CORTIR PHASE 2

Cost, Risk and Transition Zone Innovative Reinforcement

EUDP Project 64021-1054 – FINAL REPORT

Date: 28th June 2023

Authors: Find Jensen[1], Mathias Reding[1] , Shahrukh Ahmed[1] , Javier Ozores Arconada[1], Margrethe Werk[1], Tamas Nagy[1], Christian Berggreen[2], Jacob Paamand Waldbjørn[2], Edgar Arturo Gomez Meisel[2],John Dalsgaard Sørensen[3], Jannie Sønderkær Nielsen[3], Abhinav Abeendarnath[3], Peder Jacobsen[4], Yu-Huan Lin[4], Christian Løjtved[5], Rune Kirt[6], Birgit Junker[7], Nicolas Quiévy[8], Yangjiao Liao[9], Pierre Stephan[10], Hans Møller[11], Maria Asuncion Padros Razquin[12], Liane Persson[13], Francisco Garcia Lopez[14], Signe Olsson[15], Wouter Hans[16], Peter Hansen[17], David Fletcher[18], Niels Therkildsen[19], Henrik Danielsen[20], Tim Block[21]

1: Bladena
2: DTU Construct
3: AAU Build
4: Global Wind Service
5: ECC
6: Kirt x Thomsen
7: RWE
8: Engie
9: Shell
10: EDF
11: TOWII (EWII)
12: Acciona Energia
13: Arise
14: Enel
15: Statkraft
16: Equinor
17: Northland Power
18: GEV
19: FlexWind
20: Vento
21: Nordex

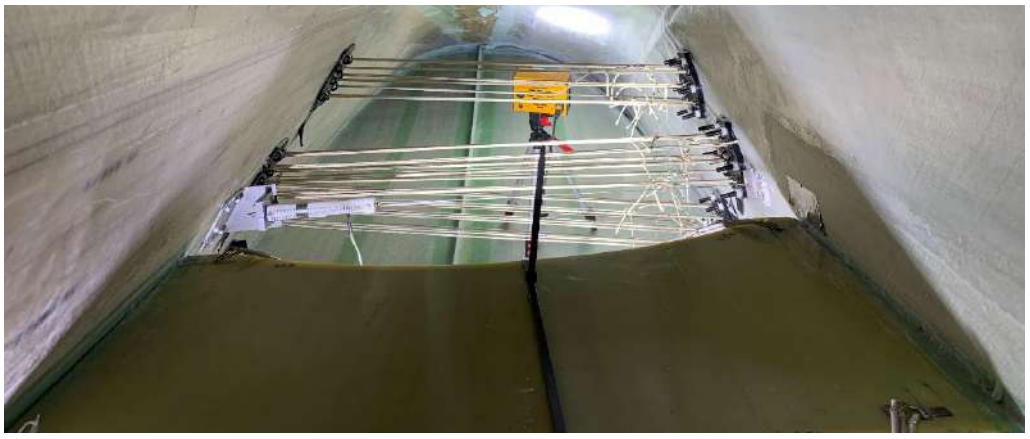

Bladena
Banestrøget 13, 1
DK-2630 Taastrup

Taastrup, June 28, 2023

Table of Contents

Bladena
Banestrøget 13, 1
DK-2630 Taastrup

Bladena
Banestrøget 13, 1
DK-2630 Taastrup

Taastrup, June 28, 2023

Project detail

Project title	Cost and Risk Tool for Interim and Preventive Repair (CORTIR Phase 2)	
File no.	64021-1054-Final Report	
Name of the funding scheme	EUDP	
Project managing company	Bladena ApS	
CVR number	34208433	
Project partners	Bladena DTU Construct AAU Build Global Wind Service ECC Kirt x Thomsen CODAN Nordex RWE Engie EDF Statkraft Equinor	TOWII (EWII) Acciona Energia Arise Enel Shell Northland Power GEV FlexWind Vent-To
Submission date	2023 June 28	

Acknowledgment

Bladena and partners would like to acknowledge the Energy Development and Demonstration Program (EUDP) for financial support under the grant number: 64021-1054 CORTIR 2 Project.

Bladena
Banestrøget 13, 1
DK-2630 Taastrup

Taastrup, June 28, 2023

Short summary

Short summary in English

The main objective of the CORTIR Phase 2 project has been to address the increasing risk of critical failure modes in the blade's transition zone mainly due to torsional loads in large wind turbine blades. During the project a retrofit solution, the Bladena patented RTZ Solution™, has been developed and demonstrated.

To validate the failure modes and its root cause, a multi-scale level test program was performed. The test results proven that under simulated field conditions the applied torsional load components lead to significant out-of-plane deformation and its direct effect can be a critical failure mode such as aft shear web disbond or/and delamination on the panels in the root transition zone.

To mitigate the investigated root cause, the RTZ Solution™ has been developed. The solution connects the two blade panels thereby, decreasing out-of-plane deformation. A testing campaign has proven the feasibility of the solution and its positive effects on the blade's performance.

Several themes and Work Packages focused on risk mitigation. Cost and Risk tool and the NIFIS developed to give educated guidelines during the decision-making progress regarding planning the correct maintenance strategy. In the NIFIS guidelines, a new Damage Categorization scheme has been developed with awareness about specific blade "hotspots" (prone to damage regions) as well as focus on the implementation of the Damage Tolerance Approach when it comes to maintenance strategy planning. Whereas WP11 dived into the topic of standards and regulations regarding testing campaigns with a special attention put on the appropriate application of torsional load components during large- and full-scale tests. Besides that, a validation process was developed in which suggestions were given on using appropriate testing methods with applied torsional load components and the use of results for more accurate blade lifetime predictions.

Additionally, the minimal viable version of the CAR Tool from a preceding EUDP CORTIR project has been improved, became more holistic and concerns more failure modes such as aft shear web disbonding in the case of large (60m+) blades.

The WTO Blade Network has been maintained and grown significantly, by now the network consists of 55 members. The conferences were held with great participation with a large part of the network being represented at the meetings.

Bladena
Banestrøget 13, 1
DK-2630 Taastrup

Taastrup, June 28, 2023

Kort resume på dansk

Det primære mål med CORTIR II projektet har været at håndtere den stigende risiko for kritiske failure modes i vinges transition zone, hovedsageligt på grund af torsional loads i store vindmøllevinger. I løbet af projektet er en retrofit-løsning, den Bladena patenterede RTZ Solution™, blevet udviklet og demonstreret.

For at validere 'failure modes' og deres 'root cause' blev et testprogram på flere skalaer udført. Testresultaterne beviste, at under simulerede feltsituationer fører, de påførte torsional load komponent, til betydelig deformation ud af plan, og dens direkte effekt kan være en kritisk failure mode, såsom aft shear web disbond eller/og delaminering på panelerne i root/transition zone.

For at mitigere den undersøgte root cause er RTZ Solution™ blevet udviklet. Løsningen forbinder de to vingepaneler (Suction Side og Pressure Side), hvilket derved reducerer deformationen ud af plan. En testkampagne har bevist løsningens gennemførlighed og dens positive effekter på vingens ydeevne.

I projektet, flere temaer og arbejdspakker fokuserede på risikoreduktion. Cost and Risk Tool samt NIFIS er udviklet for at give velinformerede retningslinjer i beslutningstagningsprocessen vedrørende planlægning af den korrekte vedligeholdelsesstrategi. I NIFIS-retningslinjerne er et nyt skadeskategoriseringssystem (Damage categorization) blevet udviklet med bevidsthed om specifikke vinge "hotspots" (områder tilbøjelige til skade) samt fokus på implementeringen af Damage Tolerance Approach, når det kommer til planlægning af vedligeholdelsesstrategi. Derimod dykkede WP11 ned i emnet standarder og regulativer angående testkampagner med særlig opmærksomhed rettet mod den passende anvendelse af torsional load komponent under store- og fuldskalatests. Derudover blev en valideringsproces udviklet, hvor der blev givet forslag til brug af passende testmetoder med påførte torsional load komponent og brugen af resultater til mere nøjagtige forudsigelser af vingens levetid.

Derudover er den minimale 'viable' version af CAR-tool fra et tidligere EUDP CORTIR-projekt blevet forbedret, er blevet mere holistisk og bekymrer sig om flere failure modes, såsom aft shear web debonding i tilfældet med store (60m+) vinger.

WTO Blade-netværket er blevet vedligeholdt og er vokset betydeligt, netværket består nu af 55 medlemmer. Konferencerne blev afholdt med stor deltagelse, med en stor del af netværket repræsenteret ved møderne.

Bladena
Banestrøget 13, 1
DK-2630 Taastrup

Taastrup, June 28, 2023

Executive summary

The wind industry is continuously growing and so are the wind turbines. With increasing blade lengths structural failures of the blades become a significantly bigger technical risk as well as financial risk, resulting in increased cost for repair and loss of Annual Energy Production (AEP). Some of the most critical structural issues of large +60m wind turbine blades such as debonding of the shear web from the load-carrying spar caps and delamination on the unsupported panels occur in the root-transition zone as an impact of torsional loads. These failure modes are today occurring more frequently due to significantly increased deformation of the unsupported blade panels. As the above-mentioned failure modes can fast lead to critical blade failures, and as of yet no repair solution has proven more than temporary, these failure modes have become a significant risk for the industry, especially for large offshore wind turbines, where limited access may result in the necessity for significant extended periods of downtime and consequently AEP losses.

For the WTOs there should be a clear focus to have more reliable blades. In the meantime, the goal is to minimize risk, especially for unplanned repairs and costly, unscheduled maintenance of blades. One way of lowering risk is to take preventive actions before blade fails. The RTZ Solution™ is such an option. Another way of mitigating risk is to become more knowledgeable about the likelihood for blade failures of various types to occur and to focus maintenance frequency, focus areas and methods to discover critical failures while the risk is low. Under NIFIS a guideline has been developed to guide WTOs and ISPs in deciding on the right maintenance strategy. In many cases, blade failures can be avoided and have a more accurate lifetime prediction by following the appropriate validation loop with relevant test campaigns using realistic load scenarios.

Shear web disbonding failure mode is a high risk

The main structural pain addressed in this project is the aft shear web disbond from the blade panels in the fish mouth region.

Many modern, large blade designs feature an aft shear web fish mouth located in the root-transition zone region. Figure 1 shows the position of the aft shear web on a typical large 60+m blade.

Bladena
Banestrøget 13, 1
DK-2630 Taastrup

Taastrup, June 28, 2023

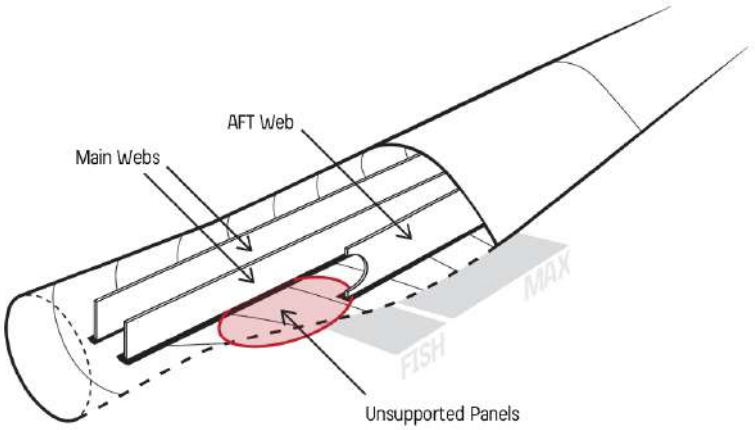

Figure 1: Large blade from root to max chord region seen in profile with the aft web fishmouth located in the transition zone.

The aft shear web failure starts as a debonding between the aft web and the blade and delaminations in the area of the fish mouth foot, see Figure 2.

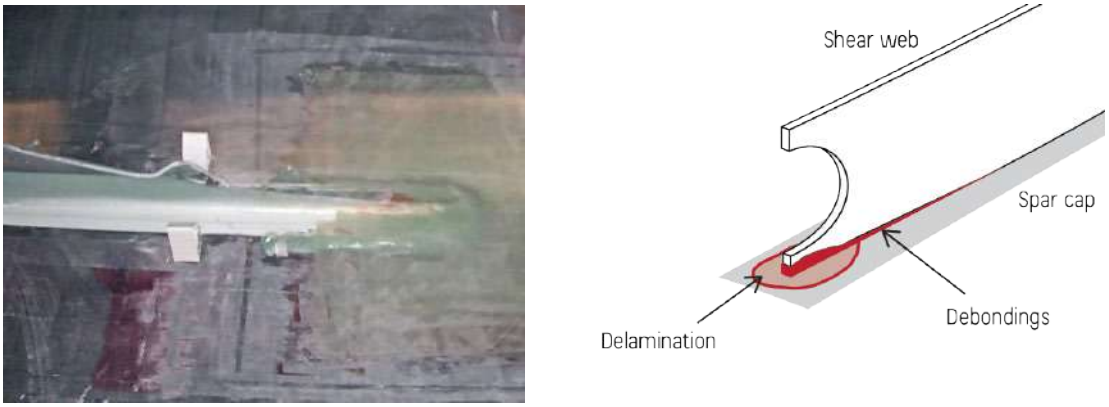

Figure 2: LEFT: Photo of a disbond of the aft web and the blade panels. RIGHT: illustration of the shear web disbond.

When the disbond of the shear web from the blade panels are initiated, it will in most cases continue to grow and in time the blade will lose the structural integrity in the area resulting in a very critical failure mode and risk of blade collapse.

The failure is prominent on large offshore blades and are seen more often in the fields during the most recent years. In general increase blade length increases the risk of structural damages. No permanent repair solution has been offered so far.

Overview of theme A, theme B and theme C

Theme A: The implementation of the Cost and Risk Tool for business analysis to assist the WTOs in their O&M decision making.

Bladena
Banestrøget 13, 1
DK-2630 Taastrup

Taastrup, June 28, 2023

Theme B: Research focused on the shear web disbond failure mode, including field measurements, large-scale sub-structural and smaller-scale sub-component testing, cohesive fracture analysis, as well as the development of the new retrofit RTZ-Solution™.

Theme C: Creation of New Innovative Field Inspection Strategy (NIFIS) including the demonstration of new monitoring techniques.

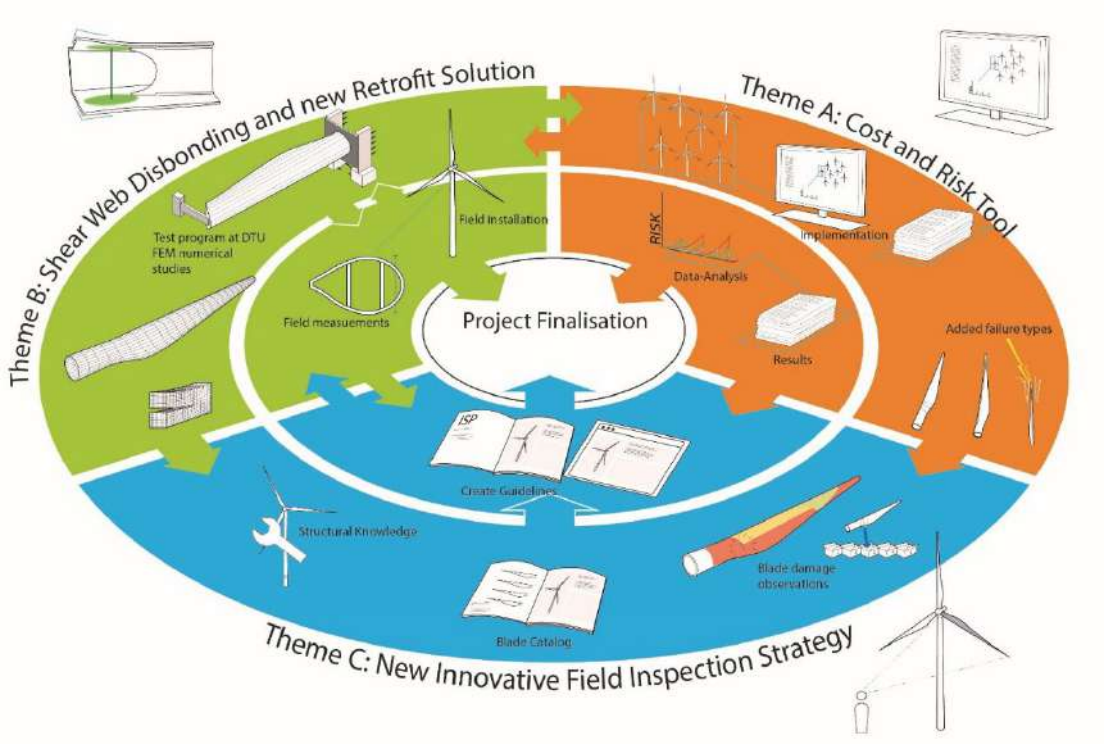

Figure 3: Project overview and interconnection between the three themes. The outer ring is the first part of the project and the inner ring is the second part with project finalization in the middle. With green is Theme A. The CAR Tool will be implemented and used to analyze maintenance strategies from the project start, where also added capabilities, such as more failure modes and advanced loading will be implemented in the tool. In the second part of the project, the CAR Tool will provide valuable data to NIFIS about the cost and risk of applying different maintenance strategies. Theme B has got the color green. This is the development of the RTZ Solution. The test and demonstration activities start in the lab and later moves out in the field. Lastly with blue is Theme C. This is the development of NIFIS, which is supported by the other two themes.

Theme A summary: CAR Tool

The main objective of Theme A is to cover from a holistic perspective relevant aspect that allow to perform a risk assessment as part of a O&M strategy simulation, so it is actually a theme that inherits knowledge from the other Themes, as well as the WP11 regarding standards on O&M.

The ultimate application of the knowledge obtained will be the development of the CAR Tool, transforming it from the current Minimum Viable Product (MVP) to an

Bladena
Banestrøget 13, 1
DK-2630 Taastrup

actual practical software that can provide an assessment to WTOs in their O&M strategies.

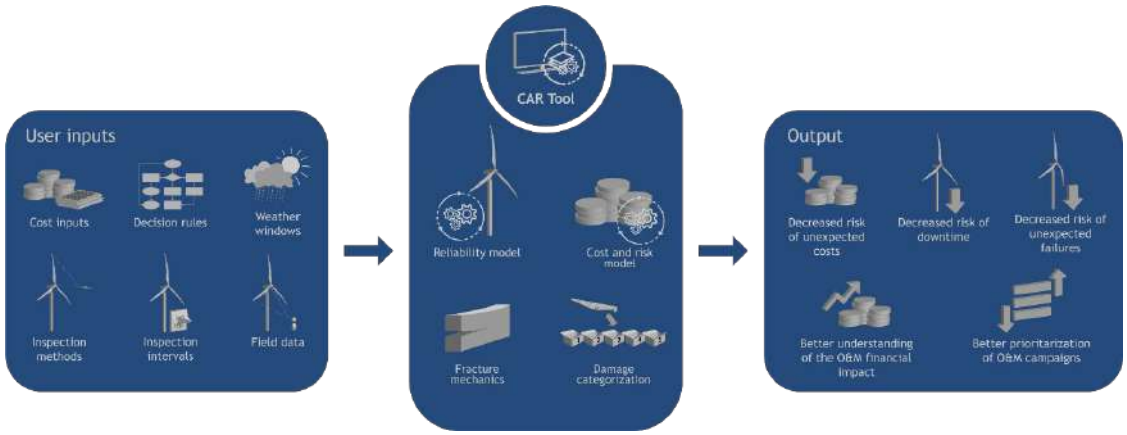

Figure 4: General scheme of the CAR Tool. On the left, the users introduce a set of variables creating a maintenance strategy that is analyzed by the CAR Tool solver (center), which calculates the risk and other economical parameters helping in the decision making for a WTO.

On one side, risk-based maintenance strategies have been investigated in more detail, both from a theoretical statistical approach and from a practical perspective. AAU has heavily contributed to this work by the analysis of reliability models and statistical approach for risk calculations. Part of this job has been gathered in the publication of a paper named “Optimization of novel heuristic strategies for inspection and maintenance”.

The main functionality of the CAR Tool is to carry out a risk analysis of specific O&M analysis. Consequently, it is required to be updated about the current common practices that Wind Turbine Owners and Independent Service implement during their inspection and repair campaign. Bladena has been in continuous contact with WTOs and ISPs in order to gather the relevant information that needs to be considered in a O&M strategy.

Regarding the development of the tool “CAR Tool”, with the intention of obtaining a holistic tool representative of the reality experienced in field conditions, the following failure modes have been analysed:

1. Leading edge erosion: a risk model has been created and fully implemented into the tool.
2. Lightning: the risk model has not been fully completed due to the complexity of the topic, but it has been studied a methodology to complete a lightning site assessment considering the risk of suffering damages from direct lightning impact through an analysis of the lightning protection system.

Bladena
Banestrøget 13, 1
DK-2630 Taastrup

Taastrup, June 28, 2023

3. Shear web disbonding: Bladena is aware that this structural issue is suffered especially on large new wind turbine blades. A fracture mechanic model after testing in DTU has been established. In addition, other approaches have been considered in detail, such as the established S-N curves method, widely used in other industries.

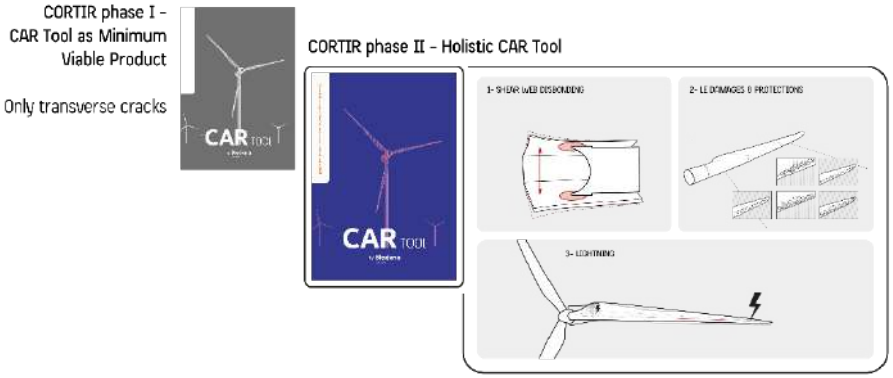

Figure 5: During the CORTIR II project the CAR Tool became more holistic with 3 additional failure modes implemented: shear web disbond, leading edge damages and lightning.

Theme B summary: RTZ Solution™

Aft Shear web dis-bonding and delamination are commonly occurring failure modes in the transition zone, especially in the newer longer (60m+) blade designs. Critical failures in long, modern blades can be translated in massive operation and maintenance (O&M) cost, especially for an offshore asset. In Theme B, the main focus is to verify and validate this failure modes utilizing numerical and experimental analysis and develop a retrofit solution to mitigate the problem.

The first step of investigation focused on performing state-of-the-art sub-component test techniques and large-scale testing with different levels of load complexity, utilizing the testing facilities in DTU Construct lab. The testing process has followed the building block approach (multi scale level approach) starting from fundamental coupon testing, manufactured by Global Wind Service, and leading to the large-scale testing. Two 15-meter-long SSP34 blade specimens were used in large-scale testing, with an aft shear web retrofitted as an evaluation area.

Complementing the lab testing investigations, the validation of the global Finite Element Model (FEM) was used to conduct a numerical study to identify how the global and panel out-of-plane deformations change for different blade types and different amount of shear webs. The obtained numerical model has determined the boundary conditions for the three levels of testing. The testing campaign included large-scale sub-structural blade section testing, smaller-scale sub-component testing, and material and fracture mechanical characterization testing.

Bladena
Banestrøget 13, 1
DK-2630 Taastrup

The obtained knowledge of the two previous steps was used as a benchmark for the performance of the newly developed solution which aims to mitigate the out-of-plane deformations in the root-transition zone of longer blades. The RTZ Solution™ is a device that is designed to be installed internally and is glued on the inner skin of the blade, without drilling through it, preventing the deformation of the panels by connecting them during operation.

The RTZ Solution™ development went through different stages of design. The final selection was optimized to address every issue that was acknowledged in the early stages of development. The solution was evaluated in different levels of testing, starting from individual component testing, both ultimate and fatigue, and finishing with testing of the entire solution.

A number of technologies were used to validate the failure mode in large-scale testing and evaluate the performance of the RTZ Solution™. Measurement sensors were installed close to the retrofitted shear web and the post-processed data were used to perform a comparison study to evaluate the performance of the RTZ Solution™. The methods used as measurements included wire potentiometers, strain gauges, and digital image correlation (DIC) cameras.

Furthermore, monitoring methods were evaluated during large-scale testing. The Sensoria system developed by MISTRAS-SENSORIA was installed on the SSP34 blade cut-outs. The acoustic emission sensors were used as a way to monitor crack initiation and propagation on the retrofitted shear web.

Theme C summary: NIFIS

During the first couple of months of the project the focus of the theme was to develop a NIFIS mobile application. After the early phase of development and the NIFIS workshop with the CORTIR partners in November 2022, the decision was made that in order to create value, the goal of the theme had to be shifted. Instead of developing a mobile application, Bladena started working on a new and improved Damage Categorization Scheme considering blade specific “hotspots” (damage prone regions/areas) and on the Damage Tolerance Approach to implement into pro-active maintenance strategies.

Besides that, different techniques were studied and their function as monitoring methods was investigated. As part of the validation process of acoustic emission sensors, Sensoria (by Mistras-Sensoria) system was used during the large-scale testing of Theme B. The use of different sensors and measurement systems were also being investigated as inspection tools in order to have more efficient inspections with identified “hotspots” of the blades matched with specific inspection methods.

Bladena
Banestrøget 13, 1
DK-2630 Taastrup

Taastrup, June 28, 2023

Regulations and standardizations (WP11), summary

Operational risk of wind turbine rotor blades can be significantly mitigated by performing sufficient tests during their testing campaign. Regarding full-scale testing, the current IEC 61400-23 standards by IEC only suggest but do not require the application of torsional loads (see in ref. [11.]). Scaling studies have proven that in the case of long (60m+) blades the torsional loads during operation are significant and can lead to severe structural damages, such as the aft shear web disbonding which was investigated in other themes of this project.

The importance of torsional loads has been highlighted in previous projects headed by Bladena, funded by the EUDP. Under the framework of Work Package 11, Bladena has performed a FEM study in which the torsional loads are investigated and quantified for long modern blades, to determine the scaling of the torsional loads with respect to length. Three blades have been analyzed with different lengths, 65m, 80m and 120m. This scaling study has been used as a key finding for the importance of torsional loads.

Besides that, Bladena in close collaboration with Aalborg University investigated the standards/guidelines related to the operation and maintenance (O&M) phase. In this project potential improvements/suggestions were developed to minimize risk in operation. Standardizations and procedures carried out in other industries (civil engineering, naval architecture, aircraft) will be used to determine relevant suggestions to the existing guidelines, where the damage tolerance approach is adopted.

Furthermore, suggestions on improving the reliability and risk in operation are also discussed in this work package. An extensive study has been carried out to investigate which approaches are described and used in the standards (e.g., semi-probabilistic, reliability-based design, etc.). On the other hand, a standardized reliability framework has been suggested for the common five-step damage categorization scheme that is used in the industry, so that it is ensured that sufficient reliability is fulfilled during the entire operational life of the blade. The gathered knowledge has been documented and a Risk-based maintenance roadmap for WTOs has been developed for the upcoming two years.

Finally, a design and validation process has been developed to estimate the lifetime more accurately utilizing sub-component testing and FEM calibration of the blade model, focusing on structurally critical measurements. This is a cost-effective way to capture any critical result before expensive prototype testing, as it mostly requires sub-component testing and FEM-modeling.

Bladena
Banestrøget 13, 1
DK-2630 Taastrup

Taastrup, June 28, 2023

Project Objectives

Main project objectives

The project ran for 2 years and had 11 Work Packages, the main focus of the project was to develop and demonstrate a new innovative retrofit reinforcement for shear web disbonding in the root-transition zone of large (60m+) wind turbine rotor blades. The development of the solution included a test campaign dedicated to verifying the failure mode and its root cause.

Besides that, the project concerned risk mitigation by developing tools assisting WTOs to plan more efficient pro-active maintenance strategies. Regarding risk mitigation the project also covered the area of standardization/regulations and currently used testing requirements.

Objectives of Theme A: CAR Tool

Holistic risk analysis, identifying and studying the main considerations for the simulation of a realistic O&M strategy, including assessment on risk and reliability models, O&M general practices understanding, and technical analysis on specific failure modes. A great proportion of all this knowledge obtained, aims to be implemented in the Cost and Risk Tool for business analysis to assist the WTOs in their O&M decision making.

Objectives of Theme B: RTZ Solution™

Research focused on the shear web disbond failure mode, including field measurements, large-scale sub-structural and smaller-scale sub-component testing, cohesive fracture analysis, as well as the development of the new retrofit RTZ-Solution™.

Bladena
Banestrøget 13, 1
DK-2630 Taastrup

Taastrup, June 28, 2023

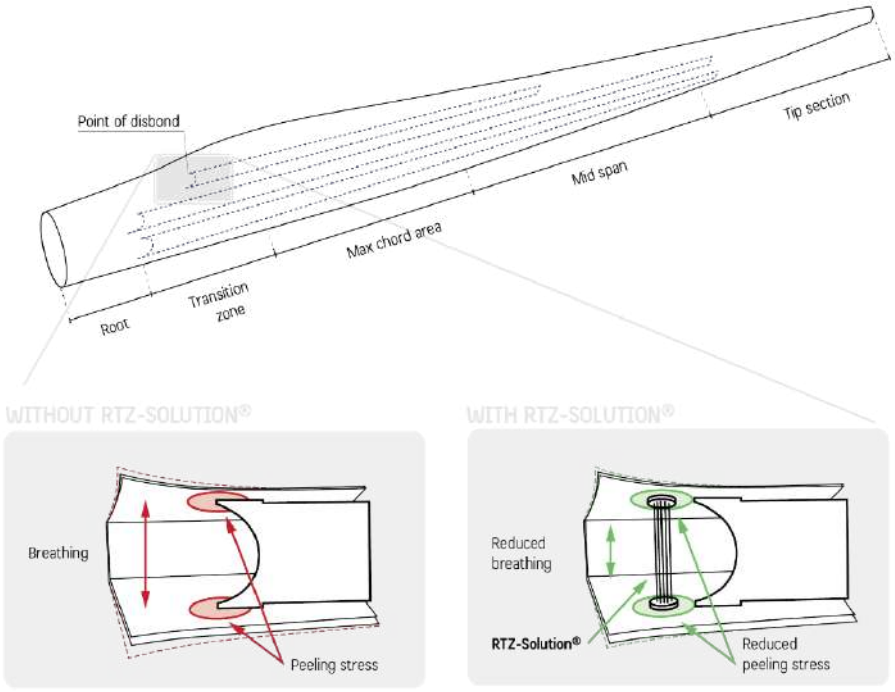

Figure 6: Panel breathing (deformation) in the transition zone generates high peeling stresses at the secondary shear web. The effect and impact of the RTZ Solution will be analysed numerically on different blade concepts.

Objectives of Theme C: NIFIS

Creation of New Innovative Field Inspection Strategy (NIFIS) including the demonstration of new monitoring techniques. The main objective of Theme C was to deliver a valuable tool for the WTOs, ISPs, and assessment companies which help them to create optimal inspection/maintenance strategies. By creating the right strategy, the maintenance strategy could be delivered more efficiently which would eventually lead to less downtime and higher AEP.

Objectives of WP11: Regulations and standardizations

The main objective of WP11 was to raise awareness about the use of relevant testing methods (large-scale or/and full-scale test with applied torsional load components) and validation (see in detail in ref. [1.]). Within the work package, a deep dive was taken into the area of required tests, the lack of precise torsional loading requirements and potential improvements of standards in order to minimize operation risk for wind turbine rotor blades.

Bladena
Banestrøget 13, 1
DK-2630 Taastrup

Taastrup, June 28, 2023

Milestones

Technical and commercial milestones were defined prior to the start of the project. The purpose was to keep track of the project.

Technical Milestones

TM1: Reconstruct blade sections by creating manhole to enter rear box and install new shear web

TM2: Final RTZ Solution™ development

TM3: Validation of FEM models against test results

TM4: Development of NIFIS guidelines

TM5: CAR TOOL ready to be utilized by WTOs as an assessment tool

Commercial Milestones

CM1: Release of Technology Roadmap of the product development of the RTZ Solution™

CM2: The delivery of "Technical Blade course fitted for ISP needs"

CM3: Bladena has hosted an international conference presenting the RTZ Solution™ and NIFIS

Overall, the project was on track during the whole time period allocated to it. Due to unpredictable failures (issues with the test rig; damaged specimen) regarding the test campaign TM2: Final RTZ Solution™ development and TM3: Validation of FEM models against test results tasks and deadlines had to be adjusted but the milestones have been met before the end of the project.

Besides the above mentioned, after the NIFIS seminar and workshop held in May 2022 the scope of Theme C concerning NIFIS has been shifted from creating an app to the development of a new damage categorization scheme and the implementation of Damage Tolerance Approach. This meant that TM4: Development of NIFIS guidelines was not relevant anymore, despite of that NIFIS is as a guideline with the mentioned focus points has been finalized by the end of the project.

Bladena
Banestrøget 13, 1
DK-2630 Taastrup

Taastrup, June 28, 2023

Project implementation

Project progress

Overall, the project has followed the initially predicted timeline. The tasks described in the work packages and in the project's Gantt chart have been completed in time, in a few cases some insignificant delays were experienced but they did not have a negative effect on the time flow of the project.

Risk in the project

The initially determined risks concerned different levels of the testing campaign of the project. First of all, a concern was raised regarding specimens for sub-component level testing. With the correct resource management, the project managed to manufacture sufficient amount of new shear web specimens which are identical to the one which were retrofitted inside the 15m blade cut out. The specimens were manufactured by Global Wind Service based on Bladena's design with DTU Construct input.

On the other hand, the risk regarding large-scale and full-scale demonstration had an impact on the project. Firstly, within the resources there were only two SSP34m blade sections available. The project faced delays due to the fact that one of the specimens had damage which was only found once it was installed on the test rig and the test was started. This caused some downtime as the section had to be taken off the rig with disassembling of the measurement/monitoring systems. Once the second specimen was on the test rig, unexpectedly DTU Construct was faced with issues with the testing equipment. The rig had broken parts which had to be fixed in order to progress with the testing, this caused delays in the testing campaign and unplanned actions had to be taken. The necessary actions were taken effectively, leaving the project with sufficient test results to conclude.

Project results

All main objectives of the project have been reached.

The RTZ Solution has been developed and benchmarked against the same conditions without the solution being installed. A test campaign was performed successfully.

The CAR Tool has been developed to a more holistic tool taking into account transverse cracks, shear web disbonds, and leading edge erosion.

As planned the CAR Tool has given input to NIFIS. NIFIS as a guideline for more efficient maintenance strategy development.

Bladena
Banestrøget 13, 1
DK-2630 Taastrup

Results for theme A: CAR Tool

Cost and reliability (WP4)

The CAR tool developed in CORTIR Phase 1 (Ref to final report) relies on a simulation-based approach for assessing the risk associated with heuristic strategies with equidistant inspections and a threshold for when to make repairs (ref.[2.]). In CORTIR Phase II, methodological developments have been made to explore the benefit of including more advanced strategies. Firstly, for damage tolerant systems, where small defects do not have to be repaired immediately, it may be preferable to use a smaller inspection interval when defects get closer to the size requiring a repair. Secondly, information from inspections may be used to reduce uncertainties in models. Within the field of inspection and maintenance planning, advanced methods have been developed recently based on e.g. partially observable Markov processes (POMDP) or deep reinforcement learning (DRL). However, the strategies coming out of these methods lack transparency, and they are consequently not easy to understand for practitioners. Therefore, the developments in this project have focused on advanced heuristic strategies. A novel Bayesian network approach was developed, where age-based inspections can be included, by including a count-down node for the time to the next inspection. This allows for including strategies, where the time for the next inspection depends on the outcome of the latest inspection in terms of the size of the defect. Due to the computational efficiency, it is possible to consider a large number of different strategies, and thereby do the optimization for specific degradation mechanisms. Further, a module for updating the model based on inspections has been developed, allowing to adapt strategies when more information becomes available.

Statistical analysis after shear web disbonding testing (WP6)

Design and assessment of wind turbine blades assisted by tests are important in verifying structural integrity of large wind turbine blades. In CORTIR II tests are performed for assessment of shear web disbanding and the RTZ Solution™ in Theme B. Tests of composites and wind turbine blades / critical details as the shear web are generally performed at an increasing level of detail illustrated by the test pyramid with many tests performed at characterization level and fewer and fewer tests performed for subcomponents with increasing size and complexity and finally only a few tests at large scale or full-scale level. In verifying structural integrity of critical details, the uncertainties related to these different levels have to be included. The uncertainties include physical uncertainty, model uncertainty, statistical uncertainty and measurement uncertainty. Physical uncertainties are generally quantified at

Bladena
Banestrøget 13, 1
DK-2630 Taastrup

characterization level where the statistical uncertainty is very small due to the large number of tests being performed. At subcomponent and large-scale test level numerical models using e.g. cohesive elements for fatigue verification are introduced. In validation of the numerical models the tests are an important tool. In this project an approach for a systematic modelling and quantification of the uncertainties is developed. Using test results the model and statistical uncertainties due to a (very) limited number of tests can be quantified with statistical uncertainty becoming more and more important at increasing subcomponent level. The uncertainty modelling related to tests and associated numerical models are developed such that they can be used to verify the structural reliability and for optimal planning of operation & maintenance in CAR Tool. The statistical modelling of test results also includes tests performed at subcomponent with reinforcement the RTZ solution included. The tests results obtained at DTU Construct are used to quantify the above uncertainties. The statistical analysis for shear web disbanding tests is described in the paper 'Stochastic modelling of wind turbine blade tests for reliability analysis and O&M planning'.

Based on the stochastic and statistical modelling of the test results and included in the numerical models, reliability verification can be performed using partial safety factors or reliability-based approaches. Further, the stochastic models for fatigue can be used as important input for cost-optimal planning of operation & maintenance including planning of inspections and monitoring in CAR Tool.

Leading edge erosion implementation (WP3)

Leading edge erosion (LEE) has been included in the CAR Tool, meaning that now users can establish O&M strategies involving LEE and its consequent risk in the overall risk calculation for decision making.

A methodology has been established as well as a numerical model for risk calculation exclusively due to LEE. The methodology is presented below.

Bladena
Banestrøget 13, 1
DK-2630 Taastrup

Taastrup, June 28, 2023

Methodology description

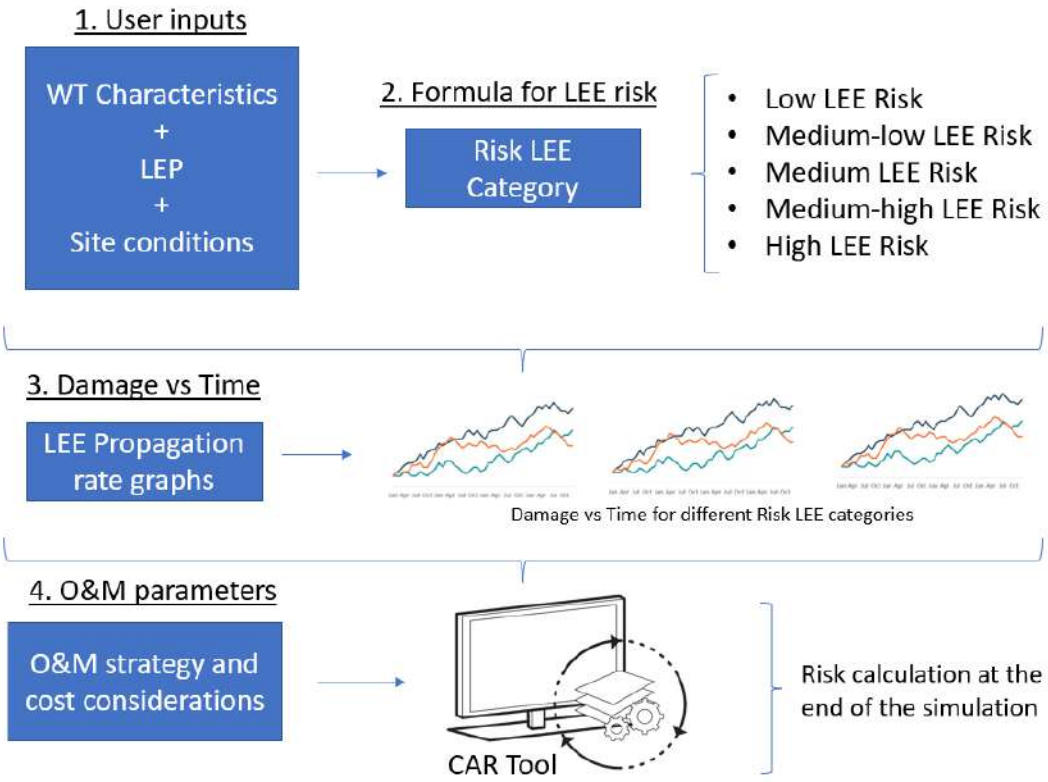

Figure 7: User scenario and workflow of the CAR Tool

The idea is that the users will provide information to the CAR Tool about wind turbine (WT) characteristics, leading-edge protection (LEP) solutions, and site weather conditions. The software will use this input to define the risk LEE category, which has been associated with a specific rate of propagation, meaning that e.g., high damage categories will be reached earlier for a high LEE risk than for a low or medium-low LEE risk.

Once the software is aware of the expected erosion propagation, a simulation will be run considering a list of relevant O&M parameters also defined by the users, including some such as inspection interval, inspection method, repair criteria, or decision rule.

A consequent risk, associated with each simulated O&M strategy, will be calculated following a reliability and risk model developed together with AAU. The final risk due to leading-edge erosion will be shown to the users individually, but also it will be combined with the other sources of risk that the CAR Tool aims to analyse to become in a holistic tool.

Bladena
Banestrøget 13, 1
DK-2630 Taastrup

Taastrup, June 28, 2023

Numerical model for LEE risk calculation description

During the last years, Bladena has been updated about the last state of the art on leading edge erosion, by reading new publications on the topic, and attending conferences and international symposiums. Relevant knowledge has been gathered as a result, which has allowed the establishment of a numerical model as part of this Theme A.

The model is based mainly on three group of variables:

1. *Wind turbine characteristics*:

   Tip speed is the main variable that should be considered.

   It has been studied the relationship between tip speed and blade length for several commercial blades, concluding that in case that the user does not have access to the maximum tip speed then the blade length could be used instead. By using commercial documentation, there is sufficient data to estimate expected tip speeds for specific blade lengths.

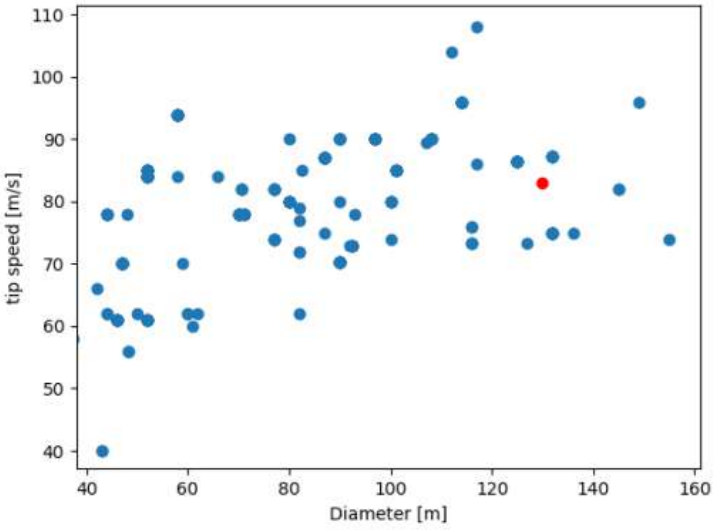

Figure 8: Analysis of relationship between maximum tip speed and diameter of different commercial wind turbines.

2. Leading Edge Protection (LEP) systems:

   LEPs are a relevant aspect to consider for the risk evaluation. Specific LEPs can be suitable for a specific wind turbine in a specific site with some weather

Bladena
Banestrøget 13, 1
DK-2630 Taastrup

conditions, but it might not be the ideal solution for a same or another wind turbine in different locations.

Therefore, understanding the main characteristics of an LEP is essential to make a sensible choice to protect against leading edge erosion and several aspects should be considered for the evaluation of a LEP, e.g., possible aerodynamic issues due to addition of extra thickness in the airfoil profile, loss of adhesion during operation, energy impact dampening capacity, resistance to each relevant environmental factor, debonding risk due to stiffness mismatch, weather window during application, and possible noise emission for onshore locations.

For the numerical model, the analysis has focused on:

- Material of LEP
- Type of LEP: shell, tape, liquid solution
- Location of the LEP in the blade

3. Weather characteristics:

The sources that influence on the risk (probability of an event to happen multiplied by the consequence of this event) in terms of developing environmental factors, have been divided in the following site conditions:

- Rain: most recognized source of risk of LEE. It is energy driven meaning that some variables like “erosivity” can be taken as a reference (include reference here)
- Hail: also, energy driven. There are available hail index maps of different areas of the world that allow to get an estimation of the possible hail events.
- Wind: the Weibull distribution of a specific site will be used as a reference
- UV: ultraviolet light irradiation has proved to influence on the degradation of some mechanical properties especially for LEPs made of polyurethane.
- Sand: sand particles travel at high speeds that erode the leading edge during sandstorms.

Due to the lack of reliable knowledge on how each of the previous parameters influence on LEE, it has been decided to follow a simple approach in which all parameters are combined in a linear function, in which weighting factors are given to each of the analysed parameters.

So, the following formula has been considered:

Bladena
Banestrøget 13, 1
DK-2630 Taastrup

$$Criticality = f(WTs, LEP, site) = W_{WT}X_{WT} + W_{LEP}X_{LEP} + W_{site}X_{site}$$

Where:

- W = weighting factor. From [0,1]. The sum of the weighting factors will never exceed 1.
- X = punctuation of the parameter. From [0,1]

Analysis of W_{WT} and X_{WT}:

It refers to the variables that will be considered for the analysis of the wind turbine characteristics. As mentioned previously, the single variable will be tip speed, as a higher tip speed will lead to a higher relative velocity between the blade and whatever particle is impacting against its surface.

A specific W_{WT} has been selected, that will be multiplied by the corresponding X_{WT} according to an internal criterion that will depend on the value of maximum tip speed.

Analysis of W_{LEP} andX_{LEP}:

Quantifying how the LEP influences in the final level of erosion is currently a challenge for which the wind energy industry does not have enough expertise nowadays. In addition, LEP by itself is not a source of LEE, but on the contrary, it is a parameter that will modify how the other two parameters (tip speed, and site conditions) will influence on the LEE.

Analysis of W_{site} and X_{site}

5 variables will be considered: wind, hail, UV, Sand, Rain.

$$X_{site} = f(S_1, S_2, S_3, S_4, S_5) = W_{s1}X_{s1} + W_{s2}X_{s2} + W_{s3}X_{s3} + W_{s4}X_{s4} + W_{s5}X_{s5}$$

Where:

- S_1: wind
- S_2: hail
- S_3: UV
- S_4: sand
- S_5: rain
- X_{si} will oscillate depending on the value of the meteorological value, and W_{si} will depend on the specific weight of that weather factor.

Bladena
Banestrøget 13, 1
DK-2630 Taastrup

Taastrup, June 28, 2023

Final risk categorization:

The final 5 LEE risk categories, considering the value of Risk (see formula of Risk above) will be:

- Low LEE risk: for $Risk \leq 0.30$
- Medium-low LEE risk: $Risk \in (0.30\,, 0.40]$
- Medium LEE risk: $Risk \in (0.40, 0.60]$
- Medium-high LEE risk: $Risk \in (0.60, 0.75]$
- High LEE risk: $Risk > 0.75$

Damage propagation in time:

In order to simulate the risk on a specific O&M strategy, it is necessary to have an estimated propagation of LEE in time, for the five different LEE risk categories commonly recognized in the industry.

Bladena has analysed different inspection reports for different wind farms. A risk analysis has been performed considering mainly the site conditions, and the wind turbine tip speeds, categorizing the risk from Low to High. As an example of a possible leading edge erosion propagation that could be shown as an output of the CAR Tool, see figure below:

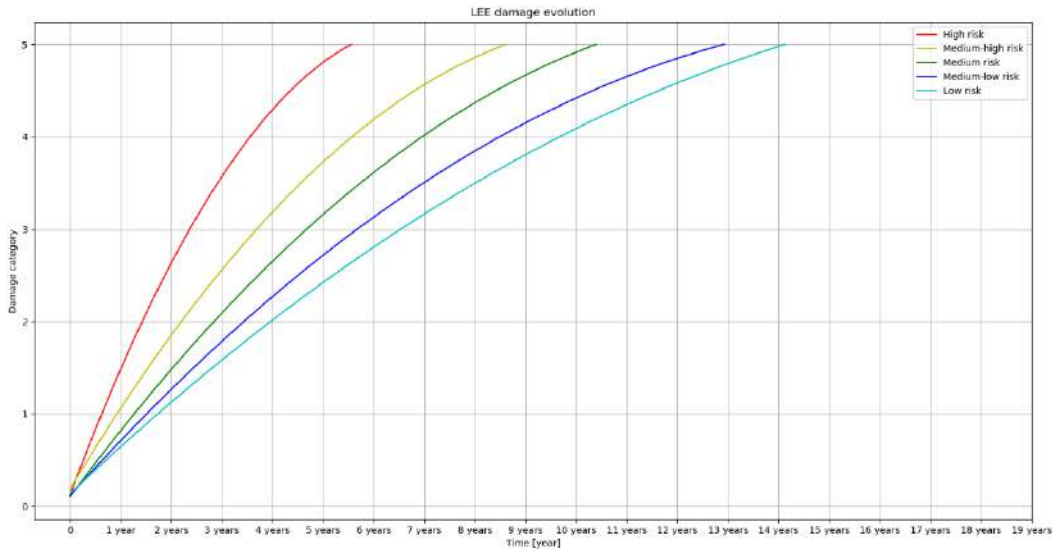

Figure 9: Damage category vs Time. Example of possible leading edge erosion propagation for different risk levels without repairs

Bladena
Banestrøget 13, 1
DK-2630 Taastrup

Shear web disbonding

Shear web disbonding is a structural failure mode that has been studied in this project. A set of different tests have been performed in DTU facilities (see section 8.2.) and a fracture mechanic model has been established consequently (see ref. [3.]).

In order to understand better the influence of shear web disbonding on the lifetime of a blade and impact on O&M strategies, this failure mode has also been studied from the perspective of S-N curves, obtaining relevant conclusions.

The fracture mechanic approach is understood as the method that will lead to highest uncertainty reduction; however, this method is not always possible to be applied due to lack of resources or even time to perform the analysis explained in Theme B.

S-N curves are lifetime curves that define the number of cycles (N) that are necessary to be experienced so that a material fails at a specific given stress range (S) in a fatigue analysis. S-N curves are extensively used in the industry, and they help to estimate the lifetime of a material exposed to fatigue conditions.

For the statistical analysis, it has been assumed that an S-N curve has the following linear shape:

$$\log(N) = \log(A) - m \cdot \log(S)$$

Where:

- N: number of cycles
- A: it would represent the point where the line would interesect with the “y” axis
- S: stress range $(F_{max} - F_{min})$

S-N curves combined with FEM analysis for estimation of lifetime reduction:

S-N curves can be a powerful tool if they are combined with a detailed FEM analysis on specific failure modes. FEM can provide results for stress and strain levels, which can work as a reference for a possible damage initiation and propagation as used in risk based planning of O&M strategies.

If this information is postprocessed, the identified stress values could be used in an S-N curve in order to determine the possible number of cycles that are required until failure is reached.

Bladena
Banestrøget 13, 1
DK-2630 Taastrup

The number of cycles can later be converted into expected number of years by making use of variables such as tip speed ratio, providing valuable informatio for the establishment of O&M strategies from a risk perspective.

In addition, if field information is available about when a specific damage has appeared, the combination of FEM and S-N curves could help to estimate when it may appear again for another blade with a similar blade geometry. This is technically possible by performing a scaling study between the two blades. However, it must be understood at this point, that uncertainty will always have to be considered for any analysis of this nature.

Example 1:

Based on the field data of a Blade 1, it is known that a damage appeared at a lifetime of X1 years of operation. By using FEM analysis, it could be determined the strain level under operational conditions that potentially could lead to the generation of that specific damage in Blade 1.

As stress and strain are proportional units, due to the following equation, a similar proportionality can be assumed for the stress levels.

$$\sigma = \varepsilon * E$$

By doing so, the stress for Blade 1 can be determined. Given the same proportionality between the two units, the stress level for the Blade 2 can also be calculated by following the approach illustrated in the figure below:

Bladena
Banestrøget 13, 1
DK-2630 Taastrup

Taastrup, June 28, 2023

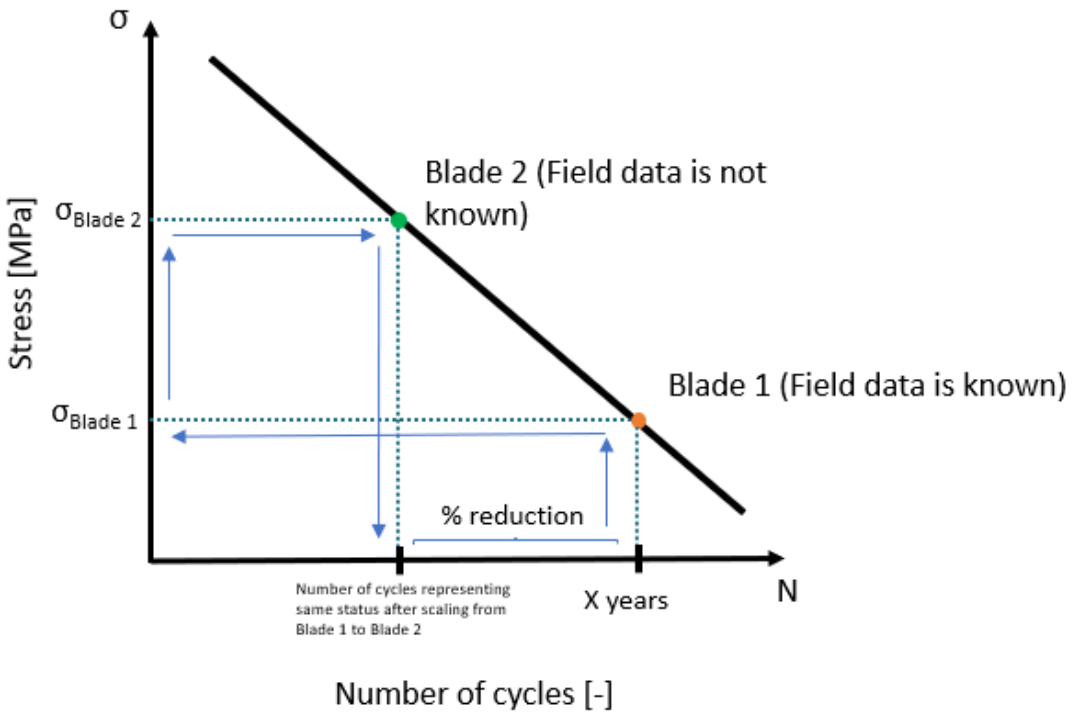

Figure 910: Impact of stress levels on an S-N curve

This method gives a good initial look of how the increased stress levels will influence the state of the Blade 2 seen from different failure modes, and how much the lifetime may be reduced from Blade 1 to Blade 2.

In a similar way, and now in direct relationship with shear web disbonding, the combination of S-N curves and FEM analysis could help to study the possible root cause of initiating this failure mode at an early stage of the lifetime of a blade. This again, could be very valuable information for a consequent risk-based O&M strategy.

Example 2:

Imagine a blade that has experienced the initiation of a field damage due to shear web disbonding after X years of operations. If it is assumed that torsional loads are the root cause of shear web disbonding, and this is confirmed from a technical perspective, consequent preventive actions could be established.

By following a similar analysis than in Example 1, FEM could study the strain levels in the shear web spar cap connection of a specific Blade 1 under operational loads. This analysis could be implemented both with and without the application of torsional loads.

Bladena
Banestrøget 13, 1
DK-2630 Taastrup

Taastrup, June 28, 2023

Thanks to the correlation between strain and stress previously mentioned, S-N curves could help to understand the possible lifetime reduction because of torsional loads.

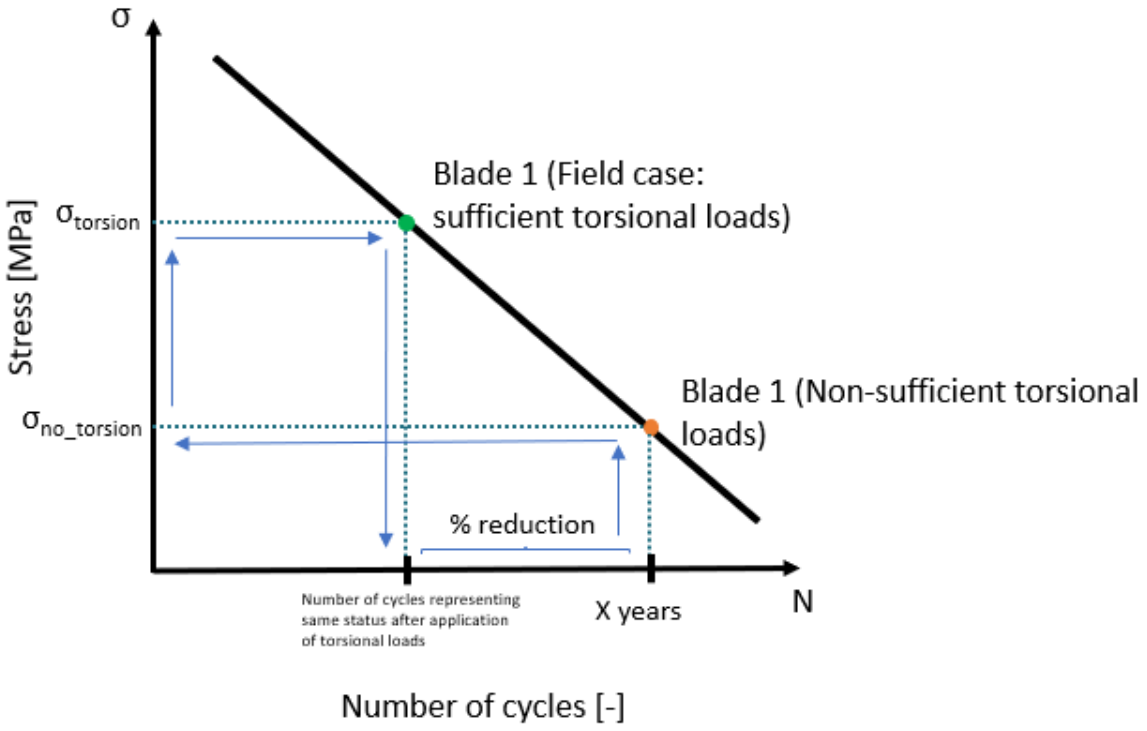

Figure 10: S-N curve showing possible life reduction due to torsional loads, which could help to establish a preventive risk-based O&M strategy

O&M information

The O&M cost contributes a significant share of the total OPEX of a wind turbine. Wood Mackenzie reported in 2019, that the global onshore wind O&M cost will reach nearly $15 billion in 2019 already, 57% of that number is allocated for unplanned repairs (ref. [12.]). Based on our experiences and knowledge this number for large offshore turbines can be even higher. Thus, to reduce the OPEX cost, it is crucial that the right choice of maintenance strategies for wind turbine blades is applied optimally. In 2023 the concern of increasing OPEX is a significantly relevant topic as DNV in a whitepaper (ref. [9.]) and GCube in an article (ref. [13.]) are also addressing the worrisome increasing costs and that with the scaling in size would increase the costs even more.

Currently, the Wind industry adapts two primary strategies: Proactive or Corrective. Corrective strategy is when an asset is run to failure and consequently performed repair, whereas proactive strategy is being proactive and utilizing various means to

Bladena
Banestrøget 13, 1
DK-2630 Taastrup

arrest the damage in the early phase, for example utilizing monitoring techniques, frequent inspections etc. The CAR Tool aims to help in the decision making of this type of proactive strategies, especially for large offshore wind turbines.

As it will be explained in more detailed in Theme C, condition monitoring is an additional approach for blades for a preventive strategy that has started to be used in the industry. Condition monitoring aims at detecting any changes from the normal behaviour and indicates developing damage or a damage initiation.

Condition monitoring is realized using Monitoring methods (such as acoustic emission, accelerometers etc.), and frequent inspections. Corrective maintenance has the advantage of fully utilizing the blades lifetime however with corrective maintenance the risk of developing secondary damage and catastrophic failure is high. Thus, Bladena suggests using preventive maintenance for critical hotspot regions of the blade, such as shear web disbonding shown in Table 1.

Failure mode	Region	Criticality level	Damage stability	Action
Shear web debonding	Transition zone/Max chord	Very High	N/A	Repair immediately.

Table 1: Potential approach to shear web disbonding. The table is not reflecting the likelihood of the failure mode, it only shows the action and the "consequence" (criticality level) if the damage occurs.

The criticality level shown in Table 1 is also an essential variable for the establishment of a risk-based O&M strategy.

Typically, damages are classified using a five-point scale which defines different levels of damage. Assigning a category to a particular damage can be uncertain as the same damage in the load-carrying region and in the aerodynamic region may not have the same category. Additionally, categorizing a damage or defect depends on various factors such as whether it has grown over time or if it has stopped. In this project, Bladena has utilized the five levels to determine the criticality level of shear-web disbonding and the rest of failure modes included in the CAR Tool. See Table 2.

Category	Definition
Very High	Is assigned to a damage which is considered to cause a total loss of the structure.
High	Damage that has potential to cause catastrophic failure if keeps growing.
Medium High	Damages that are stable but in the structural region of the blade.
Medium	Stable damage in the aerodynamic region.
Low	Mostly cosmetic damages or minor damages requiring minor repairs.

Table 2: Definition of criticality level categories utilized in the report.

Bladena
Banestrøget 13, 1
DK-2630 Taastrup

Taastrup, June 28, 2023

Results for theme B: Shear Web Dis-bonding and New Innovative Retrofit Solution (RTZ Solution™)

The main objective of Theme B is to investigate the failure mode of shear web disbonding and the development of a solution to eliminate the root cause of this failure. The shear web disbonding is a failure mode that is mostly relevant for modern, long blades (longer than 60 meters), designed with an aft shear web. Shear web disbonding is considered as a critical failure mode and as the length of installed wind turbine blades is increasing to cover the electricity needs, it will be observed more frequently in field inspections.

Shear web disbonding is a failure mode that occurs due to the panel out-of-plane deformations during operation in the root-transition zone of a blade. These localized deformations increase the peeling stresses of the bondlines on the fishmouth region of the aft shear web, especially on the pressure side where the panel is curved, and it thus deforms significantly more than the suction side panel.

The current status in repair actions on shear web disbonding issues only include temporary solutions, such as overlamination of the fishmouth region, where the crack initiates. This lack of a permanent solution raised the need for the development of RTZ Solution™. The RTZ Solution™ is a device installed internally in the root-transition zone and its purpose is to prevent the outwards out-of-plane panel deformation.

The following section is dedicated to the investigation of the failure mode. The different levels of testing will be showcased, from coupon testing to small sub-component testing and finally to large-scale testing. The configuration of each test will be discussed followed by presenting the findings of each step. Additionally, the development stages of the RTZ Solution™ will be presented, along with the evaluation of the final design.

Shear web disbonding investigation

The shear web disbonding investigation was executed in collaboration with DTU Construct at their testing laboratory (Structural Lab) in Lyngby. The testing was carried out in different levels following the Building Block Approach, adopted from the aircraft industry, thereby several experiments were done on Level 3, 4 and 5 investigating material characteristics (see in ref. [3.]) whereas on Level 2 (large-scale testing) (see in ref. [4.]) only 2 tests were executed as the allocated resources provided 2 large blade cut-outs for the project. The building block approach for the testing with the different levels are presented on the figure below.

Bladena
Banestrøget 13, 1
DK-2630 Taastrup

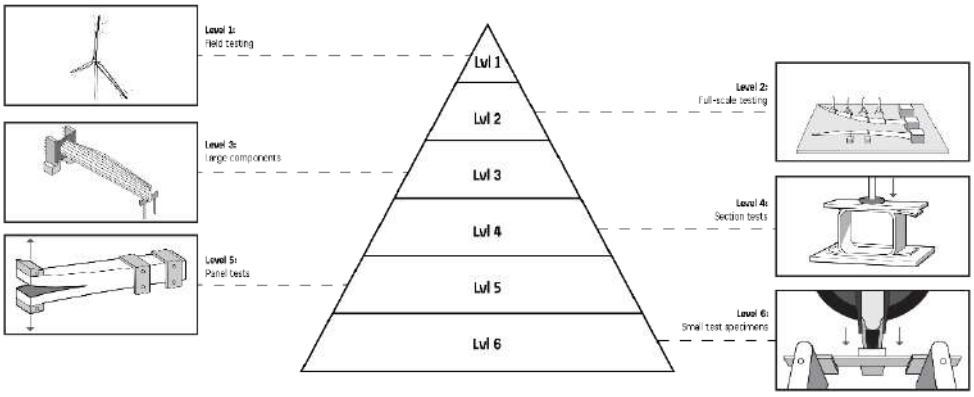

Figure 11: The followed building block approach for the testing campaign

The adoption of the Building Block Approach for wind turbine blade testing can significantly contribute to the blades' validation process (see more in the findings of Work Package 11). The test pyramid involves a series of physical and virtual fracture tests and models of increasing complexity which ensures that with increasing complexity in geometry and loading the damage mechanisms are properly captured, understood and presented in the predictive damage models. Different scale-levels are addressed sequentially starting from characterization testing, over sub-component testing, large-scale testing of a wind turbine blade section, and in-field full-scale testing. Following the pyramid from bottom levels towards the top in combination with the on-going adjustments of the numerical models with the test results, can result in significant decrease of risk once the full-scale test is performed with realistic, operational load scenarios which directly leads to a more trustworthy lifetime expectancy prediction for the blade.

The detailed findings of Level 3, 4 and 5 are presented in DTU Construct's publications which can be found as separate papers attached to the report [*Appendix C: PAPER H: Cohesive zone modelling to predict crack growth under fatigue loading (A. Gomez; C. Berggreen)*].

The purpose of the large-scale testing is to verify the findings of the initial FEM simulations which showed that due to out-of-plane deformation caused by combined loading in the root-transition zone bondline failure can occur at the aft shear web's fish mouth geometry in cases of large blades (60m+) (see in ref. [8.]). The result of the FEM scaling study is presented on the figure below.

Bladena
Banestrøget 13, 1
DK-2630 Taastrup

	Peeling Stresses (Mpa)
34 m blade	3.5
65 m blade	8.0
Change (%)	125

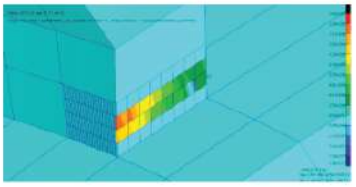

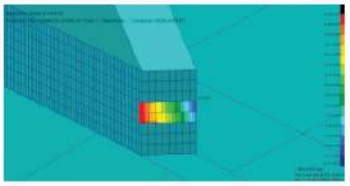

Figure 12: Scaling study on the peeling stresses in the aft shear web bondline in FEM simulation (see in ref. [8])

It was observed from the FEM studies, that the loads acting on the blade during normal operational conditions generates oscillatory transverse panel deformations or in popular terms named "breathing", which generates peeling stresses in the cohesive bondline between the inner sandwich panel face sheet and the shear-web. Exposed to continued fatigue loading, the impact of this deformation mechanism is a cohesive damage in the bondline, leading to a disbonding of the adhesive bondlines in the shear web. In order to verify this an artificial aft shear web were retrofitted in both available SSP34m blades designed by Bladena and installed by Global Wind Service. During the experiment, normal field conditions were simulated to investigate the peeling stresses in the area and their effects on the installed aft shear web. The installed shear web and the SSP34m blade cut-out on the test rig are presented on the figure below.

Figure 13: The installed artificial aft shear web (on the left), the SSP34m blade cut-out installed on the test rig at DTU Construct's Structural Lab (on the right)

For the large-scale testing campaign besides the measurement systems, Digital Image Correlation (DIC) camera, strain gauges and potentiometer wire, also the SENSORIA acoustic emission sensors by MISTRAS-SENSORIA was used as a monitoring system. For more details about the full-scale test setup, equipment and in-detail results, see in *Appendix D [Large-scale fatigue testing of a retrofitted 3rd shear web in a 34m wind*

Bladena
Banestrøget 13, 1
DK-2630 Taastrup

turbine blade section (J.P. Waldbjørn; C. Berggreen, S. Ahmed, T. Nagy]. The position of the internal measurements is presented on Figure 14.

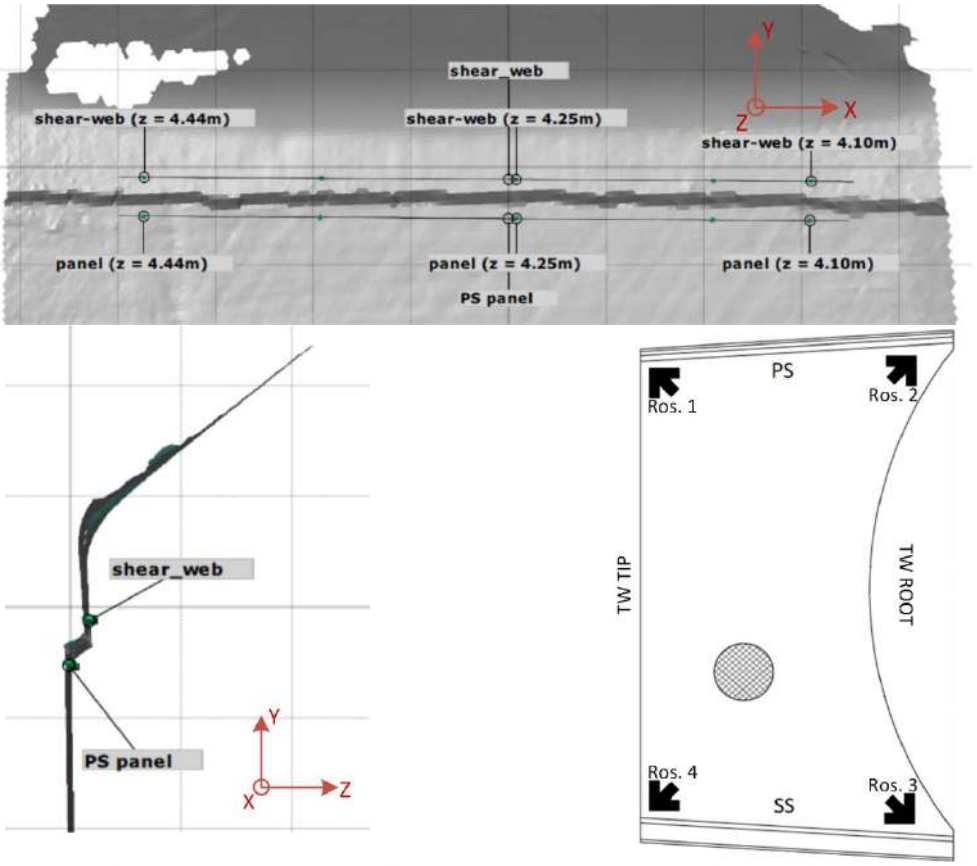

Figure 14: Internal measurement system labelling, in-plane DIC (top), out-of-plane DIC (bottom left), and strain gauges (bottom right). Source: ref. [4.].

The first SSP34 blade section with the retrofit installed aft shear web was tested under 100kN of edgewise load capacity along with a corresponding 100kNm torsional moment. These torsional load components are approximately 50% higher than those that a 34m long blade would meet in field. A failure mode different than the main investigated one occurred after approx. 280.000 cycles. The applied torsional loads introduced root bending moment which have led to a major crack in the blade's transition zone region. Further testing on the same blade section would have led to a blade collapse due to significant sudden decrease in edgewise stiffness (see Figure 15). This damage was a direct result of the applied torsional fatigue loads, causing large-scale damage on the blade shell in the root transition zone due to delamination from the out-of-plane deformation. The damage is shown on Figure 15. Such damage is considered critical, as it would require an immediate action if it happened during operation; failure to do so could potentially lead to further structural damage to the blade or other areas of the wind turbine. as if no actions were taken it could potentially lead to further structural damages on the blade or on other areas of the

Bladena
Banestrøget 13, 1
DK-2630 Taastrup

wind turbine. Delamination in this region is a failure mode which, based on Bladena's knowledge and FEM models, is a common damage due to the applied torsional loads.

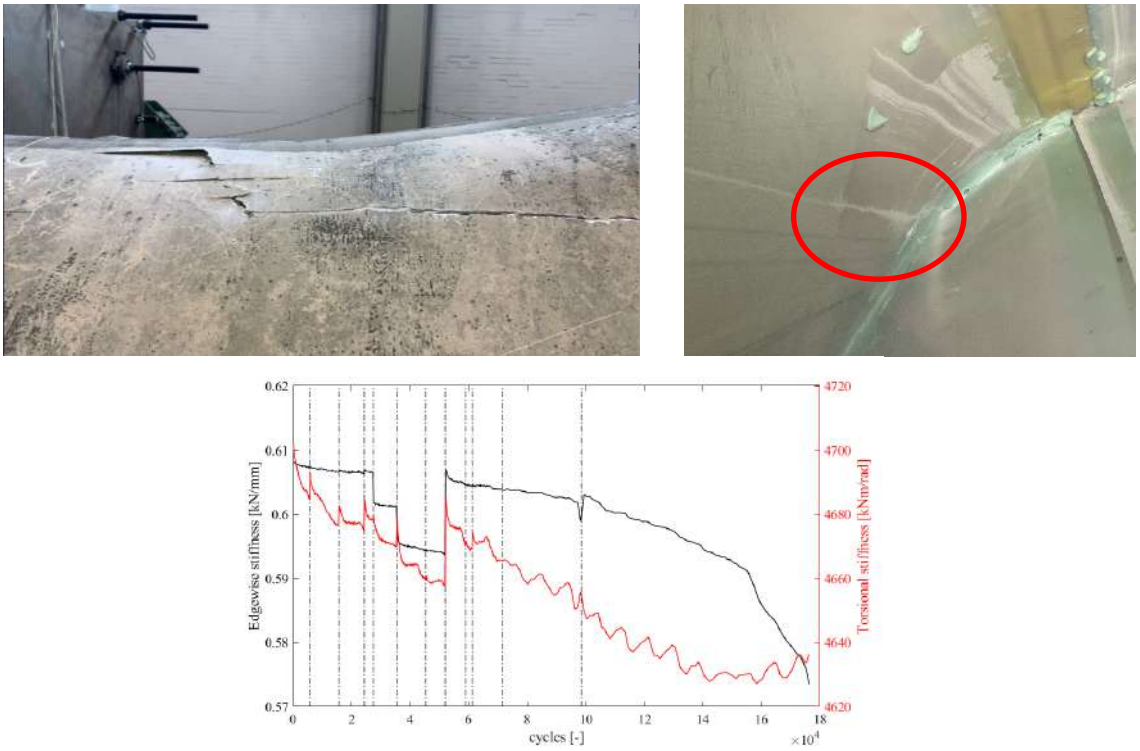

Figure 15 - Critical damage on the blade's transition zone observed after 300 000 fatigue test cycles. From outside (on the left) and from inside the blad (on the right). Plot presenting the change in edgewise and torsional stiffness (on the bottom).

The first test is considered successful for several reasons. Firstly, it has proven that high enough torsion load can be introduced to the blade section to damage the blade without damaging the cargo insertion point. Secondly, even though the damage is not in the shear web bondline, it occurred in the transition zone of the blade which shows that the introduction of torsional loads significantly impacts the load carrying transition zone. The measurements of the strain gauges installed on the aft shear web shows that the strain levels were stable with the amplitude of 7με, see Figure 15. Even though the damage happened further towards the root, it can be concluded that a severe damage can occur under lower strain levels around the aft shear web bondlines when the torsional load components are applied.

Bladena
Banestrøget 13, 1
DK-2630 Taastrup

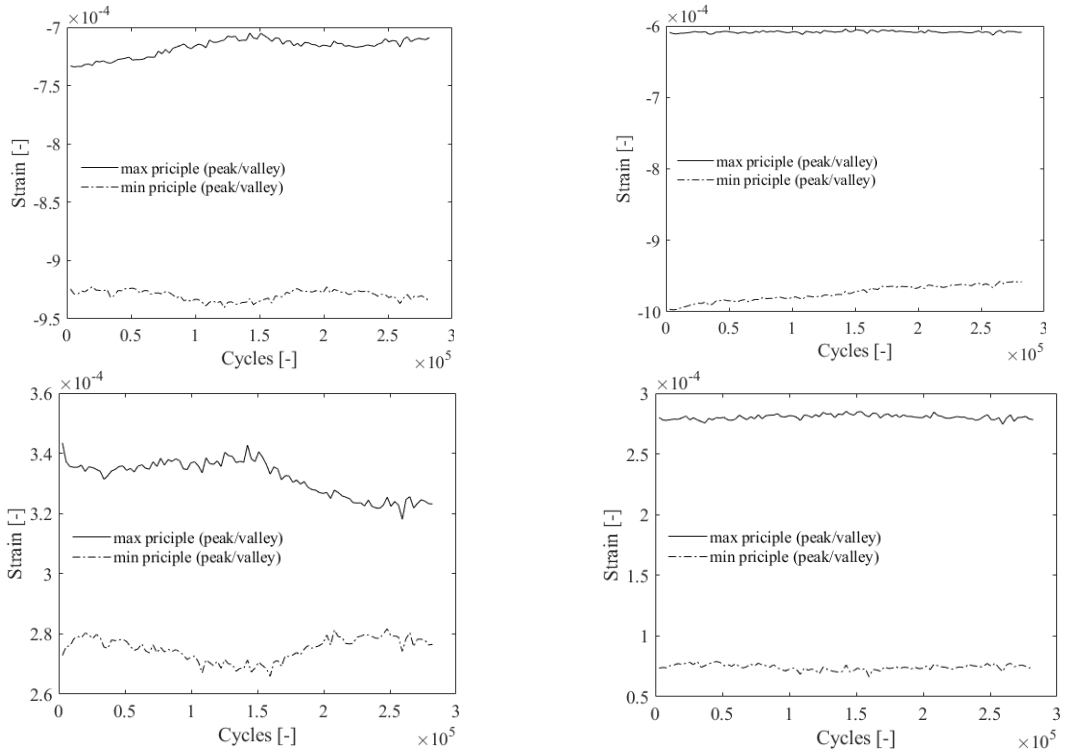

Figure 16: Strain at each corner of the shear-web including a) pos. 1, b) pos. 2, c) pos. 3 and d) pos. 4. Source: ref. [4.].

The second test specimen suffered a significant leading edge damage (approx. 3m long longitudinal crack along the bondline) only after a few cycles performed under the same fatigue conditions as in the first test. In order to continue the full-scale test the damage had to be repaired. After investigating the damage, the decision was made to remove the damaged area completely and then reinforce it with fiberglass lamination. The repair was performed by Global Wind Service. Besides the repair, the bondline of the aft shear web was cut (5cm in length) on both pressure side and suction side in order to initiate the shear web disbonding failure mode. The repaired blade and the initiated cut are presented on the figure below.

Bladena
Banestrøget 13, 1
DK-2630 Taastrup

Taastrup, June 28, 2023

Figure 17: Repaired blade section (on the left) and initiated crack in the aft shear web bondline (on the right).

Due to time and resource limitations, the test without the RTZ Solution™ being installed only ran for approximately 12000 cycles. Within the 12000 cycles from the measurements of the wire potentiometer installed 20cm in front of the aft shear web, significant increase of out-of-plane deformation was observed. As it can be seen on Figure 18, at the beginning of the test the out-of-plane deformation was approximately 10mm whereas after 12000 cycles this value reached 13mm. In comparison, during the test of the other blade the deformation was stable 7mm throughout the entire test (see in ref.[4.]). The plot of the measured deformation can be seen on the figure below.

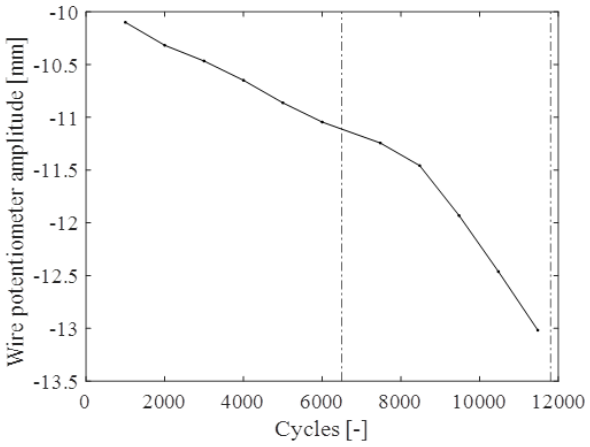

Figure 18: Out-of-plane deformation measurements plot obtained with wire potentiometer (LVDT).

The sudden increase in out-of-plane deformation could be the indication of a failure mode, therefore the blade was inspected internally. During the inspection it was observed that the manually initiated cracks in the aft shear web bondlines have significantly propagated. On the Pressure Side (PS) the crack propagation was above

Bladena
Banestrøget 13, 1
DK-2630 Taastrup

2cm whereas on the Suction Side (SS) this value was approximately 1cm. The cracks damaged bondlines are presented on the figure below.

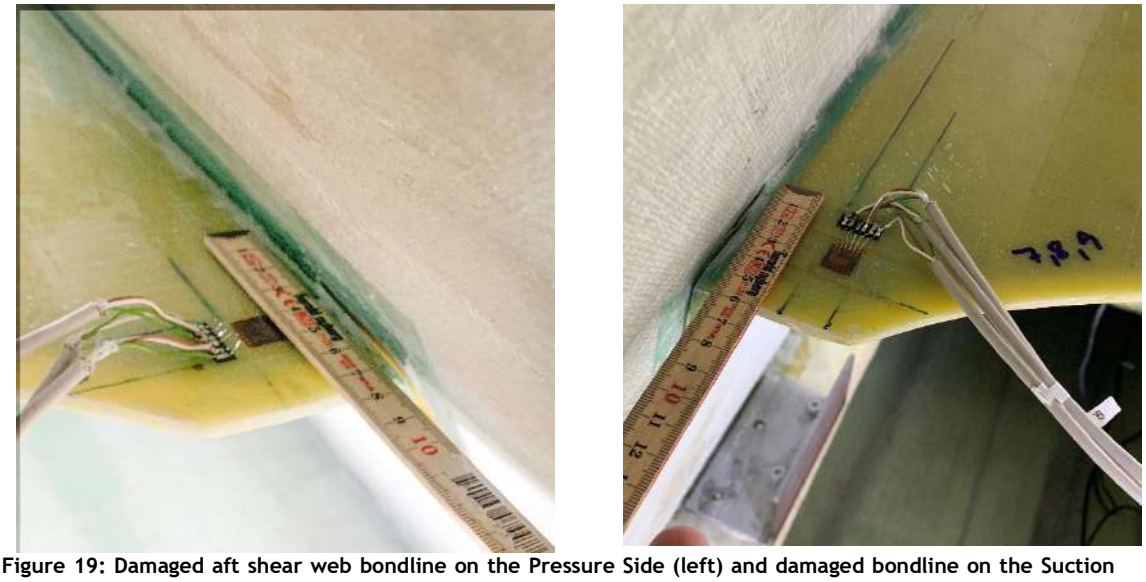

Figure 19: Damaged aft shear web bondline on the Pressure Side (left) and damaged bondline on the Suction Side (right).

In summary, increased "breathing" was observed when torsional load components were applied on the cut outs of the SSP34m blade, leading to a severe damage during large-scale testing. This outcome was noted in two separate experimental analyses, each revealing the extent of the damage caused by these loads. These tests led to the conclusion: the impact of torsional loads is not confined to only longer blades but also substantially affects shorter ones. Even a blade with a relatively short length of 34m demonstrated vulnerability to torsional loads.

RTZ Solution™ development

As a reflection of the test results a solution was developed in order to mitigate the peeling stresses and thereby eliminate bondline failures in the aft shear web's adhesive bondline. The development of the RTZ Solution™ followed a carefully developed design funnel in which from a reason for the need of the product led to the launch of the solution. The funnel is presented on the figure below.

Bladena
Banestrøget 13, 1
DK-2630 Taastrup

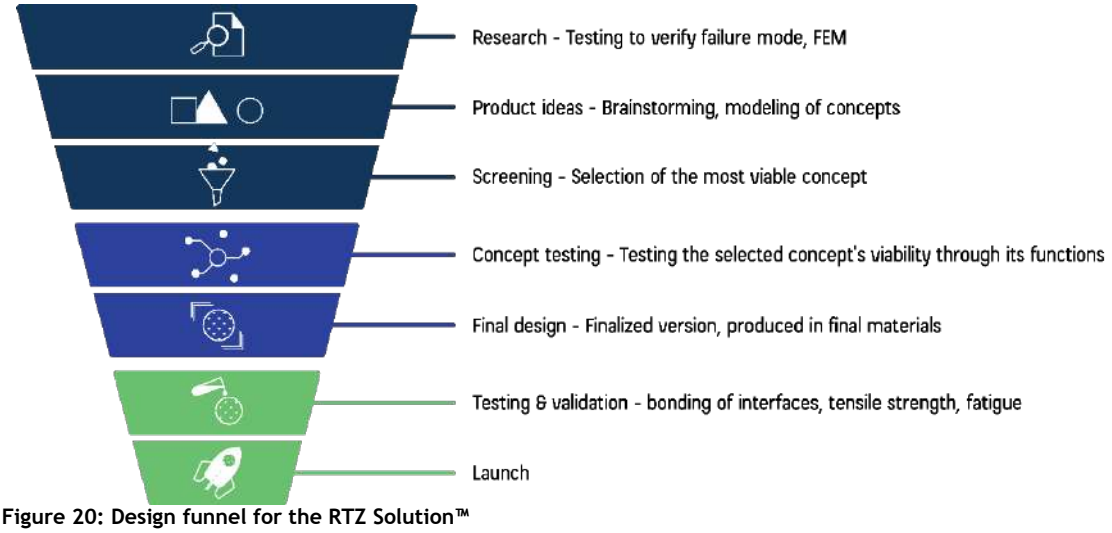

Figure 20: Design funnel for the RTZ Solution™

Following the funnel ensures that every stage of the development is done in the correct order, thereby resulting in a final solution which was built on solid groundwork with precisely defined purposes and goals.

Product testing

The FEM analysis investigated by Bladena, showed that the peeling stresses in the area in question can be significantly reduced by connecting the two shells (pressure side and suction side) of the blade together. Therefore, the main function of the RTZ Solution™ is to connect the blade panels and eliminate the oscillatory transverse panel deformations ("breathing").

During the product testing campaign, the aim was to verify the capabilities of the solution to connect the panels and eliminate the out-of-plane deformations without creating any possible causes for failure in the panels' sandwich construction. The experiments followed the similar building block approach as the shear web disbonding investigation.

On Level 4 (sub-component level) the solution was tested under both static and fatigue conditions in tension. The 1:1 prototype were installed on blade panel cut-outs and tensional loads were applied in order to find the ultimate strength/load carrying capability of the solution. Due to time limitations, the sub-component test campaign is being executed ongoingly with the time of the end of the project. During static tensile tests the weak points of the solution will be found. The tested specimens are prototypes made out of PC-ABS and manufactured by 3D printing. Therefore, the obtained values do not represent the actual strength of the solutions but it gives a clear understanding of the strengths of the solution. The test setup is presented below.

Bladena
Banestrøget 13, 1
DK-2630 Taastrup

Taastrup, June 28, 2023

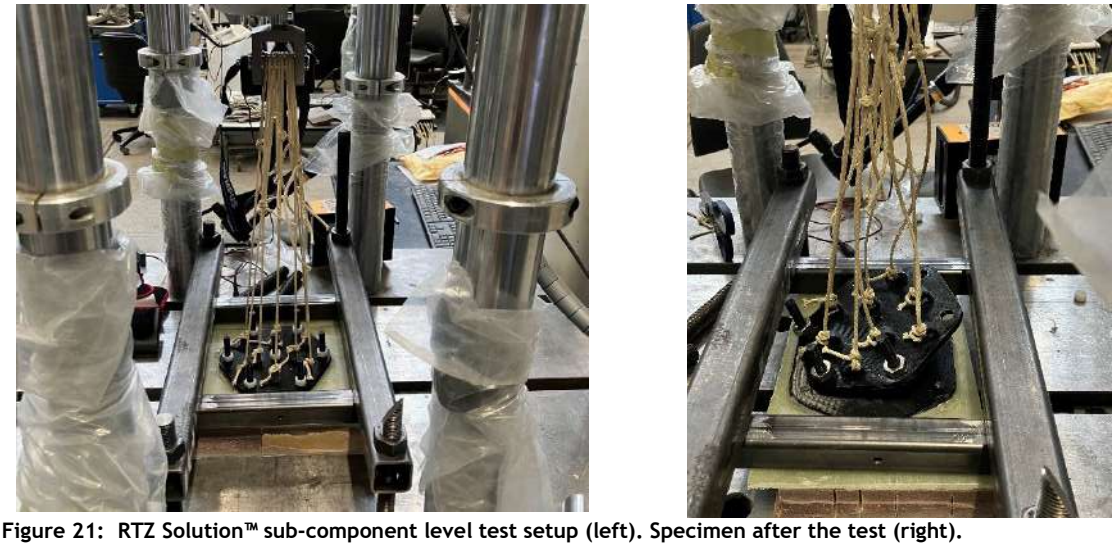

Figure 21: RTZ Solution™ sub-component level test setup (left). Specimen after the test (right).

The executed tests showed that the bolts and nuts are the weakest points of the solution. Therefore, gluing the brackets together is necessary.

On Level 3 (large-scale level) the solution was installed onto the previously tested SSP34m blade cut-out. The test under the same conditions was performed on the specimens in order to benchmark the results of the tests against the results achieved without the solution being installed. Due to time limitations the test campaign could not be fully executed within the timeframe of the project. The RTZ Solution™ is installed inside the 15m blade section after the crack on the aft shear web bondlines propagated but due to a technical issue in the mounting box girder of the blade section the test cannot be executed until a repair is done in the damaged area.

The installation of the solution is relatively easy, and the only time-consuming part of it is the curing time of the adhesive. The experience of installing the solution allows us to adjust the product for even more easier installation. For future prototypes, the bolts will be shortened as at the moment they are unnecessarily long. Besides that the PC-ABS 3D printed material is not strong enough therefore in future works glass filled ABS will be used. The installed RTZ Solution™ inside the test blade is presented on the figure below.

Bladena
Banestrøget 13, 1
DK-2630 Taastrup

Figure 22: The RTZ Solution™ installed inside the 15m blade cutout of the SSP34m blade.

Final Prototype – RTZ Solution™

The final version of the product is relying on a carefully designed looping system. The solution is four component design with the top part, bottom part and fixing part is made of glass fibre filled plastic material and the system is connected through the loops with a Vectran rope from Marlow Ropes. For simplicity during the prototyping and testing PC-ABS material was used. The figure below illustrates the solution.

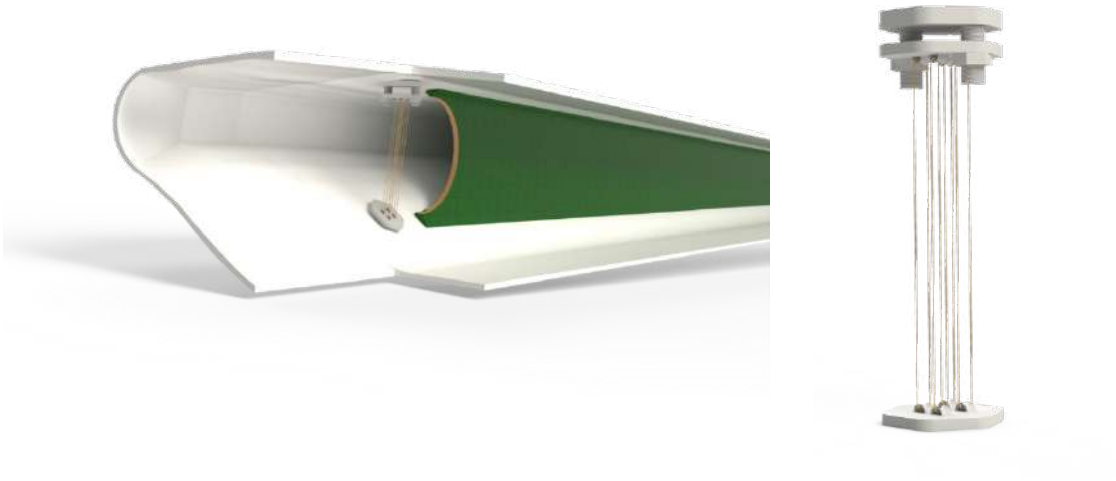

Figure 23: Concept illustrations of the RTZ Solution™, patented by Bladena

The solution must be installed inside the blade in front of the aft shear web's fish mouth geometry. The installation does not require drilling on the panels but instead

Bladena
Banestrøget 13, 1
DK-2630 Taastrup

it must be adhered onto the panels with SikaForce-800 Red(or similar). Depending on the blade size more devices can be installed, the necessary number of devices will be discussed and recommended by Bladena after the assessment of the specific blade type.

Results for theme C: New Innovative Field Inspection Strategy

Based on different schemes around the industry, the NGIR project and Bladena's damage interpretation, a combined damage categorization scheme has been created. In contrast with other damage categorization scheme, the new version focuses on the position and its effects on the blade's structure rather than only on the damage type and its size. This updated scheme is applying the Damage Tolerance Approach based on the structural severity of different damages in different blade regions. The scheme is presented on the tables below.

Bladena
Banestrøget 13, 1
DK-2630 Taastrup

Taastrup, June 28, 2023

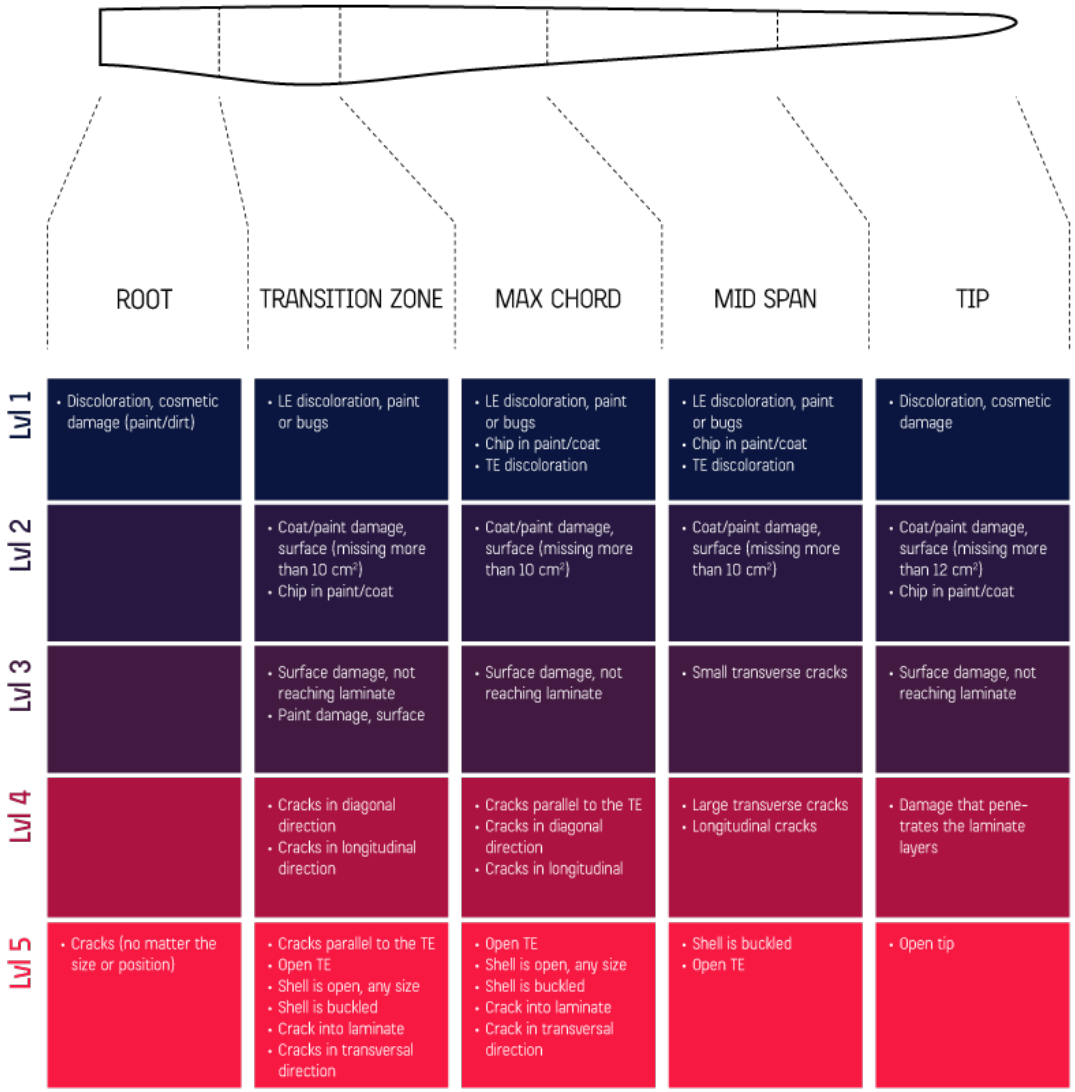

Figure 24: Updated Damage Categorization scheme with applied Damage Tolerance Approach with damage criticality depending on its position and structural importance of the blade.

The damage categorization scheme will be updated with illustrations for the different damages.

Results regarding inspection and monitoring techniques will be added once the large-scale test in Theme B is performed and a conclusion will be made by MISTRAS-Sensoria.

Bladena
Banestrøget 13, 1
DK-2630 Taastrup

Taastrup, June 28, 2023

Pro-active/preventive maintenance strategy

The current maintenance approach is to repair the blades if necessary. Implementing the use of the Damage Tolerance Approach by monitoring the "hotspots" of the blade would allow the owner to prevent severe failure modes and thereby planning a more optimal maintenance strategy. Condition monitoring of blades have started to be used but there is still limited experience. Bladena has positive experience with Acoustic Emission, in full-scale test environment, as an effective monitoring technique that can detect damage at early stages if the sensors are placed close to the determined hotspot, see Figure 12. Within the frame of Theme B the Sensoria™ acoustic emission system by MISTRAS-Sensoria was used to validate the reliability of this NDT monitoring technique. Figure 12 shows an illustration of the Acoustic Emission (AE) sensor installed at the hotspot.

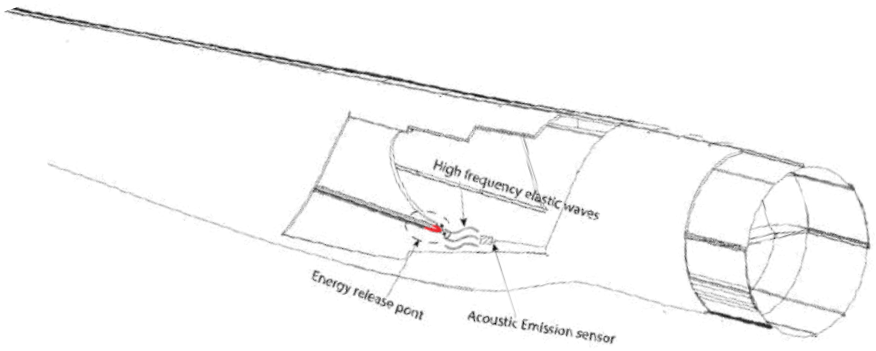

Figure 25: An illustration of an acoustic sensor placed close to the hotspot.

Moreover, to detect potential unwanted vibrations, such as flutter and Edgewise vibrations, Bladena suggests the installation of accelerometers to avoid catastrophic failures due to edgewise vibrations. The accelerometers measure the dynamic response of the blade. It is probably not relevant to install Accelerometer on all blades, maybe only on the prototype turbine if Flutter occurs, it is likely that it will be detected. Figure 13 shows an illustration for the potential installation location of an accelerometer.

Bladena
Banestrøget 13, 1
DK-2630 Taastrup

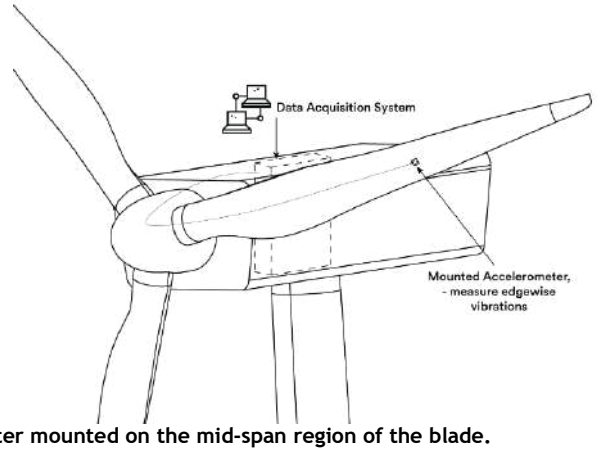

Figure 26: Accelerometer mounted on the mid-span region of the blade.

The table below provides general advantages and disadvantages of using corrective (currently used within the industry) or preventive/pro-active strategy. Various factors must be considered when choosing a relevant strategy, such as position, damage stability, region (aerodynamic or structural), etcetera. However, for the purpose of the analysis, it is assumed that the failure modes are located in the structural region.

Preventive	
Pros	**Cons**
Continuous monitoring.	Can be costly in short-term.
Repair actions are taken before a damage reaches a critical stage.	Qualified personnel to evaluate the data.
Schedulable inspections.	Limitations of monitoring systems.
Lower repair costs.	
Low risk of long downtime periods.	
Lower wating times for repairs (less dependency on weather windows).	
Corrective	
Pros	**Cons**
Adequate for low criticality damages.	Long downtimes.
Less costly (short-term).	Risk of secondary damages.
	Unforeseeable costs potentially out of the planned budget.
	Risk of catastrophic failure.

Figure 27: Table listing the advantages and disadvantages of preventive and corrective maintenance strategies. The table presents general pros and cons for the Preventive and Corrective strategies and each Pros and Cons must be read independently.

Bladena
Banestrøget 13, 1
DK-2630 Taastrup

Taastrup, June 28, 2023

Results: Regulations and standardizations

The information presented in this report empathises the importance of paying attention to shear web disbonding damages and especially to the torsional load components in a blade, as torsion is considered to be a relevant factor that influences on the formation of this failure mode.

The report presents both experimental analysis, and numerical models which both point in the same direction.

As a result, the wind energy industry is recommended to act accordingly being aware of the high risk it is exposed to for large blades, and consequently re-assess both blade designs and O&M strategies during operation in order to reduce the probability of failure of shear web disbonding and to minimize the possible failure modes derived from torsional loads.

In this relation, regulations and standardizations are a key element to promote the implementation of specific actions or steps.

One of these steps, as it will be developed more in detail in subsection 8.4.1. Figure 22, of the whole validation process.

The current section takes into account the main findings in the CORTIR Phase II project, to identity some areas which could potentially help to mitigate the risk of suffering damages from some of the structural damages related to torsional loads. The following recommendations are presented below, and they are to be considered by the wind energy industry. It is believed that a joint-venture project concerning the topic would be beneficial for the whole industry.

Full-scale static test with torsional loads

The full-scale testing program following IEC-61400-23 standard requires both flapwise and edgewise loads but in separated load cases. The static pull is close to the shear centre, hence almost no torsional loads are applied.

The importance of both torsional loads, and a combined load case is recognised in different sections of the certification, but nowhere it is imposed an application:

- Example 1: Section 7.2. Test program: “the flap and lead-lag sequence of testing may be performed on two separate blades. However, if an area of the blade is critical due to the combination of flap and lead-lag, then the entire test sequence shall be performed on one blade”. The consideration of whether an area of the blade is critical or not due to the combination of loads is open to interpretation, meaning that freedom is given to applying or not a

Bladena
Banestrøget 13, 1
DK-2630 Taastrup

combined loading full scale test. As a clarification, in this context the term lead-lag is used in a similar way as the term edgewise in the current report.

- Example 2: Annex E.6. Torsion loads: "if torsion loads are significant in the structural design of the blade they should be included in the test". Again here, it is subjective the establishment of whether torsion loads are critical or not. And even if they are considered as significant, the word "should" indicates a recommendation, not an obligation.

- Example 3: Section 9. Test loading and test evaluation: "sufficient information shall be provided to allow the test load to be accurately assessed against the target load. In principle, the six load components should be given, including phase and frequency information required to generate combined load cases. In reality, the load components lead-lag and flapwise moments are the far most important components". Again, the IEC standard highlights a combined loading scenario, but the word "should" does not force any action in this regard.

- Example 4: Section E.4. Flapwise and lead-lag combinations: "In static and fatigue tests, the results are most representative when combinations of flapwise and lead-lag loads are applied. By applying only the flapwise bending moments or only the lead lag moment, the resulting stresses and strains and/or damage rates may be lower in some areas than the target values". As a fourth time, importance is recognised, but no action is taken. The content of this example 4 is actually in alignment with the study of the impact of torsional loads on large blades that Bladena and partners present in a separate paper (see ref. [1.]). Some of the main results from this paper are also presented in section 8.4.5.

As a result of all this, it is recommended that as part of the certification and standards, the combination of flapwise and edgewise loads that generate torsion are applied at the same time. The following sketch is proposed (see Figure 24)

Bladena
Banestrøget 13, 1
DK-2630 Taastrup

Taastrup, June 28, 2023

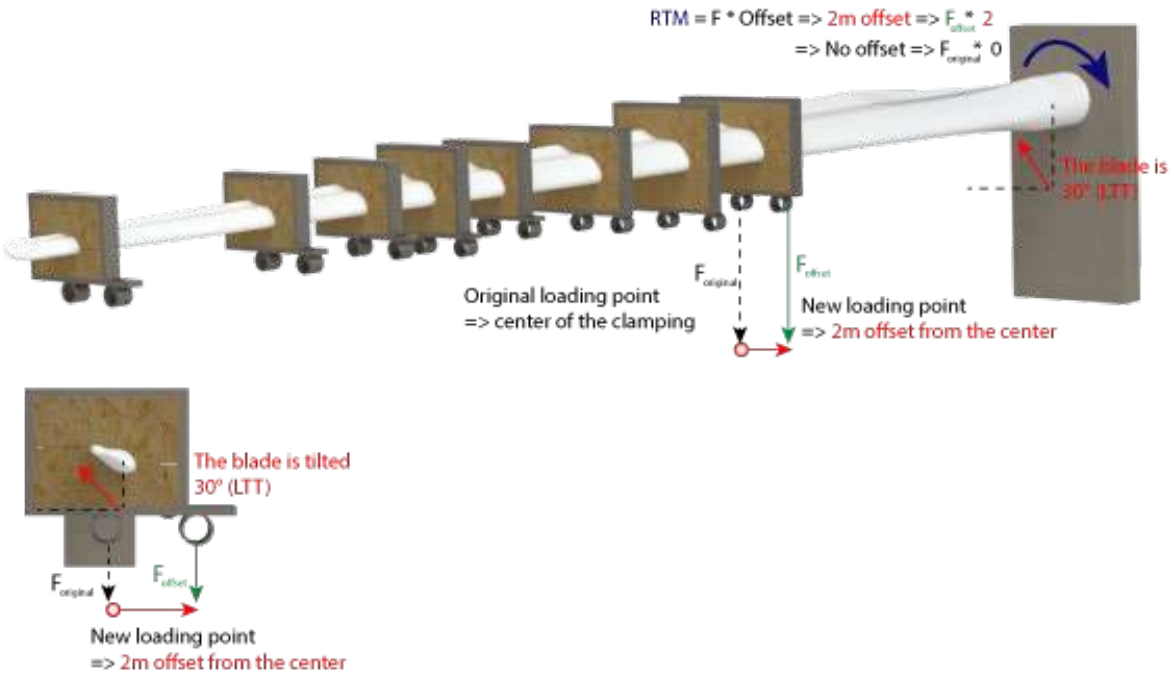

Figure 28: Recommended large scale static test setup. By having the blade tilted with 30° (LTT) when mounted on the rig, and the loading point is offset with a given distance, a certain root torsional moment (RTM) is applied.

If the combination of loads were applied, with an offset (estimated offset of around 2 meters for a large 120m blade as shown in figure above), the local deformations and distortion effects (CSSD and breathing) will be representative. To incorporate the combined flap- and edgewise loads, the blade is also recommended to be tilted (30 degrees for this case) in the direction of the leading edge toward trailing edge during the full-scale test.

The proposed full-scale test is considered to be fast, with a low cost, and easy to implement. Timewise it can be done before the certification fatigue test program is initiated helping to validate FEM models which at the same time are used to establish the boundary conditions for the following sub-component fatigue programs.

Summing up, a full-scale test including torsional loads during the testing phase adds a high value from a structural perspective and it is therefore highly recommended.

Additional measurements

At the time that the full-scale test with applied torsional loads is being carried out, additional valuable information can be extracted if specific measurements are performed.

As an example, during the current CORTIR Phase II, shear-web disbonding has been identified as a critical failure mode that increases the probability of failure on large

Bladena
Banestrøget 13, 1
DK-2630 Taastrup

offshore blades. Shear-web disbonding, in some areas like the aft-shear web fish mouth in the transition zone, is related to both breathing of the panels and cross-sectional shear distortion.

Therefore, understanding in detail the relationship between breathing, CSSD and the failure mode shear-web disbanding is key in order to:

- Gather relevant information to understand the root cause of shear-web disbonding.

- During the operational phase, prevent the damage formation by setting an alarm system that indicates when both breathing and CSSD exceed specific values that have previously been linked to the formation/initiation/propagation of shear-web disbonding.

- Validate FEM models: 3D-FEM models are a valuable source of information when it comes to variables such as peeling stresses or bending strains. FEM models can be calibrated with real field/test data that confirms that the numerical result from the FEM analytical analysis matches with the real operational/testing values.

All the previous could be obtained if additional measurements were implemented during a full-scale testing campaign. Specific areas or hotspots, prone to develop specific failure modes, could be addressed.

Deformation sensors and back-to-back stain gauges are suggested as potential measurement systems.

Figure 29. Wire potentiometer measuring relative out-of-plane deformation of the pressure side trailing edge panel

Bladena
Banestrøget 13, 1
DK-2630 Taastrup

Scaling of torsional load components

Scaling of wind turbine blades is a key topic in the wind energy industry due to the fast pace at increasing the blade's lengths in the last years. Understanding how some variables are related to the length, might be a relevant matter to highlight possible risk sources in case it is concluded that some specific variables are actually highly sensitive to scaling.

Because of this, Bladena has studied three variables as a function of the blade length: flapwise root bending moment (RBM), edgewise RBM, and torsional root torsional moment (RTM). These three variables are considered to have a significant impact on some failure modes such as the shear-web disbonding analyzed in this project.

Table 3. below shows that the three variables get influenced in an exponential way with blade length, experimenting an increase that oscillates between the power of 2.8 for the flapwise RBM, and the power of 4, for the case of torsional RTM.

Load direction	Exponent
Flapwise RBM	2.8
Edgewise RBM	3.4
Torsional RTM	4.0

Table 3. Exponent increase for as a function of blade length for flapwise RBM, edgewise RBM and torsional RTM.

It can be concluded, that increasing blade size may lead to further energy production, but at the same time, triggers some bending and torsional moments which are highly related to structural damages, increasing the probability of suffering from higher OpEx as a result of the initiation of blade structural damages during operation.

If the wind energy industry aims to continues in the current direction of continuous blade growth, certification and standards should definitely be aware of the possible associated risks, and guarantee a healthy environment where the failure rate does not force to extreme high unexpected OpEx that risks the economic viability of the wind energy sector.

Torsional loads

From Bladena's perspective, with the knowledge which has been established in the last 6-8 years e.g., together with DTU, torsional loads are of key importance, especially in large (60m+) blades. The torsional loads are occurring on a blade from two components during operation. As the blade is rotating and is exposed to flapwise and edgewise loads, it is deflecting in both directions. If each of these deflections

Bladena
Banestrøget 13, 1
DK-2630 Taastrup

are investigated independently, the two components leading to torsional loads can be easily explained.

On long (60m+) blades, the torsional loads are the main component for localized deformations, e.g., leading to increased peeling stresses and interlaminar stresses. Considering that the torsional loads are not sufficiently addressed in the design and testing, they are linked to a number of potential failure modes such as aft shear web disbonding in the root-transition zone.

Figure 15 presents a list of potential failure modes and the impact of torsional loads on them. Failure modes which are dependent on panel deformation (e.g., breathing and CSSD) are heavily impacted by the inclusion of torsional loads, whereas damages in the root (T-bolts, root inserts) are not impacted.

Failure Mode	IEC 61400-5:2020	IEC 61400-23:2014	DNV-ST-0376:2021	Used in industry	Uncertainty of tools	Impact of torsional loads
Bondlines (Peeling test)	(2)	(1)	(3)	(YES)	MEDIUM	HIGH
Skin debonding from core (Test)	(2)	(1)	(3)	(NO)	MEDIUM	HIGH
Interlaminar failure (Bending test)	(2)	(1)	(2)	(NO)	LOW	HIGH
Global strain (failure criteria)	(5)	(5)	(5)	YES	LOW	LOW
Shear web disbonding	(2)	(1)	(3)	(YES)	MEDIUM	HIGH
Root failures	(5)	(5)	(5)	YES	LOW	NO

Figure 30: Updated table from CORTIR-Handbook p. 46 (1 means there is no reference in the standard and 5 means it is required in standards). The table has been "adjusted", so it does not take vibration issues into account. An additional column with the impact of torsional loads has been included.

The correct application of torsional loads during full-scale test would significantly mitigate operational risk of severe failure modes during the lifetime of the blade. In order to achieve that testing under torsional loading must be included in the requirements specified within the wind turbine rotor blade testing standards.

The impact of torsional loads has been studied in detail in a separate paper done by Bladena, AAU, DTU, and Shell (see ref. [1.]). Some of the main results from this paper are presented in this final report to strengthen the argument that it is highly recommended that certifications and current standards consider torsion as one of the main drivers of some of the latest and more and more common structural damages on blades.

Bladena
Banestrøget 13, 1
DK-2630 Taastrup

Taastrup, June 28, 2023

Extra tip torsional loads due to tip deflection:

The current design basis considers the loads associated with displacements in the edgewise and flapwise independently and not their combined three-dimensional effect equivalent to what is found under actual operating conditions.

This simplification implies a significant underestimation of the actual movements of the blades and thus of the forces/stresses that the blades are exposed to in real life.

A large offshore blade with a blade size of 120m has been investigated in Bladena 3D non-linear FEM models. An analysis of the global tip deflection has been established, comparing the deflection of a scenario with only edgewise loads versus another one in which operational field loads are simulated, meaning the combined loading with both flapwise and edgewise loads. The flapwise loads are a result of the aerodynamic impact of the incoming wind flow, and the edgewise loads come after the torque and gravity effect.

Results are shown in Table 4, below.

120m wind turbine blade	Edge tip deflection [m]
Only edge TTL	6.6
Operational loads	9.2

Table 4: Edgewise deflection for both operational loads, and only edge load component. 120m wind turbine blade.

Regarding the edgewise direction, blades are significantly stiffer, but the deflection values increase from 6.6m to 9.2m when actual operating conditions are added. The increased edgewise deflections are equivalent to a loss of stiffness compared to the design basis; an effect that will not only influence the tip deflection, but also the stresses in the max chord area and in the transition zone.

Impact of torsion on shear-web disbonding

Shear-web disbonding is the main failure mode studied in the current project. It is a more and more common failure mode characterized by disbands in the aft shear web bondlines. Special attention has been aimed at blades which have an aft shear web with a fishmouth shape, as well as traces of delamination in the area of the fishmouth foot.

Consequently, peeling stresses is the main parameter to focus on in the 3D-solid FEM analysis in order to understand the possible initiation of this failure mode.

A comparative analysis has been established between a 80m blade and a 120m. In addition, operational loads have been studied against pure or only edgewise loads, as imposed by the current standards. By implementing this analysis, it is possible to get an idea of the:

Bladena
Banestrøget 13, 1
DK-2630 Taastrup

- Impact of blade size on the peeling stresses in the transition zone bondlines close to the aft shear web
- Impact of the torsional loads (combined loading scenario considering both flap and edgewise loads) on the peeling stresses in the transition zone bondlines close to the aft shear web

Results can be seen in Table 4 below:

Blade	Peeling stresses. Operational 90-degree azimuthal position [MPa]	Peeling stresses acc. to current standards [MPa]	Increase due to torsional loads
80m	1.4	1	+40%
120m	1.6	1.3	+23%
Comparison	+14%	+30%	

Table 5. Comparative table for shear web disbonding. Max values of peeling stresses.

Results show that peeling stresses increases with both blade size and addition of operational loads in percentages that oscillate between 14% and 40%. For a detailed analysis see ref. [1.].

The experimental analysis on the second blade section of a 34m blade also verified the impacts of torsional loads on the aft shear web bondlines. By applying 50% higher torsional load components than a 1.5MW turbine would meet in field, significant crack propagation was observed on the aft shear web bondlines both on Pressure Side (200mm growth) and Suction Side (100mm growth). The test setup and results in details are described in this report within the "Shear web disbonding investigation" in section in Theme B (pg.34-38).

Validation loop process – Design Process

This Optimal Design and Validation Process for Large Blades is in Bladena`s opinion to ensure reliable blade design. Following the process step by step, adding the realistic operational loads, testing critical joints, and using measurements to validate the process will lower the risk of critical damages in the field. Estimated associated cost of the different steps is also presented in the illustrated validation process, see on Figure 23.

This will be able to provide information that can assist with the decision-making on critical areas such as operational loads, repair strategy, etc. It, therefore, has the

Bladena
Banestrøget 13, 1
DK-2630 Taastrup

Taastrup, June 28, 2023

potential to be used as a prognostic health management system, which will change the maintenance strategies from fixed schedules and intervals towards predictive maintenance.

The validation loop for the design phase of the blade focusing on optimizing the design process with a strong emphasis on recommending the use of correct testing methods. In Theme B of this project a testing pyramid (see on Figure 11), an adaptation of the Building Block Approach from the aircraft industry is also reflected in the validation loop. By following the presented approach the risk of insufficiently tested blades being installed in-field would be significantly decreased. The test results along with the calibrated FEM numerical models can give an accurate presentation of the blade's behaviour in realistic, operational conditions which supports the lifetime prediction of the blade.

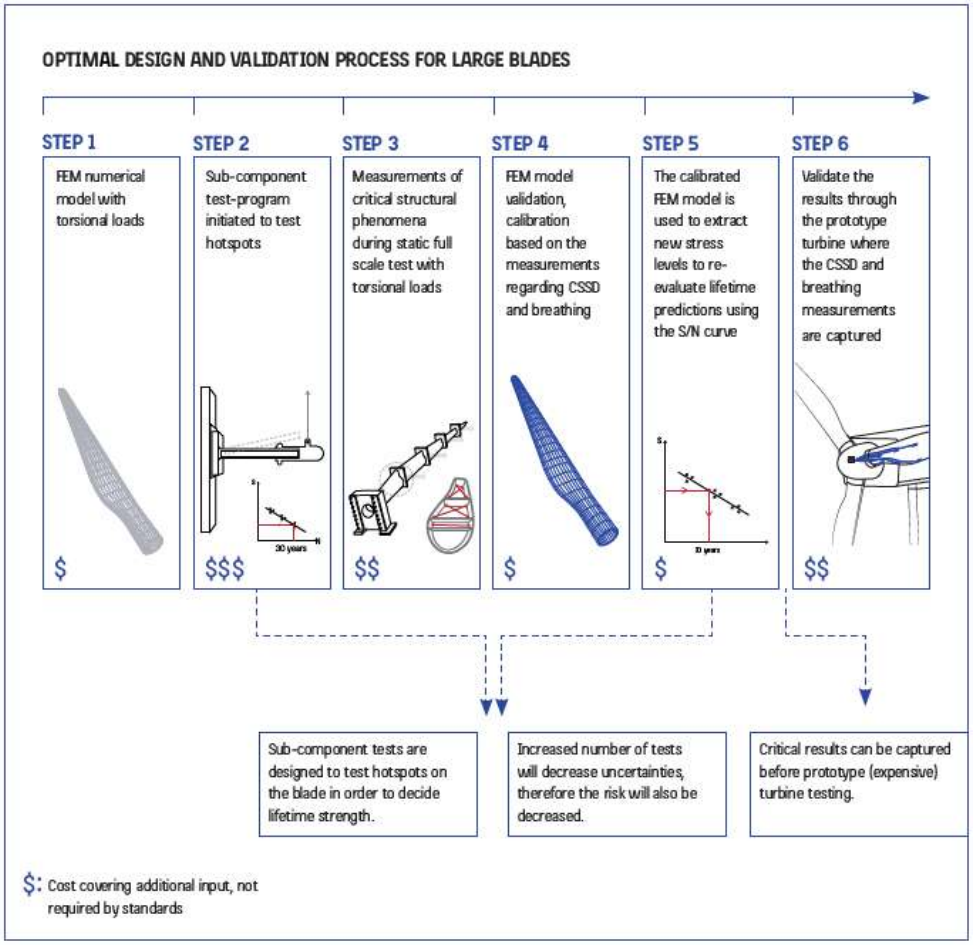

Figure 31: Validation process before commissioning of the blade developed by Bladena.

Bladena
Banestrøget 13, 1
DK-2630 Taastrup

Validation loop process – Blades in Operation

Once the blade is installed in-field on a turbine, most of the steps from the previously discussed validation loop become irrelevant. After commissioning, sub-component and large component level tests are irrelevant as most likely the tested specimens would not represent operational conditions. In many cases, even after installing the turbine the owners or asset managers still do not have access to geometrical data or layup data of the blade in operation. Using historical data, and details made available by the OEM, combined with the right measurement campaign gives the possibility of establishing a reliable FEM numerical model of the blade, for instance, bending strains could be related with actual damage growth, and test or field out-of-plane deformations or CSSD.

FEM cannot predict damage failure but based on the accurately calibrated numerical model a more efficient, optimal, risk-based maintenance strategy can be created which helps in condition maintenance which results in decrease of risk and that can directly impact the lifetime of the blade.

Commercial results

Commercial results for the RTZ Solution™

The commercial objective for the patented RTZ Solution™ was to reach TRL 7 (Technology Readiness Level) from TRL 4 by the end of the project. By developing a final concept and its positive effects validated on a large-scale test, the solution can be assessed as it reached TRL 7. As it was presented in an above section the RTZ Solution™ successfully demonstrated its function in a simulated operational environment. As a result of the project the solution is part of Bladena's product portfolio with a specified installation manual ready to be introduced in the market or to be installed on a turbine in operation.

Commercial results for NIFIS

As a direct consequence of the development of NIFIS guidelines Bladena and Mistras-Sensoria has started a commercial collaboration. SENSORIA acoustic emission system by Mistras-Sensoria can detect, to some degree, damages progressing under working condition for the blade. They are experts to recognize specific sounds and patterns indication certain types of damages. Together with Bladena's unique knowledge of blade hotspots and Bladena's damage categorization scheme, Bladena and Mistras-Sensoria can work on a monitoring setup that finds critical blade failures.

Bladena
Banestrøget 13, 1
DK-2630 Taastrup

Structural Blade Course for ISPs

During the period of the CORTIR II project, Bladena has developed its blade course to be more relevant for also ISPs to attend. The modules of the course are designed and streamlined in a way that the participants get a better understanding of wind turbine blades from a structural perspective. The findings of CORTIR II are significant part of the course along with the knowledge Bladena has acquired during the last 12 years.

Target groups

WTOs

The WTOs are dealing with the high costs of O&M on a daily basis and the feedback is that WTOs suffer from structural damages on blades which have a direct impact on the cost for repairs and loss of production due to downtime. By increasing the knowledge and awareness on shear web disbonding, supporting the development of the RTZ-Solution, giving input to the CAR Tool, and allowing the creation of the NIFIS guidelines, they are leading their way into a more reliable and efficient maintenance strategy with its corresponding reduction of O&M OpEx costs.

The RTZ Solution must be installed in blades to work as a permanent repair. For that reason, the WTOs are target users. The WTO carries a lot of risk on their blade, especially for blades after End of Warranty (EoW). As the RTZ Solution prevents the aft shear web failure mode, it makes sense to use the RTZ Solution to minimize the risk and extend the lifetime significantly.

ISPs

The ISPs are the next target. The ISPs offer their services of inspection and repair to the WTOs. After having participated in this project, ISPs has been educated in a broader understanding of blade issues and root curses. They now possess more knowledge and can give the WTOs a more risk-based plan for their blade maintenance and repair solutions.

ISPs can improve their position in the wind energy industry by gaining independency from OEMs and taking decisions with a long-term perspective based not only on the cost, but mainly on the value that they provide.

In this sense, the NIFIS guidelines and structural awareness created in this project can be perceived as an opportunity for ISPs to collaborate in creating valuable knowledge which will aim to educate themselves in maintenance strategies, inspection and repair procedures, and possible solutions to some specific damages

Bladena
Banestrøget 13, 1
DK-2630 Taastrup

like the shear-web disbonding. In addition, it will get them in close contact with their WTOs customers.

As a result of all this, the collection of knowledge will be considered as a success from the moment that it will allow them to perform according to their own educated decisions resulting in a more competitive position in the market. This project can initiate this transformation towards real independent ISPs.

OEMs

OEMs continuously wish to produce larger blades with a minimum cost (CAPEX). The increasing loads (e.g. in the shear web bondlines) will occur more frequently when blades get larger. By installing RTZ Solution™ in new blades or incorporating the Bladena product in the initial blade design, this failure mode can be removed.

In a market where WTOs are becoming more aware of blades failing which might have been prevented, more pressure has been imposed to the OEMs to address the critical failures. Therefore, OEMs should choose to upgrade their blade design and offer their customers a better and more reliable product. If the RTZ Solution™ is inserted as a part of the initial blade design, the OEMs will be able to find a business case in cost-out, where less material in the blade panels at root-transition zone panels are necessary. With more reliable blades than their competitors this will also be an advantage.

A way into the OEMs "headlight" will be for Bladena to have a close commercial collaboration with selected ISPs which already have OEMs as clients.

Dissemination of project results

As for all previous EUDP funded projects headed by Bladena, dissemination of project results, education on fundamental principles and shared knowledge between, and specifically to, partners have been top prioritized. To make the knowledge and results gathered in throughout this project reach as many interested parties as possible Bladena has taken care to communicate in different levels and with many different methods, see Table 5.

Level 1: Easy overview of blade knowledge	The Blade Handbook
Level 2: Understanding main concepts	Movies and Posters + Virtual reality
Level 3: Diving into the "How" and the work done	Short papers
Level 4: Theoretic explanations of complex topics	Extended papers

Table 6: The project dissemination plan communicates on four levels; from very easy and fast accessible to a high level of academic complexity.

Bladena
Banestrøget 13, 1
DK-2630 Taastrup

In this way of dividing communication into four defined levels it should be easy for each partner to both have an overview of all main concepts treated in the last two years and the opportunity to dive deeper into specific topics of interest and to gain from the expert knowledge and conclusions formulated during this project.

Meetings, Workshops and Seminars + an International Conference

During the project the time current results and project status have been presented to and discussed by all partners at meetings and seminars. To ensure progress founded in expert knowledge from relevant partners several technical workshops have been executed. A broader discussion across WTO, ISP, OEM and insurance companies have been possible during the bigger meetings, seminars and the international conference hosted by the project, see Table 7.

Date	Meeting / Seminar / Workshop
22-23 September 2021	**Kick-off meeting**
9 December 2021	NIFIS Workshop
21 December 2022	Technical workshop • FEM approach and Impact of torsion on large blades • Measurements and testing of wind turbine blades
17 January 2022	Damage mechanics in operation
21 January 2022	Composite material and failures
11-12 May 2022	NIFIS, Seminar and Workshops
19 May 2022	Fracture Mechanic, Uncertainty, Standards Workshop
14 July 2022	Risk Mitigation Workshop
31 August 2022	Loads and Stress, Workshop
21 September 2022	**Midterm seminar**
22 September 2022	International conference - WTG blade risk mitigation & monitoring
28-29 June 2023	**Final seminar**

Table 7: Seminars, workshops, and main meetings.

Bladena
Banestrøget 13, 1
DK-2630 Taastrup

Taastrup, June 28, 2023

International conference

The international conference gathered WTOs, OEMs and ISPs and was one of the commercial milestones in this project. 37 companies (14 WTOs) attended the event to discuss risk, risk mitigation and monitoring of wind turbine blades. Representatives from Bladena and the universities AAU, DTU Construct and DTU Wind presented amongst other topics the "Next step Roadmap for Risk Mitigation".

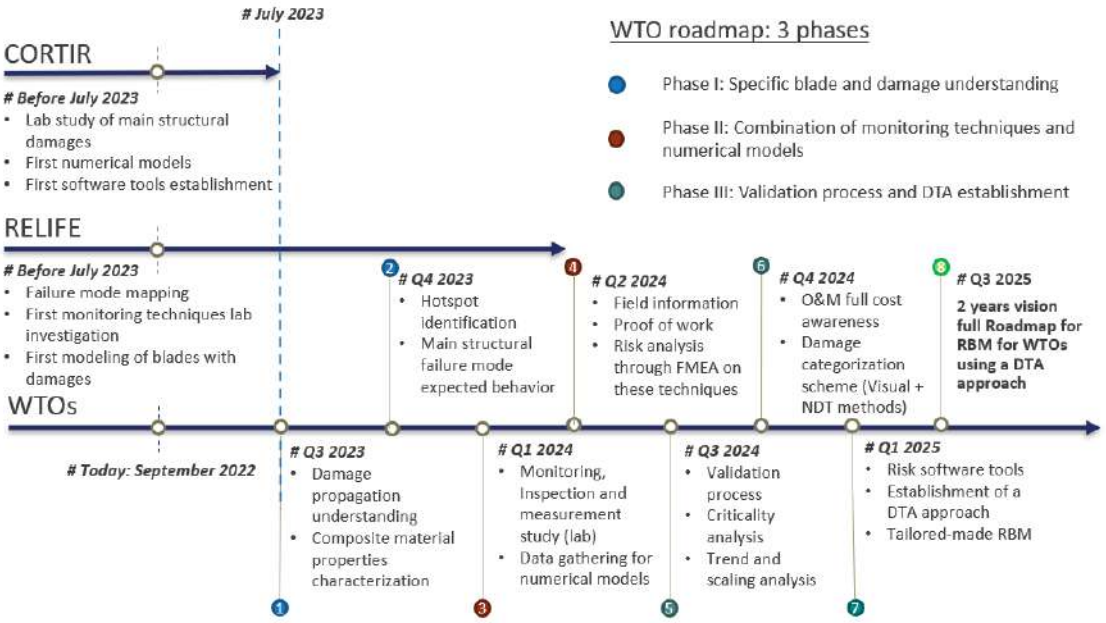

Figure 32: Roadmap: Risk mitigation for assets.

The above illustrated WTO-centric roadmap was presented with a timeline for the implementation of risk-based maintenance with a damage-tolerance approach. In Figure 12, the roadmap can be seen and provides an overview of what steps must be taken, to fast forward the use of the knowledge available, into the decision-making when prioritizing how to spend the OPEX budget in a data driven manner. Combining monitoring data, with validated FEM models reducing uncertainty and thus risk in the O&M of the fleet of blades installed. This roadmap was received positively by the audience and agreed that the steps are necessary for effective risk mitigation.

One way of mitigating risk is the use of "state-of-the-art" monitoring techniques. A guest speaker from Sensoria™ by MISTRAS Group elaborated on monitoring critical failure modes while representatives from Shell, SR Energy and Ørsted attended a panel discussion on risk-based maintenance and the impact of monitoring.

Bladena
Banestrøget 13, 1
DK-2630 Taastrup

Taastrup, June 28, 2023

Figure 33: Group photo of the attends of the International Conference, 22nd of September 2022

In September, DTU Wind is hosting a symposium during which Find Mølholt Jensen will present, as a keynote speaker, the relevant findings of the CORTIR II project regarding the impact of torsional loads on large wind turbine blades, ref. [1.]. The presented paper is accessible as Appendix A of this final report. During the same symposium Christian Berggreen, Jacob Paamand Waldbjørn and Arturo Gomez from DTU Construct and John Dalsgaard Sørensen, and Jannie Sønderkær Nielsen from AAU will also present their CORTIR II framework findings ref. [2.,3.,4.,5.], these presented papers can be found in Appendix B, C, D, E.

Newsletters

Every quarter Bladena publish a newsletter with the current development in the project described in text, figures, and photos. Each theme A, B and C presents its findings and makes it easy for partners to follow their specific topic of interest with a minimum of time invested.

LinkedIn and press releases

After each event Bladena publish a press release with a description of the activities at the meeting/seminar and acknowledging the EUDP fund. These press releases were shared on Bladena's own LinkedIn page as well as published on Bladena's website. The press releases can be obtained from www.bladena.com.

Bladena
Banestrøget 13, 1
DK-2630 Taastrup

Taastrup, June 28, 2023

The EUDP Blade Handbook

The first version of the EUDP Blade Handbook was published in 2017 as a part of the EUDP LEX project. Even then the book received very positive feedback as the Blade Handbook was the first (and still only) of its kind and much needed in the wind industry to further blade education, understanding and communication between different companies and positions in the wind industry. Since the first version of the Blade Handbook, Bladena, Kirt x Thomsen and partners have continued to improve and add to the book. The Blade Handbook experiences an immense success across the whole value chain because of its short and precise explanations coupled with excellent illustration of different blade topics.

Figure 34: Blade Handbook cover and its rewarded awards.

During this project, the Blade Handbook was heavily updated with new chapters, complementing the existing content, covering more aspects relevant to the wind industry. Firstly, a new chapter in monitoring and measurements presents how these technologies can be used for risk mitigation purposes. Furthermore, leading edge erosion and lightning are illustrated, along with their respective protection systems. Additionally, a new chapter on risk and its implementation on operation and maintenance strategies is presented. Finally, a new chapter on digital twin shows how structural knowledge can optimize such technologies.

Bladena
Banestrøget 13, 1
DK-2630 Taastrup

The EUDP Blade Handbook in pdf format can be acquired from Bladena's webpage:

https://www.bladena.com/all-downloads.html

Or hard copies of the Blade Handbook can be obtained by contacting Bladena:

info@bladena.com

Professional high-quality Movies, posters and Virtual reality

Having Kirt x Thomsen as a partner for professional visual communication as part of the CORTIR 2 team has greatly added to the cohesion of the project and the many partners form different wind backgrounds. A high priority has been given to general communication and education of project results and knowledge giving the premises for the project.

During the project several movies has been made in a collaboration between Bladena and Kirt x Thomsen:

- Torsion movie: Explaining the impact of torsional loads on the blades.

The torsion movie is an excellent example of technical knowledge communicated in a way that can resonate with everybody. As such, the movie become an argument for the ground premiss of the project: Torsional forces in large blades creates out-of-plane deformation in the root-transition area and brings the need for the permanent repair solution, the RTZ Solution™.

The movies developed in this project can be seen here:

The torsion movie will be uploaded to Bladena's webpage soon.

Another way of communicating knowledge between partners and indeed to all in the industry, has been through the development of XX posters:

- Torsion on blades poster 1.
- Torsion on blades poster 2.
- Cost and Risk Tool poster
- Shear web disbonding and new innovative solution poster
- New Innovative Field Strategies

The poster collection can be downloaded here:

https://www.bladena.com/uploads/8/7/3/7/87379536/poster_collection_formatted.pdf

Bladena
Banestrøget 13, 1
DK-2630 Taastrup

Taastrup, June 28, 2023

An advantage of being part of an EUDP project is that it gives the partners room to investigate and try out something new. In this project KirtxThomsen has developed 3D models in different sizes from 35m, 70m and 125m. The blades could be experienced at the International Conference, September 2022, though virtual reality.

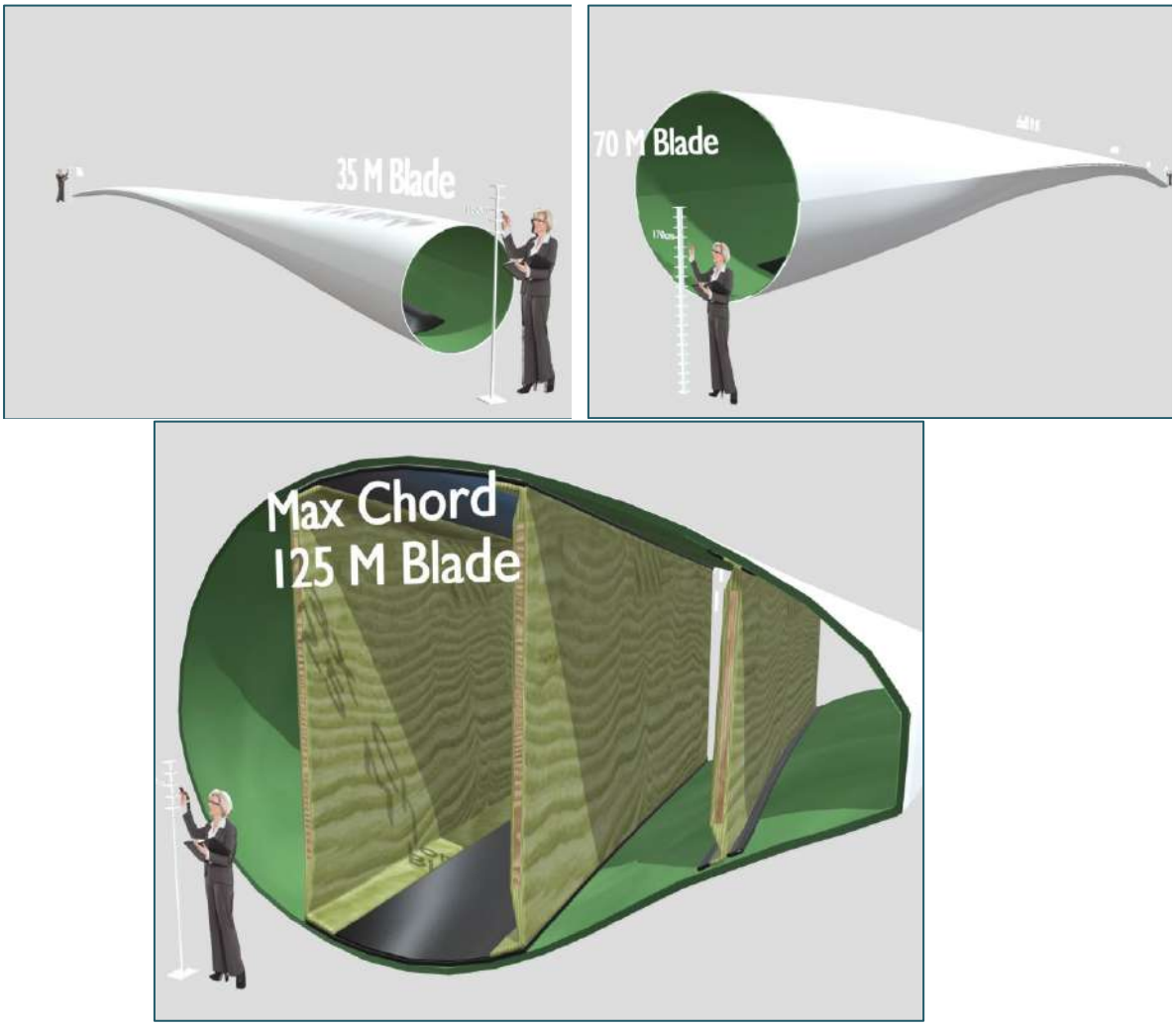

Figure 35: Scaling of blades presented in Virtual Reality. In the VR setup the user can compare the average human size to the size of different wind turbine blades.

This gave people the opportunity to get up close and personal with a large blade and experience there through size, when compared to our own small human self. The event drew much curiosity and positive feedback.

Short Papers and Extended papers published on important topics

Regarding the CORTIR II project 7 papers have been made, 4 of papers (1.-4.) which are going to be published as journal papers after being presented at the DTU Wind symposium in September 2023. These 4 papers are in the review phase, so minor

Bladena
Banestrøget 13, 1
DK-2630 Taastrup

changes can be made on them until the official journal paper release. The list of the published papers is the following:

1. Jensen F.M., Arconada J.O., Werk M., Berggreen C., Sørensen J.D., Zhong G., Haans W., (2023),"Torsional impact on wind turbine blades and impact on field damages", *Bladena, DTU, AAU, and Shell;* see in Appendix A. This paper has been submitted to the Material Symposium held by DTU Wind in Risø. The paper will be presented as an invited keynote speaker during the symposium.

2. Gomez A., Berggreen C., (2023),"Cohesive Zone Modelling to predict crack growth under fatigue loading", *DTU Department of Civil and Mechanical Engineering;* see in Appendix B. This paper has been submitted to the Material Symposium held by DTU Wind in Risø.

3. Waldbjørn J.P., Berggreen C., Ahmed S., Nagy T., (2023),"Large-scale fatigue testing of a retrofitted 3rd shear web in a SSP34M wind turbine blade", *DTU and Bladena;* see in Appendix C. This paper has been submitted to the Material Symposium held by DTU Wind in Risø.

4. Waldbjørn J.P., Berggreen C., Jensen F.M., Ley O., (2023)," Large-scale fatigue testing of a wind turbine root end section", *DTU Department of Civil and Mechanical Engineering, Bladena, Mistras* see abstract in Appendix D. This paper will be published later in 2023.

5. Nielsen J.S., Sørensen J.D., (2023),"Optimization of novel heuristic strategies for inspection and maintenance", *AAU Department of The Built Environment;* see in Appendix E. The approach described in this journal paper was presented at the Wind Energy Science Conference, Glasgow May 2023 - Utilizing digitalization through heuristic risk-based blade maintenance for leading edge erosion.

6. Sørensen J.D., Abeendarnath A., Nielsen J.S., Gomez A., (2023), "Stochastic modelling of wind turbine blade tests for reliability analysis and O&M planning", *AAU Department of The Built Environment and DTU Department of Civil and Mechanical Engineering;* see the draft version in Appendix F.

7. Bladena, (2022), "Structural weaknesses of blades in operation", *Bladena whitepaper*. The whitepaper is available under the following link: https://www.bladena.com/uploads/8/7/3/7/87379536/whitepaper_1_structural_understanding_bladena_13.04.2022_compressed.pdf

8. Bladena, (2022), "Risk considerations on upscaling wind turbine blades", *Bladena whitepaper*. The whitepaper is available under the following link: https://www.bladena.com/uploads/8/7/3/7/87379536/white_paper_scaling_and_risk_bladena.pdf

Bladena
Banestrøget 13, 1
DK-2630 Taastrup

Taastrup, June 28, 2023

The WTO Blade Network

The WTO Blade Network is a growing group of WTOs who are meeting and discussion shared topics of relevance. Bladena was asked in 2014 to be the coordinator of the topic "Structural blade design and testing" and has since invited WTOs to many seminars on the subject. The CORTIR Project offers an opportunity to keep creating relevant seminars and gathering WTOs for discussions and knowledge sharing.

The WTO Blade Group Network has received several new members during the time span of the CORTIR Project.

Now we have officially reached 55 all registered on the member list at www.wto-network.com with company description and logo. Inquiries regarding joining the network occur often and a few companies have indicated their intention to be part of it but yet to deliver information to share on the webpage.

During the CORTIR Phase 2 project the WTO Blade Network showed great interest in the organized conferences and seminars. The turn out on these events were higher than expected allowing us to discuss the relevant topics with a wide range of wind turbine owners.

Utilization of project results

For the future utilization of commercial results, the RTZ Solution™ will be on the market and accessible as a permanent repair solution for failure modes in the blade's transition zone.

To strengthen the commercial incentive to choose the RTZ Solution™ as a damage preventive maintenance option, the NIFIS guidelines and the CAR Tool both provides arguments creating a business case for the RTZ Solution™.

The technical results of the project are used to build understanding and argumentation for the input to NIFIS.

Turnover….. Private investors… Additional employees…

Bladena has gained a closer collaboration with the partner ISPs during this project getting insight into their business, but also having the possibility to work with a business model with advantages to both ISPs and Bladena. A structural blade course was developed specifically focusing on the needs of ISPs. Several ISPs from all over the world showed interest in participating one of the courses and many of them

Bladena
Banestrøget 13, 1
DK-2630 Taastrup

decided to join, three structural courses were held during the span of this CORTIR project (November 2022, January 2023, March 2023) meeting the demands of ISPs.

Another very positive outcome has been the relationship and collaboration with Mistras-Sensoria. The unique and very advanced method of monitoring goes hand in hand with Bladenas wish to create a better knowledge foundation of the actual structural failures in wind turbine blades under operation.

The development of a permanent solution addressing aft shear web disbond also raised interest within the industry. Several WTOs are interested in the test results of the solution and considering installing it on their own fleet.

Competition

For Bladena's patented structural enhancement products (the RTZ Solution™), currently, the competition should not be seen as other products directly competing with the developed solutions. Competition is considered repairs in the aftermarket, or the worst-case scenario replacement of the blades when they fail. However, repair should be considered carefully, as the industry has adopted new methods and improved the possibilities of repairs quite significantly in the latest years. Most of the ISPs offer prefabricated service deals at different levels depending on the customer's needs, but there is an urgent need for the WTOs to be self-serving as their WTG fleets growth.

There is no competitive retrofit solution for the shear web disbond failure mode in the root-transition zone of large turbines. The repair solutions offered has to be repeated and often do not show to be sufficiently strong, whereas the RTZ-Solution are designed to last for 20-25 years on large blades. The competition is based on the OEM design criteria and expectations to their known patch solutions or the industry's standard by continuing to repair reoccurring damages. In only seldom cases the root causes are removed, as the RTZ Solution™ will do.

As mentioned above, repairs are the current way to deal with the blade damages. Since shear web disbond can lead to the critical failure mode of cracks in the trailing edge root-transition zone and eventually blade collapses. Field experience have shown that repairs in this zone does not last if the root is not removed.

Thus, one possible solution for OEMs would be to remove the root cause through improved design of new blades of the root-transition zone on large blades. They could refrain from having shear webs end in the region. Contrarily, they could also implement Bladena*s RTZ Solution™.

Bladena
Banestrøget 13, 1
DK-2630 Taastrup

Taastrup, June 28, 2023

Sales barriers / Market barriers

The Wind industry is still a young industry and the knowledge about the importance of the torsional loads are still not sufficiently acknowledged. The wind industry players are used to recognizing a problem in the same way and applying the same solutions as last year. But the industry faces strong competition from other green energy providers and to increase AEP and reduce LCoE a new way of thinking must be nurtured in the industry. The gained focus on non-fossil fuels within Power-to-X technologies emphasizes the importance of the wind industry to be cost efficient and reliable.

Bladena's patented innovative structural RTZ Solution™ is still not chosen as a solution, perhaps because the industry is not well-aware of it yet. In order to fully understand the benefits of the RTZ Solution™, sufficiently high level of structural knowledge is required, e.g. impact of torsional loads. To mitigate this, Bladena is continuously trying to heighten the shared discussion and understanding level in the industry. During EUDP projects Bladena has come a long way to move project partners in how they look at and understand the structural issues of blades more in-depth. The tools applied has been focused on superb communication and a solid knowledge sharing flow coupled with blade courses and seminars held by Bladena to lift the knowledge level for the participants. An example is the Blade Handbook™, which manages to communicate essential and complicated blade knowledge in a simple way. In this project, an updated version have been published and shared globally to the entire value chain.

To introduce Bladenas new innovative RTZ Solution™ to the damages in the root-transition zone, the industry must be guided, where they are willing to see the advantages of using a new solution to a known and sadly recurring problem. To achieve this, the RTZ Solution™ will be backed up by appropriate documentation and results. To ensure costumers about the validity of product specification and capacity, the test program carried out during and after the development phase must live up to all relevant market standards and regulations.

Just as important is the overall communication and mutual understanding in the industry. It might also be necessary to shake the old structures of dependencies within industry players. It is the aim that both WTOs and OEMs should consider their alternatives when it comes to business models and inspection, repair and maintenance strategies. The ISPs will then be able to offer a broader spectrum of blade services and solutions, coupled with knowledge on blades and future consequences of the choices made. OEMs may have to look outside internal R&D and engineering groups to find solutions beneficial for the OEMs and the full supply chain.

Bladena
Banestrøget 13, 1
DK-2630 Taastrup

Time will be another mitigating effect. As blade lengths increase, the shear web disbond failure mode will happen with a higher frequency and a more severe degree. This will push the need for an innovative solution which does not require the turbines to be stopped for repair every time the failure reappears. WTOs will be more and more likely to the new innovative solution instead of old failed ones.

Project contribution to realizing the energy policy objectives

Stronger blades with longer operational time and less downtime has a higher AEP. For that reason, and since the whole project is within the green continues energy, this project works to give Wind Energy a larger competitive edge in the race to produce the cheapest, and hopefully, greenest power.

1. With better maintenance planning and with more reliable blades, the operational team of the turbines will be more steady securing energy supply.
2. With a more stable supply of wind energy, knowing the cost and risk and how to mitigate the problems, independence from fossil fuels is reduced.
3. With the lower O&M costs and higher uptime, the LCoE will be reduced. This will strengthen the wind energy industry in the competition against fossil fuels and have a positive environmental impact as a consequence.
4. Especially for offshore turbines there is a higher risk bound to blade failures due to the often-challenging environments to operate, inspect and repair in. This will affect the LCoE if risk is not handled correctly and minimized where possible.
5. The developed RTZ-Solution™ will cause more uptime of wind turbines due to reduction of structural repairs and the better planning and service actions on blades which means the annual energy production (AEP) will increase, which is a direct increase in the energy efficiency of wind turbines.
6. With the implementation of suggested test campaigns and the use of the Validation Loop Process can ensure that the blades are tested sufficiently before they are installed in-field and would give a more accurate lifetime prediction for the blades.

Project conclusion and perspective

During the timespan of the CORTIR II project, a huge emphasis was placed on investigating the impact of torsional loads on wind turbine blades. On several levels it has been demonstrated that the appropriately applied torsional load components can lead to critical damages especially on large (60m+) offshore wind turbine blades.

Bladena
Banestrøget 13, 1
DK-2630 Taastrup

By scaling up rapidly in size the torsional loads in operation significantly increase too. This increase may lead to severe damages and blade failures. The project is focused on decreasing the risk of these damages from several perspectives.

In different stages of the blade's lifetime, suggestions were given in CORTIR Phase II with the objective of mitigating the risk of critical failure modes due to torsional loads. In the design phase (before commission), a Validation Process has been developed supported by a test pyramid (Building Block Approach adopted from the aircraft industry) which aims to ensure that the blade has been sufficiently tested under operational conditions and a credible numerical model is created supporting blade lifetime prediction and determining "hotspots" (damage prone areas) on the blade.

This established knowledge, together with the CAR Tool, will help to create a blade specific risk-based maintenance strategy. The accurate prediction of failure modes is not possible yet to our knowledge but by optimizing the maintenance strategy, the occurrence of damages can be minimized, and the planning of inspections/maintenance can be optimized with less downtime as its main direct result.

As the testing campaign executed has demonstrated, operational torsional loads can lead to critical damages. The bi-axial full-scale test resulted in serious damages which can potentially lead to blade collapses. The applied torsional load components resulted in significant out-of-plane deformation of the unsupported panels in the transition zone of the blade which is the root cause of several failure modes such as aft shear web disbonding and delamination of the skin on the blade panels on the first tested blade. Whereas during the test of the second blade where small, 5cm long cracks were introduced to the aft shear web and only after 12000 fatigue test cycles significant crack propagation was observed due to the increasing out-of-plane panel deformations. DTU Construct has successfully built the new test rig which allowed the project to use the test setup with applied torsional load components.

Through FEM numerical models, it was discovered that with operational loads the edgewise deflection increases, as a result of the fact that the large flapwise deflection, makes the blade lose stiffness in the edgewise direction. The softer blades will result in increasing torsional loads which increase e.g., breathing and cross-sectional shear distortion in the max chord and transition zone.

In order to decrease the out-of-plane deformation, the Bladena patented, RTZ Solution™ was developed. By connecting the pressure and suction side, the localized deformation is minimized thereby the root cause of severe failure modes is removed. FEM numerical models and the experimental test setup validated that by connecting the unsupported panels, the out-of-plane deformation can be significantly mitigated.

Bladena
Banestrøget 13, 1
DK-2630 Taastrup

The out-of-plane deformation introduced by the applied torsional load components can be the direct cause of aft-shear web debonding and skin delamination in the blade panel's sandwich structure. These failure modes are severe and can lead to serious repair work or even blade collapses. By installing the RTZ Solution™ the risk of these damages can be minimized which results in a more reliable blade with possibly extended lifetime without necessary unplanned repair campaigns for the transition zone of the blade.

The RTZ Solution™ has been developed with the focus on easy installation without modifying the blade's structural integrity. The installation must be performed inside the blade without drilling into the panels, the mounting of the solution is performed with a certified adhesive. Based on the size of the blade, the number of installed RTZ Solution™ can differ, as larger blades have increased torsional loads acting on them which results in higher out-of-plane deformation.

The next step in the RTZ Solution's development is to install the solution in-field during which it will be demonstrated that the solution works efficiently not only in test environment but also in operation. Within the CORTIR II framework, different monitoring methods for different blade "hotspots" and failure modes were investigated. The installation of monitoring systems can indicate failure modes in time which would significantly support the WTOs and ISPs to act on them accordingly.

In order to achieve a better, common understanding of structural damages a new Damage Categorization Scheme was developed. The new scheme implements the Damage Tolerance Approach and focuses not only the size of the damages but also on their position and how much impact they can have on the blade's structural integrity. Once the damage is found by using the scheme and input from Bladena, in many cases the turbine can be kept in operation, but the use of a suggested monitoring technique is needed to ensure that the damage is stable and not growing.

The implementation of the findings of the project in the wind industry would significantly impact energy production and heavily support the lifetime expectancy of wind turbine blades. The first step of implementing several suggestions of the project will be to acknowledge the impact of torsional loads.

The industry is in a process of maturing and in 2023 the topic is getting more and more relevant, as DNV (standardisation and certification body) already acknowledged the lack of torsional loads during test campaigns in one of their recent whitepapers (ref. [9.]). Therefore, delivering the message of the CORTIR Phase II project will further assist the industry to become more mature by raising awareness of the impact of torsional loads. In Bladena's paper about the impact of torsional loads on large wind turbine blades (ref. [1.]), three suggestions are given for the wind industry to

Bladena
Banestrøget 13, 1
DK-2630 Taastrup

consider about mitigating the risks associated with torsional loads. Some of these suggestions, are also highlighted in section 8.4.

The first suggestion is regarding the full-scale testing of the blade, which recommends using a static test with combined (edgewise, flapwise, torsional) load components applied. The cost of this is low, and the value of it is high, as it can support giving a more accurate lifetime prediction of the blade. The second recommendation is the use of additional measurements during the full-scale test of a blade. This again would have low cost and give a clearer understanding of strains and deformations on the blade under realistic conditions. The third suggestion is the application of torsional loads in non-linear 3D FEM analysis. That would also have low costs but significantly increase the accuracy of the lifetime prediction of the blade.

Taken the findings and suggestions into consideration, a validation process roadmap was developed. The validation process suggests certain steps with the implementation of the testing pyramid (similar to the building block approach from aircraft industry). By following the steps of the loop, lifetime estimations would be more qualified, as a result, among other reasons, of calibrated numerical 3D-FEM models under realistic operational conditions.

A validation roadmap was developed for blades in operation, supporting WTOs to plan an efficient risk-based maintenance strategy.

References

[1.] Jensen F.M., Arconada J.O., Werk M., Berggreen C., Sørensen J.D., Zhong G., Haans W., (2023),"Torsional impact on wind turbine blades and impact on field damages", *Bladena, DTU, AAU, and Shell;* Appendix A

[2.] Sørensen J.D., Nielsen J.S., (2023),"Optimization of novel heuristic strategies for inspection and maintenance", *AAU Department of The Built Environment;* Appendix B

[3.] Gomez A., Berggreen C., (2023),"Cohesive Zone Modelling to predict crack growth under fatigue loading", *DTU Department of Civil and Mechanical Engineering;* Appendix C

[4.] Waldbjørn J.P., Berggreen C., Ahmed S., Nagy T., (2023),"Large-scale fatigue testing of a retrofitted 3rd shear web in a SSP34M wind turbine blade", *DTU and Bladena;* Appendix D

[5.] Berggreen C., (2023),"Large-scale structural testing on a wind turbine blade through single-component hybrid simulation", *DTU Department of Civil and Mechanical Engineering;* Appendix E

Bladena
Banestrøget 13, 1
DK-2630 Taastrup

[6.] Bladena and partners, (2022),"Wind turbine blades - Handbook", *Edition 2022 CORTIR II, EUDP*

[7.] Bladena, (2022),"Structural weaknesses of blades in operation", *Bladena whitepaper;* *https://www.bladena.com/uploads/8/7/3/7/87379536/whitepaper_1_structural_understanding_bladena_13.04.2022_compressed.pdf*

[8.] Bladena, (2022),"Risk considerations on upscaling wind turbine blades", *Bladena whitepaper;* *https://www.bladena.com/uploads/8/7/3/7/87379536/white_paper_scaling_and_risk_bladena.pdf*

[9.] Griffin D.A., (2023),"The challanges of wind turbine blade durability", *DNV whitepaper;* *https://www.dnv.com/Publications/the-challenges-of-wind-turbine-blade-durability-243601*

[10.] Waldbjørn J.P., Buliga A., Berggreen C., Jensen F.M., (2020), "Multi-axial large-scale testing of a 34m wind turbine blade section to evaluate out-of-plane deformations of double-curved trailing edge sandwich panels within the transition zone" *DTU and Bladena journal paper* *https://journals.sagepub.com/doi/abs/10.1177/0309524X20978408*

[11.] International Electrotechnical Commission, (2015), "International Standard: Wind turbines – Part 23: Full-scale structural testing of rotor blades", *IEC 61400-23 Edition 1.0*

[12.] Wood Mackenzie, (2019), "Unplanned wind turbine repairs to cost industry $8 billion+ in 2019", *Wood Mackenzie: One minute read press release* *https://www.woodmac.com/press-releases/unplanned-wind-turbine-repairs-to-cost-industry-$8-billion-in-2019/*

[13.] Richard C., (2023) "Offshore wind turbine arms race accelerating component failures", *GCube* *https://www.windpowermonthly.com/article/1821773/offshore-wind-turbine-arms-race-accelerating-component-failures-%E2%80%93-gcube*

[14.] Jensen, F.M., "Ultimate strength of a large wind turbine blade," Risø DTU, PhD Thesis, 2008. *https://backend.orbit.dtu.dk/ws/portalfiles/portal/5434131/ris-phd-34.pdf*

[15.] Bladena and Partners, (2019), "Project Report: Root Area Transition Zone RATZ and Reduction O&M cost of WT blades, Energy Development and Demonstration Program (EUDP) RATZ project, 64015-0062,",

Bladena
Banestrøget 13, 1
DK-2630 Taastrup

https://www.bladena.com/uploads/8/7/3/7/87379536/eudp_ratz_-_project_final_report_-_eudp_ref._j64015-0602.pdf

[16.] Brøndsted, P., & Nijssen, R. (Eds.) (2023), "Advances in wind turbine blade design and materials." Woodhead Publishing. *Woodhead Publishing Series in Energy No. 47* http://www.woodheadpublishing.com/en/book.aspx?bookID=2548

[17.] Bladena and Partners, (2021), "Cost and risk tool for interim and preventive repair (CORTIR) EUDP project 64018-0507 – Final Report", https://www.bladena.com/uploads/8/7/3/7/87379536/eudp_cortir_-_project_final_report_-_ref._64018-0507.pdf

Appendices

Appendix A Jensen F.M., Arconada J.O., Werk M., Berggreen C., Sørensen., J.D., Zhong G., Haans W., (2023), "Torsional impact on wind turbine blade main operational field damages", Bladena, DTU, AAU and Shell

Torsional Effects on Wind Turbine Blades and Impact on Field Damages

F. M. Jensen[1], J. O. Arconada[1], M. Werk[1], C. Berggreen[2], J. D. Sørensen[3], G. Zhong[4], W. Haans[4]

[1]Bladena, Banestrøget 13, 2630 Taastrup, Denmark.

[2]Technical University of Denmark, Department of Civil and Mechanical Engineering, Koppels Allé, Building 404, 2800 Kgs. Lyngby, Denmark.

[3]AAU, Department of The Built Environment, Thomas Manns Vej 23, 9220 Aalborg, Denmark.

[4]Shell Global Solutions International B.V., 2596 HR Den Haag, Netherlands.

05th of July

Email: fmj@bladena.com

Abstract.
The purpose of this paper is to present the importance of torsional loads when understanding the significant increase in structural damages on large wind turbine blades. By comparing the stress state of two blades of different length, it is shown that torsional loads grow with an exponent of four (4). Thereby, a function of the length of the blades leading to a new range of challenges that are not met by the current process for design, testing and certification.

The paper presents the study of these new challenges in detail, based upon:
- An experimental perspective, with results from large-scale cyclic loading tests on two blade cut-outs conducted under controlled laboratory conditions in. Both blades were tested to failure.
- A numerical perspective, non-linear geometrical 3D FEM simulations has been performed to study the impact of torsional loads on relevant current structural failure modes on large wind turbine blades.

The conclusion is that the larger torsional loads may explain shear-web disbond, as well as sandwich skin debonding in both the transition zone and in the max chord area of wind turbine blades. In view of the findings, the paper includes proposals for remedies that are expected to mitigate some of the significant failures currently seen in the field.

Abbreviations

Leading edge	LE
Trailing edge	TE
Pressure side	PS
Suction side	SS
Cross-Sectional Shear Distortion	CSSD
Root torsional moment	RTM
Root bending moment	RBM
Number of cycles to failure for given cyclic stress of specific material	S-N curves
Trailing edge Towards Leading edge	TTL

Table 8. List of abbreviations

Introduction

Background

Publications in recent years have highlighted an increase in structural blade failures (ref.[2.], [5.], [11.]), a fact that has been recognized not only by wind turbine owners, but also by manufacturers and certification bodies (ref.[2.]).

Published articles, see ref. [1.-14.], report reoccurring blade issues on several platforms with large blades on 5MW to 8MW turbines. In some of the reported blade collapses, the operators have shown concern that the critical damage is not a one-off event (ref.[5.]).. Therefore studies have been conducted of whole fleets such as in 2021 at a Norwegian wind farm, see ref.[2] and in 2020 at a wind farm in the USA, see ref.[3]. Furthermore, DNV has recently published a whitepaper acknowledging the relevance of the topic, see ref.[2].

The trend that structural related failures occur early at the large blade's lifetime, suggests that the methodologies used in the development and testing phase of blades need improvements, see ref.[4]. In some instances when similar blade failure happens on the same platform on different wind farms, it can be a clear sign of insufficient testing of the specific blade type, see ref.[5].

The importance of torsional loading is becoming an increasingly significant topic, as found in the studies performed for different blade sizes and presented in this paper. These studies have clearly demonstrated that increasing the length of the blades only adds to the severity of the challenges.

A comprehensive analysis of the importance of the torsional loads for large blades is presented in this paper. According to the current testing standards (ref.[19.]), both edgewise and flapwise load cases are

Bladena
Banestrøget 13, 1
DK-2630 Taastrup

required, but not the operational load case. For large blades, edgewise loading is often the most critical and is therefore used for comparison in this paper. However, neither the edgewise or the flapwise test load cases include significant torsional loads.

The reason why this topic has been addressed is the rising concerns that out-of-plane panel deformations is a major root cause of critical stresses in adhesive bondlines as well as between the composite layers (interlaminar stresses), especially, the interface between sandwich skin and sandwich core materials. The term sandwich skin is used in this context to refer to the face sheets, thus the outer- or inner-most layers of sandwich panels.

Torsional Load Overview

The current design basis considers the loads associated with displacements in the edgewise and flapwise independently and not their combined three-dimensional effect equivalent to what is found under actual operating conditions.

Figure 1 shows the three-dimensional tip deflection in both directions when the blade is in operation. This deflection is a consequence of the combination of flapwise loads due to the aerodynamic impact of the incoming wind, and edgewise loads, due to gravity forces and blade dynamics during rotation. These movements cause forces to act not exactly at the blade's shear centre, thereby creating an arm that generates a Root Torsional Moment (RTM). The direction of this RTM depends on the magnitude of the applied loads and the stiffness of the blade. As blades increase in length, the tip deflection also increases significantly, leading to notable rise in the RTM. This will be further discussed in the subsequent section of the paper.

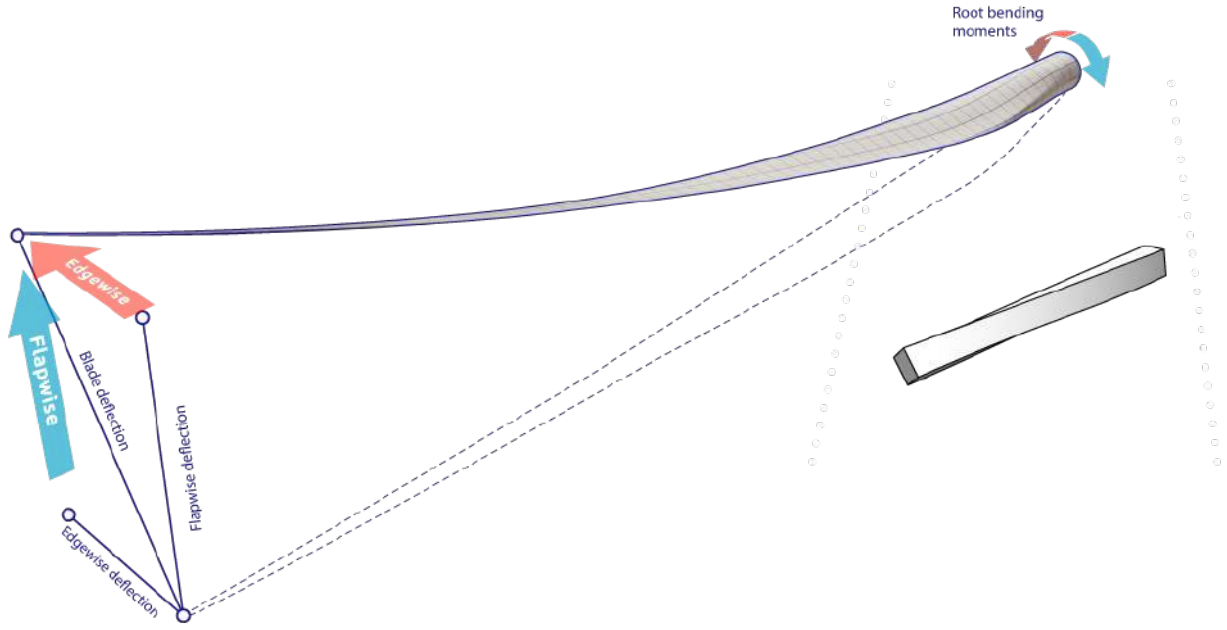

Figure 36. Flapwise and edgewise load components and tip deflection generate Root Torsional Moments (RTM).

The torsional load components cause localized panel deformations in the transition zone and in the max chord area of the blade (ref.[13.]). As a result of out-of-plane deformation, bending strains in the panels are generated. This occurs mainly in the transition zone and in the max chord area. The deformations also cause peeling stresses in the bondlines of blade designs with an aft shear web.

Bladena
Banestrøget 13, 1
DK-2630 Taastrup

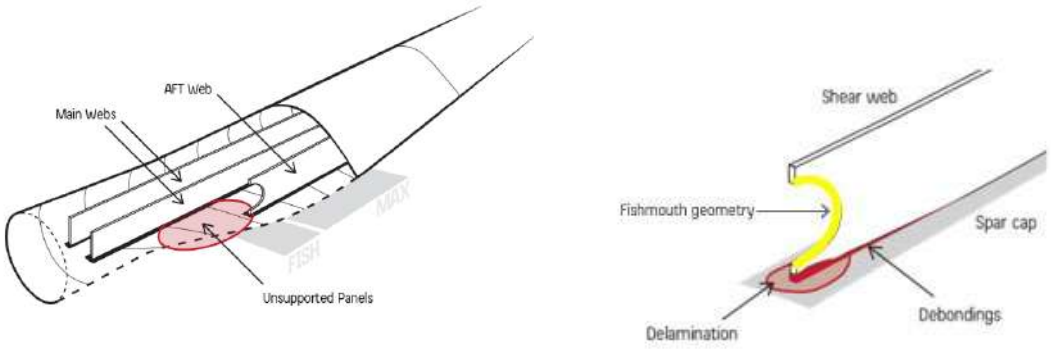

Figure 37. Transition zone of blade with 2 main shear webs and one aft shear web with unsupported panels, the red ellipse illustrating the area where the unsupported panels are located (left). Connection between the aft shear web fishmouth and the spar cap. Highlighted, initiation of delamination and debonding (right).

Localized bending of the sandwich panels in the transition zone (see Figure 3 for further information about the transition zone),often results in peeling in the bondlines of blade designs with an aft shear web. This occurs more frequently due to the peeling stresses caused by the out-of-plane deformation of the unsupported panels, which are carried by the bondlines of the aft shear web. In blades without an aft shear web, the peeling stresses are carried by the bondlines in the trailing edge and at the main shear web.

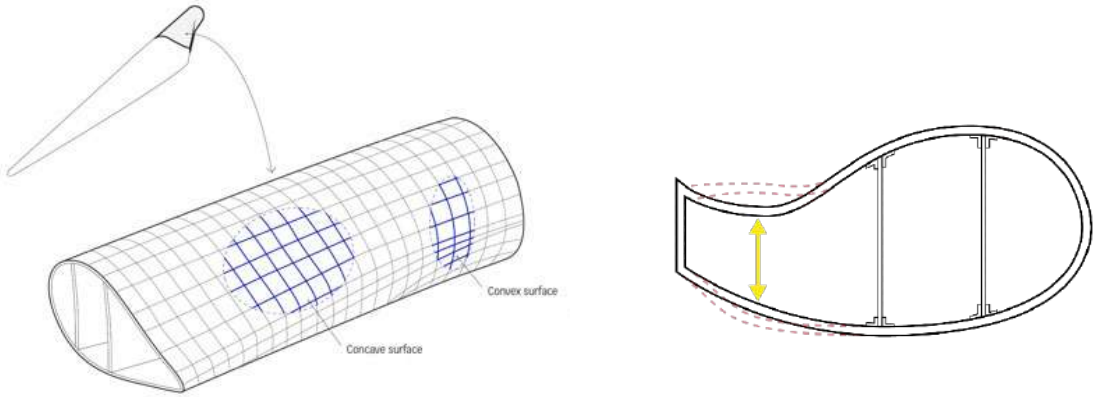

Figure 38. Transition zone of a large blade where the complex geometry can be appreciated, moving from a convex to concave shape, and changing in tapering in 3 directions. On the right, localized bending of the panels is represented, the solid lines represent the un-deformed positions and the dashed lines present the deformed positions.

Furthermore, the torsional loads cause additional cross-sectional shear distortion (CSSD), which results in additional peeling stresses (ref. [13.]) being transferred to the bondlines, see Figure 4. This phenomenon is in many cases driving structural related failures early in the lifetime of large wind turbine blades, see ref. [1]. In a previous study conducted by Bladena, it was concluded that both cross sectional shear distortion, and especially out-of-plane deformation of the panels in the transition zone, are the two main root causes of shear-web disbonding in the transition zone, see ref.[9].

Bladena
Banestrøget 13, 1
DK-2630 Taastrup

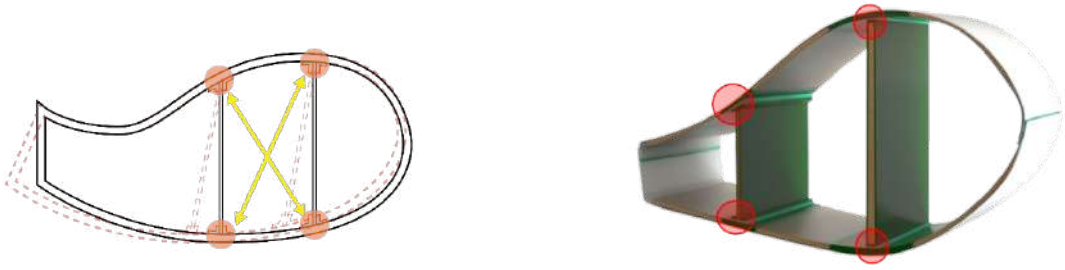

Figure 39. Blade cross-section. On the left, the solid lines represents the un-deformed position wand the dashed lines show the deformed position. On the right, bondlines highlighted in red circles on a blade cross section..

The significance of the torsional loads and the associated deformations is tied to the fact that they increase with a power of 4 in relation with the length of the blades. Hence, what was considered an acceptable risk for a certain size of blade may become out of control as the blades increase in length, even leading to failures shortly after the blades have entered into operation.

The paper presents results of non-linear geometric 3D-solid FEM simulations to quantify these phenomena.

Experimental analysis: Large-scale testing applying torsional fatigue loads

Background and experimental methods

A large-scale test campaign was performed by utilizing the strong-floor test facilities. The purpose of the test campaign was to demonstrate the impact of torsional loads on a blade's transition zone region. A detailed description of the test program is presented in ref.[6]. Based on the 3D FEM analysis - as a direct impact of torsional loading - significant out-of-plane panel deformation occurs in the blade sandwich shells on both pressure and suction side. This oscillatory out-of-plane panel deformation is generating peeling stresses in the adhesive bondline connecting the aft shear web to the shells.

The blade type used for this test campaign was a 34m blade manufactured by SSP Technology using a prepreg manufacturing process (pre-impregnated fiber mats without autoclave) (ref. [17.]). High resin content was selected for the laminates close to the PVC foam core and mold to ensure adequate resin quantity According to the manufacturer a modification of the Ampreg 22 epoxy laminating system was used (ref. [18.]). Although, this blade type is considerably smaller than the blades typically discussed when addressing failure in the transition zone and newer blade designs are more likely to use balsa wood or PET foam for the core material. Despite, it is still sufficient to develop the test method and to demonstrate the effect of torsional loads with the use of right setup. A 15m root end section cut-out of the SSP34m blade was utilized with a retrofitted aft shear web in the transition zone. Since the blade originally has a box spar design, a retrofit aft shear web was necessary (ref. [15]). This web was installed 4m from the root towards the tip section, positioned midway between the load carrying box girder and the trailing edge. The position was determined based on previously conducted test results which indicated the highest out-of-plane deformation in this area, see ref. [1.]). The main body of the aft shear web is a sandwich structure consisting a 10mm core material (PVC foam) and four layers of bi-axial glass fiber. The strong-floor setup and the retrofitted aft shear web are presented on the Figure 5.

Bladena
Banestrøget 13, 1
DK-2630 Taastrup

Figure 40. Large-scale strong-floor based test setup, the root section is mounted on a vertical strong-floor and the tip end is mounted onto the load train, the load introduction is explained on Figure 6 (left). Retrofitted aft shear installed in the 2 blade cut-outs (middle). The position of the retrofitted aft shear web illustrated (right).

Since the large-scale test was performed on the inner 15m section containing the transition zone, it is noted that the large-scale test will not be able to address one of the main conclusions explained below in subsection 4.2. Here the deflection of the tip of a large blade gets significantly amplified when both edgewise and flapwise loads are acting simultaneously, creating a large torsional arm that will lead to a high torsion on the structural regions of the blade.

In order to account for this limitation, and to avoid a testing campaign that could last for multiple years using conventional full-scale blade test methodologies, an accelerated fatigue test was carried out using the large-scale test setup and section test configuration. Thus, the loads applied are higher than the tested blade would ever experience in field conditions. Also, the layout and geometrical characteristics of the tested blade differs from current large blade types. Nonetheless, results from the test are illustrative of the field scenario for larger blades.

The torsional cyclic loads which have been applied in the large-scale tests are 50% higher than those that a 1.5MW old blade will meet in the field. The reason is that the objective is to demonstrate the importance of torsional loads on a larger blade. Ideally, a large modern blade should have been tested, but that has not been possible within the framework and budget of this research project.

The loading arrangement consists of two structural actuators which are capable of applying loads at the free end of the root section compromising two degree-of-freedoms: edgewise load along with torsional moment around the longitudinal axis of the blade. The maximum loading used during this fatigue test was 100kN edgewise load component (F_Y) and 100kNm as torsional moment (M_Z) respectively and with a frequency of 0.1Hz. Figure 6 below shows the test setup actuator configuration of the loading at the 15m reinforced cross-section. More details about the test setup can be found in ref. [7]. Figure 6 illustrates the test setup and the actuator specifications with the related coordinate system. During the test campaign various instruments were used, including a Digital Image Correlation (DIC) system, 4 strain gauges mounted on the retrofitted aft shear web, acoustic emission sensors and a wire potentiometer, more details about the instrumentation (e.g. instrument specification, positioning, etc.) see in ref. [7.]. The illustration shows the mounted position of the blade on the test rig and visualizes the applied load components.

Bladena
Banestrøget 13, 1
DK-2630 Taastrup

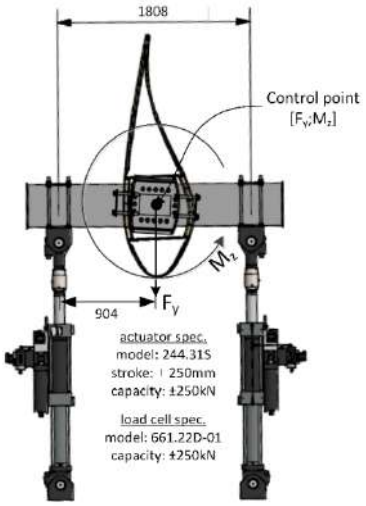

Figure 41. Active coordinate system and notation of the load train. Source: ref. [7]

Experimental results

The test resulted in a critical damage in the transition zone area on the pressure side panel in the trailing edge region of the blade in approx. 280.000 load cycles. More info about the damage and the test can be found in ref. [7.]. Further testing on the same blade section would have led to a blade collapse due to significant sudden decrease in edgewise stiffness (see Figure 7). This damage was a direct result of the applied torsional fatigue loads, causing large-scale damage on the blade shell in the root transition zone due to delamination from the out-of-plane deformation. The damage is shown on Figure 7. Such damage is considered critical, as it would require an immediate action if it happened during operation; failure to do so could potentially lead to further structural damage to the blade or other areas of the wind turbine. as if no actions were taken it could potentially lead to further structural damages on the blade or on other areas of the wind turbine.

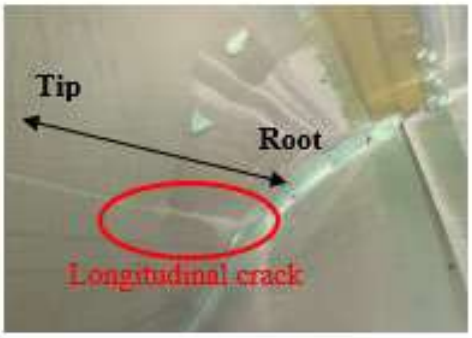

Bladena
Banestrøget 13, 1
DK-2630 Taastrup

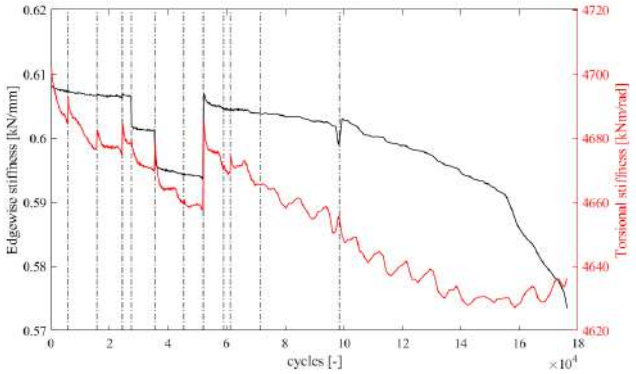

Figure 42. Picture presents the critical damage occurred on the 15m blade section of a 34m blade after 280.000 cycles in fatigue testing, where torsional loads are applied. The external condition of the blade (on the left), the crack observed internally (on the right). Plot presenting the change in edgewise and torsional stiffness (on the bottom).

Even though the measurements in the large-scale test focused on the bondlines of the retrofitted aft shear web, limited data is available for the position of the initial damage location (approximately 1-1.5m from the root towards the tip section). However, the initiated damage is highly relevant, as the results show that the application of torsional load components lead to critical damage in the root transition zone on the unsupported panels.

The potentiometer installed 200mm from the front of the aft shear web towards the root (approximately 3.8m from the root has captured out-of-plane deformations in the transition zone. Since the damage occurred further towards the root, the panel deformation is likely significantly higher where the panels are unsupported. At the position where the measurements were made, the aft shear web supported the blade shells which indicates that the out-of-plane deformation of the panels are likely lower in this area. The mounted wire potentiometer is presented in Figure 8 below.

Figure 43. The mounted wire potentiometer measured out-of-plane deformation of the blade panels. The potentiometer was installed 3.8m from the root and 200mm from the retrofitted aft shear web.

The findings suggest that in case the aft shear web is helping to reduce out-of-plane deformation where it is installed, increased "breathing" will occur on the blade further towards the root section which leads to skin delamination and that result in a catastrophic failure mode.

Additionally, a second 15m blade section of a SSP34m blade was tested with a 5cm crack introduced manually into the bondlines on both sides of the retrofitted aft shear web. The test was executed under the same conditions as the first fatigue test (100kN edgewise load component (F_Y) and 100kNm torsional moment (M_Z) with the frequency of 0.1Hz). However, the test was halted after approximately 12000 cycles

Bladena
Banestrøget 13, 1
DK-2630 Taastrup

due to technical issues with the mounting box girder installed onto the tip section of the blade which mounts the blade onto the test rig. During the 12000 cycles significant increase in out-of-plane deformation was observed, from the initial 10mm deformation, it increased to 13mm. as represented on Figure 9, below.

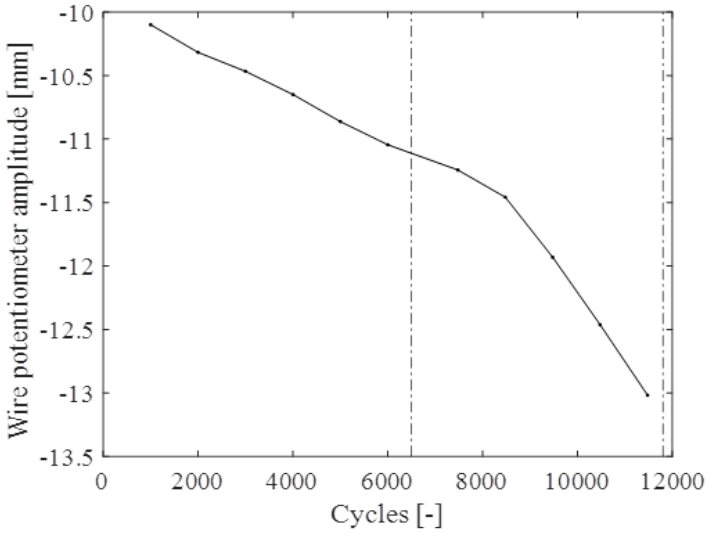

Figure 44. The measurements obtained from the wire potentiometer regarding out-of-plane deformation during the second test.

In Figure 9, a plot is presented of the magnitude of out-of-plane deformations and the nr. of cycles. A sudden drop (a drop in the plot shows an increase in the out-of-plane deformations) is observed on the plot at around 8000 cycles, show that damage is growing faster, hence is unstable. Upon inspecting the aft shear webs bondline, a clear crack propagation of over 10mm was observed on both bondlines of the aft shear web, see Figure 10.

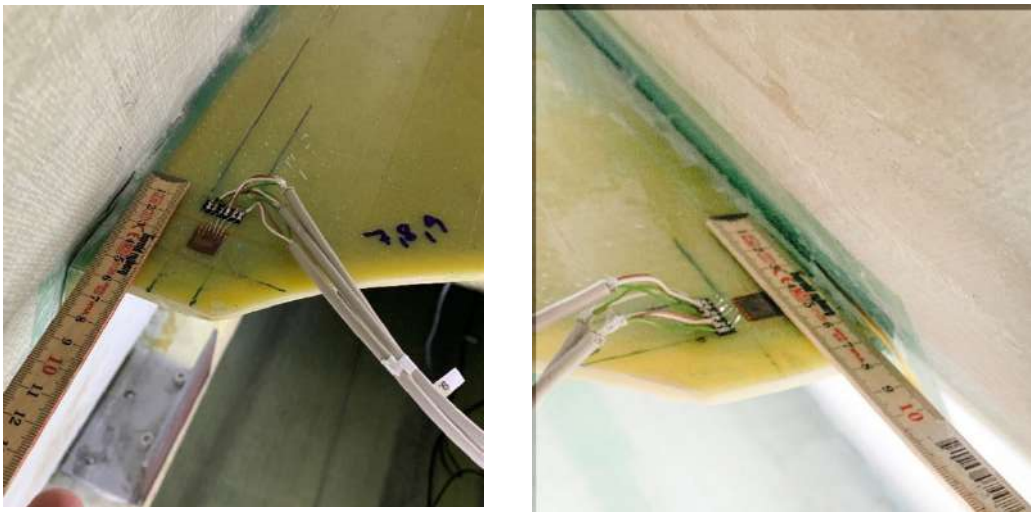

Figure 45. Approximately 10mm crack propagation on the Suction Side (on the left). Approximately 20mm crack propagation on the Pressure Side (on the right).

Figure 10 shows the results of inspection. A 10mm crack and a 20mm crack was observed on the SS and PS, respectively causing a halt to the testing.

Bladena
Banestrøget 13, 1
DK-2630 Taastrup

In summary, increased "breathing" was observed when torsional load components were applied to the 15m blade cut-outs, leading to a severe damage during large-scale testing. This outcome was encountered during two separate experimental analyses, each revealing the extent of the damage caused by these loads. These tests led to the finding: the impact of torsional loads is not confined to only longer blades but also substantially affects shorter ones. Even a blade with a relatively short length of 34m demonstrated vulnerability to torsional loads. This conclusion emphasizes the importance of considering torsional loads in the design and testing phases of wind turbine blades, regardless of their size.

FEM Analysis

Three different analyses have been conducted. Firstly, simulations were performed comparing the additional tip deflection and consequent torsional loads representing actual operational conditions to a scenario with only edgewise loads. This scenario is expressed in several tables below as “Only edge TTL”, meaning that the loads are exclusively considered in the edgewise direction, from trailing edge to leading edge. Secondly, torsional moments have been quantified for different blade sizes, obtaining scaling factors for RTM and edgewise and flapwise RBM. Thirdly, 3D FEM analysis have been applied to determine the influence of torsional loads on peeling stresses and bending strains on three hotspots (damage prone regions) of the blade:

1. Max chord area, unsupported panels
2. Transition zone, fishmouth of the aft shear web
3. Transition zone, unsupported panels

Two failure modes are covered for these hotspots: shear web disbonding, and skin debonding.

These hotspots were selected based on the author’s in-field experience regarding damage occurrence during operation.

Each hotspot is analysed for the blade position where the highest values were found. Two operational load positions, 90-degree azimuthal position and 270-degree azimuthal position have been used. To clarify this, the azimuthal degree indicates the position of the blade during rotation. As an example, 0-degree represents a blade in a vertical position with the tip pointing up, and 180-degree azimuthal position the blade is also vertical with the tip facing down. For further details, see Figure 11.

The two blade FEM models have been established using state-of-the-art structural and FEM numerical knowledge.

The FEM blades are modelled using HEX8 elements and 3D layered solids which are modelled with composite properties (e.g. layers of glass fibres – biax, triax and unidirectional - are built up in specified directions and with a core in the panels). This modelling approach is very effective at capturing out-of-plane deformations as well as strains and stresses in the lamina. This feature is used to extract strains from the outer and inner layer of panels and calculate bending strains.

The loads applied are calculated by adapting operational loads for specific blades familiar to the author, to fit the 80m blade and the 120m blade.

Operational loads cause extra Tip Deflection leading to additional Torsional Loads

The current design basis considers the loads associated with displacements in the edgewise and flapwise independently and not their combined three-dimensional effect equivalent to what is found under actual operating conditions.

This simplification implies a significant underestimation of the actual movements of the blades and thus of the forces/stresses that the blades are exposed to in real life. For the 120m blade the global edge tip deflections are presented in Table 2.

Bladena
Banestrøget 13, 1
DK-2630 Taastrup

120m wind turbine blade	Edge tip deflection [m]
Only edge TTL	6.6
Operational loads, 90-degree azimuthal position	9.2

Table 9. Edgewise deflection for both operational loads, and only edge load component. 120m wind turbine blade.

Regarding the edgewise direction, blades are significantly stiffer than in the flapwise direction, but the deflection values increase from 6.6m to 9.2m when actual operating conditions are added. The increased edgewise deflections are equivalent to a loss of stiffness compared to the design basis. This effect will not only influence the tip deflection, but also the stresses in the max chord area and in the transition zone.

Quantification of Torsional moments

The load contributions that introduce a root torsional moment on the blade arise from the aerodynamic forces and gravity working on the already deformed blade under operation. The aerodynamic forces can be divided in a purely flapwise component as well as a tangential component in relation to the rotor plane, acting as an edgewise load, in relation to the aerodynamic profile of the blade. Additionally, gravitational loads are also acting in the edgewise direction, see Figure 11.

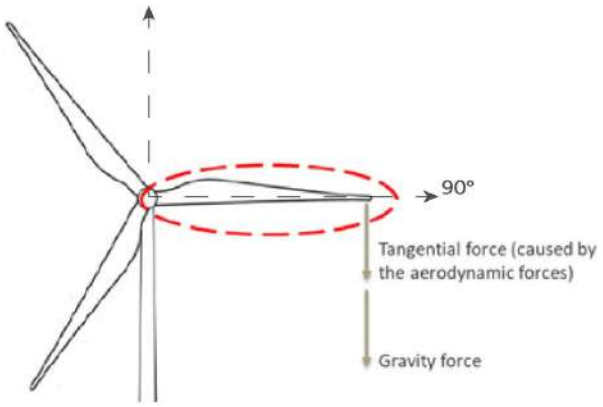

Figure 46. Investigated blade in 90-degree azimuthal position as the blade rotates. The arrows next to the forces indicate direction only, the gravity forces act at the center of gravity of the blade whereas the tangential forces act along the blade..

When the blade is loaded and deflected, torsional loads are generated. The edgewise aerodynamic loads working on a flapwise deformed blade twist the blade in a clockwise direction if the blade is seen from the tip towards the root. At the same time aerodynamic flapwise loads work on the edgewise deflected blade and the twist direction generated by this depends on the direction of the edgewise deflection. While the tangential aerodynamic loads (if the aerodynamic loads are split into two, based on directions, we can define normal direction and tangential direction) are always working towards LE, the gravitational load switch direction relative to the blade between the two horizontal positions. Figure 9 shows 90-degree azimuthal position where the aerodynamic tangential forces and gravity works in the same direction. For this position the flapwise loads generate a counter-clockwise twist to the blade when seen from tip towards the root. Figure 10 illustrates the resulting torsional moments due to the operational loads.

Bladena
Banestrøget 13, 1
DK-2630 Taastrup

Taastrup, June 28, 2023

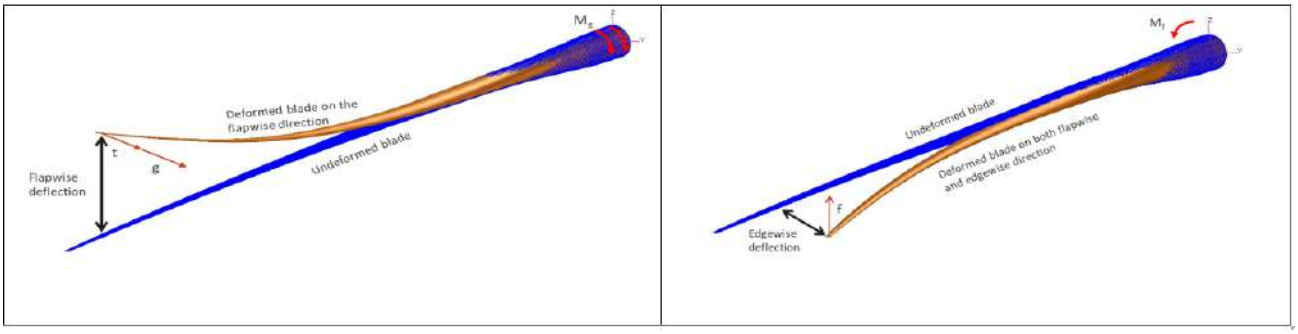

Figure 47. Left: RTM when gravity and tangential forces are in the same direction. Right: Root Torsional Moment induced by flapwise forces. Moment is acting in a different direction than the ones from the edgewise loads. On the figures "t" indicates tangential force and "M" indicates torsional moment.

A scaling study was carried out using two generic blade FEM-models, i.e., a typical 80m blade (corresponding to 7-9MW) and a typical 120m blade (corresponding to 15-18MW).

In the scaling study of the two blades, an 80m blade and a 120m blade, the blade characteristics can be compared. Both blades which are considered large (60m+), share a flatback design with two main shear webs and an aft shear web starting in the transition zone. They also both have carbon in the caps. Despite its large size, the 120m blade is very slender and lacks a clearly defined max chord, instead featuring a max chord region. This means that even though one blade is much larger, they have the same "max chord" profile length of approximately 5m. The sandwich panels are built up with layers of glass fibers (biax, triax, unidirectional).

The three torsional moment contributions and the total moment are listed in Table 3. It is seen that the total root torsional moment is 4 times higher in the 120m blade compared to the 80 m blade.

Torsional load contribution	Generic 80m blade	Generic 120m blade
Gravitational contribution	200 kNm	1600 kNm
Tangential contribution	160 kNm	700 kNm
Flapwise contribution	-160 kNm	-1500 kNm
Total	200 kNm	800 kNm

Table 10. The torsional moment contributions for 80m and 120m blades for 90-degree azimuthal position. A positive moment is defined as the moment that twists the blade clockwise if the blade is seen from the tip towards the root.

Table 4 below shows the result of a study conducted to understand how the RBM and RTM change for different blade sizes. The exponents shown below correspond to a curve fitting performed with the values from this study in which in the x-axis the blade length was presented, and the RBM or RTM in the y-axis. So RBM and RTM are represented as a power function with an exponent x.

$$f(x) = ab^x$$

Where:

- $f(x)$: RTM or RBM
- a: value different to 0

Bladena
Banestrøget 13, 1
DK-2630 Taastrup

- b: blade length
- x: exponent shown in table below

Load direction	Exponent
Flapwise RBM	2.8
Edgewise RBM	3.4
Torsional RTM	4.0

Table 11. Exponent increase for as a function of blade length for flapwise RBM, edgewise RBM and torsional RTM.

In all cases, magnitudes increase as a function of the blade length, especially in the case of torsional RTM. The mathematical relationship between the three studied variables (Flapwise RBM, edgewise RBM, and torsional RTM) and its dependency on blade length (exponent shown in Table 4) shows a scaling exponential behaviour up to the power of 4 for the torsional RTM.

Finally, Table 5 presents a list of potential failure modes and the impact on them from of torsional loads. Failure modes which are dependent on panel deformation e.g., breathing and CSSD are heavily impacted by the inclusion of torsional loads, whereas damages in the root (T-bolts, root inserts) are not impacted.

Failure mode	IEC 61400-5:2020	IEC 61400-23:2014	DNV-ST-0376:2021	Used in industry	Uncertainty of tools	Impact of torsional loads
Bondlines (Peeling test)	(2)	(1)	(3)	(YES)	MEDIUM	HIGH
Skin debonding from core (Test)	(2)	(1)	(3)	(NO)	MEDIUM	HIGH
Interlaminar failure (Bending test)	(2)	(1)	(2)	(NO)	LOW	HIGH
Global strain (Failure criteria)	(5)	(5)	(5)	YES	LOW	LOW
Shear web disbonding	(2)	(1)	(3)	(YES)	MEDIUM	HIGH
Root failures	(5)	(5)	(5)	YES	LOW	NO

Table 12. Table regarding potential failure modes and the impact of torsional loads on them, ref. [16] p. 46 (1 means there is no reference in the standard and 5 means it is required in standards). The table does not take vibration issues into account. An additional column with the impact of torsional loads has been included. Regarding this column, it must be said that the impact depends on the section of the blade where this is analysed.

4.3 Impact of Torsional Loads on Selected Failure Modes

This sub-section addresses the impact of applying torsional loads in non-linear geometric 3D-solid FEM models for different failure modes.

The objective is to quantify the influence of torsional loads on variables such as peeling stresses, and bending strains, which have a direct relationship with some of the most common structural field damages seen during operational conditions.

The root transition zone of the blade has a complex geometry and contains tapering shell panels in 2 directions double curved in addition to the concave-convex double curved geometry. In addition, depending on the blade model, these panels in the TE box often have a large unsupported panel area in some sections of the blade, since the aft shear web usually starts around the max chord area or at the very end of the root transition zone.

Shear web disbonding

As explained in the introduction, shear web disbonding is a frequently occurring failure mode seen for a variety of larger blades. This failure mode is characterised by disbonds in the aft shear web bondlines, initiating from the spar cap fishmouth region. Thus, special attention has been aimed at blades which have an aft shear web with a fishmouth shape, as well as traces of delamination in the area of the fishmouth foot, see Figure 2.

Consequently, peeling stresses is the main parameter to focus on in the 3D-solid FEM analysis in order to understand the possible initiation of this failure mode.

In the following, results from two different studies will be presented on this topic for two different blade sizes, namely 80m and 120m. The fishmouth region of the aft shear web is located between the trailing edge and the trailing edge shear web, and situated at a distance of 3.5m towards the root for the 80m and 9,8m for the 120m blade. These are the positions where the aft shear web starts for the two blades with different length.

1. 80m wind turbine blade

Operational loads have been compared against only edgewise loads.

Results are presented in terms of maximum values. Maximum values show the highest stress or strain calculated by FEM in the selected hotspots. They are considered as being the most likely locations for initiation of damages.

Table 6 below shows the maximum peeling stresses in the transition zone. An increase of 40% can be observed due to the impact of torsional loads.

Transition zone	**Peeling stresses. Operational 90-degree azimuthal position [MPa]**	**Peeling stresses acc. to current standards [MPa]**	**Increase due to torsional loads**
80m	1.4	1.0	+40%

Table 13. Maximum values for peeling stresses comparison for an 80m blade in the shear-web disbonding transition zone. The two load cases analysed is an operational 90-degree azimuthal position and a pure edgewise loading.

It cannot be stated whether this increase in stresses is critical or not, and no literature has been found for reference. Such an evaluation will vary from blade design to blade design. In addition, standard methodologies representing fatigue analysis such as SN curves are not considered to be accurate enough for the analysis of interlaminar strength (ref [21] and [22]). A correlation with field damage would be required in order to

Bladena
Banestrøget 13, 1
DK-2630 Taastrup

estimate peeling stress values that may lead to the initiation of the damage, particularly in the form of shear web disbonding.

However, it must be considered at this point that the transition zone is the main load carrying area of the blade. Thus, damages in this area can influence the structural integrity of the entire blade. Bondlines in this area may suffer from high peeling stresses caused by localised deformations, probably due to the breathing of the panels and the cross-sectional shear distortion of the structure, composed by the spar caps and the shear webs. Increases, like the 40% shown in this paper, may be enough to exceed the stress limit that can be carried by the bondlines.

Figure 13 below shows an example of where the peeling stresses are extracted from the 3D-solid FEM analysis.

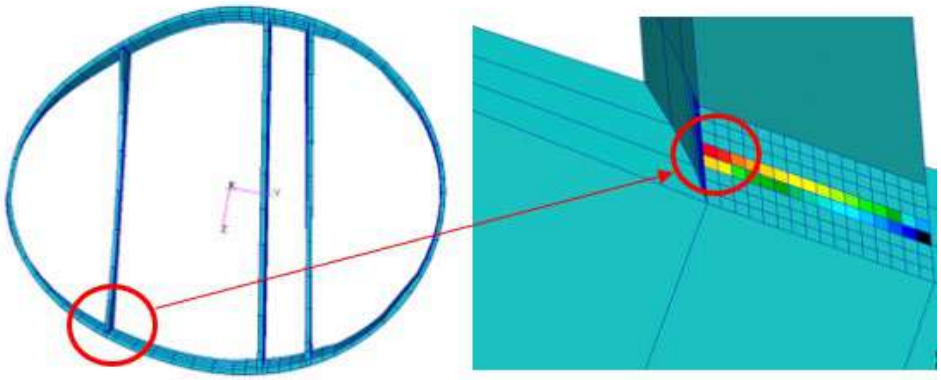

Figure 48. An example of the location where peeling stresses are extracted. The cross section is of a root-transition zone area and the peeling stresses are extracted at the aft shear web fish mouth foot as highlighted in red circle. The illustration is an indication of the increased peeling stresses in the investigated area.

2. 120m wind turbine blade

Again, a comparison between operational loads and edge loads as they are assessed in the current industry design basis has been established.

Results are presented in Table 7 below, in which an increase of 23% is deducted from the application of torsional loads.

Transition zone	**Peeling stresses. Operational 90-degree azimuthal position. [MPa]**	**Peeling stresses acc. To current standards [Mpa]**	**Increase due to torsional loads**
120m	1.6	1.3	+23%

Table 14. Max values for peeling stresses comparison for a 120m blade in the shear-web disbonding transition zone.

When comparing results from both the 80m blade and the 120m, see Table 8, it can be observed that, on one side, the values for the 120m blade are between 14% and 30% higher than for the 80m. This result is expected from a theoretical point of view, as the larger torsional arm created in the case of 120m blade, should generate a higher RTM and consequently higher peeling stresses in sensitive structural areas. It may be noted, that for the generation of torque, there must be a force component applied in the perpendicular direction to the

Bladena
Banestrøget 13, 1
DK-2630 Taastrup

line of action of this force from the point around which it is calculated. In other words, if the torsional arm increases, the twisting of the structure will be higher, which will lead to deformation of the blade cross section. As a result, increase in peeling stresses due to both cross section shear distortion and local bending of the unsupported panels between the trailing edge and the aft shear web in the transition zone will be present.

On the other hand, by analysing the percentage increase due to torsion, it can be seen how the impact of torsional loads is increasing faster in the 80m blade than in the 120m blade. The reason for the smaller increase is most likely due to the position of the aft shear web, which is very sensitive.

The most important observation is that for all blade types there is a significant increase in the peeling stresses when torsional loads are applied.

Blade	**Peeling stresses. Operational 90-degree azimuthal position [Mpa]**	**Peeling stresses acc. To current standards [Mpa]**	**Increase due to torsional loads**
80m	1.4	1	+40%
120m	1.6	1.3	+23%
Comparison	+14%	+30%	

Table 15. Comparative table for shear web disbonding. Max values

When comparing the max values for operational load 90-degree azimuthal position between the 80m blade and the 120m, an increase of 14% is found. For the case of pure edgewise load case, the value reaches a +30%. In this case, results are aligned with expectations, showing that peeling stresses increase with the blade size.

Consequently, the reason for the high number of failures due to shear web disbonding in the transition zone is probably due to torsional loads in large wind turbine blades. Only with field data will it be possible to fully validate the results herein. For this purpose, a validation process would be required, in which field and test measurement campaigns would be carried out in specific critical hotspots, measuring the physical response of the blade, and obtaining essential knowledge to validate the FEM models and numerical results obtained. A validation process is considered a key element to reduce risk in large blades. For further information, see ref. [10].

Skin (face sheet) Debonding from Sandwich Core in the Root Transition Zone

This failure mode is also more commonly seen in large blades in operation based on the author's in-field experience. Breathing of the panels due to out-of-plane deformations will potentially initiate skin debonding between the thin skins and the balsa or foam core of the sandwich shell panels. When sandwich panels are subjected to bending there is a risk that the interlaminar strength is not sufficient, causing skin debonding to initiate. If this occurs the bending stiffness of the sandwich panel will decrease significantly, and further crack propagation might develops rapidly. As a result of this, measuring bending strains through FEM will provide an indication of the behavior and possible breathing and bending of the panels which is understood as a possible root cause of this failure mode. Bending strains are calculated as the absolute difference between the outer strain and the inner strain of the panel.

The performed FEM analysis allows for comparison of the bending strains due to only edgewise loads with the operational loads. Results are presented for both the 80m and for the 120m wind turbine blades. For the

Bladena
Banestrøget 13, 1
DK-2630 Taastrup

80m blade, the bending strains have been measured at 3m from the root and 0.7m from the TE. For the 120m blade, the measured area is around 8m from the root and 1.2m from the TE in the chordwise direction.

The strain value is taken in the surface plane direction transverse of the blade profile (as opposed to longitudinal strains). This direction is best at capturing out-of-plane panel deformation. The complex geometry of the area changing from concave to convex and tapering in two directions is the main explanation for that the out-of-plane deformations are highest in this region, see figure 3.

Results for bending strains will in some cases give negative values, while in others they will be positive. A negative strain is defined as whenever the bending is experienced inwards in relation to the blade cross section, and a positive value indicates that the bending is outwards. Whether positive or negative is not important; the importance is the magnitude, as the focus is on the amount of bending, regardless of whether the bending is inwards or outwards.

1. 80m wind turbine blade

Transition zone. Max values. Results are shown in the table below.

Transition zone	**Bending strains. Operational 270-degree azimuthal position [με]**	**Bending strains acc. To current standards [με]**	**Increase due to torsional loads**
80m	-450	69	+550%

Table 16. Max values. Bending strains for skin debonding in transition zone. Operational 270-degree azimuthal position vs Only edgewise loads. 80m wind turbine blade. The deviation in percentages is for the absolute values, since the magnitude and not the direction of bending is what matters.

Bending strains increase due to the increased level of bending and breathing of the panels. The transition zone is the main area of the blade carrying the loads, meaning that even small modifications in the load distribution may have an impact in this structurally critical area.

It can be seen how bending strains are increased 550% under the impact of torsional load. It can also be observed that the direction of strains changes from positive to negative. This sign is not important for the interlaminar stresses between the layers.

One reason that could explain this finding could be that when operational loads are included in the analysis, the panels may suffer an increased bending due to the loss of stiffness in the edgewise direction, as seen in Table 2 whenever the tip deflection was compared with and without applied torsional loads. This loss of stiffness has been studied only in a 120m blade; however, it is expected that the 80m blade also experiences a softer edgewise deflection that could explain the big percentual difference in the impact of torsional loads in the transverse direction versus the longitudinal one.

Max chord area. Max values. Results are shown in the table below.

Max chord.	**Bending strains. Operational 90-degree azimuthal position [με]**	**Bending strains acc. To current standards [με]**	**Increase due to torsional loads**
80m	-360	-280	+29%

Table 17. Max values. Bending strains for skin debonding in max chord area. Operational loads vs pure edgewise loads. 80m wind turbine blade.

Bladena
Banestrøget 13, 1
DK-2630 Taastrup

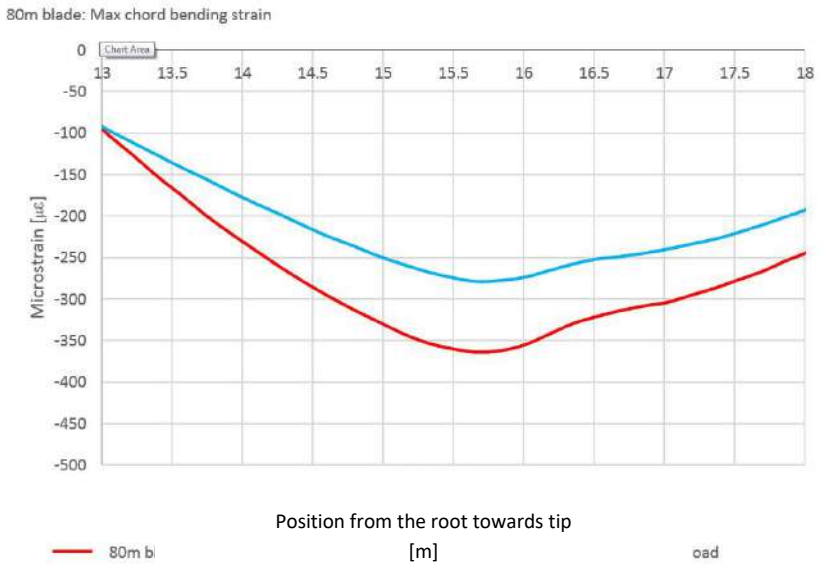

Figure 49. Bending strain compari *al loads 90-degree azimuthal position vs Only Edgewise loads.*

For the max chord area Table 10 shows that bending strains increase around 30% whenever torsional loads are included.

It is also important to highlight that values for operational conditions are lower in the max chord area (360με) than in the transition zone (450με) which strengthens the hypothesis that the transition zone is the most critical and sensitive area from a structural point of view.

2. 120m wind turbine blade

Transition zone. Max values:

The evaluation focuses on the transition zone region, specifically between 8m and 9m along the blade length. The increase in the bending strains due to torsional loads are 120%, as can be seen in Table 11.

Transition zone	**Bending strains. Operational 270-degree azimuthal position [με]**	**Bending strains acc. To current standards [με]**	**Increase due to torsional loads**
120m (transverse)	630	430	+46%

Table 18. Max values. Bending strains for skin debonding in transition zone. Operational load 270-degree azimuthal position vs Pure edgewise load, 120m wind turbine blade.

Bladena
Banestrøget 13, 1
DK-2630 Taastrup

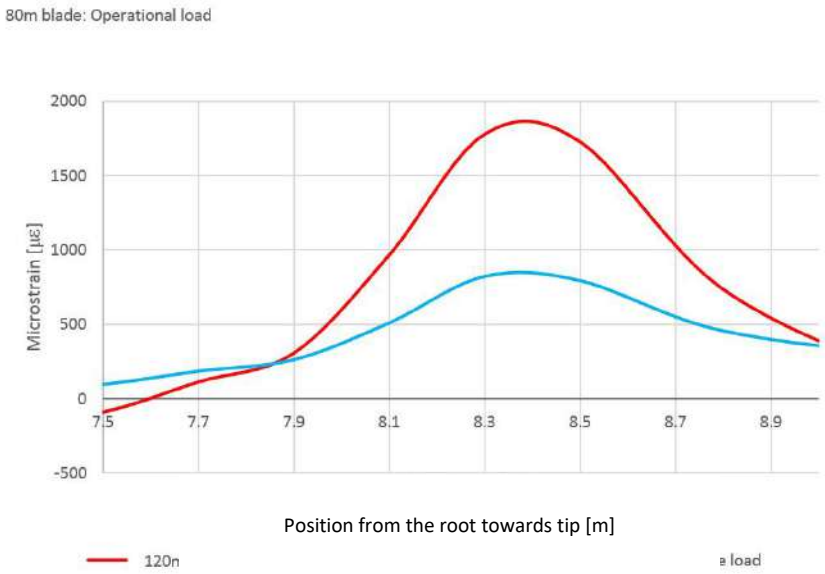

Figure 50. Bending strain comparison for 120m blade in the transition zone PS, operational load 270-degree azimuthal position max values vs Pure edgewise load max values.

Table 11 also indicates that bending of the panels is more severe in a 120m than in the 80m blade, shown in table 9. The difference in bending strains with operational loads reaches a +40% (630με vs 450με).

Consequently, it may be concluded that bending strains in the transition zone could increase linearly to the size of the blade.

Max chord area. Max values:

Max chord.	**Bending strains. Operational 90-degree azimuthal position [με]**	**Bending strains acc. To current standards [με]**	**Increase due to torsional loads**
120m	-1090	-740	+47%

Table 19. Max values. Bending strains for skin debonding in max chord area. Operational loads, 90-degree azimuthal position vs pure edgewise loads, 120m wind turbine blade.

Regarding the max chord area, the increase in the bending strain due to torsional loads is of around +47%. Summary table for skin debonding with max values is shown in Table 13.

Bladena
Banestrøget 13, 1
DK-2630 Taastrup

Summary. Bending strains	Operational [με]	Bending strains acc. To current standards [με]	Increase due to torsional loads
80m TZ	-450	69	+550%
80m Max chord	-360	-280	+29%
120m TZ	630	430	+46%
120m Max chord	-1090	-740	+47%

Table 20. Comparative table for skin debonding with max values.

Two main observations and results from the analyses can be highlighted:

- 80m blade vs 120m blade: the bending strains of the larger blade are significantly higher than for the smaller one, which emphasizes the thought that large blades have a much smaller structural reliability than medium or small blades. When values are compared between the 80m blade and the 120m applying operational loads:
  - Max chord area, transverse bending strains: +200% (from -360με to -1090με)
  - Transition zone panels, transverse bending strain: +40% (from -450με to 630με)

- Transition zone vs Max chord area: the transition zone does not always experience higher bending strains than the max chord area.
  - 80m, transverse direction bending strains: +25% (from -360με to -450με)
  - 120m, transverse direction bending strains: -71% (from -1090με to 630με)

Impact of torsional loads on lifetime – Discussion of results

The information presented in this paper emphasizes the importance of the torsional load components in order to correctly assess the durability of a given blade. Publicly available information on field damages, experimental analysis, and numerical models all points in the same direction: the larger turbine blades necessitate high maintenance costs (ref.[20.]).

As a result, it seems logical that the wind industry would adapt to the ongoing changes and challenges. This would mean reassessment of the design principles and O&M (Operation and Maintenance) strategies of large modern blades. Moreover, predicting the lifetime of these blades is a complex task, particularly because the traditional S-N curve method may not be accurate enough when it comes to analysing interlaminar strength (ref [21] and [22]). It is a well-established understanding among composite material experts that the S-N curve approach cannot be used to predict the lifetime of bondlines within these materials. Instead, these experts, including the authors of this paper, propose using a fracture mechanics approach. This method offers increased accuracy and allows for the implementation of a damage tolerance approach. The damage tolerance approach is about predicting when damage will occur and understanding how the structure will behave once a damage is present. Our main research project, see ref. [10], over the past two years, has been focused on these aspects. The majority of our research projects' participants and partners are Wind Turbine Owners whose goals are to minimize operating expenses (OPEX) and maximize the annual energy production (AEP). They are not typically involved in the design process, and therefore have not adopted the classical damage tolerance

Bladena
Banestrøget 13, 1
DK-2630 Taastrup

approach. However, in our views, the traditional methods are viewed from a perspective that is relevant not only to wind turbine owners but, hopefully, to manufacturers and companies involved in service and management. Doing this aims to bring a fresh understanding and approach that benefits all parties involved.

Conclusions

The current design and validation testing of large wind turbine blades omit substantial loads on the blades and that these omissions may very well explain the high level of unwanted maintenance costs that are currently found in the industry on large blades; an effect which increases exponentially with increasing blade lengths.

The paper presents non-linear 3D-solid FEM comparisons between different load scenarios as they come out of the current design practice and stresses as they come out when the more realistic 3D non-linear behaviour of the blades is accounted for.

Numerical analysis using non-linear geometric 3D-solid FEM, for the study of shear web disbonding and skin debonding, can conclude that peeling stresses and bending strains are found significant for large blades due to the high torsional loads generated when the blade is in operation.

The results may be summarized as follows:

- The torsional loads that are found under actual operating conditions cause additional and critical out-of-plane deformation of the unsupported panels and also distortion effects such as CSSD and breathing. The localized deformations cause peeling in the bondlines, interlaminar stresses between the composite layers, and in between the sandwich skin and the core material. Layered composite structures and adhesive bondlines do not have a high load carrying capacity for those failure modes.
- The edgewise tip deflection increases by 40% for a 120m blade when the non-linear 3D behavior is accounted for. Amongst others, the larger deflection implies a loss of stiffness which in turn leads to significant increase in bending stresses and peeling stresses.
- Scaling factors have been quantified concluding that RTM's increase with a power of 4 with blade length.
- Experimental testing using large-scale section testing has demonstrated that critical damage in the root transition zone appears when torsional fatigue loads are applied.
- On the second blade shear web disbanding occur and showed an unstable crack development

It should be noted that even though the authors are confident that the results from the FEM models used for the study are valid, it should also be considered that the operational loads used for the analysis may differ from reality, as field measurements for large blades were not available thereby it is not sufficiently covered in this study. Also, layup and geometry are not accurate from any specific blades in the field and therefore, results must be perceived as a trend rather than accurate values.

However, despite any uncertainty of the results, the value of the FEM analysis results, and their conclusions are considered to be significant because the results demonstrate that critical loads are not accounted for in the current industry practice.

Recommendations

Taking all this into consideration, some areas have been identified which could potentially help to mitigate the risk of suffering damages from some of the structural damages related to torsional loads. The following recommendations are areas recommended to the wind energy industry to consider. We believe that a joint-venture project concerning the topic would be beneficial for the whole industry.

<u>Suggestion 1. Application of torsional loads during the static blade full scale testing program</u>

The full-scale testing program following IEC-61400-23 standard requires both flapwise and edgewise loads but in separated load cases (ref.[19.]). The static pull is close to the shear centre, hence almost no torsional

Bladena
Banestrøget 13, 1
DK-2630 Taastrup

loads are applied. The importance of both torsional loads, and a combined load case is recognised, but no obligation is imposed.

As an example, the IEC-61400-23 states that "the flap and lead-lag sequence of testing may be performed on two separate blades. However, if an area of the blade is critical due to the combination of flap and lead-lag, then the entire test sequence shall be performed on one blade" (ref.[19.]). The consideration of whether an area of the blade is critical or not due to the combination of loads is open to interpretation, meaning that freedom is given to applying or not a combined loading full scale test.

Another example that emphasizes that torsion is understood as a relevant matter, but not forced to be considered, is the following quote from Annex E in the same IEC-61400-23: "if torsion loads are significant in the structural design of the blade they should be included in the test" (ref.[19.]). Again here, it is subjective the establishment of whether torsion loads are critical or not. And even if they are considered as significant, the word "should" indicate a recommendation, not an obligation.

Therefore, the application of the torsional load components is suggested, as more realistic scenario, but nothing is imposed. As stated also in DNV's whitepaper, see in ref. [2], with the increasing size, the torsional loads and displacement of the shear centre are significant contributors to loading.

If the combination of loads were applied, with an offset, shown on the sketch in Fig. 18, the local deformations and distortion effects (CSSD and breathing) will be representative. To incorporate the combined flap- and edgewise loads, the blade was tilted 30 degrees in the direction of the leading edge toward trailing edge during the full-scale test performed in an earlier executed full-scale blade test study, see ref. [1]. At this full-scale test, the purpose was also to test the buckling capacity of the trailing edge. In this paper the focus is on the structural strength of the max chord region and the root transition zone and therefore the sketch show another load direction, in the positions where the torsional loads are highest.

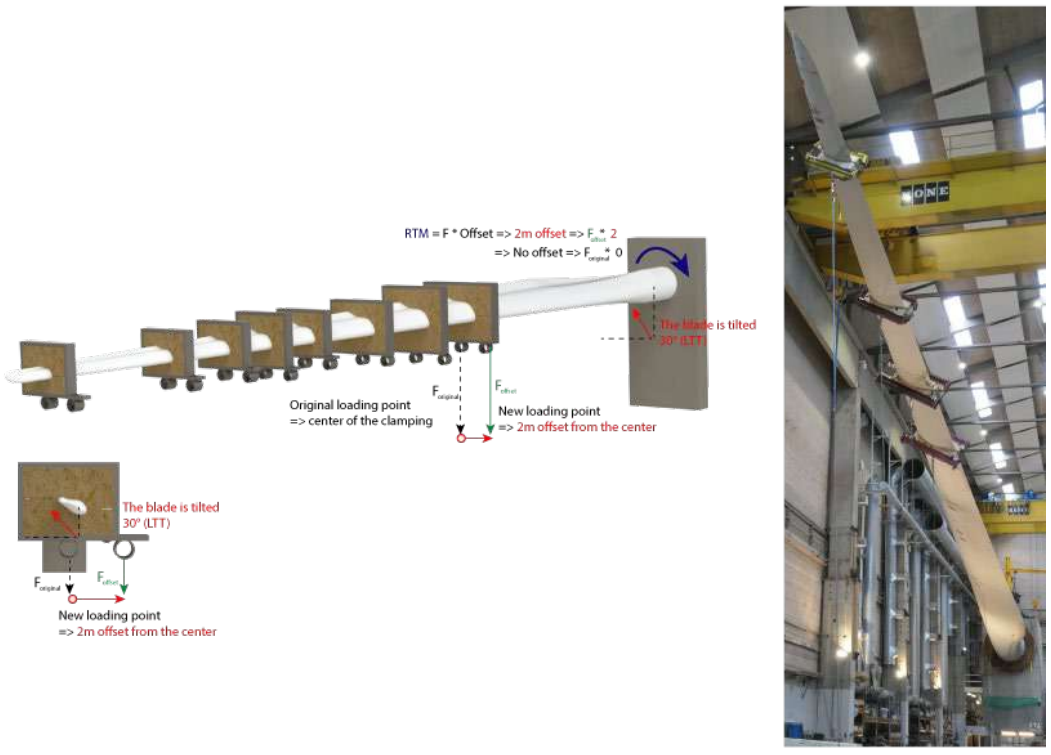

Figure 51: Sketch of a full-scale static test setup with applied torsional load components (left). Photo to the right show a full-scale test of a LM58,7m blade with combined statis loads performed at a commercial test center in collaboration with LM-Windpower and Bladena, see ref. [1] EUDP RATZ project.

Bladena
Banestrøget 13, 1
DK-2630 Taastrup

This full-scale static test campaign is fast and easy to perform, and the costs are low. Furthermore, the additional load case can be done before the certification fatigue test program is started, and this is important since the measurement, is needed as early, as possible in order to validate FEM-models. When the FEM model is validated the boundaries for of the performed fatigue test sub-component program, can be updated.

More details regarding the needed measurement and the validation program can be found in the following two suggestions. Fig. 18 includes a photo from a full-scale test, Bladena and LM WindPower performed together in a commercial test centre. The static full-scale test with combined load was successfully performed, but at that time the test was performed, the knowledge about size of the torsional loads was known and furthermore the blade was only 58,7m, so the torsional arm offset should not have been as large as illustrated on the sketch.

The calculated torsional arm offset for a 120m blade has been calculated to be approximate 2m offset from the shear centre. 8 load clamps have been estimated, but of course this has been analysed for the actual blade and it can also be considered not to have the same offset for all load clamps, as long the sufficient torsional loads are applied it is not so important how it done.

Suggestion 2. Additional measurements

During a full-scale test campaign, additional measurements, are recommended to be implemented to identify localized deformation in the critical inner third of the blade e.g., cross-sectional shear distortion and breathing. This can be considered as a relevant step prevent from some of the failure modes here studied, as an example, the phenomenon “breathing” of sandwich panels in the trailing edge region, can influence both the formation of transverse cracks due to skin debonding followed by skin fatigue cracks, and the opening of the trailing edge due to high peeling stresses in the adhesive bondlines close to the trailing edge.

The additional measurements would also help to validate the FEM-simulations, so the boundaries for the fatigue sub-component test program for a lifetime estimation can be updated.

Moreover, back-to-back strain gauges on the unsupported panels in the transition zone is highly recommended. By measuring back-to-back strains, the localized bending causing potential critical interlaminar stresses can be determined.

Suggestion 3. Torsional loads during the 3D FEM modelling

Modern aero-elastic load simulations include the torsional loads in the analysis. However, according to the author’s knowledge, these loads are not always included in the following non-linear 3D FEM analysis. This will also result in insufficient loading applied to the sub-component fatigue test program.

If the above three suggestions are implemented, potential issues can be found, and design improvements can be performed before the turbine is in operation.

Acknowledgement

Bladena would like to acknowledge the Energy Development and Demonstration Program (EUDP) for financial support under the grant number: 64021-1054 CORTIR II Project. Within the frame of the CORTIR II project considerable work has been done by DTU Construct regarding the experimental analysis and Global Wind Service supporting the large-scale test program and visualization work on several illustrations by Kirt X Thomsen.

References

[1]. Bladena and Partners, (2019), "Project Report: Root Area Transition Zone RATZ and Reduction O&M cost of WT blades, Energy Development and Demonstration Program (EUDP) RATZ project, 64015-0062,",

Bladena
Banestrøget 13, 1
DK-2630 Taastrup

https://www.bladena.com/uploads/8/7/3/7/87379536/eudp_ratz_-_project_final_report_-_eudp_ref._j64015-0602.pdf
[2]. Griffin, D.A., (2023), "The challenges of wind turbine blade durability" DNV Whitepaper, 2023, https://www.dnv.com/Publications/the-challenges-of-wind-turbine-blade-durability-243601
[3]. Renews.biz, (2020), "Vestas, EDPR probe blade failure at Ohio wind farm.", Renews 2020 September 9. https://renews.biz/63000/vestas-blade-failure-at-edps-ohio-wind-farm/
[4]. Harrison, C., (2019), "Limitations of legacy certification standards and benefits of new standards demonstrated on a100m wind turbine blade", DNVGL, WindEurope Offshore Conference, Copenhagen, 2019 November.
[5]. Rajgor, G. (2022). "GE Renewable Energy investigates second Cypress wind turbine failure in two months", Windpower Monthly, 2022 March 16. https://www.windpowermonthly.com/article/1749796/ge-renewable-energy-investigates-second-cypress-wind-turbine-failure-two-months
[6]. Bladena and Partners, (2021), "Cost and risk tool for interim and preventive repair (CORTIR) EUDP project 64018-0507 – Final Report", https://www.bladena.com/uploads/8/7/3/7/87379536/eudp_cortir_-_project_final_report_-_ref._64018-0507.pdf
[7]. Waldbjørn, J.P., Berggreen, C., Ahmed, S., Nagy, T., "Large-scale fatigue testing of a retrofitted 3rd shear web in a 34m wind turbine blade section" DTU Construct & Bladena, 2023
[8]. Bladena, (2022), "Risk considerations on upscaling wind turbine blades", Bladena whitepaper, 2022. https://www.bladena.com/uploads/8/7/3/7/87379536/white_paper_scaling_and_risk_bladena.pdf
[9]. Bladena, (2022), "Structural weaknesses of blades in operation" Bladena whitepaper, 2022. https://www.bladena.com/uploads/8/7/3/7/87379536/whitepaper_1_structural_understanding_bladena_13.04.2022_compressed.pdf
[10]. Bladena and Partners, (2023), "Cost and risk tool for interim and preventive repair (CORTIR Phase II) EUDP project 64018-0507 – Final Report"
[11]. Karlsen, T. (2021), "76 meter langt turbine blad deiset i bakken – kan ikke si hvor utbredt turbinen er i Norge", Teknisk Ukeblad, 2021 November 15. https://www.tu.no/artikler/136-meter-langt-turbinblad-deiset-i-bakken-kan-ikke-si-hvor-utbredt-turbinen-er-i-norge/515102
[12]. Brøndsted, P., & Nijssen, R. (Eds.) (2023), "Advances in wind turbine blade design and materials." Woodhead Publishing. Woodhead Publishing Series in Energy No. 47 http://www.woodheadpublishing.com/en/book.aspx?bookID=2548
[13]. Jensen, F.M., "Ultimate strength of a large wind turbine blade," Risø DTU, PhD Thesis, 2008. https://backend.orbit.dtu.dk/ws/portalfiles/portal/5434131/ris-phd-34.pdf
[14]. Bladena and Partners, (2016), "Torsional Stiffening of Wind Turbine Blades - Mitigating leading edge damages, EUDP project, 64013-0115", https://www.bladena.com/uploads/8/7/3/7/87379536/eudp_lex_project_final_report_september_2016.pdf
[15]. Waldbjørn J.P., Buliga A., Berggreen C., Jensen F.M., (2020), "Multi-axial large-scale testing of a 34m wind turbine blade section to evaluate out-of-plane deformations of double-curved trailing edge sandwich panels within the transition zone" DTU and Bladena journal paper, 2020, https://journals.sagepub.com/doi/abs/10.1177/0309524X20978408
[16]. Bladena and partners, (2022), "Wind turbine blades - Handbook", Edition 2022 CORTIR, EUDP.

Bladena
Banestrøget 13, 1
DK-2630 Taastrup

[17]. Jensen F.M., Falzon B.G., Ankersen J., Stang H., (2005), "Structural testing and numerical simulation of a 34m composite wind turbine blade", Composite Structures, October 2005, https://www.sciencedirect.com/science/article/abs/pii/S0263822306002480
[18]. Gurit, (2020), "Ampreg 22 – Epoxy Laminating System", https://pdf.directindustry.com/pdf/gurit/ampreg-22-epoxy-laminating-system-v17/37817-79061.html
[19]. International Electrotechnical Commission, (2015), "International Standard: Wind turbines – Part 23: Full-scale structural testing of rotor blades", IEC 61400-23 Edition 1.0
[20]. Wood Mackenzie, (2019), "Unplanned wind turbine repairs to cost industry $8 billion+ in 2019", Wood Mackenzie: One minute read press release https://www.woodmac.com/press-releases/unplanned-wind-turbine-repairs-to-cost-industry-$8-billion-in-2019/
[21]. M. Quaresimin, M. Ricotta, (2005), "Fatigue behaviour and damage evolution of single lap bonded joints in composite material", University of Padova, Italy, 2005

[22]. A.J. Kinloch, (1997), "Adhesives in engineering", University of London, 1997.

Bladena
Banestrøget 13, 1
DK-2630 Taastrup

Taastrup, June 28, 2023

Appendix B Gomez A., Berggreen C., (2023), "Cohesive Zone Modelling to predict crack growth under fatigue loading", *DTU Department of Civil and Mechanical* - WORK IN PROGRESS

Cohesive zone modelling to predict crack growth under fatigue loading

A. Gomez, C. Berggreen

Technical University of Denmark, DK-2800 Kgs. Lyngby, Denmark

eagme@dtu.dk

Abstract. This draft manuscript presents the development of numerical models based on Cohesive Zone Modelling, to analyse quasi-static and fatigue crack propagation in the adhesive interface between fibre laminates and structural epoxy adhesive in a wind turbine blade 3rd shear-web connection to the trailing edge panels. Fracture characterization experiments using the Double Cantilever Beam with Unequal Bending Moments (DCB-UBM) specimen are performed, and results are used to determine different modelling parameters, such as the mixed-mode cohesive laws and fatigue damage parameters for cohesive crack propagation. The developed numerical model is compared and validated against sub-component testing on two different scale levels, using a Modified Tear Test (MTT) specimen geometry with simplified geometry and loading, and a more complex geometry sub-component specimen with a simplified Shear Web Disbond Test (SBDT), also retrofitted into a 34 m long wind turbine blade section at a higher scale-level, see Figure 1. The work is carried out as part of the CORTIR-II project, funded by the Danish Ministry of Energy.

1. Introduction

A wind turbine's blade comprises an outer aerodynamic shell, and shear webs that join the upwind and downwind sections of that shell. These webs are bonded to one another at the leading and trailing edges. Typically, a blade has two shear webs that run almost the entire length of the blade from the transition zone (denoted by the shear web fish mouth).

Due to the increasing global demand for clean and sustainable energy, wind turbines have become more prevalent over the past few decades. This surge in interest has driven manufacturers to develop larger wind turbines that are more efficient and cost-effective than their smaller counterparts. However, the continuous increase in size has resulted in higher loads, which require additional strengthening. This challenge is addressed by adding a third shear web to the blades. Unfortunately, this leads to a failure phenomenon known as shear web disbonding, where cracks in the adhesive interface between the shear web footing and spar cap propagate due to large deflections in the aerodynamic skins near the third shear web. If the crack grows too large this could compromise the integrity of the blade, eventually causing the wind turbine to collapse.

Bladena
Banestrøget 13, 1
DK-2630 Taastrup

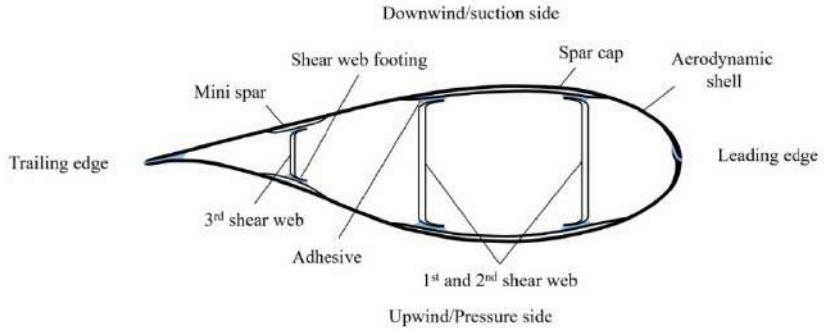

Figure. Example of a wind turbine blade section

To address this issue, Bladena has partnered with wind turbine owners and operators, The Technical University of Denmark (DTU) and Aalborg University, to initiate the CORTIR-II project, which aims to investigate shear web disbonding in large wind turbine blades. The project is divided into four stages to investigate the issue in detail. It starts with characterisation and moves on to sub-component testing with more detail, before finally conducting large-scale testing.

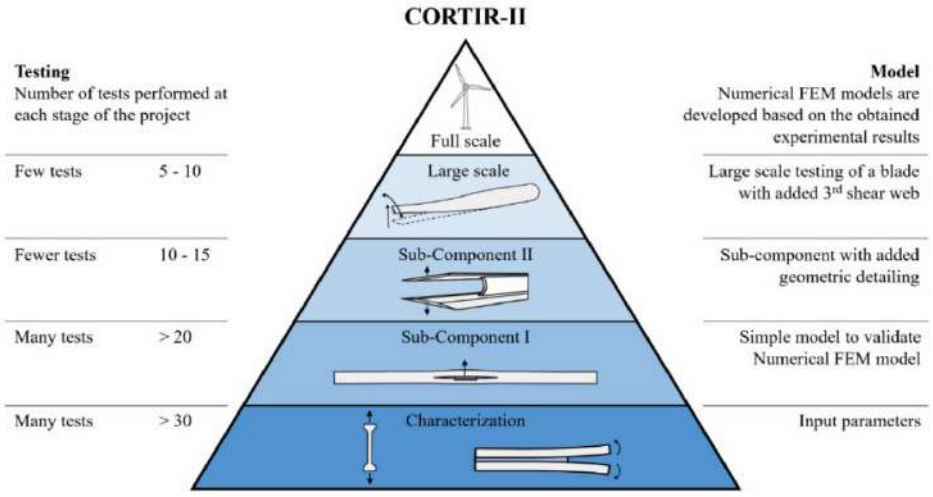

Figure. Building block approach for Cortir II project

This work presents the current state of part of this project which is focused on developing numerical models based on Cohesive Zone Modelling to analyze quasi-static and fatigue crack propagation in the adhesive interface between fibre laminates and structural epoxy adhesive. The modelling parameters are determined from results obtained in an experimental campaign using the Double Cantilever Beam under Uneven Bending Moments (DCB-UBM) testing, which is a novel test

Bladena
Banestrøget 13, 1
DK-2630 Taastrup

method for mixed-mode fracture characterization. The developed numerical modelling will be validated using the Modified Tear Test (MTT), and sub-component testing method.

2. Cohesive zone modelling

The fibre bridging phenomenon occurs when the fibres in neighbouring laminate plies bridge the debonding plane, serving as crack arrestors. As a result, the debonding resistance and inter-laminar fracture toughness are enhanced. Non-linear fracture mechanics such as the computation of the J integral is often necessary to study problems that involve extensive bridging. However since no analytical solution is available it is necessary to determine a bridging/cohesive law from experimental testing (Sørensen, 2022)

Cohesive Zone Modeling (CZM) is a useful tool for predicting and modelling crack initiation and propagation in situations where Linear Elastic Fracture Mechanics (LEFM) cannot be assumed and over the last 20 years, researchers have increasingly shown interest in CZM applied in finite element modelling.

CZM incorporates nonlinear behaviour into the material's constitutive response, making it capable of predicting failure in ductile crack problems with significant process zones. The length of the process zone is critical in the fracture process as it can indicate if the fracture is ductile or brittle. If the process zone is much smaller than other characteristic lengths of the specimen such as crack length, specimen length, width, etc., brittle fracture occurs. CZM has previously been applied to the study of various failures in concrete, metals, composites, bi-material interfaces, and adhesive joints.

In the CZM the fracture process zone (FPZ) is substituted with a cohesive region, where the exchange of stress between the two artificial crack surfaces is defined using a relationship between the traction and separation of the FPZ.

2.1. Traction separation law

In practical FEA analysis, the cohesive zone model is commonly applied by a single layer of cohesive elements, which are placed along the expected path of crack propagation. Each element follows a constitutive response which uses a strength-based criterion to predict the onset of damage and the degradation of the material stiffness.

Commercial FEA software packages such as Abaqus required a set of parameters that govern the traction-separation law:

- K_{nn}, the stiffness of the cohesive element in the linear elastic regime
- Traction t_n^0 (or separation δ_n^0) for damage onset
- G_n^c, fracture energy release rate
- Damage evolution law

There are multiple traction-separation laws used in literature. Some of the most common bi-linear, exponential, and trapezoidal behaviors although non-standard (tabulated) laws computed directly from experimental tests are also employed.

Bladena
Banestrøget 13, 1
DK-2630 Taastrup

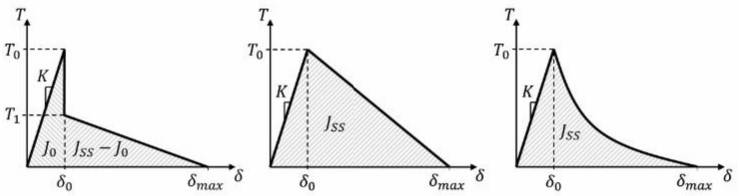

Figure 1. Different traction-separation functions evaluated in the current project

CZM also allows studying the fracture process when mode-mixity is present using the power law fracture criterion based on the energy required to propagate a crack under pure mode conditions.

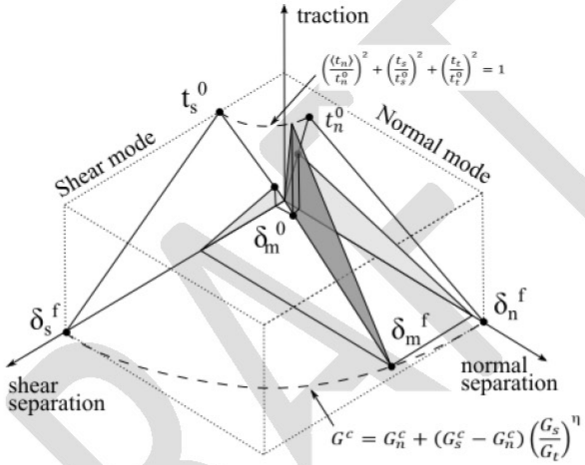

Figure 2. Mixed mode traction-separation and criteria for damage onset and failure

It is generally agreed that the key parameters of traction-separation law should be obtained from direct experimental testing although some other studies have used calibration methods based on trial-and-error search or a combination of both.

One of the aims of the present study is to obtain traction-separation law directly from an experimental fracture test following the methodology proposed by [1] which involves the computation of the J integral and the measurement of the crack tip separation in a quasi-static DCB-UBM test. In this method, the traction-separation law is obtained by the partial differentiation of the fracture resistance J_R and the crack tip separation. In pure mode I (opening) for example, the traction-separation law can be obtained by:

$$t_n(\delta_n, \delta_t) = \frac{\delta(J_R(\delta_n, \delta_t))}{\delta(\delta_n)}$$

While for model II (shear):

$$t_t(\delta_n, \delta_t) = \frac{\delta(J_R(\delta_n, \delta_t))}{\delta(\delta_t)}$$

2.2. Modelling fatigue with cohesive zone models

Bladena
Banestrøget 13, 1
DK-2630 Taastrup

A novel approach to consider the deterioration of materials caused by fatigue loading is to degrade the traction-separation response as the number of cycles increases. In this approach the cohesive strength and critical fracture energy decrease following a fatigue damage evolution law of the following form [2]:

$$\frac{\Delta D_i}{\Delta N} = \alpha(\varepsilon_{max} - \varepsilon_{th})^{\beta}$$

where ΔD_i is the damage accumulated over ΔN cycles while α, β and ε_{th} are material parameters which must be calibrated against experimental results.

ε_{max} is the maximum overall strain defined in terms of the normal and shear strains in the cohesive element:

$$\varepsilon_{max} = \frac{\varepsilon_n}{2} + \sqrt{\left(\frac{\varepsilon_n}{2}\right)^2 + \left(\frac{\varepsilon_t}{2}\right)^2}$$

In the beginning, the damage parameter D_i for each element within the cohesive zone is set to zero and damage accumulation in the load cycle only occurs if the maximum overall strain is larger than the threshold value ε_{th}. The damage parameter which ranges between 0 and 1 can be computed after each load cycle (or set of load cycles) and update the effective traction and energy release rate used to estimate the crack propagation.

$$t_i = D_i t_0$$
$$G_{c,i} = D_i G_{C,0}$$

Where i denotes the current time step, and t_0 and $G_{C,0}$ is the initial cohesive strength and fracture energy respectively.

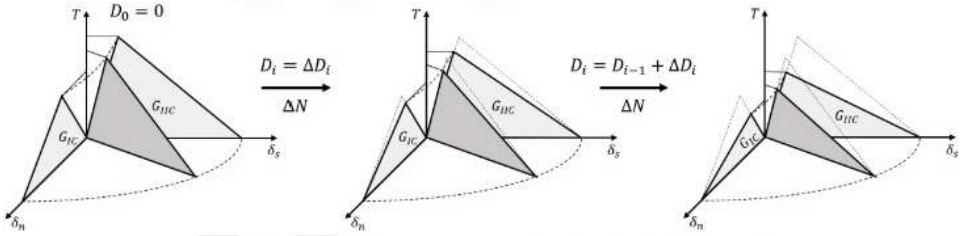

Figure 3. Evolution of the traction-separation law due to fatigue cycles

3. DCB-UBM tests (Level -0)

Three different experimental tests are carried out to study the quasi-static and fatigue debonding phenomena. An initial characterization test campaign with the Double Cantilever Beam under Uneven Bending Moments (DCB-UBM) test method, which aims to assess the critical fracture parameters such as energy release rates and cohesive damage law under various mixed-mode loading conditions.

For validation purposes, two additional tests are proposed: First, a new test approach, referred to as the Modified Tear Test (MTT), derived from the Sandwich Tear Test (STT), is specifically designed for Sub-component level 1 testing. And second a setup for a simplified shear web geometry (Sub-

Bladena
Banestrøget 13, 1
DK-2630 Taastrup

component II testing) which considers the knowledge acquired from conducting the aforementioned tests and includes external load conditions closer to those encountered in a full-scale blade scenario.

3.1. DCB-UBM test set-up

The DCB-UBM test, as introduced by [1], involves the application of uneven bending moments to the crack flanks' tips in the specimen. By adjusting the ratio of these applied moments, crack propagation can occur under different fracture modes, ranging from pure mode I to pure mode II. This characteristic of DCB-UBM tests eliminates the requirement for three separate characterization tests, making it an appealing and efficient method for fracture characterization in general. Since the load applied to the specimen solely originates from bending moments, both the energy release rate and the mode-mixity angle remain unaffected by the crack length. Another advantage of employing pure bending moments for loading, particularly in cases involving large process zones, is that the applied load remains constant throughout the entire process zone.

The tests were performed in a DCB-UBM servo-hydraulic testing machine developed in-house at DTU. Pure moments on the edges of the specimen are applied by two separate servo-hydraulic torsional actuators. To maintain pure moment loading, it is required to minimize any in-plane and out-of-plane forces so the carriage plates are mounted on raceway shafts, utilizing track rollers.

The DCB-UBM specimens have overall dimensions of 450 mm x 30 mm x 18.2 mm and are made from two GFRP laminates bonded on top of each other (Figure 4). The specimens were manufactured by Global Wind Services by hand layup, manufacturing the laminates separately and then bonding them together by secondary bonding and vacuum bag consolidation. A 50 mm pre-crack is made by inserting a Teflon film during the consolidation process. The top laminate is made from a triaxial/biaxial fabric with the following stacking sequence 8[45/0/-45/ ±45] and an average cured thickness of 10 mm. The bottom laminate is made from biaxial fabric with a stacking sequence of 10[±45] and an average cured thickness of 6.8 mm.

The specimen configuration was determined through preliminary studies, utilizing CSDE analysis to calculate mode mixity angles and energy release rates. Due to the significant tip rotations, potential laminate failure and limited fixation options, two 6 mm thick steel reinforcement plates (doublers) were bonded to the top and bottom surfaces of the specimen using an epoxy structural adhesive. Additionally, a clamp was installed to prevent crack initiation between the specimen and plates.

Bladena
Banestrøget 13, 1
DK-2630 Taastrup

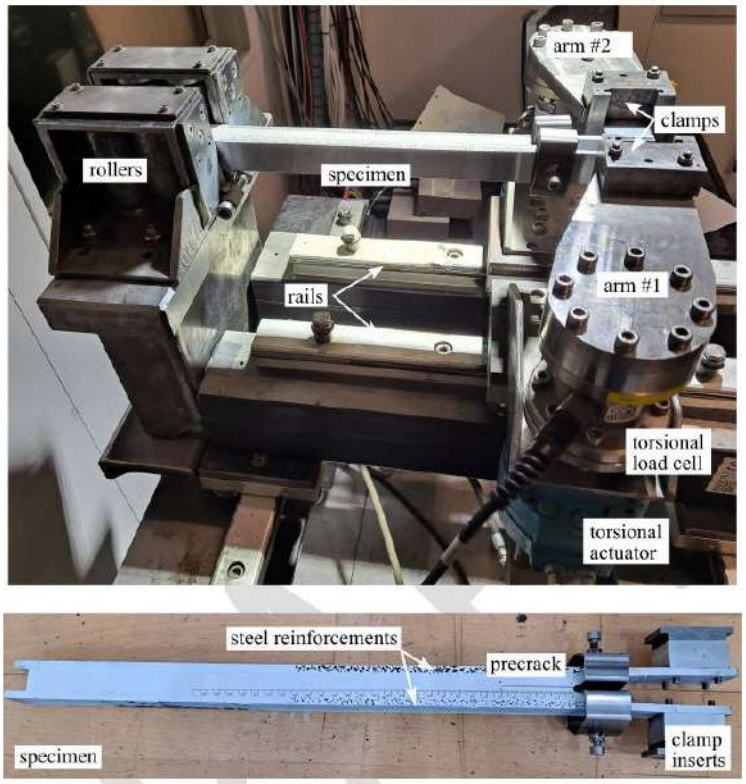

Figure 4. DCB-UBM test set-up and specimen

The moments and rotations of the loading arms are directly obtained from the sensors of the test machine through the MTS data acquisition system. Additional data such as crack length and separation of the crack tip is collected using the iMetrum Non-Contact Video Measurement live-tracking software. The displacements of the tracked crack flanks, which are utilized to determine the phase angle, should be closely monitored near the crack tip and adjacent to the crack flank surface. To ensure precise tracking of crack propagation, it was crucial to accurately define the crack path and initial crack length. Additionally, to enhance the image correlation results, all specimens' surfaces were meticulously sanded and painted white, and speckle patterns were applied to the steel plates.

Quasi-static and fatigue tests were conducted to establish the key parameters of the cohesive laws. The moment ratios (MR = M2/M1) were determined to obtain phase angles of 0° (MR=-1.2), 15° (MR = -0.714), 30° (MR = -0.4). Phase angles larger than 30° (including Mode II) were not considered due to limitations in the load capacity of the testing machine. At least three specimens were tested for each phase angle.

The crack propagation rate in fatigue is assessed under various load levels equivalent to 60%, 70%, and 80% of the critical energy release rate at the same moment ratios studied in the quasi-static test. Due to the presence of a time delay, the actual moment ratio between arms 1 and 2 underestimates the moment on arm 2. Thus, the input moment ratio used for fatigue analysis needs to be slightly calibrated from the desired value. Additionally due to the longitudinal movement of the specimens and

Bladena
Banestrøget 13, 1
DK-2630 Taastrup

the opening/closing of the crack flanks the live-tracking features are unfit for this test. Consequently, the crack length is manually measured from the video frames.

3.2. DCB-UBM tests results

It was discovered that the interface failure was primarily controlled by extensive fibre bridging on a large scale, both during testing under quasi-static and fatigue loading. Fibre bridging was observed across all tested modes, with its greatest impact occurring in the proximity of mode I.

The presence of voids within the adhesive, as well as variations in the thickness of the bondline, and internal preload caused by imbalanced composite face-sheets, result in variations in the fracture resistance of each specimen. In some instances, the crack deviated towards the opposite interface from the location of the pre-crack, forming a kink. Besides this, most experiments were successfully performed.

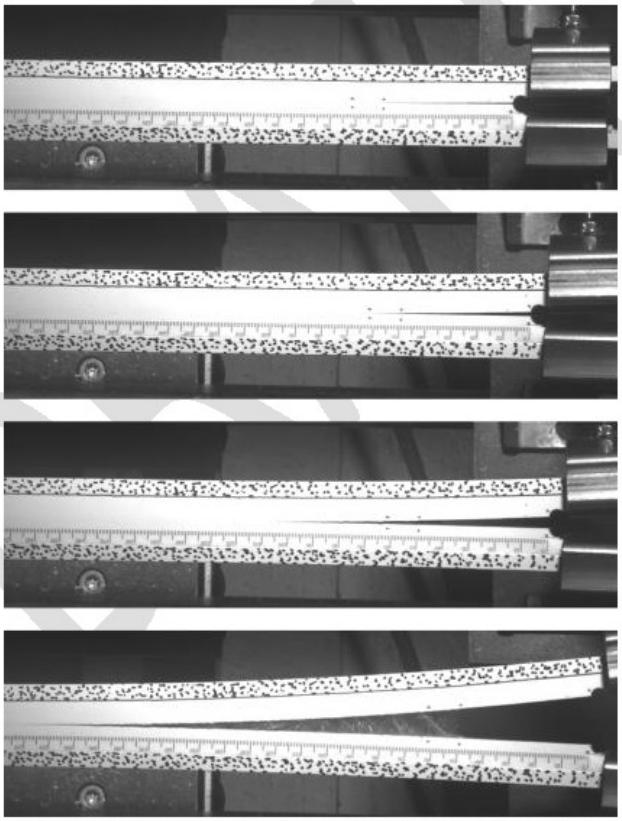

Figure 5. Photograms showing crack propagation in a quasi-static DCB-UBM test (M2/M1=-1.2). Fully developed fibre bridging is visible in the last photogram

The obtained data was post-processed in MATLAB to obtain the fracture resistance R-curve by computing the J-integral at each instant taking as input the applied moments (M1 and M2), crack

Bladena
Banestrøget 13, 1
DK-2630 Taastrup

extension (Δa) and tip-end separation (δ_n , δ_t). The J-integral formulation presented by [3] was modified to account for the asymmetry due to the difference in the thickness and material properties of the top and bottom laminates. The close-form solution is described in detail in Appendix A:

An example of the post-processed data is shown in Figure 6.

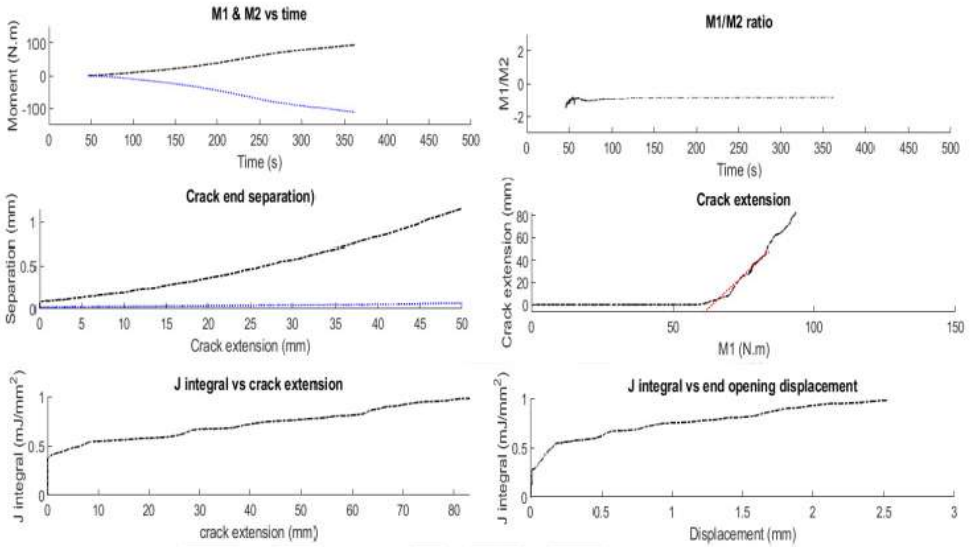

Figure 6. Example of postprocessed data for MR = -1.2 (Ψ = 7.4°)

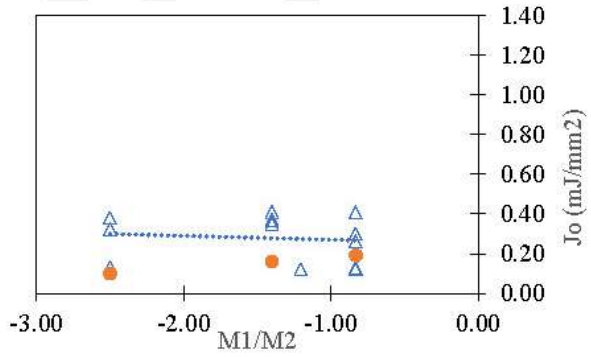

Bladena
Banestrøget 13, 1
DK-2630 Taastrup

Taastrup, June 28, 2023

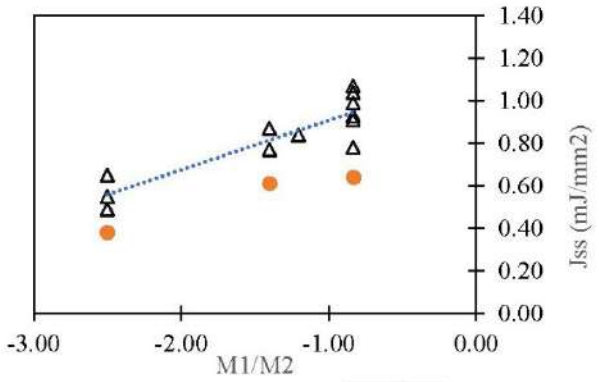

The fracture resistance for crack initiation (J_o) and steady-state crack growth (J_{ss}) are compared at different phase angles. Results show that J_{ss} is larger than J_o for all studied phase angles which shows the relevance of the fibre-bridging toughening effect, particularly at low phase angles.

To obtain the cohesive traction-separation laws it is convenient to graph the fracture resistance for each test as a function of the normal crack end opening and the tangential crack end opening. Due to the high data scattering surface polynomial fitting is utilized, yielding a parametric function that enables the estimation of the traction-separation cohesive laws.

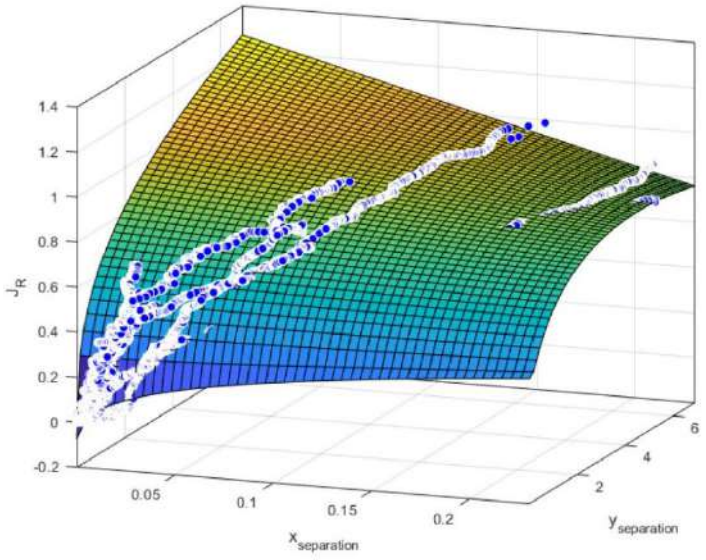

Bladena
Banestrøget 13, 1
DK-2630 Taastrup

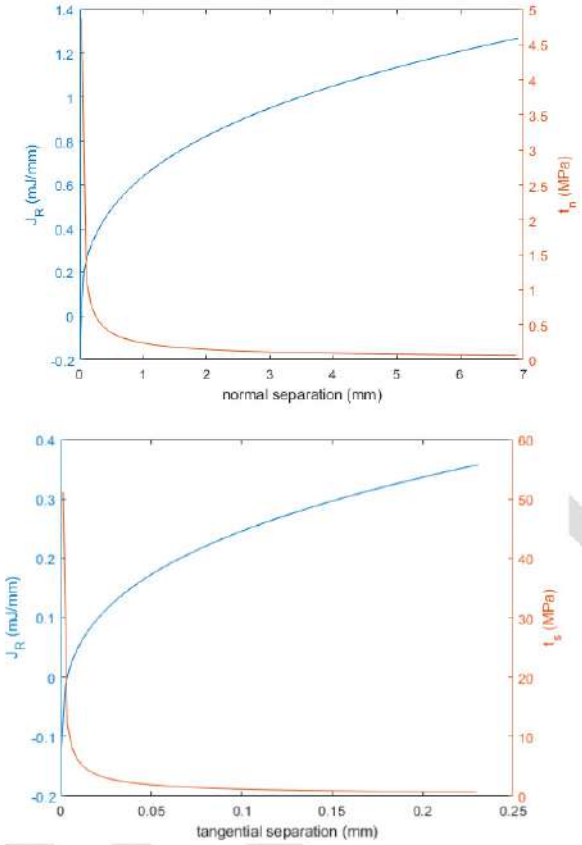

Figure 7. Cohesive traction separation law obtained analytically from quasi-static DCB-UBM tests. a) Mode I, b) Mode II

Fatigue crack propagation rates were assessed at different moment ratios and the parameters of the material-specific Paris' law equation were determined through curve fitting.

Bladena
Banestrøget 13, 1
DK-2630 Taastrup

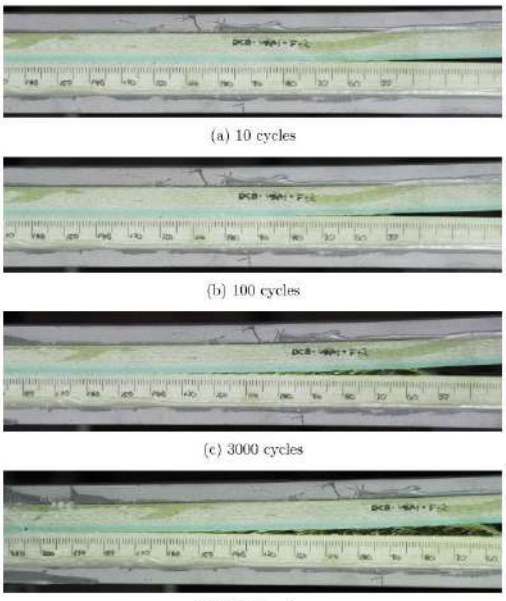

(a) 10 cycles

(b) 100 cycles

(c) 3000 cycles

(d) 15000 cycles

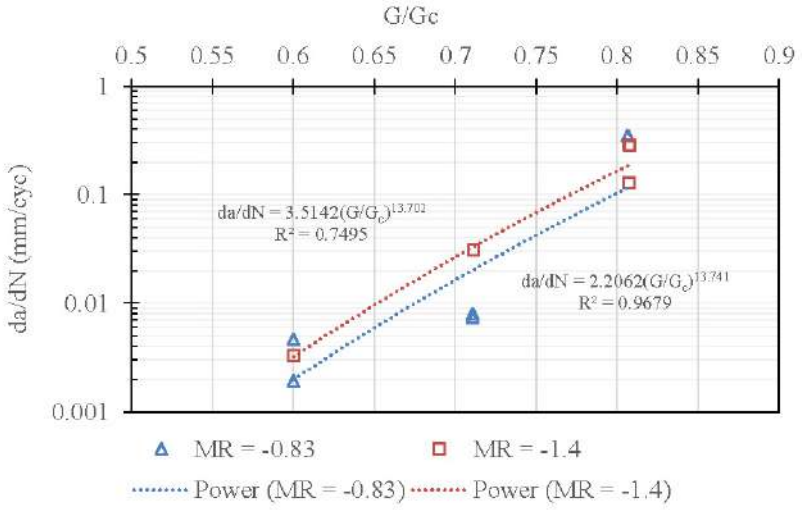

3.3. FEA models of DCB-UBM tests.

Two independent FEA models were created in Abaqus 2021 to replicate the experimental DCB-UBM test explained in the previous subsection. However, each model was generated with a different purpose.

Bladena
Banestrøget 13, 1
DK-2630 Taastrup

The first model is based on Linear Elastic Fracture Mechanics (LEFM) particularly the method of Crack Surface Displacement Extrapolation (CSDE) method. The purpose of this model is to initially determine the geometric configurations of the test specimens, based on different criteria such as expected energy release rate and phase angle, DCB-UBM machine loading range, and yielding of the doubler plates. Additionally, results from this FEA model are used to find the ratio of arm moments M2/M1 to be used in the DCB-UBM experimental test to obtain a desired phase angle Ψ.

On the other hand, the second FEA model uses a cohesive zone model to predict damage initiation and crack propagation both in quasi-static and fatigue loading. For this purpose, cohesive elements COH2D4 are used together with element deletion to track crack propagation in two alternative ways: when damage initiates (damage variable D>0) and complete failure occurs (D=1).

In the case of fatigue loading the fatigue damage criteria are described in section 2.2. was implemented in a VUSDFLD Fortran subroutine. Since modelling fatigue loading cycle-by-cycle is computationally non-practical a different strategy is implemented in which bundles of multiple load cycles are represented into a single period.

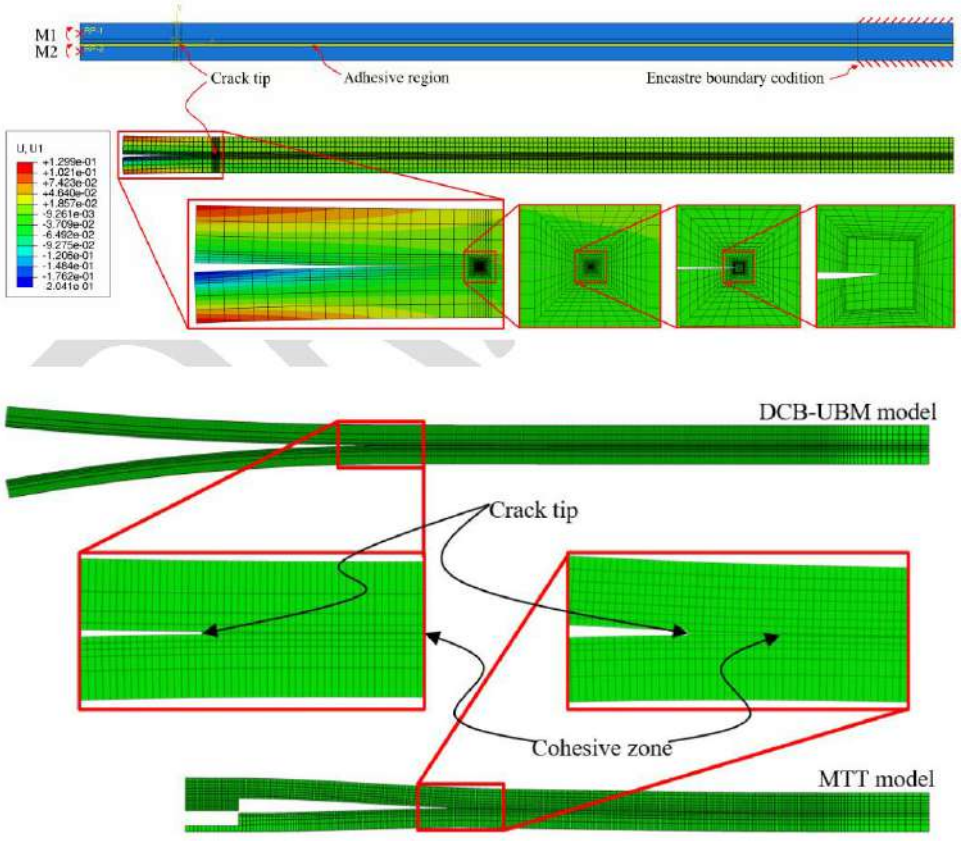

Figure 8. FEA model using cohesive zone model. a) DCB-UBM test, b) MTT test. Source: [4]

Bladena
Banestrøget 13, 1
DK-2630 Taastrup

To construct the geometry the laminates and adhesive layer are modelled as separate geometric bodies joined at the interface using a tie constraint. The laminates are modelled as orthotropic materials while the adhesive material and the material for the doubler stiffeners an isotropic materials. Material properties for the laminates were obtained by coupon testing during Cortir I project and are summarized in Table 1. The models are mesh using 2D CPE8R, quadratic plane strain elements with reduced integration. In the case of the CSDE model, the crack tip has a very fine mesh to capture with accuracy the flank displacements for the CSDE extrapolation. While in the case of the cohesive zone FEA model the mesh size in the bondline is less fine but it is kept constant to ensure continuity in the element size as the crack propagates.

Property	Units	Top laminate	Bottom laminate
E_1	MPa	20159	10067
E_2	MPa	10126	9597
G_{12}	MPa	8705	8962
G_{21}	MPa	9365	9229
Xt_1	MPa	262	119
Xt_2	MPa	90	102
S_{12}	MPa	75	203
S_{21}	MPa	129	206
v_{12}	-	0.44	0.54
v_{21}	-	0.03	0.56

Table 1. Laminate material properties

Two concentrated moments (M_1 and M_2) are applied over reference points located on the left side of the specimen which are coupled to the specimen's external surface by a rigid body constraint. The specimen is restrained on the opposite side simulating the rollers

3.4. FEA model results of DCB-UBM test

The CSDE model provides an approximate prediction of the fracture energy release rate (G) and phase angle (Ψ) for a given moment ratio (M1/M2). This estimation is used to determine the maximum possible phase angle within the DCB-UBM machine loading capability. From this analysis, it is also clear that the difference in thickness and material between the top and bottom laminates creates an asymmetry in the fracture behaviour. As a result pure mode I don't not occur at M1/M2 = 1, but instead, it is expected to occur at M1/M2 = -1.16.

Bladena
Banestrøget 13, 1
DK-2630 Taastrup

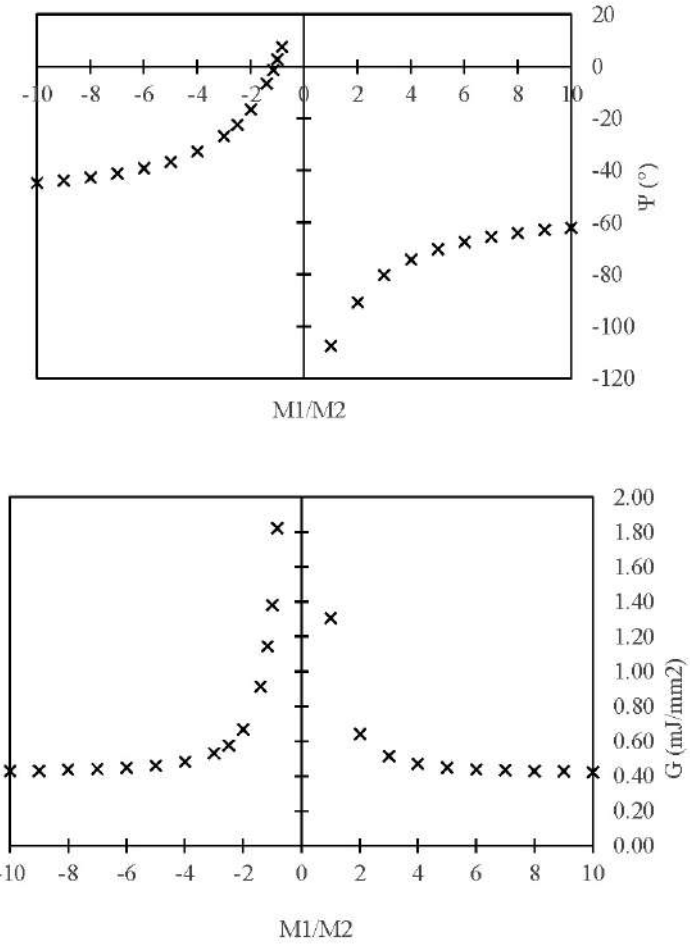

Figure 9. CSDE prediction of energy release rate (a) and phase angle (b) for different moment ratios. Values of G are estimated assuming a limit moment arm (M1 = 120 N.m), due to DCB-UBM machine load cell admisible range.

Bladena
Banestrøget 13, 1
DK-2630 Taastrup

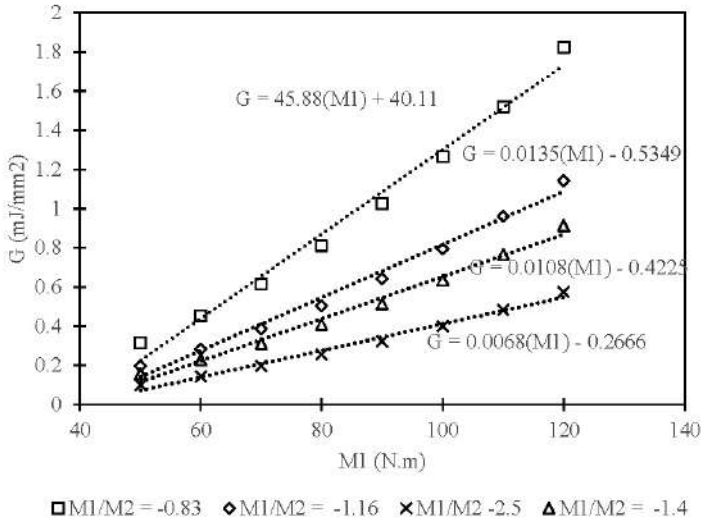

Figure 10. CSDE predictions of G as a function of moment arm M1 for a given moment ratio. Information used for test preparation.

The quasi-static cohesive FEA model is primarily used to calibrate and validate the cohesive law estimated analytically from the experimental test results. Due to the large data scattering in the experimental results, the calibration procedure requires a clear measure of the error between experimental and FEA results. Since the primary objective of a cohesive law approach is to be able to predict both crack initiation and crack growth rate, both measurements are used to define a combined mean squared error of the following form:

$$e_{comb}(\%) = \sqrt{\left(\frac{M_1^{FEA} - M_1^{EXP}}{M_1^{EXP}}\right)^2 + \left(\frac{\frac{da}{dM_1}^{FEA} - \frac{da}{dM_1}^{EXP}}{\frac{da}{dM_1}^{EXP}}\right)^2} * 100$$

Where M_1 and $\frac{da}{dM_1}$ are the moment in arm 1 and crack growth rate at crack initiation onset and the superscripts FEA and EXP mean FEA results and experimental results respectively.

Bladena
Banestrøget 13, 1
DK-2630 Taastrup

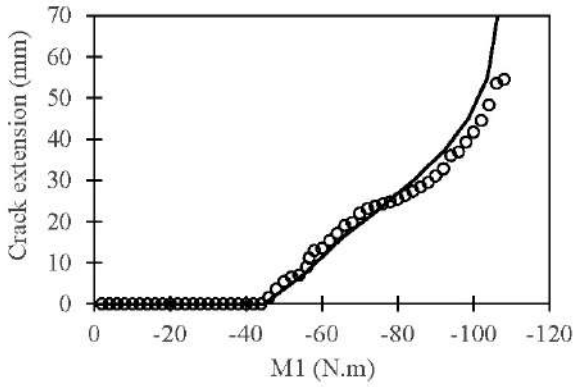

Figure 11. Comparison between FEA and experimental results for a quasi-static DCB-UBM test

SPACE INTENTIONALLY LEFT IN BLACK (COHESIVE LAW CALIBRATION USING RELATIVE ERROR)

Similarly, the fatigue cohesive FEA model is used to calibrate the fatigue damage parameters α, β, ε_{th} trying to fit the FEA results to the experimental DCB-UBM test data.

SPACE INTENTIONALLY LEFT IN BLACK (PARAMETERS CALIBRATION)

4. MTT tests (Level – 1)

The objective of conducting sub-component level I tests is to replicate the real-life occurrence of shear web disbonding using simple test setups and specimens. While it is commonly assumed that shear web disbonding occurs under mode I condition, the presence of mode mixes can occur due to membrane forces in aerodynamic shells or the torsional shear induced by global loading on wind turbine blades. To explore how these factors might influence the problem, it was necessary to devise a test method in which mode mixity varies during crack propagation. Additionally, this test enables the validation of the cohesive law parameters across different mode mixity angles that are estimated in level-0 of the building block approach.

The Modified Tear Test (MTT) is derived from the Sandwich Tear Test (STT) method, which is utilized to examine interface failure between the adhesive and laminates while considering different mixed mode conditions. In this test, the upper laminate is pulled upwards, so the in-plane membrane forces escalate significantly as the test proceeds. This escalation leads to an increase in the mode-mixity angle, transitioning from an initial pure mode I opening condition to mixed fracture modes (opening and shear). A new test set-up was developed and produced, incorporating some components from a previous STT setup while redesigning and manufacturing the majority of them specifically for this test.

Bladena
Banestrøget 13, 1
DK-2630 Taastrup

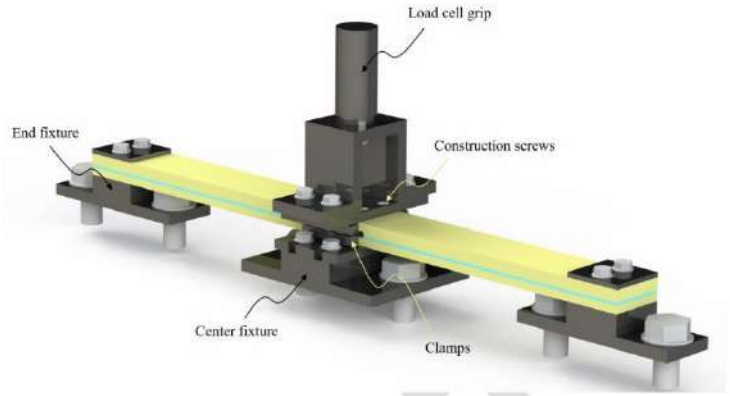

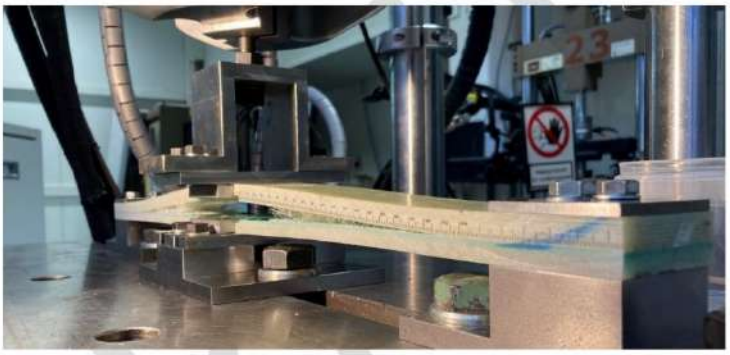

Figure 12. MTT test setup. Source: [4]

The specimen materials, layup and manufacturing method are the same as for the DCB-UBM test. However, the specimen length is 600 mm while the width is 50 mm. Additionally, the MTT specimen pre-crack is located in the mid-section and has a length of 150 mm. For conducting the tests, a four-column MTS 810 test machine is utilized with a load cell of 100 kN. Quasi-static tests are initially performed to measure the compliance of the structure as well as the load for crack initiation. This test is carried out under displacement control since it promotes stable crack propagation by allowing the energy release rate to increase with the extension of the crack length. Fatigue tests were carried out under load control at three different maximum loads. These values we selected above the critical load for crack initiation obtained in the quasi-static test while the minimum load was set to 20%-30% of the maximum load. The crack extension in the quasi-static tests was measured by the iMetrum tracking software while for the fatigue tests crack opening/closing presented a challenge for this method and visual measurements from the video frames were taken instead.

4.1. MTT tests results

During MTT testing, the fatigue crack propagation exhibited a predominantly stable behaviour, even under high loads. As a result, the MTT produced highly predictable and consistent results across all fatigue tests. The impact of the experimental setup on the test results seems minimal.

Bladena
Banestrøget 13, 1
DK-2630 Taastrup

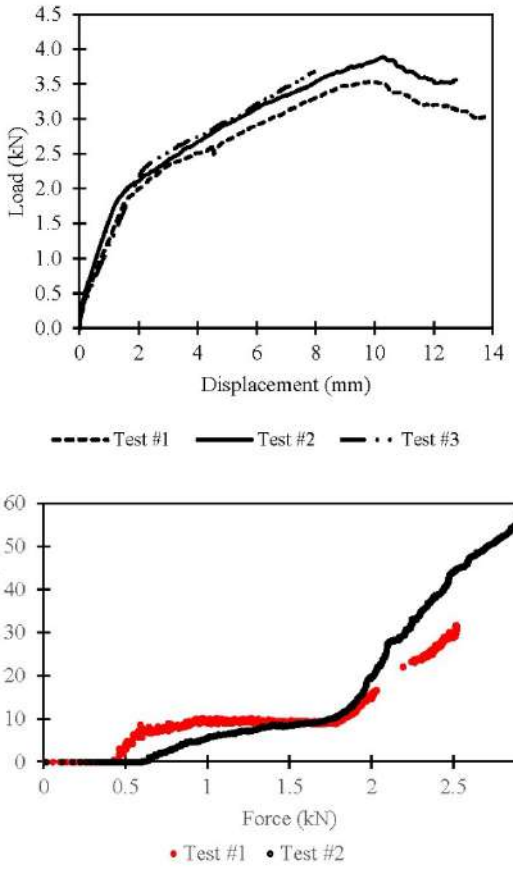

Figure 13. Quasi-static MTT test results. a) Load vs displacement curve, b) crack extension vs load

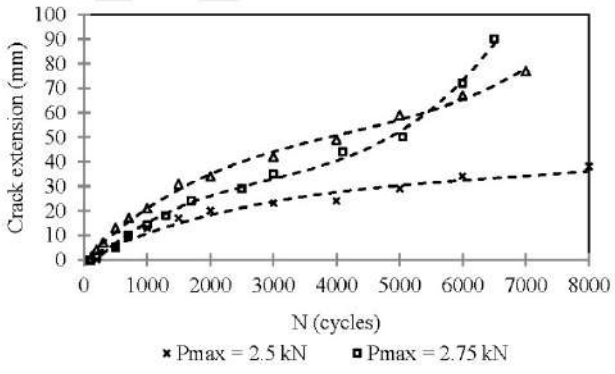

Figure 14. Fatigue MTT test result. Crack length vs Number of cycles

Bladena
Banestrøget 13, 1
DK-2630 Taastrup

4.2. FEA models of MTT test

Two different FEA models were prepared to validate the MTT test. The first is a 2D model like the one described for DCB-UBM but with the corresponding boundary conditions for MTT test (Figure 8) while the second model is a simplified quarter symmetry 3D FEA model. For both models symmetry boundary conditions are applied in the midsection. The end fixture is modelled by restraining all degrees of freedom in the top and bottom surfaces of the left side. The same boundary condition is applied to the bottom surface over the central section to model the clamps in the centre fixture.

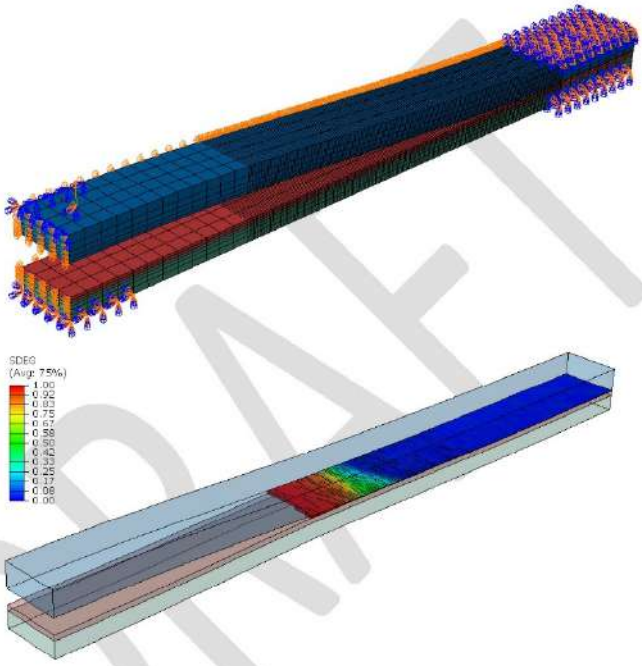

Figure 15. 3D FEA model for MTT test. a) boundary conditions, b) example of crack growth extension and damage variable

SPACE INTENTIONALLY LEFT IN BLACK (FEA MODEL VALIDATION RESULTS)

4.3. Subcomponent Level II test – Shear Web Disbond Test (SWDT)

The purpose of the subcomponent level II test is to study the simplified geometry and loading conditions of a real shear web installed in a wind turbine blade paying particular attention to the bonded interface between the shear web flange and the blade outer shell. The test specimens are a representative simplified version of only half the shear web and a portion of the outer shell to which it is bonded with a 50 mm long pre-crack inserted in the bondline. Four specimens were manufactured by *Global Wind Services*, manufacturing the shear webs and laminates separately by hand layup and

Bladena
Banestrøget 13, 1
DK-2630 Taastrup

vacuum bag consolidation and then joining them by secondary bonding. The top laminate and shear web flange have the same composite layup as those used in level-I and level-II tests.

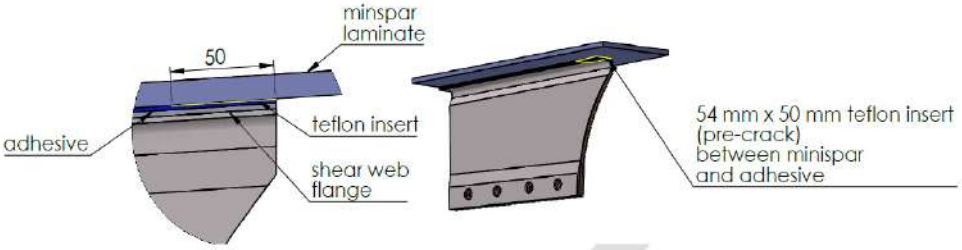

The complexity of the test required the design and manufacturing of a whole load transfer assembly which is briefly described below:

A force is applied to the upper shell laminate simulating a distortion of the blade cross-section while the bottom of the half-shear web is clamped to the test bed. A link with rod end bearings on both sides transfers the load from the clevis to the grip assembly and avoids the transfer of moments into the specimens due to the translation/rotation of the pinpoint. Since torsional coupling is expected due to the asymmetry of the shear web section, it was necessary to design a mechanism to adjust the lateral location of the pinpoint for load application (Figure 16).

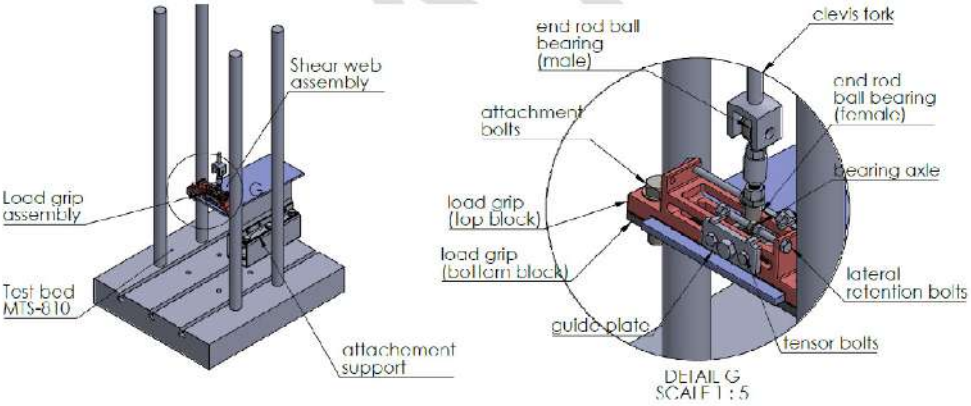

Figure 16. SWD test set-up and load transfer assembly

Bladena
Banestrøget 13, 1
DK-2630 Taastrup

Figure 17. SWDT specimens and load transfer assembly

For conducting the tests, a four-column MTS 810 test machine is utilized with a 10 kN load cell which is placed directly in the linkage connecting the clevis and the grip assembly.

Initially, one specimen is tested under quasi-static load with displacement control to measure the compliance of the structure as well as the load for crack initiation. The location of the load transfer pinpoint is carefully selected to avoid excessive rotation of the top laminate and try to reproduce the strain levels encountered in a full-scale blade. For this purpose, it is decided to install strain gauges in the corners of the specimen (over the straight side). Additionally, the rotation of the top laminate is measured through a camera located in front of the specimen. Crack propagation is measured visually by placing a camera to the side and underneath the specimen and using a metric tape attached to the specimen. The specimen is painted in white to increase contrast with the crack tip and direct light is applied to ensure no shadows will compromise the measurements.

Similarly, three specimens were tested in fatigue under load control with fluctuating loads with a load ratio R=0.2. The same maximum load was applied in all cases and its magnitude was selected above the critical load for crack initiation obtained in the quasi-static test (still to choose a percentage 60%, 70% or 80% depending on the crack growth rate)

SPACE INTENTIONALLY LEFT IN BLACK FOR FUTURE UPDATES

4.4. FEA model of the SWDT test

A fully detailed 3D FEA model was implemented in Abaqus to study the behaviour of the shear web specimen and the fracture behaviour at the bondline in both quasi-static and fatigue loading conditions. A detailed 3D CAD model was initially prepared in SolidWorks which includes the most important geometrical features of the specimens (e.g. shear web flange, local reinforcements, core-laminate transition, laminate drop-offs, insert holes). Each part was imported independently in Abaqus as a 3D solid and modelled with 8-node linear brick elements with reduced integration (C3D8R). Contact interactions and tie constraints were applied between interacting bodies as required. The bondline is modelled using cohesive elements using the same traction separation in the same way as in the previous scale levels (levels 0 and 1). The external force is applied as a point load over a reference point and transmitted to a region of the top laminate using rigid-body constraint. The same technique is used to react the structure to the inserts located in the root.

Bladena
Banestrøget 13, 1
DK-2630 Taastrup

Taastrup, June 28, 2023

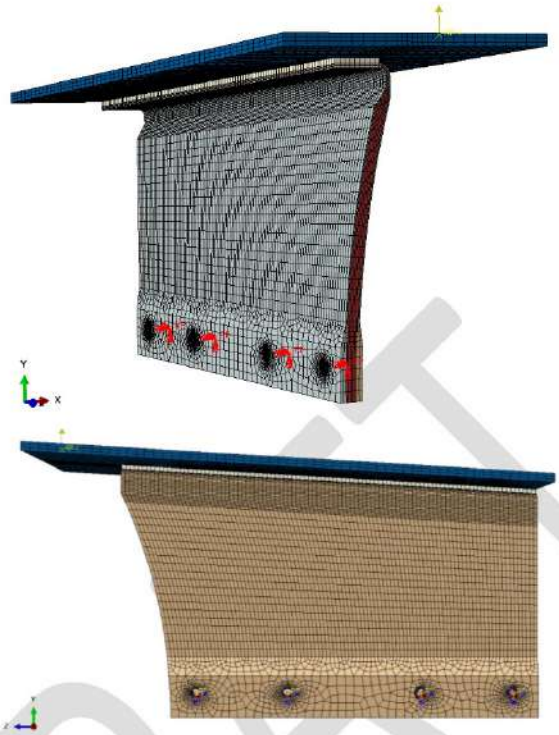

Figure 18. Detailed 3D FEA model of the SWD test. a) Isometric view, b) Left view

This FEA model was initially used to predict the elastic response of the specimen under the expected load levels. Preliminary results suggest that torsional coupling occurs due to the asymmetry of the shear web flange and could generate an asymmetric crack onset in the bondline. This information was used in the design of the test set-up. Future research tasks with this FEA model include the validation of quasi-static and fatigue tests.

SPACE INTENTIONALLY LEFT IN BLACK (FEA MODEL RESULTS)

Conclusions

At the moment of writing the current report, most of the research activities are either completed or near complete. However, due to unforeseen time and logistical delays, some research activities are still ongoing. Therefore this section presents only partial conclusions to day results.

A building block methodology has been implemented to study crack initiation and propagation in bonded joints of glass fibre laminates and epoxy adhesives, typically encountered in shear webs in wind turbine blades. The phenomena have been studied from an experimental and numerical perspective at three different levels of complexity starting from fracture DCB-UBM characterization

Bladena
Banestrøget 13, 1
DK-2630 Taastrup

tests followed by two subcomponent validation fracture tests, MTT test and SWDT (Shear Web Disbond Test).

Experimental study:

Quasi-static DCB-UBM tests show that the crack propagation behaviour is dominated by a large fibre bridging zone in the bondline which acts as a toughening mechanism, particularly at small mode mixites phase angles (mode I, and opening-dominated fracture). Measurements of the fracture resistance (R) through the J integral show a large increase from the crack onset (J_o) to steady-state propagation with fully developed bridging (J_{ss}). The measurements of the fracture energy release rate were highly scattered probably due to differences in the bondline thickness, void content and curvature (due to the asymmetry of top and bottom laminates). Since the manufacturing method, materials and sizes used in the specimen fabrication are representative of those employed in the wind industry for similar applications similar deviations in the fracture resistance could be expected in operating wind turbine blades. It was also possible to determine the traction-separation law directly from the experiments for a range of phase angles by measuring crack tip displacements and applying the data reduction proposed by Sorensen together with nonlinear surface extrapolation. However, due to limitations in the test machine, it was not possible to test phase angles near mode II and therefore the validity of the predicted fracture behaviour in this region is still unknown.

Fatigue DCB-UBM tests were found to be challenging due to large machine vibrations, and difficulties to set the PDI controller, for this reason, a limited amount of tests were performed. Besides this, it was possible to measure the crack growth rate at different loading conditions and results suggest that the crack growth rate (da/dN) follows a power law function which depends on the mode mixity. Due to the large data scattering it was not possible to estimate this dependency quantitatively with enough reliability so additional tests are carried out at this moment to reduce the statistical uncertainty of the curve fitting estimation.

For the subcomponent level-1 (MTT) test a new experimental set-up was successfully designed, manufactured and implemented. Results were highly repeatable with some data scattering due to minor variations in the tested specimens. However, the force required to trigger crack growth showed some variability which could be related to the large scattering in the fracture resistance for crack onset (J_o) observed in DCB-UBM tests. Quasi-static MTT test allowed us to observe the crack growth transition between pure mode I (opening) towards higher mixed modes (combined opening and shear). It was observed that at small crack lengths where mode I is dominant, fibre bridging is present and the bondline fracture resistance is large, however as the crack extends fibre bridging is less dominant and shear tearing starts playing a larger role. This shear tearing is associated with a higher crack growth rate (in terms of applied force) which in turn seems to be associated with the lower fracture resistance observed in the DCB-UBM experiments for mixed-mode fracture.

The fatigue MTT test shows that the crack growth rate is highly dependent on the load range. As expected tests performed at higher maximum cyclic loads show larger crack growth rates. It was also observed that the crack growth rate is not constant but decreases as the crack extends, something that occurs since the tests were load controlled and therefore the effective crack tip forces are lower as the crack grows.

For the subcomponent level-2 test (SWDT) a new experimental set-up was successfully designed, manufactured and implemented to study a simplified geometry and loading conditions of a real shear web installed in a wind turbine blade paying particular attention to the bonded interface between the shear web flange and the blade outer shell. Quasi-static and fatigue testing are currently ongoing.

Bladena
Banestrøget 13, 1
DK-2630 Taastrup

Taastrup, June 28, 2023

Numerical study:

Multiple FEA models have been developed in parallel to the experimental tests at all scale levels of the testing pyramid. These FEA models are used to predict the fracture behaviour of the bondline under the corresponding levels of complexity validating FEA results against experimental ones. Since the fracture phenomena are dominated by fibre bridging the main focus of this work is the cohesive zone modelling method although linear elastic fracture mechanics (LEFM) have been used on a few occasions for preliminary analysis to support the design of experiments.

For characterization (DCB-UBM) tests, 2D finite element analysis (FEA) models have been developed to calibrate the cohesive traction-separation laws obtained in experimental tests. Different traction separation laws have been tested and compared including bi-linear, exponential, and tabulated (based on traction separation curves obtained in experiments). For mode, I tabulated cohesive-law can capture with accuracy crack onset and crack propagation behaviour. However, minor calibrations were required for some cohesive law parameters using trial-and-error search methods.

A novel approach to model fatigue crack growth in the bondline was successfully implemented through a material user subroutine in which a fatigue damage law is coupled with the cycle jump technique. The same 2D FEA model was used to calibrate the fatigue damage law parameters using trial-and-error search methods. Preliminary results suggest that the proposed approach can capture with some accuracy the crack growth rate. However further improvements could be achieved by extending the formulation of the fatigue damage law to account for mix mode dependency and applying more advanced calibration methods.

Validation of the proposed quasi-static and fatigue cohesive damage models was carried out initially through the subcomponent MTT tests. Both 2D and 3D FEA models were developed under the same test set-up conditions. Correlation between FEA results and experimental data shows that stiffness, crack growth initiation, and early crack growth are well captured by the quasi-static FEA models. However, critical failure is overpredicted, probably due to inadequate estimates of the mixed mode fracture behaviour, yielding much more conservative estimates than in real life. MTT fatigue models have also been successfully developed and the validation against experimental data is still ongoing.

For the SWDT test a detailed 3D FEA model was implemented to study the behaviour of the tested shear web specimen under a more complex load and geometrical details. This model has been successfully used to design the experimental test set-up by predicting the structural response of the shear web specimen. Preliminary results indicate that torsional coupling due to the asymmetry of the shear web profile could induce non-homogeneous peeling forces over the bondline leading to an asymmetric crack onset. No direct comparison has been made yet between FEA results and experimental results since the last ones are still not available.

Acknowledgements

The authors would also like to acknowledge the Danish Ministry of Energy for funding this work as well as all the Cortir-II team members for their support during the different project activities, in particular, Find Moholt, Tamas Nagy (Bladena), Yu-Huan Lin (Global wind services), Daniel Søndergaard, Rasmus Thomasen (DTU Construct).

Bladena
Banestrøget 13, 1
DK-2630 Taastrup

Taastrup, June 28, 2023

Reference

[1] Sørensen, "Cohesive laws for assessment of materials failure: Theory, experimental methods and application," *Downloaded from orbit.dtu.dk*, 2022, Accessed: Jun. 14, 2022. [Online]. Available: www.risoe.dtu.dk.

[2] H. Khoramishad, A. D. Crocombe, K. B. Katnam, and I. A. Ashcroft, "Predicting fatigue damage in adhesively bonded joints using a cohesive zone model," *Int. J. Fatigue*, vol. 32, no. 7, pp. 1146–1158, Jul. 2010, doi: 10.1016/J.IJFATIGUE.2009.12.013.

[3] V. Saseendran, C. Berggreen, and L. A. Carlsson, "Fracture Mechanics Analysis of Reinforced DCB Sandwich Debond Specimen Loaded by Moments," doi: 10.2514/1.J056039.

[4] D. S. Rasmussen, "Cohesive web joints in wind turbine blades Using cohesive zone modelling to predict crack growth under fatigue loading," 2022. [Online]. Available: www.mek.dtu.dk.

Bladena
Banestrøget 13, 1
DK-2630 Taastrup

Taastrup, June 28, 2023

Appendix A. Modified J-integral calculation for an asymmetric DCB Sandwich Debond Specimen Loaded by Moments.

This appendix shows the modifications to the close analytical solution proposed in [3] to account for a DCB specimen with different laminate thickness and material properties. The methodology to obtain the J integral as well as the mathematical notation are kept the same. However, minor changes in the stiffness coefficients were required to account for the difference in material stiffness.

Coupling and bending stiffness (A, B, D) for the debonded and substrate beam sections

For the debonded beam:

$$y_0 = 0 - (H_1/2)$$
$$y_1 = h_r - (H_1/2)$$
$$y_2 = h_r + h_u - (H_1/2)$$
$$A_d = E_u(y_1 - y_0) + E_r(y_2 - y_1)$$
$$B_d = \frac{1}{2}(E_u\,(y_1^2 - y_0^2) + E_r(y_2^2 - y_1^2))$$
$$D_d = \frac{1}{3}(E_u\,(y_1^3 - y_0^3) + E_r(y_2^3 - y_1^3))$$
$$e_d = \frac{B_d}{A_d}$$

For the substrate beam:

$$y_0 = 0 - (H_2/2)$$
$$y_1 = h_r - (H_2/2)$$
$$y_2 = h_r + h\_fl - (H_2/2)$$
$$y_3 = h_r + h\_fl + h\_c - (H_2/2)$$

$$A_s = E_r(y_1 - y_0) + E_{fl}(y_2 - y_1) + E_c(y_3 - y_2)$$
$$B_s = \frac{1}{2}(E_r\,(y_1^2 - y_0^2) + E_{fl}(y_2^2 - y_1^2) + E_c(y_3^2 - y_2^2))$$
$$D_s = \frac{1}{3}(E_r\,(y_1^3 - y_0^3) + E_{fl}(y_2^3 - y_1^3) + E_c(y_3^3 - y_2^3))$$
$$e_s = B_s/A_s$$

$$E_{dhd} = (E_r\,h_r) + (E_{fu}h_{fu})$$

$$E_{shs} = (E_r h_r) + (E_{fl}h_{fl}) + (E_c h_c)$$

V1, V2 and V3 parameters

$$V_1 = \frac{1}{2}(E_c\,h_c + E_{fl}h_{fl} + E_r h_r)$$

Bladena
Banestrøget 13, 1
DK-2630 Taastrup

Taastrup, June 28, 2023

$$V_2 = \left(\frac{E_c}{2}\right)\left(\left(\frac{h_c}{12}\right)((3\,h_r^2) + (6h_r h_{fl}) + (3h_{fl}^2) + (h_c^2)) - (e_s\,h_c)\,(h_{fl} + h_r) + (e_s^2)\,h_c\right) + (E_{fl}/2)\,((h_{fl}/12)\,((3\,h_r^2) - (6\,h_r\,h_c) + (h_{fl}^2) + (3h_c^2)) - (e_s\,h_{fl})\,(h_r - h_c) + (e_s^2)\,h_{fl}) + \left(\frac{E_r}{2}\right)\left(\left(\frac{h_r}{12}\right)((h_r^2) + (6h_{fl}h_c) + (3h_{fl}^2) + (3h_c^2)) + (e_s h_r)\,(h_c + h_{fl}) + (e_s^2)\,h_r\right)$$

Modified V3 term:

$$V_3 = E_c\,[(-h_c/2)\,(h_{fl} + h_r) + e_s\,h_c] - E_{fl}\,[(h_{fl}/2)\,(h_r - h_c) - e_s\,h_{fl}] + E_r\,[(h_r/2)\,(h_c + h_{fl}) + e_s\,h_r]$$

$$\delta_1 = H_1/2 + e_d$$
$$\delta_2 = H_2/2 + e_s$$
$$\delta_1' = H_1 - \delta_1$$
$$\Delta_1 = H_3 - \delta_1' - \delta_2$$
$$L^1 = \frac{1}{2}\,(E_r\,hr + E_u\,h_u)$$

$$L^2 = \left(\frac{E_r}{2}\right)\left(\left(\frac{hr}{12}\right)((3\,h_u^2) + (hr^2)) - (e_d\,h_u\,h_r) + (e_d^2)h_r\right) + \left(\frac{E_u}{2}\right)((h_u/12)\,((h_u^2) + (3\,h_r^2)) + (e_d\,h_u\,h_r) + (e_d^2\,h_u))$$

$$L_3 = -(E_r\,((h_u\,h_r/2) - (e_d\,h_r)) - E_u\,((h_u\,h_r/2) + (e_d\,h_u)))$$

$$H_d = D_d - (B_d^2/A_d)$$
$$H_s = D_s - (B_s^2/A_s)$$

Factors used to obtain G

$$a_1 = (L_1/(E_{dhd}^2)) + (V_1/(E_{shs}^2)) + (V_2(\Delta_1^2)/(H_s^2)) + (V_3(\Delta_1)/(E_{shs} * H_s))$$

$$a_2 = (L_2/(H_d^2)) + (V_2/(H_s^2))$$

$$a_3 = ((-2V^2\Delta_1)/(H_s^2)) - L_3/(E_{dhd}H_d) - V_3/(E_{shs}H_s)$$

Base beam:

$$y_0 = -H_3/2$$
$$y_1 = y_0 + h_r$$
$$y_2 = y_1 + h_{fl}$$
$$y_3 = y_2 + h_c$$
$$y_4 = y_3 + h_u$$
$$y_5 = y_4 + h_r$$

$$A_b = E_r\,(y_1 - y_0) + E_{fl}\,(y_2 - y_1) + E_c\,(y_3 - y_2) + E_u\,(y_4 - y_3) + E_r\,(y_5 - y_4)$$

Bladena
Banestrøget 13, 1
DK-2630 Taastrup

$$B_b = \frac{1}{2}\left(E_r\left(y_1^2 - y_0^2\right) + E_{fl}\left(y_2^2 - y_1^2\right) + E_c\left(y_3^2 - y_2^2\right) + E_u\left(y_4^2 - y_3^2\right) + E_r\left(y_5^2 - y_4^2\right)\right)$$

$$D_b = \frac{1}{3}\left(E_r\left(y_1^3 - y_0^3\right) + E_{fl}\left(y_2^3 - y_1^3\right) + E_c\left(y_3^3 - y_2^3\right) + E_u\left(y_4^3 - y_3^3\right) + E_r\left(y_5^3 - y_4^3\right)\right)$$

$$e = \frac{B_b}{A_b}$$

c2 and c3 parameters defined for asymmetric beam.

$$c_2 = \left(E_u\left(\left(y_4^2\right) - \left(y_3^2\right)\right) + E_r\left(\left(y_5^2\right) - \left(y_4^2\right)\right)\right) / \left(2\left(D_b - B_b^2/A_b\right)\right)$$

$$c_3 = \left(E_u\left(\frac{1}{2}y_4^2 - \frac{1}{2}y_3^2 + (y_4 - y_3)(-y_3 - e)\right) + E_r\left(\frac{1}{2}y_5^2 - \frac{1}{2}y_4^2 + (y_5 - y_4)(y_3 - e)\right)\right) / \left(D_b - \frac{B_b^2}{A_b}\right)$$

J-integral calculation:

$$M_d = M_1 - c_3 M_3$$
$$P = -c_2 M_3$$
$$J = a_1 P^2 + a^2 M_d^2 - a^3 P M_d$$

Bladena
Banestrøget 13, 1
DK-2630 Taastrup

Taastrup, June 28, 2023

Appendix C Waldbjørn J.P., Berggreen C., Ahmed S., Nagy T., (2023), "Large-scale fatigue testing of a retrofitted 3rd shear web in a SSP34M wind turbine blade", *DTU Department of Civil and Mechanical Engineering and Bladena*

Large-scale fatigue testing of a retrofitted 3rd shear web in a 34m wind turbine blade section

J. P. Waldbjørn[1], C. Berggreen[1], S. Ahmed[2] and T. Nagy[2]

[1]Technical University of Denmark, Department of Civil and Mechanical Engineering, Koppels Allé, Building 404, 2800 Kongens Lyngby, Denmark
[2]Bladena ApS, Banestrøget 13, 2630 Taastrup, Denmark

Email: jpwa@dtu.dk

Abstract. Utilizing a fatigue-rated multi-axial strong-floor based test rig, the effect of a retro-fitted fish-mouth third shear-web geometry detail located within the double-curved trailing edge sandwich panels are evaluated in an inner 15m root section from a 34m wind turbine blade manufactured by SSP Technology. From previous research, a load configuration is identified, capable of triggering the breathing/pumping deformations in the trailing edge panels within the root and transition zone, which will drive the propagation on the shear-web disbonding mechanism. Investigation and evaluation of the shear web disbonding and associated mitigation are acquired through strain gauges, wire potentiometer and digital image correlation (DIC) measurements inside the root section.

1. Introduction

Wind turbines are progressively used as a substitute to fossil fuel energy resources, enhancing the demand for larger and more efficient wind turbine blades [1]. With an increasing size of wind turbine blades a growing need is emerging to address structural challenges due to higher utilization of the structural capacity – especially within the root, transition zone and max. chord region [2]. Among one of the increasingly encountered in-field damages found in wind turbine blades, regardless of blade make and model, is transverse cracks within the transition zone and max chord region [3]. This hypothesis is from an operational perspective, supported by the wind turbine owners (WTOs), who are reporting a gradually increasing amount of transverse cracks. Believed to be the root cause of these transverse cracks are, among others, the out-of-plane deformations in the large double curved trailing edge aerodynamic sandwich panels on the pressure side within the max-chord region and towards the root – referred to here as breathing [4]. These deformations, often referred to as 3D longitudinal

out-of-plane bending, leads to critical bending stresses in the area, where the trailing edge panels are connected/kinked into the stiff cylindrical root section. To mitigate these critical bending stresses in the trailing edge panels, a retro-fitted fish-mouth third shear-web geometry detail is installed in the inner 15m section of a 34m wind turbine blade designed and built by SSP Technology – referred to here as the root section, connecting the inner skin of the trailing edge pressure side (PS) and suction side (SS) sandwich panels through an adhesive bond line.

The scope of this paper is to investigate and evaluate the overall structural integrity of the retro-fitted third shear-web along with the mitigation associated with the shear web disbonding mechanism triggered by breathing of the trailing edge panels. This breathing is primary triggered by i) the edgewise dominated loading governed by gravity which have to be carried by the large curved sandwich panels combined with ii) a torsional moment around the longitudinal axis of the wind turbine blade, generated by the flap-wise deformation, which acts as an in-plane eccentricity to the edgewise load [5]. Utilizing a fatigue rated multi-axial test rig, this dual degree-of-freedom (dof) load configuration is applied to the free end of the root section through a servo-hydraulic loading arrangement. Magnitude and phase shift of the dual dof load configuration capable of triggering the maximum breathing deformations in the trailing edge panels within the root and transition zone, which will drive the propagation on the shear-web disbonding mechanism, are identified in accordance to [6]. Investigation and evaluation of the shear web disbonding and associated mitigation are acquired through internally mounted strain gauges, wire potentiometer and digital image correlation (DIC) measurements.

2. Test specimen and installed third shear-web

The 34m wind turbine blade used in this application was used on a 1.5MW wind turbine. General blade dimensions and properties are outlined in table 1.

Table 1: Overall blade dimensions

Type	SSP34
Blade net weight	4500 [kg]
Weight of the truncated blade	2800 [kg]
Original length of blade	34 [m]
Length of the truncated blade	15 [m]
Diameter at the root	1.8 [m]
Max chord position from blade root	7.0 [m]
Chord position from blade root	2.7 [m]
Structural configuration	Box bar construction
Sandwich panel locations	Leading edge (LE) and trailing edge (TE)

The blade is produced using a high quality production method including pre-impregnated fibre mats without autoclave [7]. To ensure adequate resin quantity towards the core and mold a high resin content (HRC) is selected for the laminates next to those regions. The resin system used is unknown to the authors, but according to SSP Technology a modification of the Ampreg 22 epoxy laminating system [8] was used. At a distance of 4m from the root ($z = 4$m) a retrofitted fish-mouth third shear-web is installed connecting the inner skin trailing edge PS and SS sandwich panels through a single lap adhesive bond line according to figure 1. The main body of the shear-web consists of a sandwich structure with 10mm core material covered by 4 layers of bi-axial ($\pm 45^{o}$) glass fibre on both sides (equivalent to a skin thickness of approximately 2mm).

Bladena
Banestrøget 13, 1
DK-2630 Taastrup

Taastrup, June 28, 2023

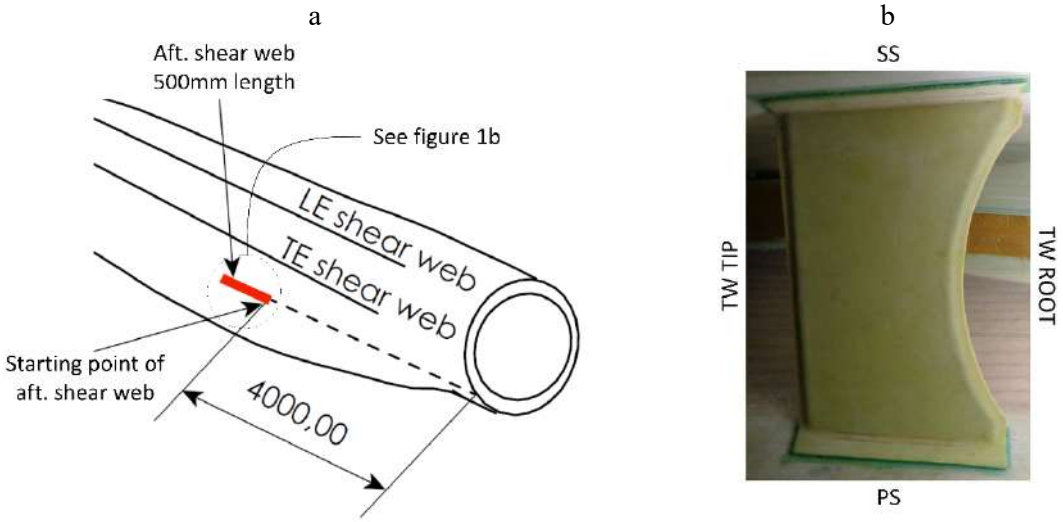

Figure 1: Retro-fitted 3rd shear-web including: a) overall position and b) photographic illustration of installation

3. Experimental test setup

A fatigue rated multi-axial test rig for structural assessment of the root section has been established on the strong floor [6]. A 3D illustration of the test setup including the loading arrangement and clamped support is presented in figure 2.

Bladena
Banestrøget 13, 1
DK-2630 Taastrup

Taastrup, June 28, 2023

a

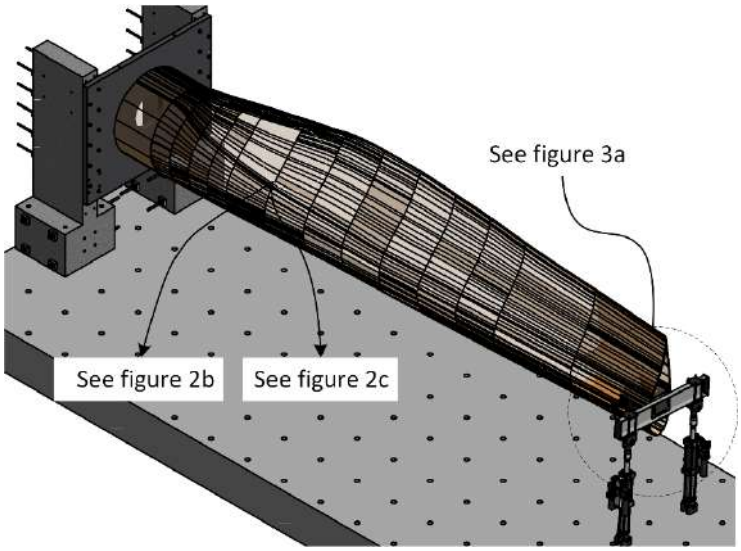

b

c

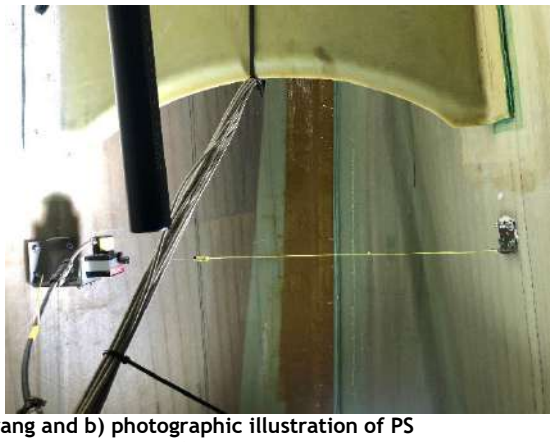

Figure 2: Test setup including: a) the multi-axial loading arrang and b) photographic illustration of PS bondline monitored by DIC and c) photographic illustration of aft - mounted wire potentiometer

The fatigue rated clamped support of the root section is achieved using a mobile strong wall consisting of i) two strong floor mounted concrete towers and ii) steel plate attached to the concrete towers. The root section is center mounted on the steel plate. All connections are established using pretensioned threaded bars. Pretensioning levels of critical connections are monitored with "donut" load cells of the type: K-181/N550-G31 by Lorenz Messtechnik GmbH.

The complete loading arrangement – consisting of two structural actuators – is capable of applying discrete loads at the free end of the root section comprising two dofs including: edgewise load (F_y) along with a torsional moment (M_z) around the longitudinal axis of the blade. Actuator specifications are provided in figure 3b. A servo hydraulic control system is operated in load control through a Proportional Integral Derivative (PID) controller of the type MTS FlexTest using the MTS 793 software suite. The coupling between the control point, located in the center of the load carrying box girder and the corresponding force of each actuator, are

Bladena
Banestrøget 13, 1
DK-2630 Taastrup

defined through the MTS 793.15 Degree of Freedom Control software following the assumption of rigid body motion. Related coordinate system and notation is presented in figure 3b.

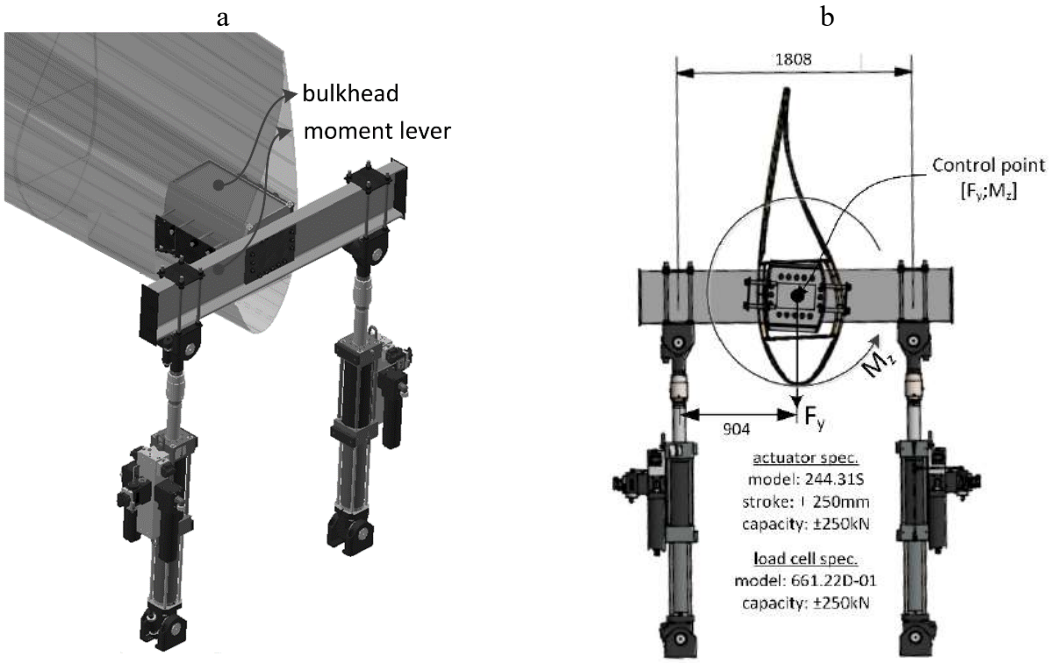

Figure 3: Load train including: a) detailed 3D illustration of multi-axial loading arrangement and b) active coordinate system and notation

The load is transferred to the free end of the root section through a steel bulkhead, which is extending 750mm into the free end of the load carrying box girder, and fixed to the inner surface of both spar caps using glue and threaded bars. To avoid critical peeling stresses in the adhesive bondline connecting the trailing edge (TE) and leading edge (LE) panels with the spar caps, the free end of the root section is fully constraint against in-plane distortion by closing the cross section with plates of over laminated plywood. The tip end region – covering approximately 2m towards the root – is over laminated using GFRP fabrics. This over-lamination is solely added to avoid structural damages generated by the localized loading induces trough the steel box girder. The zone of interest – referred to here as the gauge zone – is located around the trailing edge panels at the transition zone. According to a numerical study further described in [6], no influence on the breathing response were detected within the gauge zone. The loading arrangement and clamped support presented in figure 2a constitutes a fatigue rated structural test setup with an edgewise load capacity of 100kN and moment capacity of 100kNm around the longitudinal axis.

Investigation and evaluation of the retrofitted fish-mouth third shear-web disbonding and associated mitigation is monitored through strain gauges, wire potentiometer and DIC. Strain gauge rosettes are applied on all four corners of the shear-web to monitor the overall transfer of shear loads from the connected trailing edge panels. These strain gauge rosettes are applied at the surface towards the trailing edge of the shear-web and labelled according to figure 4a. The breathing of the large double curved trailing edge aerodynamic sandwich panels are monitored through a wire potentiometer located 200mm aft of the shear-web according to figure 2c. The out-of-plane and in-plane deformation of the PS single lap adhesive bonde-line relative to the adjacent trailing edge sandwich panel (see figure 4b) is monitored through full-field 3D DIC system of

Bladena
Banestrøget 13, 1
DK-2630 Taastrup

the type: ARAMIS 12M supplied by Gesellschaft für Optische Messtechnik GmbH (GOM GmbH). The camera setup and performance are presented in table 2.

Table 2: Setup and performance of the 3D-DIC system

Technique	3D DIC system
used	32x32px
Subset	6px (81% overlap)
Shift	
Camera	Dalsa Falcon2 FA-80-12M1H with an 12-bit,
Field of View	4096x3072pixel
Measurement	CMOS (6.00µm
points	pitch) censor and 24mm lens
	380x305mm
	(4050x2882px)
	9531
Displacement	
Spatial	1.62mm, 17px
resolution	
Resolution	0.045mm, 0.48px
In plane	0.090mm, 0.96px
Out of plane	

By tracking the out-of-plane (z-direction) and in-plane (xy-direction) deformation of the three points located at the PS single lap adhesive bonde-line (named: shear-web) and adjacent pressure side trailing edge panel (named: ps panel) through DIC, the relative peak/valley deformation is derived.

Bladena
Banestrøget 13, 1
DK-2630 Taastrup

Taastrup, June 28, 2023

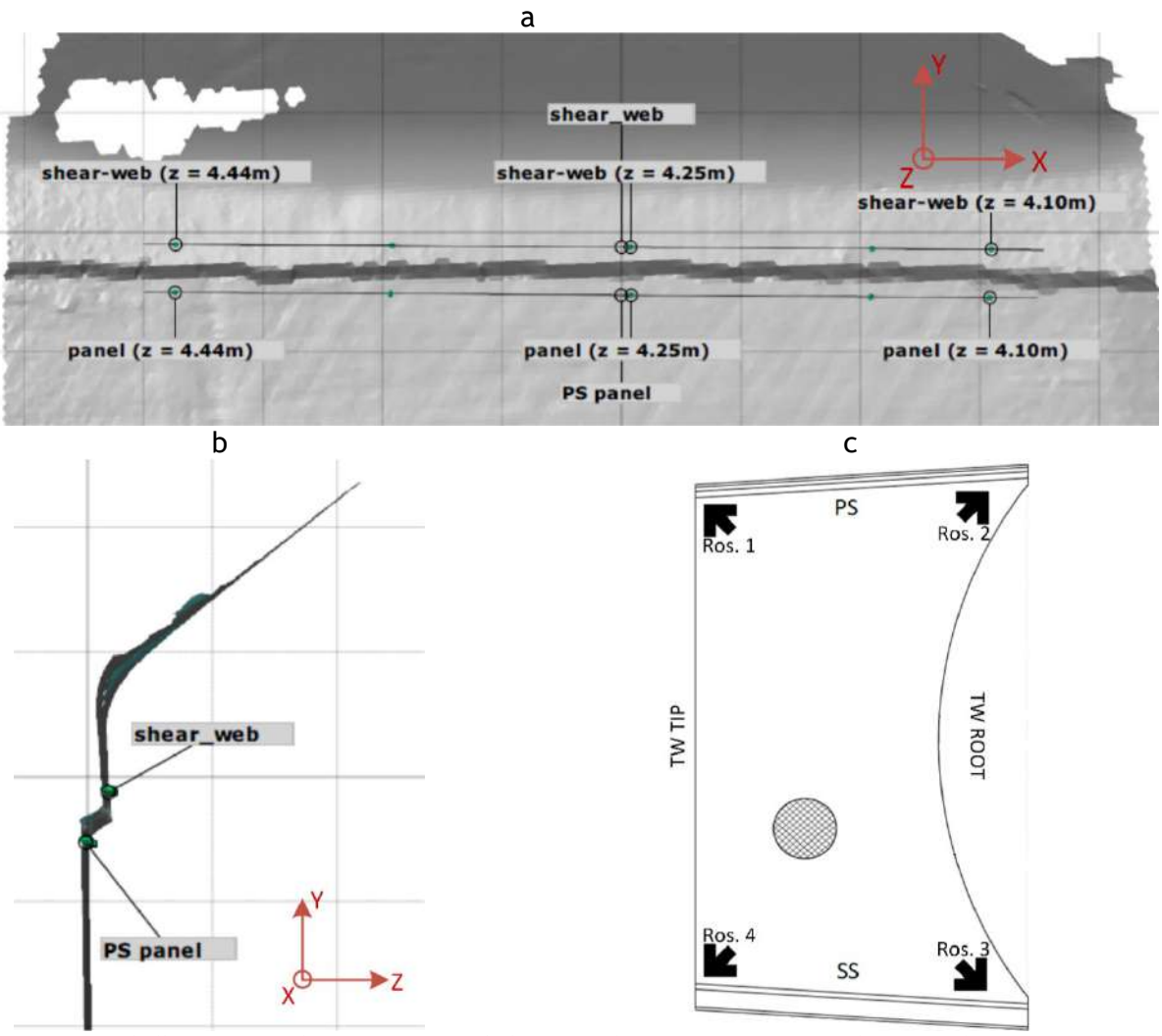

Figure 4: Labelling of internal measuremens including a) in-plane DIC measurements, b) out-of-plane DIC measurements and c) strain gauges

4. Results and discussions

The root section is loaded in a fatigue test campaign comprising approximately 280.000 load cycles with a combined load configuration of two dofs including F_y and M_z. With a sinusoidal waveform, execution frequency of 0.1Hz and phase shift of 90 degrees – F_y and M_z is applied a max load of 100kN and 100kNm respectively both with R=-1 according to figure 5. This load configuration is according to [6] found to generate the highest magnitude of breathing of the large double curved trailing edge aerodynamic sandwich panels. As the retrofitted 3rd shear web is installed to mitigate these deformations, that load configuration is established with the highest possible load magnitude to redice the number of cycles required for design validation process – even though the shear forces are different and higher than the in-service loads of the full-scale blade. A stable phase shift error of 0.7 sec between F_y and M_z were detected throughout the entire testing campaign. This phase shift error could not be lowered further with the available compensators.

Bladena
Banestrøget 13, 1
DK-2630 Taastrup

Taastrup, June 28, 2023

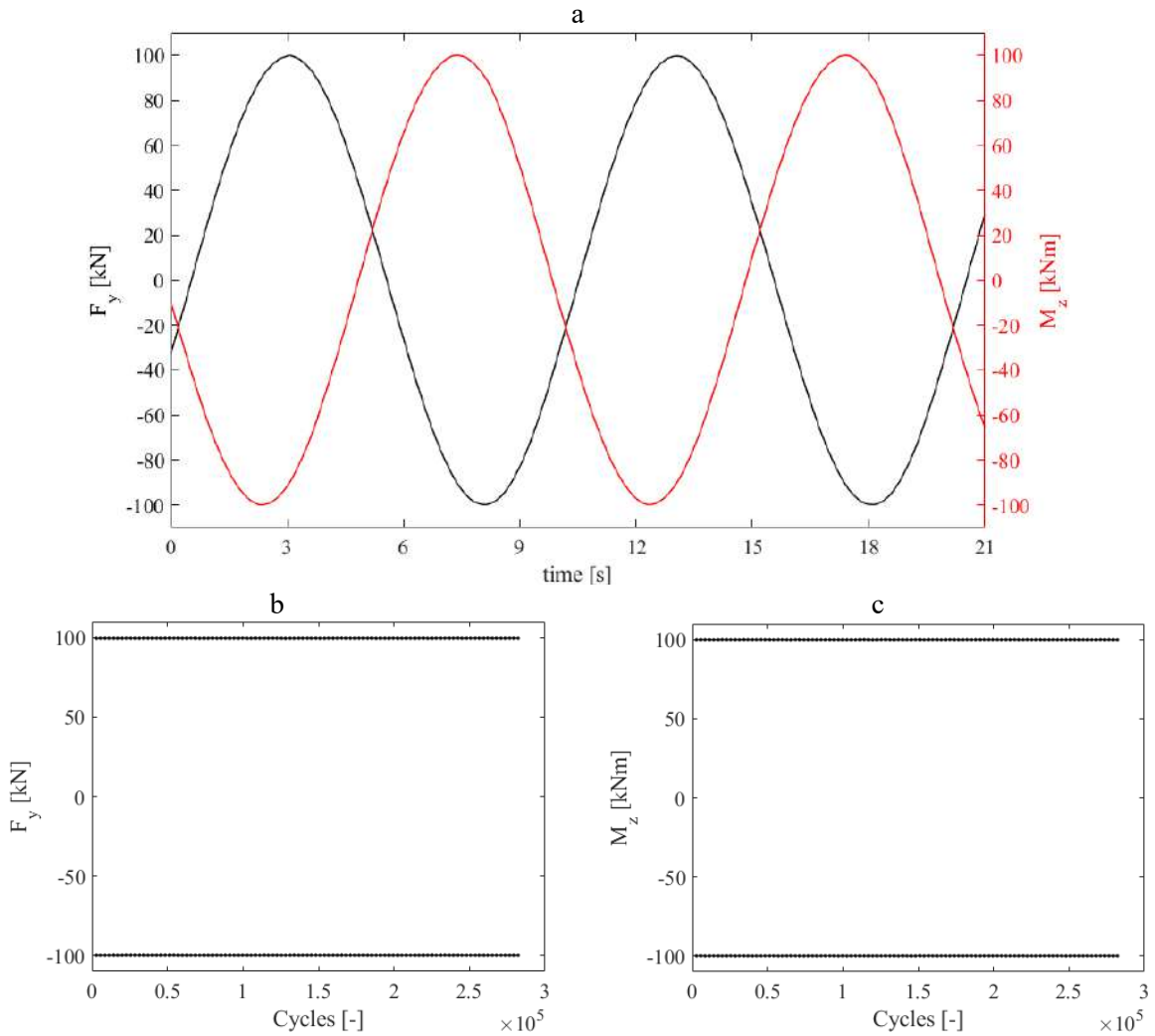

Figure 5: Fatigue loading of root section including a) timed loading sequence, b) peak/valley edgewise load and c) peak/valley torsional load

The wire potentiometer, monitoring the breathing of the PS and SS trailing edge sandwich panels, are stable throughout the entire test campaign with an amplitude of approximately 7mm.

Bladena
Banestrøget 13, 1
DK-2630 Taastrup

Taastrup, June 28, 2023

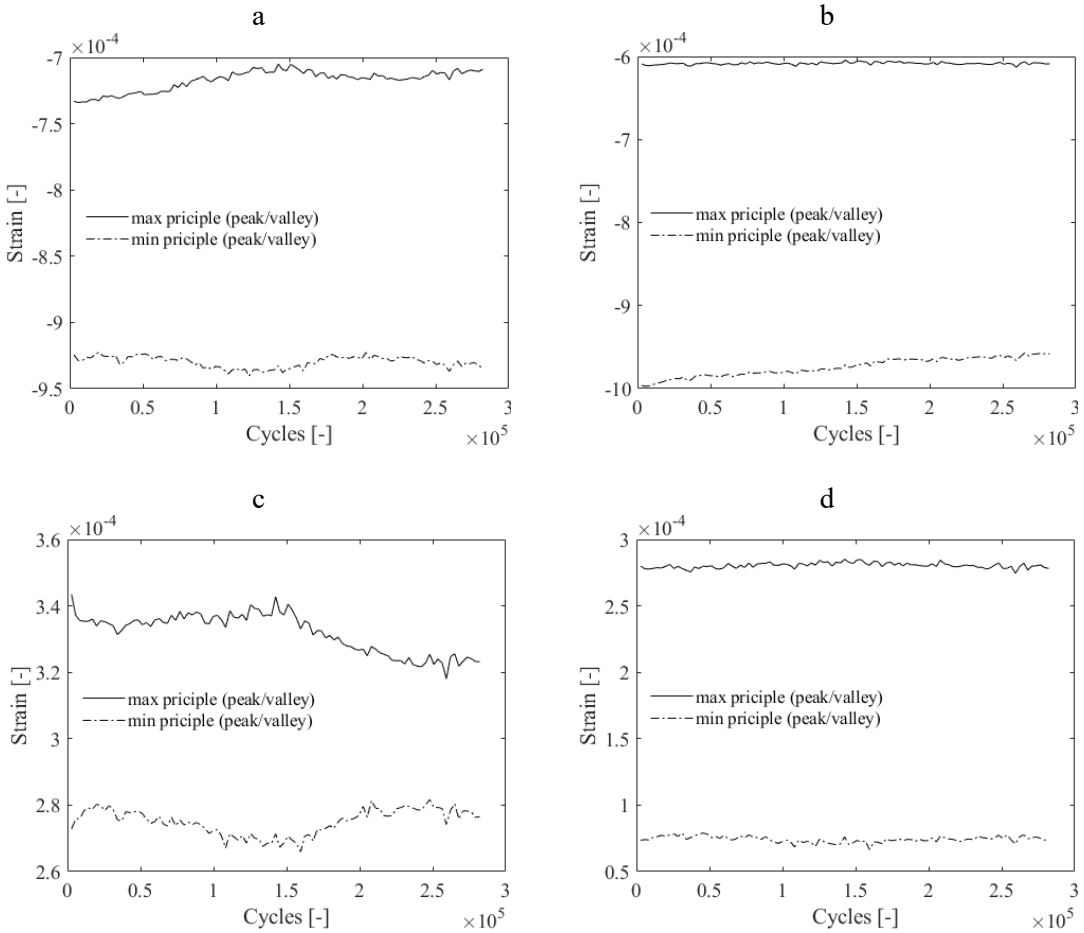

Figure 6: Principle strain at each corner of the shear-web including a) Ros. 1, b) Ros. 2, c) Ros. 3 and d) Ros. 4

From the max- and min principle strain provided in figure 6, no significant and consistent variation of the magnitude is detected throughout the fatigue test campaign indicating that the peak/valley strain field throughout the third shear-web is unchanged during the fatigue test campaign. Furthermore, no rotation of the principal axis is detected during the fatigue test campaign.

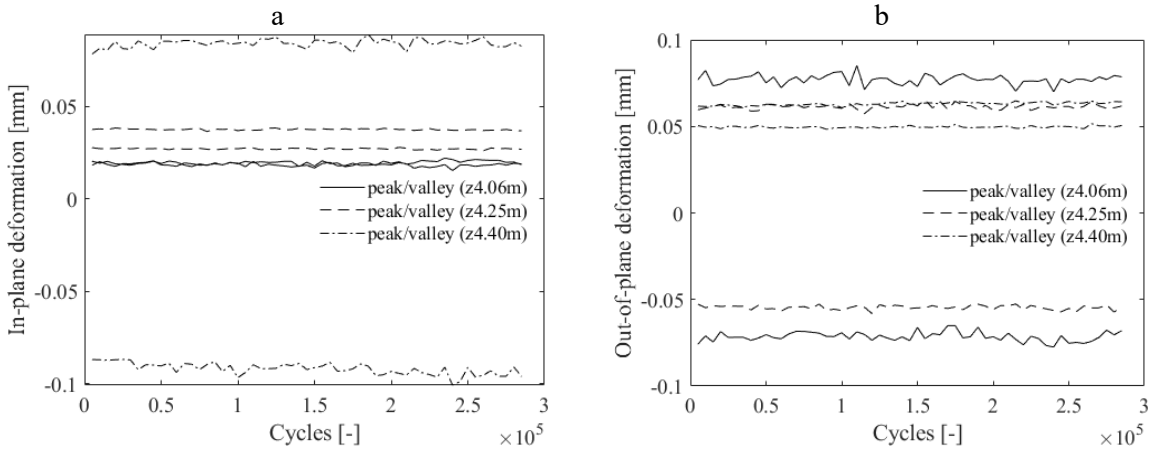

Figure 7: Relative deformation of PS single lap adhesive bonde-line and adjacent trailing edge panel including a) in-plane and b) out-of-plane

Bladena
Banestrøget 13, 1
DK-2630 Taastrup

From the DIC measurements of the peak/valley in-plane (resulting deformation in the xy-plane) and out-of-plane (deformation in the z-direction) deformation of the PS single lap adhesive bonde-line and adjacent trailing edge panel is stable throughout the entire fatigue test campaign. From all the above measurements on the third shear web and visual inspection of both the shear-web and SS and PS bondline, it is concluded that the adhesive connection between the trailing edge sandwich panels and single lap bondline is undamaged.

5. Conclusion and further work

To investigate and evaluate the overall structural integrity of the retro-fitted third shear-web along with the mitigation associated with the shear web disbonding mechanism triggered by breathing of the trailing edge panels, a fatigue test campaign was conducted covering 280.000 load cycles. Monitored by strain gauges, a wire potentiometer and DIC, the structural behavior of the third shear-web was evaluated. Here it was found that the shear-web and single lap bondline connecting the shear web with the trailing edge was undamaged at this point. To accelerate the process, it is intended to initiate a damage/crack in the bondline between the third shear-web and adjacent trailing edge sandwich panels.

6. Acknowledgement

The authors would like to acknowledge the Energy Development and Demonstration Program (EUDP) for financial support under the grant number: 64021-1054 CORTIR II project. Within the frame of the CORTIR II project, considerable work has been done by Global Wind Service supporting the large-scale test program.

References

[1] S. Singh, "Wind power: Future lies within," in *7th India International Conference on Power Electronics, Patiala, 2016*.

[2] G. Sieros, P. Chaviaropoulos, J. D. Sørensen, B. H. Bulder and P. Jamieson, "Upscaling wind turbines: theoretical and practical aspects and their impact on the cost of energy," *Wind Energy, vol. 15, no. 1, pp. 3-17, 2012*.

[3] F. M. Jensen, M. Werk, A. Buliga, T. Pardalakis, C. Berggreen, J. Waldbjoern and J. D. Sørensen, "Root Area Transition Zone – RATZ and Reduction O&M cost of WT blades," *Bladena A/S, Taastrup, 2019*.

[4] F. M. Jensen, "Ultimate Strength of Large Wind Turbine Blade," *Department of Civil Engineering, Technical University of Denmark, Kgs. Lyngby, 2008*.

[5] F. M. Jensen, M. Werk, A. Buliga, C. Berggreen, J. P. Waldbjoern, J. D. Sørensen, Y. Yang and E. S. Jensen, "Root and Transition zone (RATZ) and reduction O&M cost of WT blades," *Bladena A/S, Roskilde, 2019.*

[6] P. Waldbjørn, A. Buliga, C. Berggreen and F. M. Jensen, "Multi-axial large-scale testing of a 34m wind turbine blade section to evaluate out-of-plane deformations of double-curved trailing edge sandwich panels within the transition zone," *Wind Engineering, p. 0309524X2097840, 2020*.

[7] F. M. Jensen, B. G. Falzon, J. Ankersen and H. Stang, “Structural Testing and Numerical Simulation of a 34m Composite Wind Turbine Blade,” *Composite Structures, vol. 76, no. 1-2, pp. 52 - 61, 2006.*

Bladena
Banestrøget 13, 1
DK-2630 Taastrup

https://pdf.directindustry.com/pdf/gurit/ampreg-22-epoxy-laminating-system-v17/37817-79061.html. [Accessed 8 June 2023].

Appendix D Waldbjørn J.P., Berggreen C., Jensen F.M., Ley O., (2023)," Large-scale fatigue testing of a wind turbine root end section", *DTU Department of Civil and Mechanical Engineering, Bladena, Mistras* - Abstract

As the wind turbines are progressively growing in size, blade durability has become a significant challenge within the wind turbine industry. Wind turbine blades are usually made from composite materials including glass and carbon fibre reinforced plastics along with lightweight cores such as e.g. honeycomb, foam, etc. Hence, the ambition to improve the structural and operational performance within the industry of wind turbines has resulted in extensive research within large composite structures. In these efforts, testing has primarily been focusing on two length scales including laminate and structural scale testing. Structural scale testing provides valuable knowledge concerning structural behavior but is time consuming and expensive to perform. Here, the structure is typically tested in a simple load configuration which is a significant simplification compared to the actual forces acting on the blade during service. To investigate the material characteristics of the individual materials in the composite structure, coupon testing on laminate scale is conducted. Such tests are performed on specially designed specimens, resulting in idealized stress and strain states. Consequently, they do not account for the complex stress states and interactions, which often occur within structural scale testing leading to advanced failure modes among this mixed mode de-lamination, laminate failure, etc. Such failures often initiate from joints, bearings and other critical details, thereby weakening the structure locally and change the structural response. To ensure a proper and efficient design process of a wind turbine blade, experimental testing across length scales from micro through structural scale testing is required. This fact is supported by similar industries like aviation and maritime. This paper presents and demonstrates a fatigue rated multi-axial test rig and methodology, in which the inner 15m section of a 34m wind turbine blade manufactured by SSP technology, is installed. This substructural test setup enables structural assessment of the root, transition zone and max chord region, which have become increasingly critical due to the higher loads, governed by the demand for larger and more effective wind turbine blades. Loaded in the tip end by up to three hydraulic actuators, the blade can be handled in 3 degrees-of-freedom including edge- and flap wise loading and torsional moment around the longitudinal axis of the blade. The free end of the root section is fully constrained against in-plane distortion to avoid critical peeling stresses. Overall structural health including both specimen and test rig is successfully monitored using acoustic emission. Additionally, pre tensioning of critical bolted connections are monitored using donut load cells. The test rig is demonstrated through a couple of test campaigns related to the installation of 2 different retrofitted reinforcement solutions capable of supporting the large double curved trailing

Bladena
Banestrøget 13, 1
DK-2630 Taastrup

edge panels located in the transition zone from max. chord to the stiff root region towards out-of-plane deformation – referred to here as breathing. The rig has successfully reached more than 1e6 loading cycles.

Appendix E Nielsen J.S., Sørensen J.D., (2023),"Optimization of novel heuristic strategies for inspection and maintenance", AAU Department of The Built Environment - Draft

Optimization of novel heuristic strategies for inspection and maintenance

Jannie Sønderkær Nielsen[a]*

[a*]*Department of the Built Environment, Aalborg University, Aalborg, Denmark, jsn@build.aau.dk;*

Taastrup, June 28, 2023

Optimization of novel heuristic strategies for inspection and maintenance

The decision problem for inspection and maintenance planning for structures is complicated, and generally an exact solution cannot be found. Numerous methods have been developed based on heuristic strategies, partially observable Markov decision processes (POMDP), and deep learning approaches. While the heuristic strategies are often preferred by the industry due to the simplicity and transparency, the more use advanced approaches can often lead to lower costs. This paper presents a novel heuristic approach, which is able to include inspection intervals which depends on the most recent inspection interval, and in an numerical example it is shown that this leads to 8-10 % cost reductions compared to the use of equidistant inspections. Further, it is shown that the use of adaptive strategies, where the optimization is rerun using a model updated with inspection information from the first 10 years of operation, may also lead to cost reductions, if equidistant inspection intervals are used.

Keywords: inspection and maintenance; decision theory; Bayesian networks

1 Introduction

The importance of optimal planning of inspections and maintenance for structures has been recognised for years, and so has fact that it is a challenging problem. Inspection and maintenance optimization involves solving a sequential decision problem, where decisions are made under uncertainty (Faber, 2002). Based on the Bayesian statistical decision theory, the optimal decisions are chose maximizing the expected utility, or equivalently, minimizing the expected lifecycle costs (Raiffa & Schlaifer, 1961). Once the system defined, there exist in principle one or more optimal solutions. However, for most problems it becomes computationally intractable to solve the problem by simply evaluating all branches in the associated decision tree (Straub & Faber, 2006). This has motivated a search for approximate methods for solving inspection and maintenance decision problems, to make the Bayesian decision theory

Bladena
Banestrøget 13, 1
DK-2630 Taastrup

applicable for application such as offshore structures (Moan, 2005), bridges (Robelin & Madanat, 2007), wind turbines support structures (P G Morato, Mai, Rigo, & Nielsen, 2018), or wind turbine blades (Jannie S. Nielsen, Tcherniak, & Ulriksen, 2020).

Early attempts/traditional RBI approaches were based on reducing the decision tree to a single branch, and having a single decision parameter to schedule inspections (Faber, Sørensen, Tychsen, & Straub, 2005) (Lotsberg, Sigurdsson, Fjeldstad, & Moan, 2016). The introduction of dynamic Bayesian networks for deterioration modelling (Straub, 2009) lead to new possibilities within I&M planning. For example, limited memory influence diagrams (LIMIDS) was used by (Friis-Hansen, 2000) and (J. J. Nielsen & Sørensen, 2011) optimize I&M decisions. However, these only took into consideration the most recent inspection outcome, and the often used single policy updating (SPU) algorithm for optimization would often fail to reach the optimum, if multiple decision types were included. However, when using the LIMIDS in an adaptive way (i.e. update the strategies every time an inspected was made) (J. J. Nielsen & Sørensen, 2011) showed that it would provide much better results than using the initial strategies.

Another approach was to use heuristics, i.e. define strategies based on a few parameters defining the decision rules for when to inspect and when to repair. The use of Bayesian network for optimization of simple time based inspections and repair decision rules based on observations could be performed efficiently using exact inference algorithms (Jannie Sønderkær Nielsen & Sørensen, 2018). The simple decision rules were not ideal in all cases, for example when information from monitoring were available. Here, strategies where inspections are scheduled based on the failure probability could be applied instead to exploit the additional information. Here, Bayesian networks proved useful in a different way (Jannie Sønderkær Nielsen &

Bladena
Banestrøget 13, 1
DK-2630 Taastrup

Sørensen, 2018). For simulated lifetimes of observations, a Bayesian network was updated with all observations, and was thereby used to calculate an updated failure probability, to be used for inspection scheduling. While the updating of the network was performed efficiently using exact inference algorithms, time consuming simulations were necessary to estimate the life cycle costs for a given strategy, and therefor also for the optimization of strategies. The use of the failure probability for the scheduling of inspections were especially beneficial when information from monitoring was available, but it also gave a benefit in other cases, because it led to age-based inspections instead of time based.

Bayesian network also proved useful tor system reliability modelling (Tien & Der Kiureghian, 2017) and updating (Luque & Straub, 2016). Further, (Luque, Straub, Bismut) developed heuristic strategies for systems, taking into consideration the system effects using Bayesian networks, and (Bismut & Straub, 2021) showed that the use of adaptive strategies where strategies were updated through the life provided more optimal planning.

An alternative approach to sequential decision problems are the modelling as POMDPs (Papakonstantinou & Shinozuka, 2014) (Corotis, Ellis, & Jiang, 2005). For Markov decision processes, the optimal decision only depends on the current state, and when fully observed, this can be exploited for decision optimization. However, generally the state is not fully observed, and in POMDPs the optimal decision only depends in the current (updated) distribution for current state. Point based solvers exploiting the POMDP properties has proved fast and efficient, (e.g. SARSOP (Kurniawati, Hsu, & Sun Lee, 2008)) whereas grid based approaches were only efficient for simple models with only few states (Jannie Sønderkær Nielsen & Sørensen, 2015).

Bladena
Banestrøget 13, 1
DK-2630 Taastrup

Taastrup, June 28, 2023

POMDP papers generally considered deterioration processes which were Markovian, whereas the focus in heuristic papers were often on processes which included time-invariant parameters. However, (Pablo G. Morato, Papakonstantinou, Andriotis, Nielsen, & Rigo, 2020) showed that state augmentation could successfully be applied to convert the BN model to a Markov process, thus enabling the use of point-based POMDP solvers. Deep learning approaches has also shown promising capabilities to handle larger systems (Andriotis & Papakonstantinou, 2019) (Andriotis & Papakonstantinou, 2021).

In addition to the approximation regarding the decision optimization, the system definition also imply an approximation, where the model may not capture all aspects correctly. Optimization is performed wrt. the prior model, but it may not be correct. The used of adaptive or flexible POMDP strategies may make up for this, but generally the conditional probability distributions and model structure are not updated. For example, for new SHM methods, the value can be estimated prior to the installation, but the assessment depends on the probabilistic modelling of SHM. Measurement campaigns can give an indication, but may not be representative. (Jannie S. Nielsen, 2022) showed that the modelling of temporally correlated observations as uncorrelated, may lead to bad decisions, leading to much larger costs than expected. The modelling of inspections and SHM has been done in different ways in different branches of research using probability of detection (PoD) and receiver operating characteristic (RoC) curves, and Bismut showed that a more detailed modelling provided better decisions (Bismut & Straub, 2022).

While the advanced methods show great potential in providing more optimal strategies, a challenge lies in the boundary between the human decision makers and the technology, requiring a balance between optimality and simplicity. The need for simple

Bladena
Banestrøget 13, 1
DK-2630 Taastrup

understandable strategies favours the heuristic strategies, which are easier to understand and apply for practitioners. However, heuristic approaches which require simulations for optimization are time consuming to optimize, and large computation time is needed. Strategies which can be included directly in a Bayesian network can be evaluated very fast, but this has been limited to simple strategies, with equidistant inspections, or decisions for a current action depending directly on an observed variable in the current or previous time step. In the present paper, a novel heuristic approach is presented, where inspection times depends on the most recent inspection outcome. The method is an extension of previous Bayesian network approaches, and the paper is structured as follows. The method is described in Section 2, and a numerical example is presented in Section 3. Conclusions are given in Section 4.

2 Methodology

The section presents a novel heuristic approach for optimal scheduling of inspections and repairs for a deteriorating component. The deterioration model, inspection model and repair model are described by probabilistic models and are modelled using Bayesian networks. For the deterioration model, both time variant- and time-invariant uncertainties are included. A cost model describes the costs associated with inspections, repairs, and failures.

The aim is to find the strategy S, which minimize the expected lifetime costs. The strategy S defines decision rules for the timing of inspections and repairs based on inspection outcomes. When an inspection has been made, the next inspection is scheduled based on the outcome, and repairs can be performed following an inspection.

In order to estimate the expected lifetime costs for strategies in an efficient way, a discrete Bayesian network model is developed where the decision rules are modelled

Bladena
Banestrøget 13, 1
DK-2630 Taastrup

directly by conditional probability tables. This makes is possible to estimate the probability of inspection, repair and failure for each time step using efficient exact inference algorithms. The main novelty of the present work is that the strategies include the possibility to differentiate the time to the next inspection based on the most recent inspection outcome.

Further, the methodology includes the use of adaptive strategies. The initially optimal strategy depends on the probabilistic model and the cost model, and assumes that this strategy is used throughout the lifetime. However, if the deterioration is progressing unusually fast or slow compared to the prior model, it might be beneficial to change strategy. After inspections are made, the observations can be used to update the deterioration model using Bayesian updating. For this updated model, the optimization can be re-run to find the optimal strategy. In this way the strategy can be adapted to the new knowledge. Every time the strategy is changed, the expected benefit of changing the strategy can be evaluated.

2.1 Bayesian network model

The core in the methodology is a discrete dynamic Bayesian network with the structure shown in Figure 1. The network consists of identical time slices, one for each time step in the model. Each time slice consists of the following five nodes, which are all modelled as discrete nodes, although they may represent continuous variables:

- M_i: time-invariant parameter in deterioration model. The node has one state for each interval for the parameter.
- D_i: damage state. The node has one state for each deterioration state; the last state is fault.

Bladena
Banestrøget 13, 1
DK-2630 Taastrup

Taastrup, June 28, 2023

- I_i: inspection outcome. The node includes the dummy outcome 'no inspection', one state for each inspection outcome, and the last state 'fault'.
- R_i: repair decision. The node has two states 'no repair' and 'repair'.
- TI_i: time to next inspection. The node models the timing of inspections. After each inspection, it sets the time to the next inspection according to the strategy, and between inspections, it works as a countdown node. The node has a state for each integer from one to the largest inspection interval used in the strategies.

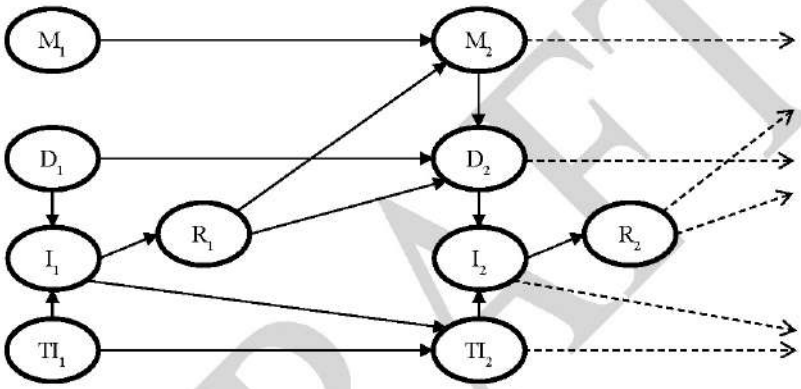

Figure 1. Bayesian network structure.

Deterioration is modelled by the conditional distribution $P(D_i|D_{i-1}, M_i)$, the prior distribution for the model parameter $P(M_1)$, and the prior distribution for the initial damage state $P(D_1)$. The distribution $P(M_i|M_{i-1})$ is the identity matrix as M is time-invariant. The nodes D and M also have the repair node as a parent, as repairs affect the damage state and possibly the time-invariant model parameter. If both D and M are affected by the repair such that the distributions after a repair are $P(D_0)$ and $P(M_0)$, the conditional distributions for D and M are:

- $P(D_i|D_{i-1}, M_i, R_{i-1})$

Bladena
Banestrøget 13, 1
DK-2630 Taastrup

Taastrup, June 28, 2023

- $P(D_i|D_{i-1}, M_i, R_{i-1} = '\text{ no repair}') = P(D_i|D_{i-1}, M_i)$
- $P(D_i|D_{i-1}, M_i, R_{i-1} = '\text{ repair}') = P(D_0)$

- $P(M_i|M_{i-1}, R_{i-1})$
  - $P(M_i|M_{i-1}, R_{i-1} = '\text{no repair}') = P(M_i|M_{i-1})$
  - $P(M_i|M_{i-1}, R_{i-1} = '\text{repair}') = P(M_0)$

If the model parameter is not affected by a repair, the distribution for $R_{i-1} = '\text{repair}'$ is instead:

$$(M_i|M_{i-1}, R_{i-1} = '\text{repair}') = P(M_i|M_{i-1})$$

The inspection node is defined by the distribution $P(I_i|TI_i, D_i)$. If the value of TI is one, an inspection is made, and the inspection model $P(I_i|D_i)$ describes the outcome:

$$P(I_i|TI_i = 1, D_i) = P(I_i|D_i)$$

If the value of TI is larger than one, no inspection is made, and the inspection node will always have the state 'no inspection':

$$P(I_i = '\text{no inspection}'|TI_i > 1, D_i) = 1$$

An exception is when there is a fault, as faults are assumed to be self-announcing, thus the inspection outcome is 'fault' when the damage size is 'fault', regardless of whether an inspection is made (regardless of the value of TI_i):

$$P(I_i = '\text{ fault}'|TI_i, D_i = '\text{ fault}') = 1$$

2.2 Strategy

The strategy is modelled by the probability distributions for R and TI: $(R_i|I_i)$, $P(TI_0)$, $P(TI_i|I_{i-1}, TI_{i-1})$. These distributions are defined depending on the following decision parameters:

- I_{th}: inspection threshold for repair (one value)

Bladena
Banestrøget 13, 1
DK-2630 Taastrup

Taastrup, June 28, 2023

- I_{int}: time to next inspection dependent on the inspection outcome (one value for each inspection outcome except for 'no inspection').

All potentially feasible preventive strategies are generated as vectors consisting of values: $[I_{th}, I_{int,1}, I_{int,2}, \dots, I_{int,1}]$. For a strategy to be potentially feasible it is required:

- The initial inspection interval $I_{int,1}$ is used after repairs and failures: thus $I_{int,j} = I_{int,1}$ for $j \geq I_{th}$
- The inspection interval for more severe damages will be smaller or equal to the interval for the milder damage.

The potentially feasible strategies can be generated based on the considered inspection intervals, and the number of strategies depends on the number of inspection outcomes, and the number of considered inspection intervals. Based on the strategies, the probability tables are generated:

- $P(R_i|I_i)$: Implements the repair decision which is decided by the decision parameter I_{th} - the inspection outcome resulting in repair.
  - $P(R_i = \text{'repair'}|I_i \geq I_{th}) = 1$
  - $P(R_i = \text{'no repair'}|I_i < I_{th}) = 1$
- $P(TI_1)$: Implements the decision on the time of the first inspection, i.e. the probability of being in the state corresponding to the initial inspections interval is one.
- $P(TI_i|I_{i-1}, TI_{i-1})$: Implements the decision on the time to the next inspection, based on the inspection outcome. When no inspection is made ($I_{i-1} =$ 'no inspection' and $TI_{i-1} > 1$), TI acts as a countdown node, always subtracting one from the previous value, thus the probability distribution has ones just above

Bladena
Banestrøget 13, 1
DK-2630 Taastrup

Taastrup, June 28, 2023

the diagonal for $TI_{i-1} > 1$. When an inspection is made ($I_{i-1} \neq' no\ inspection'$ and $TI_{i-1} = 1$) or a failure occurs ($I_{i-1} =' fault'$), TI is set to the value I_{int} given by the strategy, i.e. the probability of being in the state corresponding to the inspections interval given by the strategy for the given inspection outcome is one.

2.3 Bayesian network inference algorithm

When the Bayesian network is specified through the probability distributions, the probability of inspection, repair, and failure can be estimated using inference algorithms. For the specific Bayesian network model, an inference algorithm based on variable elimination was developed, inspired by the forward operation by Straub (Straub, 2009) and by the forward operation of the frontier algorithm and interface algorithm by Murphy (Murphy, 2002). Since the three nodes TI, M, D are connected to the previous time step, the algorithm should calculate the joint distribution of these variables, based on the conditional distributions and the joint distribution for the previous time slice. The algorithm can be written as follows:

$$P(TI_i, M_i, D_i)$$
$$= \sum_{R_{i-1}} \sum_{D_{i-1}} P(D_i|D_{i-1}, M_i, R_{i-1}) \sum_{M_{i-1}} P(M_i|M_{i-1}, R_{i-1}) \sum_{I_{i-1}} P(R_{i-1}|I_{i-1}) \sum_{TI_{i-1}} P(TI_i|I_{i-1}, TI_{i-1}) P(I_{i-1}|TI_{i-1}, D_{i-1}) P(TI_{i-1}, M_{i-1}, I$$

The largest of the probability tables generated in these operations will dominate the computation time. The order of variable elimination has been chosen to minimize computation time. In practice, it was implemented in five lines as follows:

$$P(TI_{i-1}, M_{i-1}, D_{i-1}, I_{i-1}) = P(I_{i-1}|TI_{i-1}, D_{i-1}) P(TI_{i-1}, M_{i-1}, D_{i-1})$$

$$P(M_{i-1}, D_{i-1}, I_{i-1}, TI_i) = \sum_{TI_{i-1}} P(TI_i|I_{i-1}, TI_{i-1}) P(TI_{i-1}, M_{i-1}, D_{i-1}, I_{i-1})$$

$$P(M_{i-1}, D_{i-1}, TI_i, R_i) = \sum_{I_{i-1}} P(R_{i-1}|I_{i-1})\, P(M_{i-1}, D_{i-1}, I_{i-1}, TI_i)$$

Bladena
Banestrøget 13, 1
DK-2630 Taastrup

$$P(D_{i-1}, TI_i, R_i, M_i) = \sum_{M_{i-1}} P(M_i|M_{i-1}, R_{i-1})\, P(M_{i-1}, D_{i-1}, TI_i, R_i)$$

$$P(TI_i, M_i, D_i) = \sum_{R_{i-1}} \sum_{D_{i-1}} P(D_i|D_{i-1}, M_i, R_{i-1}) P(D_{i-1}, TI_i, R_i, M_i)$$

The algorithm is used recursively to find the distribution for all time steps.

2.4 Adaption of strategy

With the adaptive strategies, the decision maker can at any point in time decide to use past observations to obtain the updated current joint distribution $P(TI_i, M_i, D_i)$, and then re-run the optimization for future time steps. The algorithms used here are basically the same as described in section 2.3, but for past time steps, distributions are instantiated with the observations/decisions for the nodes I and R.

3 Numerical example

This section presents a numerical example, where the novel approach with flexible inspection intervals and adaptive strategies are demonstrated. Generic models for deterioration and inspections are used to study the influence of model parameters on the optimal strategies. This knowledge can be used as a basis for investigations on specific models. The applied generic deterioration model is a continuous linear deterioration model with damage initiation which is representative for deterioration processes such as erosion, corrosion, and some fatigue problems. Inspections are modelled assuming a measurement method is applied, where the damage size is measured with some uncertainty, and the damage category is determined based on this.

Bladena
Banestrøget 13, 1
DK-2630 Taastrup

Taastrup, June 28, 2023

3.1 Models

3.1.1 Deterioration model

The generic deterioration model includes uncertainties related to the initiation time, the overall damage rate, and the damage increment for individual time steps. Often, damage initiation does not happen totally random (as a Poisson process), but instead due to some fatigue process in the material. In order to model the damage initiation process properly, damage initiation is modeled using a fictive negative damage size. While the damage size is below zero, damage is not detectable. Detectable damage is between 0 and 1, and exceedance of 1 result in failure. The deterioration model is defined through the following parameters:

- D_0: Initial damage size (models damage initiation)
- $M = \frac{dD}{dN}$: Model parameter (models time-invariant uncertainties on material parameters, environmental conditions and the model)
- ΔN: Equivalent number of exposures/cycles/impacts in time step (models time-variant uncertainties related to the exposure)

The damage increment in each time step is calculated as:

$$\Delta D_i = \frac{dD}{dN} \cdot \Delta N = M_i \cdot \Delta N_i$$

The damage size can then be calculated based on the damage size in the previous time step:

$$D_i = D_{i-1} + \Delta D_{i-1}$$

For the baseline model, the distribution type and parameters are shown in Table 1, and Figure 2 shows 100 simulated histories of damage sizes. The length of the time step is one month.

Variable	Distribution	Mean	COV	Discretization

Bladena
Banestrøget 13, 1
DK-2630 Taastrup

Taastrup, June 28, 2023

D_0	Normal	-0.5	0.3	-1:0.01:1
M_0	Lognormal	1.3	0.25	0.4:0.1:2.4
ΔN_i	Lognormal	0.01	1	-

Table 1. Degradation model distribution types and parameters.

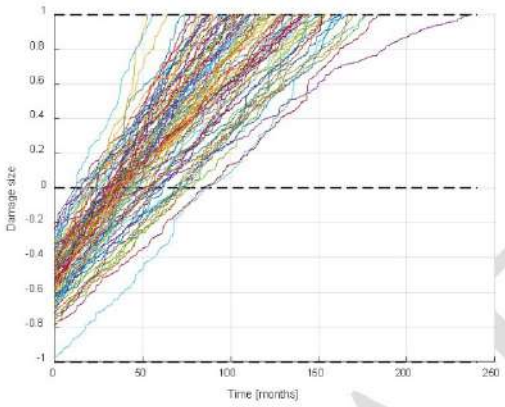

Figure 2. 100 simulated histories of damage sizes. Damage sizes below zero are non-initiated (non-detectable) damage.

Based on this model, a Bayesian network model is made. The discretization for the nodes D_0 and M_0 is shown in Table 1 and the discretization scheme for D_0 is also used for the damage size for the other time steps. The variable ΔN_i is not included as a node in the DBN, but is used to generate the conditional probability table $P(D_i|D_{i-1}, M_i)$. The nodes for D_0 and M_0 are represented by the prior distributions $P(D_0)$ and $P(M_0)$. The discrete probability tables are found directly by discretization of the continuous distributions. The nodes D_i are defined by the conditional probability distribution $P(D_i|D_{i-1}, M_i)$. The discrete probability table is generated using the midpoint values in 10 subintervals for D_{i-1} and M_i, and for each subinterval, using 100 random values of ΔN_i. Using this procedure, and the discretization given in Table 1, good agreement was

Bladena
Banestrøget 13, 1
DK-2630 Taastrup

Taastrup, June 28, 2023

found between the Bayesian network model and the continuous model, as shown in Figure 3.

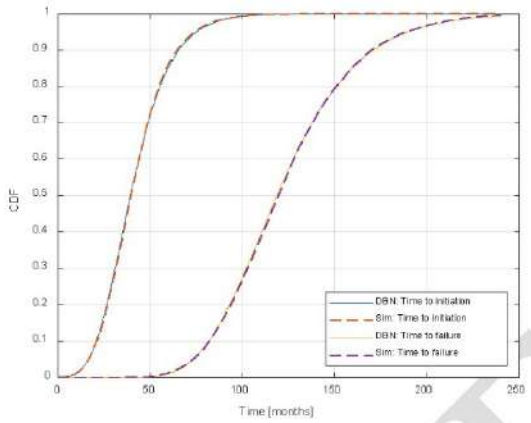

Figure 3. Comparison of CDF for time to damage initiation and time to failure calculated using the discrete DBN model and using 10000 Monte Carlo simulations from the continuous model.

3.1.2 Inspection model

Based on the continuous damage size, the damage is classified in damage categories, and the category determines the action, i.e. the time of the next inspection, and whether to make a repair. The classification is performed based on exceedance of thresholds of the measured damage size. The measurement s modelling the outcome of the inspection is given by:

$$s = D + \varepsilon$$

Where ε is a normal distributed error with mean zero and standard deviation $\sigma_\varepsilon = 0.1$. The damage categories CAT2, CAT3, CAT4, CAT5 are defined by exceedance of the thresholds 0.2, 0.4, 0.6, 0.8, and CAT 5 is assumed to be a self-announcing failure. If no threshold is exceeded, it is referred to as CAT1. The probability of the inspection categorizing a damage in each category is shown in Figure

Bladena
Banestrøget 13, 1
DK-2630 Taastrup

Taastrup, June 28, 2023

4.

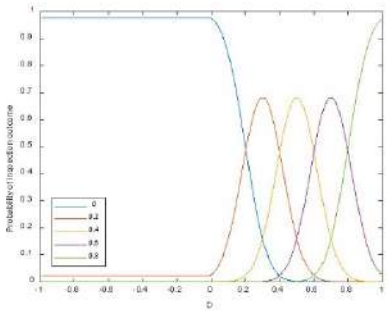

Figure 4. Probability of each inspection outcome as function of damage size.

3.1.3 Cost model

The cost model defines the total costs of inspection, repair, and failure. The costs are formulated as relative costs, as the absolute value does not affect the relative performance of strategies. The repair costs may depend on the damage category.

Bladena
Banestrøget 13, 1
DK-2630 Taastrup

Taastrup, June 28, 2023

Action	Inspection	Repair CAT1	Repair CAT2	Repair CAT3	Repair CAT4	Repair CAT5	Repair Fault
Fixed preventive repair costs	1	50	50	50	50	50	500
Variable preventive repair costs	1	20	20	50	100	200	500

Table 2. Cost model.

3.1.4 Strategies

The model has been run for equidistant inspections intervals from 6 to 36 months (in 6 month jumps), and repair thresholds CAT2 to CAT5. Further, a strategy with only corrective repairs (following failure) has been run. This results in 25 strategies. Additionally, the model has been run for all potentially feasible strategies, where the time to the next inspection may depend on the inspection outcome, but will never increase for more severe defects. Using the same possible intervals as for the equidistant strategies, this results in a total of 210 strategies. In all strategies, corrective repairs are performed following a failure.

3.2 Results

The model has been run for a lifetime of 20 years for both the case where a repair affects the model parameter M, and the case where it is assumed not to be affected by repairs. Two cost models have been considered: the fixed and variable, and two types of strategies have been considered: equidistant inspections, and variable inspection intervals. In Figure 5, the expected number of inspections and repairs of each type is shown for each equidistant strategy, when the model parameter is affected by repairs. The strategies are ordered with increasing repair threshold and increasing inspection interval (6, 12, 18, 24, 30, 36 months) within each block of six strategies with same

Bladena
Banestrøget 13, 1
DK-2630 Taastrup

Taastrup, June 28, 2023

repair threshold (CAT2, CAT3, CAT4, CAT5). The last strategy include none inspections, and repairs are only made in case of failure. It is seen that the expected number of repairs decrease with increasing repair threshold and inspection interval, whereas the category of the repairs increases.

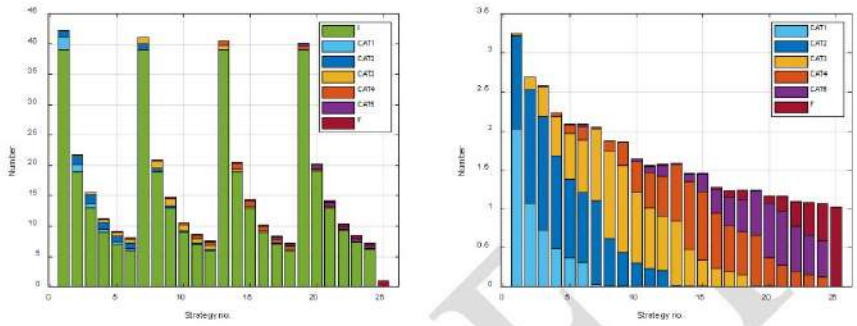

(a) (b)

Figure 5. Expected number of inspections and repairs of each type (a), and expected number of each repair type (b) for each equidistant strategy. M is assumed affected by repairs.

Figure 6 shows the expected costs for all strategies for the cost model with fixed (a) and variable (b) repair costs. Using variable repair costs reduces the costs for strategies with low thresholds and increase the costs for strategies with high thresholds. With fixed repair costs, the optimal strategy is no. 11 and for variable repair costs no. 4.

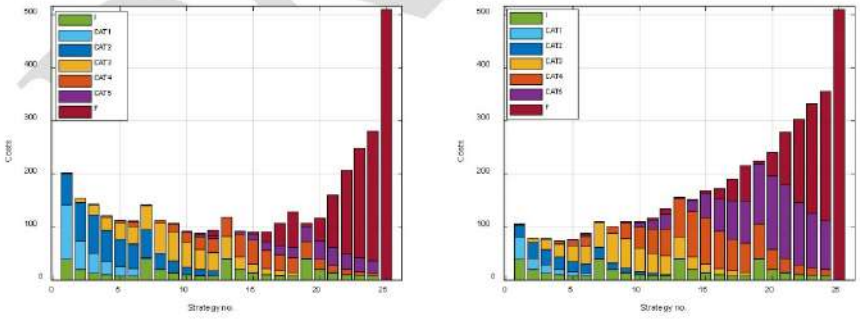

(a) (b)

Figure 6. Expected costs for each strategy for the cost model with fixed repair costs (a), and the cost model with variable repair costs (b). M is assumed affected by repairs.

Bladena
Banestrøget 13, 1
DK-2630 Taastrup

Taastrup, June 28, 2023

The optimal strategy and associated costs for each combination is shown in Table 3. For the cost model with fixed repair costs, the use of variable inspection interval strategies is seen to result in lower expected costs than the equidistant strategies (8-10% cost reduction). The inspection intervals are gradually reduced for larger defects, and repairs are made for larger defects than when equidistant inspections are used. For the cost model with variable repair costs, it is optimal to use equidistant inspections, and no savings are possible. Generally, it leads to 5-7% larger costs, when the model parameter is not affected by repairs, but the optimal strategies are mostly the same.

M affected by repair	Costs	Inspection interval	Repair threshold	Inspection intervals CAT1-5, Fault	Expected costs	Savings using variable inspection interval
Yes	Fixed	Equidistant	CAT3	30	88.17	
Yes	Fixed	Variable	CAT5	36, 18, 12, 6, 36 ,36	79.18	10.2%
Yes	Variable	Equidistant	CAT2	24	73.41	
Yes	Variable	Variable	CAT2	24, 24, 24, 24, 24, 24	73.41	0%
No	Fixed	Equidistant	CAT3	30	92.32	
No	Fixed	Variable	CAT4	36, 24, 12, 36, 36, 36	84.50	8.5%
No	Variable	Equidistant	CAT2	24	77.31	
No	Variable	Variable	CAT2	24, 24, 24, 24, 24, 24	77.31	0%

Table 3. Expected costs, repair threshold, and inspection intervals for the optimal strategy for each of the considered combinations.

Figure 7 shows a comparison between the optimal equidistant and variable strategy, when M is affected by repairs, and the fixed cost model is used. Figure 7(a)-(b) show the probability of inspection and repair of each category in each time step, Figure 7(c)-(d) show the distribution of costs over time, and Figure 7(e)-(f) show the probability of each defect category as function of time. Is it seen that in the strategy with variable inspection intervals, the inspections are being spread more over time, and only the first time of inspection, they are all inspected.

Bladena
Banestrøget 13, 1
DK-2630 Taastrup

Taastrup, June 28, 2023

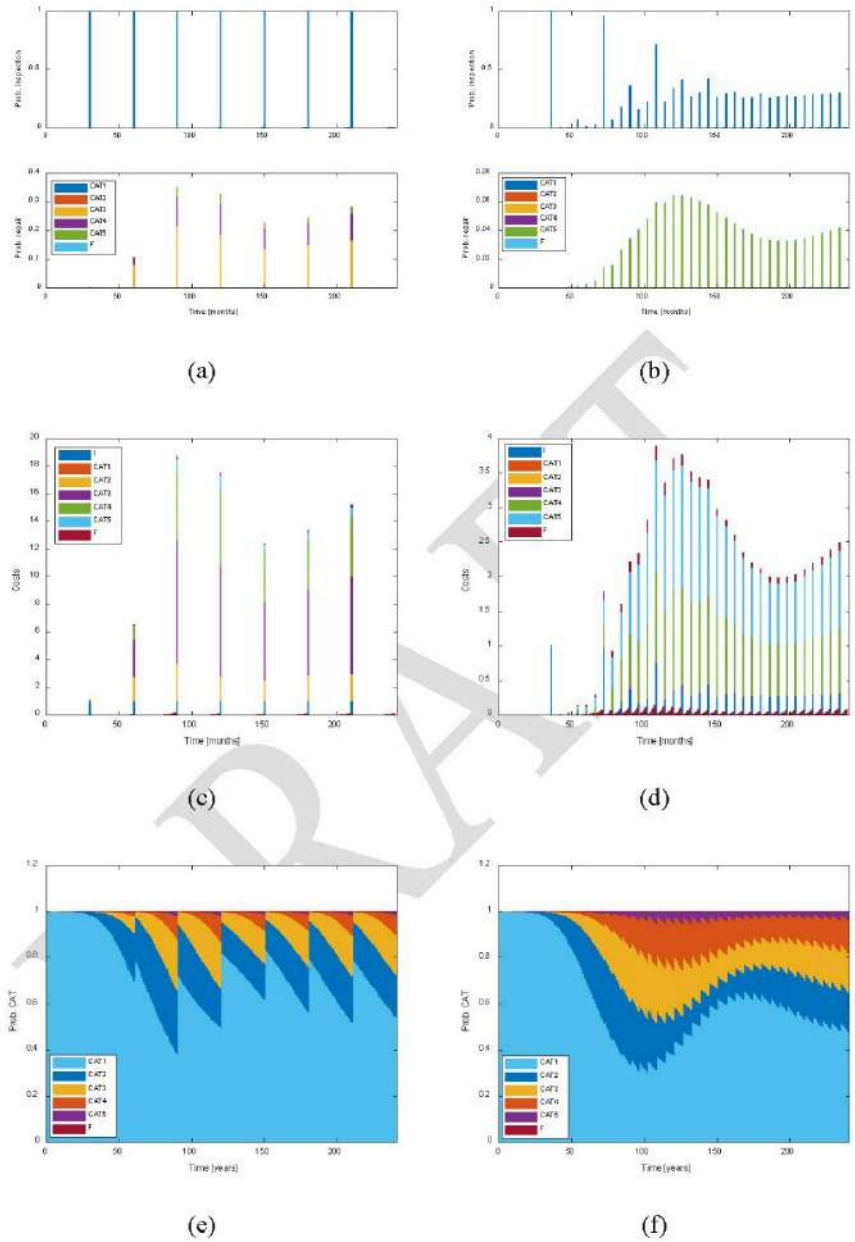

Figure 7. Distribution over time of expected number of inspections and repairs of each type (a)-(b), expected costs (c)-(d), and the probability distribution of the defect category (e)-(f). Subfigures(a),(c),(e) are for the best equidistant strategy, and (b),(d),(f) are for the best variable strategy. M is assumed affected by repairs, and the fixed cost model is used.

Bladena
Banestrøget 13, 1
DK-2630 Taastrup

3.2.1 *Adaptive strategy*

The expected costs shown in Table 3 assumed that the same strategy is used throughout the lifetime. However, after having followed the initial strategy for some years, information from inspections is available for updating the model. As an example, it is assumed that the strategy is updated after 10 years of operation, and that the inspections performed according to the originally optimal strategy does not lead to detection of damage, i.e. the inspection outcome is CAT1. For the variable inspection interval, this means that three inspections are made within the first 10 years, after 3, 6, and 9 years respectively. For the equidistant inspection interval, the initial interval is 30 months, and thus four inspections are made after 2.5, 5, 7.5, and 10 years respectively. Table 4 shows the expected costs for the initially optimal strategy and the adapted optimal strategy for both the equidistant and variable inspection intervals and when M is or is not affected by repair. All results are shown for the fixed cost model. In Table 4, results from equidistant and variable inspection intervals should not be compared, as the history of observations is different due to different initial strategies. It is seen that when equidistant inspections are used, savings of around 44% can be obtained by changing strategy after 10 years, with the given history of inspections. The changed strategies use larger repair thresholds and slightly smaller inspection intervals. For the strategies with variable inspection intervals, only smaller changes of the strategies are seen, and the savings are much smaller, as the original strategy is already more flexible. When M is not affected by repairs the savings are 3%, and when M is affected, they are only 0.7%.

Bladena
Banestrøget 13, 1
DK-2630 Taastrup

Taastrup, June 28, 2023

M affected by repair	Inspection interval	Strategy	Expected costs	Repair threshold	Inspection intervals CAT1-5, Fault	Savings from adapting strategy
Yes	Equidistant	Initial	43.93	CAT3	30	
Yes	Equidistant	Adapted	24.38	CAT5	24	44.5%
No	Equidistant	Initial	43.42	CAT3	30	
No	Equidistant	Adapted	24.37	CAT5	24	43.9%
Yes	Variable	Initial	50.26	CAT5	36, 18, 12, 6, 36 ,36	
Yes	Variable	Adapted	49.91	CAT5	36, 30, 12, 6, 36 ,36	0.7%
No	Variable	Initial	51.07	CAT4	36, 24, 12, 36, 36, 36	
No	Variable	Adapted	49.47	CAT5	36, 30, 12, 6, 36 ,36	3.1%

Table 4. Expected costs in remaining life, repair threshold, and inspection intervals for the initial and adapted optimal strategy. The fixed cost model is used.

4 Conclusions

The paper presented a novel heuristic approach to include age-based inspections and variable inspection intervals based on the most recent inspection outcome, and to update the strategies in an adaptive way. The approach is developed to provide near optimal strategies, without compromising transparency. For the inspection and maintenance professionals, the decision rules are presented as simple if-then rules. Further, the strategies can be updated in any point in time, and thereby adapted to the data from the specific inspection history.

The results of the study show that the use of variable inspection intervals may be feasible if the repair costs do not increase with damage category. In the numerical example it led to 8-10 % reduction of the expected costs. In the example, where the repair costs were increasing with defect category, it was optimal to use equidistant inspection. The difference can be explained by it being preferable to repair as late as possible, but still prior to failure, when the costs are fixed, whereas it may be preferable to early as possible, when repair costs increase with category. It was shown that the use of adaptive strategies could be very beneficial, when equidistant inspection intervals were used, whereas the potential for savings were much less, when variables inspection intervals were used.

Bladena
Banestrøget 13, 1
DK-2630 Taastrup

Taastrup, June 28, 2023

Disclosure statement

No potential conflict of interest was reported by the author.

Acknowledgements

The work on this paper has been supported by the Danish Energy Agency through the EUDP CORTIR – Phase II Cost, Risk and Transition zone Innovative Reinforcement (Grant Number 64021-1054). The support is greatly appreciated.

5 References

Bismut, E., & Straub, D. (2021). Optimal adaptive inspection and maintenance planning for deteriorating structural systems. *Reliability Engineering and System Safety, 215*, 107891. https://doi.org/10.1016/j.ress.2021.107891

Bismut, E., & Straub, D. (2022). A unifying review of NDE models towards optimal decision support. *Structural Safety, 97*, 102213. https://doi.org/10.1016/j.strusafe.2022.102213

Corotis, R. B., Ellis, J. H., & Jiang, M. (2005). Modeling of risk-based inspection, maintenance and-life cycle cost with partially observable Markov decision processes. *Structure and Infrastructure Engineering, 1*(1), 75–84.

Faber, M. H. (2002). Risk-based inspection: The framework. *Structural Engineering International: Journal of the International Association for Bridge and Structural Engineering (IABSE), 12*(3), 186–194.

Faber, M. H., Sorensen, J. D., Tychsen, J., & Straub, D. (2005). Field implementation of RBI for jacket structures. *Journal of Offshore Mechanics and Arctic Engineering, 127*(3), 220–226.

Friis-Hansen, A. (2000). *Bayesian networks as a decision support tool in marine application*. Technical University of Denmark.

Kurniawati, H., Hsu, D., & Sun Lee, W. (2008). SARSOP: Efficient Point-Based POMDP Planning by Approximating Optimally Reachable Belief Spaces. *Robotics: Science and Systems IV*. https://doi.org/10.15607/RSS.2008.IV.009

Lotsberg, I., Sigurdsson, G., Fjeldstad, A., & Moan, T. (2016). Probabilistic methods for planning of inspection for fatigue cracks in offshore structures. *Marine*

Bladena
Banestrøget 13, 1
DK-2630 Taastrup

Structures, *46*, 167–192. https://doi.org/10.1016/j.marstruc.2016.02.002

Luque, J., & Straub, D. (2016). Reliability analysis and updating of deteriorating systems with dynamic Bayesian networks. *Structural Safety*. https://doi.org/10.1016/j.strusafe.2016.03.004

Moan, T. (2005). Reliability-based management of inspection, maintenance and repair of offshore structures. *Structure and Infrastructure Engineering*, *1*(1), 33–62. https://doi.org/10.1080/15732470412331289314

Morato, P G, Mai, Q. A., Rigo, P., & Nielsen, J. S. (2018). Point-based POMDP risk based inspection of offshore wind substructures. *Proceedings of IALCCE 2018: The Sixth International Symposium on Life-Cycle Civil Engineering*, 3069–3076.

Morato, Pablo G., Papakonstantinou, K. G., Andriotis, C. P., Nielsen, J. S., & Rigo, P. (2020). Optimal Inspection and Maintenance Planning for Deteriorating Structures through Dynamic Bayesian Networks and Markov Decision Processes. *Structural Safety*. Retrieved from https://vbn.aau.dk/da/publications/optimal-inspection-and-maintenance-planning-for-deteriorating-str

Murphy, K. (2002). *Dynamic Bayesian networks: Representation, inference and learning*. University of California, Berkeley.

Nielsen, J. J., & Sørensen, J. D. (2011). Risk-based operation and maintenance of offshore wind turbines using Bayesian networks. *Applications of Statistics and Probability in Civil Engineering -Proceedings of the 11th International Conference on Applications of Statistics and Probability in Civil Engineering*.

Nielsen, Jannie S. (2022). Value of information of structural health monitoring with temporally dependent observations. *Structural Health Monitoring*, *21*(1), 165–184. https://doi.org/10.1177/14759217211030605

Nielsen, Jannie S., Tcherniak, D., & Ulriksen, M. D. (2020). A Case Study on Risk-Based Maintenance of Wind Turbine Blades with Structural Health Monitoring. *Structure and Infrastructure Engineering*, 1–17. https://doi.org/10.1080/15732479.2020.1743326

Nielsen, Jannie Sønderkær, & Sørensen, J. D. (2015). Risk-based decision making for deterioration processes using POMDP. *12th International Conference on Applications of Statistics and Probability in Civil Engineering, ICASP 2015*.

Bladena
Banestrøget 13, 1
DK-2630 Taastrup

Taastrup, June 28, 2023

Vancouver, Canada: University of British Columbia.

Nielsen, Jannie Sønderkær, & Sørensen, J. D. (2018). Computational framework for risk-based planning of inspections, maintenance and condition monitoring using discrete Bayesian networks. *Structure and Infrastructure Engineering*, *14*(8), 1082–1094. https://doi.org/10.1080/15732479.2017.1387155

Papakonstantinou, K. G., & Shinozuka, M. (2014). Planning structural inspection and maintenance policies via dynamic programming and Markov processes. Part II: POMDP implementation. *Reliability Engineering and System Safety*, *130*, 214–224. https://doi.org/10.1016/j.ress.2014.04.006

Raiffa, H., & Schlaifer, R. (1961). *Applied statistical decision theory*. Boston: Harvard University.

Robelin, C.-A., & Madanat, S. M. (2007). History-Dependent Bridge Deck Maintenance and Replacement Optimization with Markov Decision Processes. *Journal of Infrastructure Systems*, *13*(3), 195–201. https://doi.org/10.1061/(asce)1076-0342(2007)13:3(195)

Straub, D. (2009). Stochastic modeling of deterioration processes through dynamic bayesian networks. *Journal of Engineering Mechanics*, *135*(10), 1089–1099.

Straub, D., & Faber, M. H. (2006). Computational aspects of risk-based inspection planning. *Computer-Aided Civil and Infrastructure Engineering*, *21*(3), 179–192. https://doi.org/10.1111/j.1467-8667.2006.00426.x

Tien, I., & Der Kiureghian, A. (2017). Reliability Assessment of Critical Infrastructure Using Bayesian Networks. *Journal of Infrastructure Systems*, *23*(4), 04017025. https://doi.org/10.1061/(ASCE)IS.1943-555X.0000384

Appendix F Sørensen J.D., Abeendarnath A., Nielsen J.S., Gomez A., (2023), "Stochastic modelling of wind turbine blade tests for reliability analysis and O&M planning", AAU Department of The Built Environment and DTU Department of Civil and Mechanical Engineering

Bladena
Banestrøget 13, 1
DK-2630 Taastrup

Taastrup, June 28, 2023

DRAFT, June 2023

Stochastic modelling of wind turbine blade tests for reliability analysis and O&M planning

John Dalsgaard Sørensen[1], Edgar Arturo Gomez Meisel[2], Abhinav Abeendarnath[1] and Jannie Sønderkær Nielsen[1]

1) Department of the Built Environment, Aalborg University, Denmark; 2) Department of Civil and Mechanical Engineering, Technical University Denmark, Denmark

Abstract

Design and assessment of wind turbine blades assisted by tests are important in verifying the structural integrity of large wind turbine blades. Tests of composites and wind turbine blades are performed at an increasing level of detail illustrated by a test pyramid with many tests performed at the characterization level and fewer and fewer tests performed for subcomponents with increasing size and complexity and finally only a few tests at large scale or full-scale level. In verifying the structural integrity of critical details, the uncertainties related to these different levels have to be included. The uncertainties include physical uncertainty, model uncertainty, statistical uncertainty, and measurement uncertainty. Physical uncertainties are generally quantified at the characterization level where the statistical uncertainty is very small due to the large number of tests being performed. At subcomponent and large-scale test level, numerical models using e.g. cohesive elements for fatigue verification are introduced. In validation of the numerical models the tests are an important tool. In this task, an approach for systematic modelling and quantification of the uncertainties is described. Using test results, the model and statistical uncertainties due to a (very) limited number of tests can be quantified with statistical uncertainty becoming more and more important at increasing subcomponent level. The uncertainty modelling related to tests and associated numerical models is developed such that the models can be used to verify the structural reliability. The statistical modelling of test results also includes tests performed at subcomponents with reinforcement components included,e.g. the RTZ solution by Bladena [Jensen et al. 2023]. The test results are used to quantify the above uncertainties.

By combining the stochastic and statistical modelling of the test results and with numerical models, reliability verification can be performed using partial safety factors or reliability-based approaches. Further, the stochastic models for fatigue can be used as an important input for cost-optimal planning of operation & maintenance including planning of inspections and monitoring.

1. Introduction

Wind turbine blades contribute with a significant part of the costs for operation & maintenance of wind turbines, especially offshore wind turbines and farms. Cost-efficient planning of inspections, monitoring, maintenance, strengthening, repair, and potential exchange of blades requires a reliability modelling of fatigue and damage development with time. Fatigue of blades made of composites and glued parts is a complicated process. Traditionally, design based on standards use SN-curves together with linear damage accumulation by Miners rule. Methods based on fracture mechanics are able to

Bladena
Banestrøget 13, 1
DK-2630 Taastrup

Taastrup, June 28, 2023

model much better the damage / crack evolution, but they also are much more complicated. However, for cost-optimal planning of inspections etc. a fracture mechanics approach is needed.

Fracture mechanics models are subject to different uncertainties which need to be accounted for in a reliability analysis. The uncertainties include physical uncertainties related to material properties and the fatigue load. Generally, these uncertainties cannot be reduced. Other so-called epistemic uncertainties which may be reduced are model uncertainties connected to the models being used, i.e. the fracture mechanics models and the fatigue load models; statistical uncertainty connected to a limited number of tests used to calibrate models and to determine the statistical parameters; and measurement uncertainties connected to the test equipment.

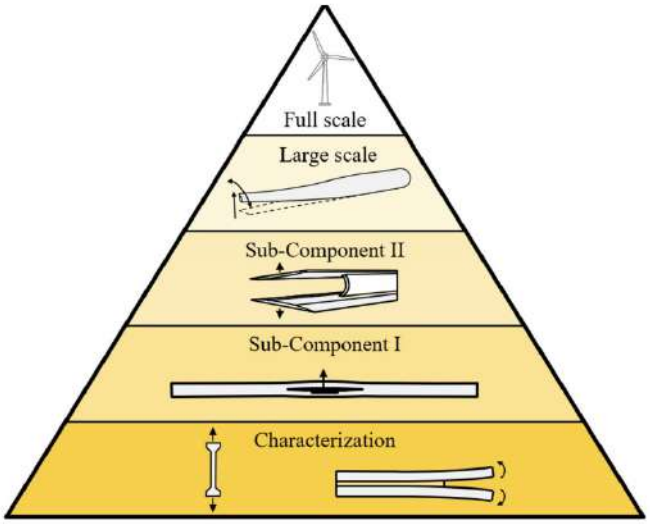

Figure 1. Test pyramid from [Jensen et al., 2023].

Tests performed to model and assess the structural capacity of wind turbine blades are generally done on different levels of size and complexity illustrated by a test pyramid, see Figure 1. At the blade development stage, a large number of tests are performed to determine the basic material properties (classification tests); many tests are performed at small subcomponents; and a decreasing number of tests are performed when the size and complexity of subcomponents are increased; and finally only one or a few tests are performed at the full-scale blade. In addition, tests may be performed at operating blades when the series production of blades has started. This paper describes the stochastic modelling of the various uncertainties in the test pyramid associated with the development of fracture mechanics based models for fatigue damage. Further, it is described how the stochastic models can be applied for reliability analysis in relation to cost-optimal planning of inspections, monitoring, and operation & maintenance.

Section 2 describes a model for estimating the crack growth. In section 3 a probabilistic model is formulated introducing physical, model and statistical uncertainties and it is described how the reliability can be determined. Section 4 describes how the stochastic modelling can be used in reliability analysis. In section 5 illustrative examples are presented.

Bladena
Banestrøget 13, 1
DK-2630 Taastrup

Taastrup, June 28, 2023

2. Crack growth modelling

Crack propagation in adhseive joins involving composites of glass fiber and polymeric matrix have found to be dominated by fiber bridging. The fiber bridging phenomenon occurs when the fibers in neighboring laminate plies bridge the debonding plane, serving as crack arrestors. As a result, the debonding resistance and inter-laminar fracture toughness are enhanced. Non-linear fracture mechanics such as the computation of the J integral is often necessary to study problems that involve extensive bridging. However since no analytical solution is available it is necessary to determine a bridging/cohesive law from experimental testing [Sørensen, 2010].

Bridging/cohesive laws can be obtained from a DCB-UBM test, as introduced by [Sørensen 2010]. Which involves the application of uneven bending moments to the crack flanks' tips in the specimen. By adjusting the ratio of these applied moments, the crack propagation can occur under different fracture modes, ranging from pure mode I to pure mode II. This characteristic of DCB-UBM tests eliminates the requirement for three separate characterization tests, making it an appealing and efficient method for fracture characterization in general.

2.1 Cohesive zone model

In the cohesive zone model the fracture process zone (FPZ) is substituted with a cohesive region, where the exchange of stress between the two artificial crack surfaces is defined using a relationship between the traction and separation of the FPZ. The material follows a constitutive response which uses a strength-based criterion to predict onset of damage and the degradation of the material stiffness. For a simplified bilinear traction-separation law, see Figure 2, the following parameters govern the traction-separation law:

- K_{nn}, the stiffness of the cohesive element in the linear elastic regime
- Traction t_n^0 (or separation δ_n^0) for damage onset
- G_n^c, fracture energy release rate
- Damage evolution law

The fracture energy release rate required for crack initiation can be related to the area under the T vs δ curve for the first linear elastic segment. Similarly the critical energy release rate required for steady state propagation corresponds to the total area. Since both values can be obtained directly from DCB-UBM tests by computing the J integral (Kardomateas et al., 2013) , they receive the notation J_0 and J_{ss}.

Bladena
Banestrøget 13, 1
DK-2630 Taastrup

Taastrup, June 28, 2023

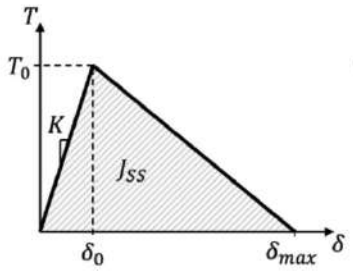

Figure 2. Cohesive law [Rasmussen, 2022].

The basic cohesive law parameters: J integral for crack initiation J_0, J integral for steady crack growth J_{ss}, and the cohesive law traction T_0 are determined by tests for different moment ratios and for the three fatigue modes I, II and III.

A novel approach to consider the deterioration of materials caused by fatigue loading, is to degrade the traction-separation response as the number of cycles increases. In this approach the cohesive strength and critical fracture energy decrease following a fatigue damage evolution law (Khoramishad et al., 2010). The damage accumulation D_i as a function of number of cycles N in each cohesive element is given by:

$$\frac{\Delta D_i}{\Delta N} = \begin{cases} \alpha(\varepsilon_{max} - \varepsilon_{th})^{\beta} & , \varepsilon_{max} > \varepsilon_{th} \\ 0 & , \varepsilon_{max} \leq \varepsilon_{th} \end{cases} \quad (1)$$

where ΔD_i is the damage accumulated over ΔN cycles while α, β and ε_{th} are material parameters which must be calibrated from FEA trial and error results against experimental DCB-UBM fatigue characterization tests using a cyclic load S with constant amplitude. Due to the data scattering, the calibration process is carried out by a curve fitting analysis for a single fracture mode, so in this formulation α, β and ε_{th} can be considered as mode dependent. For this reason, a collection of FEA analysis results is required to handle different test results. However in practical application, mode I parameters could produce acceptable results. The maximum overall strain is given in terms of opening ε_n and shear strains ε_s during the a fatigue load cycle by:

$$\varepsilon_{max} = \frac{\varepsilon_n}{2} + \sqrt{\left(\frac{\varepsilon_n}{2}\right)^2 + \left(\frac{\varepsilon_t}{2}\right)^2} \quad (2)$$

At the beginning, the damage parameter D_i is set to zero and damage accumulation in the load cycle only occurs if the maximum overall strain is larger than the threshold value ε_{th}. The damage parameter which ranges between 0 and 1 can be computed after each load cycle (or set of load cycles) and is used to update the effective traction and energy release rate used to estimate the crack propagation as follows:

$$t_i = D_i t_0 \quad (3)$$

$$G_{c,i} = D_i G_{C,0} \quad (4)$$

where i denotes the current time step, and t_0 and $G_{C,0}$ is the initial cohesive strength and fracture energy respectively.

Bladena
Banestrøget 13, 1
DK-2630 Taastrup

Taastrup, June 28, 2023

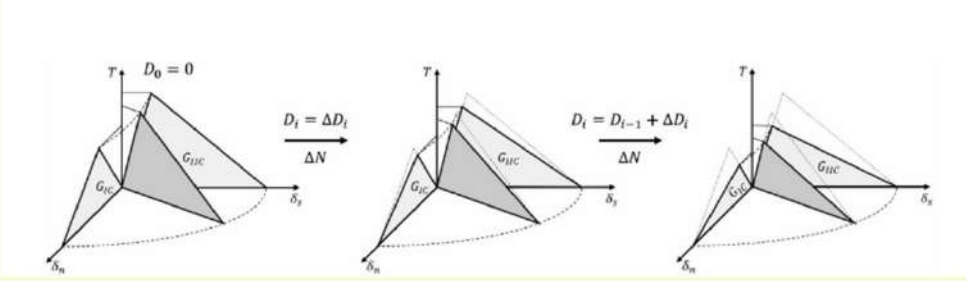

Figure 3. Cohesive model development during damage increase [Rasmussen, 2022].

It is noted that all three fatigue modes are considered simultaneously and the fatigue mode dominating the crack growth may change when the crack grows. The strains ε_n and ε_s are dependent on the fatigue load S which directly related to the load range in a fatigue load cycle.

The basic material parameters are subject to physical and statistical uncertainty which can be quantified based on characterization tests, see below.

Subcomponent tests with increasing level of size and complexity can be performed next and a FEM model prepared using the basic material parameters from the characterization tests.

The cohesive law based model thus models the crack size development and can be formulated by a Crack Propagation Rate (CPR):

$$\frac{d\,a}{d\,N} = CPR^{NUM}(J_0, J_{ss}, T_0, \alpha, \beta, \varepsilon_{th} a, S) \quad (5)$$

2.2 Simplified engineering model

A simplified, engineering model for the increase over time of the crack size a can be developed based on Paris law and the numerical modelling, and can be used for reliability analysis and planning of operation & maintenance:

$$\frac{d\,a}{d\,N} = C\left(\Delta G(a,S)\right)^m = CPR^{O\&M}(C, m, a, S) \quad (6)$$

where C and m are material / component specific parameters determined by tests, and ΔG is the energy release rate. CPR is the Crack Propagation Rate.

Bladena
Banestrøget 13, 1
DK-2630 Taastrup

Taastrup, June 28, 2023

3. Stochastic modelling

Figure 3 and Table 1 show a test matrix consisting of 6 levels indicating the typical number of tests performed and the complexicity of the model. These parameters are important for establishing stochastic models. Physical, model and statistical uncertainties can be modelled using the tets at level 3, 4, 5 and 6 as described in the following. It is noted that gross / human errors are not included in these stochastic models and have to be handled by quality control procedures.

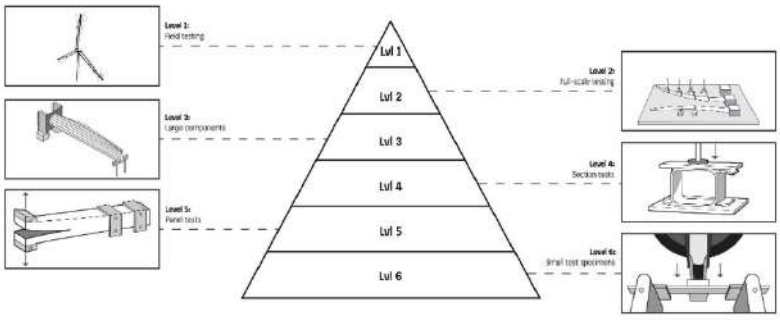

Figure 3. Test matrix with number of tests at each level [Jensen et al., 2023].

Level	Test model	Statistical uncertainty Typical number of tests	Model uncertainty Complexicity of model
1			Very complex
2	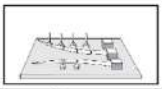	Very few Proof loading	Very complex
3		Very small number: 3-5	Complex subcomponent
4	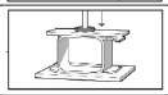	Small number: 4-8	Complex section
5	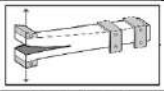	Many: 5-15	Simple
6	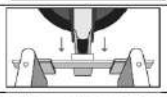	Large number: > 30	

Table 1. typical number of tests and complexicity of model.

This section describes a general approach for statistical analysis and stochastic modelling of the tests at level 6, 5, ...,1. The tests may be used in different ways:

Bladena
Banestrøget 13, 1
DK-2630 Taastrup

Taastrup, June 28, 2023

- In full-scale tests the tests are performed to a certain load level and the test is successful if no failure occur. The tests can thus be considered as a proof-load tests. The tests at level 1 and 2 are also used to verify the overall behaviour as modelled by the aeroelastic model.
- At level 3, 4 and 5, the tests can be used to estimate directly the load bearing capacity / resistance of the sub-component (large components, sections, panels) if the test is conducted to failure and a representative load is applied. Based on the tests chaacteristic and design resistances can be obtained.
- Alternatively at level 3, 4 and 5, a numerical model of the resistance can be validated and the model uncertainty related to the model can be modelled, see below. Additionally statistical uncertainty has to be included due to a limited number of tests, see below.
- At level 6, the characterization tests can be used to model the physical uncertainties related to parameters used in the numerical models investigated at level 2, 4 and 5. At level 6 the statistical uncertainty can often be neglected due to a large number of tests.

The parameters obtained by the characterization tests J_0, J_{ss}, T_0 and $\alpha, \beta, \varepsilon_{th}$ are denoted $X_1, X_2, \ldots$ in the following. Similarly for the simple 'engineering' model the material parameters are denoted $X_1, X_2, \ldots$.

3.1 Tests at level 6: characterization tests with 'real' specimens incl. manufacturing defects

Tests at level 6, see Figure 3, are characterized by: The number of tests N is very large; the crack size a and $\frac{da}{dn} = CPR$ as a function of a can be measured in each test; The test matrix contains a number of combinations of (S, d) where d models the geometry; Model uncertainty can be assumed negligible, since the tests are permed with a very basic structural model; Statistical uncertainty is negligible because a large number of tests are assumed to be performed.

The materiel parameters $X_1, X_2, \ldots$ are modelled by stochastic variables in order to include the effect of manufacturing defects. They are assumed Normal distributed with mean values, $\mu_{X_1}, \mu_{X_2,\ldots}$ and coefficients of variation (COV), $V_{X_1}, V_{X_2,\ldots}$ which are estimated e.g. by the Maximum Likelihood Method. In addition statistical / parameter uncertainty can be included for these statistical parameters. Alternatively, a Lognormal distribution may be used. It is also assumed that the test specimens are manufactured fulfilling the requirements to tolerances ans have passed the quality control requirements.

3.2 Tests at level 5: simple subcomponent tests with 'perfect' material properties

It is here assumed that the material parameters have small uncertainty obtained by controlled / perfect manufacturing. The objective of these test is to validate 1) complex numerical model using cohesive elements and of 2) simplified 'engineering' model based on Paris law. The tests can be characterized by: the number of tests N is not very large; the crack size a and $\frac{da}{dn} = CPR$ as a function of a are measured in each test; the test matrix consists of a number of combinations of $(X_1, X_2, \ldots, S, d)$ where $X_1, X_2, \ldots$ are values from the characterization tests assumed to be known with negligible uncertainty, i.e. the materiel used is almost without manufacturing defects allowing the tests to be used to quantify the model uncertainty.

Two CPR functions are considered:

Bladena
Banestrøget 13, 1
DK-2630 Taastrup

Taastrup, June 28, 2023

- A complex numerical model using cohesive elements: $CPR_5^{NUM}(X_1, X_2, \dots, S, d, a)$
- An 'engineering' model based on Paris law and to be used in planning of operation & maintenance: $CPR_5^{O\&M}(X_1, X_2, , \dots, S, d, a)$

Model uncertainties $X_{M_5}^{NUM}$ and $X_{M_5}^{O\&M}$ are introduced such that

$$\frac{da}{dn} = X_{M_5}^{NUM} CPR_5^{NUM}(X_1, X_2, \dots, S, d, a) \quad (7)$$

when the numerical model is used and

$$\frac{da}{dn} = X_{M_5}^{O\&M} CPR_5^{O\&M}(X_1, X_2, \dots, S, d, a) \quad (8)$$

when the simplified Paris law model is used. The model uncertainty: $X_{M_5}^{NUM}$ and $X_{M_5}^{O\&M}$ are assumed LogNormal distributed with mean values (bias) $\mu_{X_{M_5}^{NUM}}, \mu_{X_{M_5}^{O\&M}}$ and coefficients of variations $V_{X_{M_5}^{NUM}}, V_{X_{M_5}^{O\&M}}$. Statistical uncertainty is to be included.

$\mu_{X_{M_5}^{NUM}}, \mu_{X_{M_5}^{O\&M}}$ and $V_{X_{M_5}^{NUM}}, V_{X_{M_5}^{O\&M}}$ are estimated e.g. by the Maximum Likelihood Method which also makes it possible to estimate the statistical uncertainty related to these parameters if the number of tests is larger than approximately 25.

The statistical parameters (mean values and standard deviations) to be estimated are denoted $(\alpha_1, \alpha_2, \dots, \alpha_m)$. In general the parameters $(\alpha_1, \alpha_2, \dots, \alpha_m)$ are determined using a limited number data and are therefore subject to statistical uncertainty. The parameters are estimated by the Maximum Likelihood Method and they become asymptotically Normally distributed stochastic variables with expected values equal to the Maximum Likelihood estimators and covariance matrix equal to, see e.g. [Lindley 1976]:

$$\boldsymbol{C}_{\alpha_1,\alpha_2,\dots,\alpha_m} = [-\boldsymbol{H}]^{-1} = \begin{bmatrix} \sigma_{\alpha_1}^2 & \rho_{\alpha_1,\alpha_2}\sigma_{\alpha_1}\sigma_{\alpha_2} & \cdots \\ \rho_{\alpha_1,\alpha_2}\sigma_{\alpha_1}\sigma_{\alpha_2} & \sigma_{\alpha_2}^2 & \vdots \\ \vdots & \cdots & \cdots \end{bmatrix} \quad (9)$$

where $\boldsymbol{H}$ is the Hessian matrix with second order derivatives of the log-Likelihood function. The statistical uncertainty can easily be included in a reliability analysis using FORM (First Order Reliability Method), see below.

Statistical uncertainty may also be estimated by bootstrapping or by Bayesian inference through the Markov Chain Monte Carlo (MCMC) method which also makes it possible to include prior knowledge.

The model uncertainties are basically determined in connection with the validation of the two CPR functions, i.e. by assessing the discrepancy between the test results and estimates obtained using the two CPR functions, following the approach in [IEC 61400-1, 2019], Annex K and [ISO 2394, 2015]. A two-level approach can be used to estimate the model uncertainty of the 'engineering', simple *CPR* function, $CPR_5^{O\&M}(X_1, X_2, , \dots, S, d, a)$. First the model uncertainty related to the numerical complex CPR function, $CPR_5^{NUM}(X_1, X_2, \dots, S, d, a)$ is estimated; next additional test results are generated by simulation using $CPR_5^{NUM}(X_1, X_2, \dots, S, d, a)$ and the associated model uncertainty. These additional test results are combined with the real experimental tests and used to estimate the model uncertainty of the simple CPR function, $CPR_5^{O\&M}(X_1, X_2, , \dots, S, d, a)$.

Bladena
Banestrøget 13, 1
DK-2630 Taastrup

Taastrup, June 28, 2023

3.3 Tests at level 4: complex subcomponent tests with 'perfect' manufactured specimens

At test level 4 larger and more complex subcomponents are being tested. The procedure for uncertainty modelling is in principle the same as for tests at level 5. Fewer tests are performed and both the model uncertainties and statistical uncertainties can be expected to be larger compared to level 5.

3.4 Tests at level 3: large scale subcomponents with 'perfect' manufactured specimens:

Similar to tests at level 4 the same approach is used to model and quantify model uncertainties. Statistical uncertainties require more refined methods due to the very limited number of tests, and therefore e.g. MCMC methods may be applied.

3.5 Tests with reinforcement components

If a component is introduced to strength the blade the subcomponent tests can be performed as described above.

In addition tests have to be performed to be used to verify that both the reinforcement components and the clamping of the reinforcement component to the blade have sufficient reliability both for extreme loads and for fatigue loads.

4. Reliability analysis

4.1 Reliability verification of structural blade detail

In previous sections, a stochastic model is established for the crack growth including aleatory and epistemic uncertainties. In order to estimate the reliability / probability of failure a limit state equation dependent on time t is formulated if the 'engineering' CPR function is used:

$$g(t) = a_{cr} - a\left(X_{M_S}^{O\&M}, X_1, X_2, \dots, X_W\, X_{SCF}\, S, d, t\right) \qquad (10)$$

here a_{cr} is the critical crack size defining failure, $a(t)$ is the crack size at time t with the number of fatigue load cycles determined as $\nu\, t$ where ν is the number of fatigue load cycles per year. X_W and X_{SCF} are model uncertainties related to the fatigue load and estimation of the stresses at the considered detail, see e.g. IEC 6100-1, Annex K and [Sørensen & Toft, 2014].

The following parameters are modelled as stochastic variables:

X_W	model uncertainty fatigue load. This uncertainty depends on the degree that the fatigue load is driven by turbulence (large uncertainty) and by gravity (small uncertainty)
X_{SCF}	model uncertainty estimation of the stresses
X_1, X_2	uncertainty (aleatory) of material parameters with mean values $\mu_{X_1}, \mu_{X_2}, \dots$, standard deviations $\sigma_{X_1}, \sigma_{X_2}, \dots$ and correlation coefficients $\rho_{X_1,X_2}, \dots$
$\mu_{X_1}, \mu_{X_2}, \dots$, $\sigma_{X_1}, \sigma_{X_2}, \dots$	may be (correlated) stochastic variables modelling statistical / parameter uncertainty

Bladena
Banestrøget 13, 1
DK-2630 Taastrup

Taastrup, June 28, 2023

$X_{M_5}^{O\&M}$ model uncertainty *CPR* function with mean value $\mu_{X_{M_5}^{O\&M}}$ and coefficient of variation $V_{X_{M_5}^{O\&M}}$

$\mu_{X_{M_5}^{O\&M}}, V_{X_{M_5}^{O\&M}}$ may be (correlated) stochastic variables modelling statistical / parameter uncertainty

Using the limit state equation the accumulated and annual probability of failure are estimated by

$$P_f(t) = P(g(t) \leq 0) \quad (11)$$

$$\Delta P_f(t) = P(g(t) \leq 0) - P(g(t-1y) \leq 0) \quad (12)$$

or alternatively the annual probability of failure conditional on survival up to year $t-1y$

$$\Delta P_f(t) = \frac{P(g(t)\leq 0) - P(g(t-1y)\leq 0)}{1 - P(g(t-1y)\leq 0)} \quad (13)$$

If an inspection is performed at time T_1 with no detection of a crack and with an inspection technique with Probability Of Detection (*POD*) curve then an updated accumulated probability can be estimated by

$$P_f^U(t) = P(g(t) \leq 0 | h(t) > 0) \quad (14)$$

where $h(t) = a_d - a\left(X_{M_1}^{O\&M}, X_1, X_2, \dots, X_W\, X_{SCF}\, S, d, t\right)$ with the distribution function of a_d equal to $POD(a)$. Similarly the updated annual probability can be estimated.

If monitoring is performed the model uncertainties X_W and X_{SCF} typically decrease depending on the type of monitoring.

These probability of failure can be estimated by simulation or by FORM/SORM methods [Madsen, Krenk & Lind, 1986].

4.2 Reliability verification of reinforcement component

If reinforcement components are added, the reliability of these is to be verified using test results preformed as described in section 3. The following reliability verifications are preformed:

- The structural detail reinforced should be verified as described in section 4.1 but using the test results with reinforcement component included in the subcomponent tests.
- The structural reinforcement component should be verified having sufficient reliability with respect to extreme loads and fatigue loads.
- The location in the blade where the reinforcement component is attached should be verified having sufficient reliability with respect to extreme loads and fatigue loads since the blade my be weakened by the attachment.

4.3 Reliability requirement

Sufficient reliability to be verified in section 4.1 and 4.2 for structural details critical for the blade structural integrity can be done by using partial safety factors following e.g. [DNV-ST-0376, 2021], [IEC 61400-1, 2019] and [IEC 61400-5, 2020] or by a reliability based approach following [IEC 61400-1, 2019], Annex K. The target reliability level to be verified is corresponding to an annual probability of failure equal to $5 \cdot 10^{-4} - 10^{-4}$.

Bladena
Banestrøget 13, 1
DK-2630 Taastrup

Taastrup, June 28, 2023

5. Results

This section shows preliminary test results from DTU Construct (CORTIR II report 2023). Figure 4, 5 and 6 show test results for the cohesive law parameters J0, JSS and tn for Ψ = 0°, 15° and 30°.

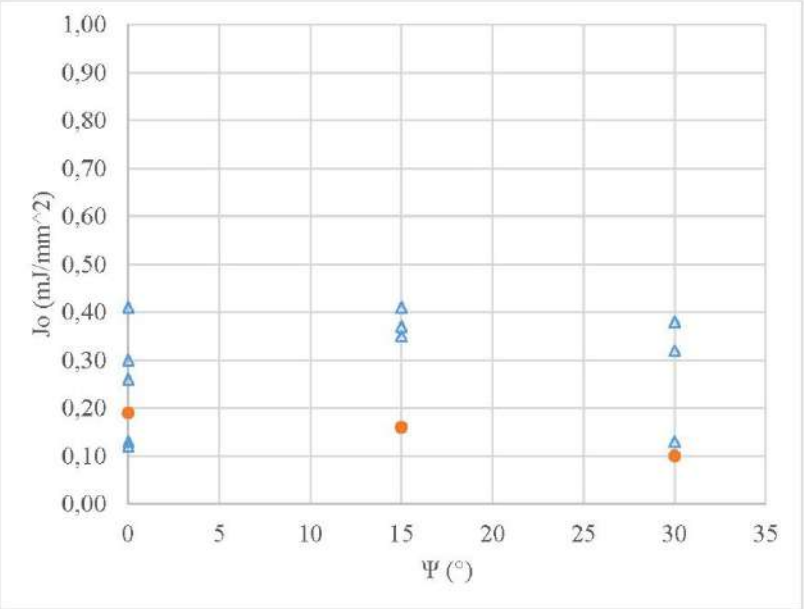

Figure 4. Test results level 6: J0 as a function of Ψ.

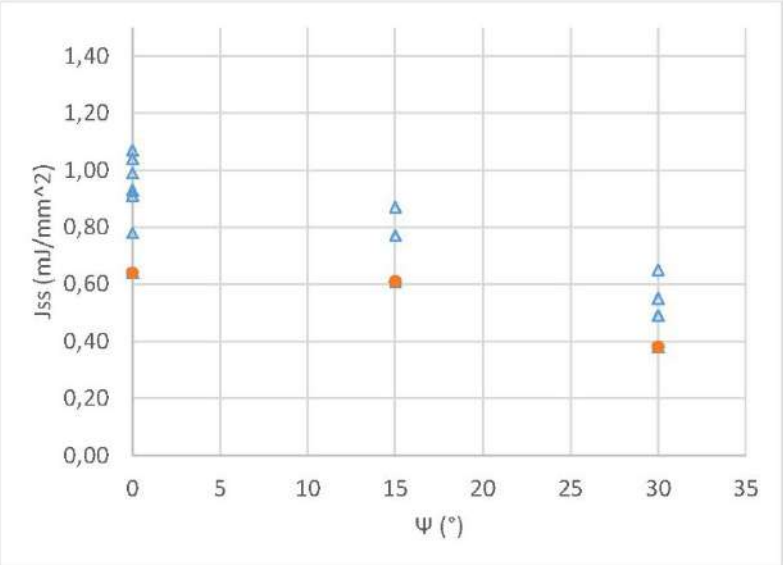

Bladena
Banestrøget 13, 1
DK-2630 Taastrup

Taastrup, June 28, 2023

Figure 5. Test results level 6: JSS as a function of Ψ.

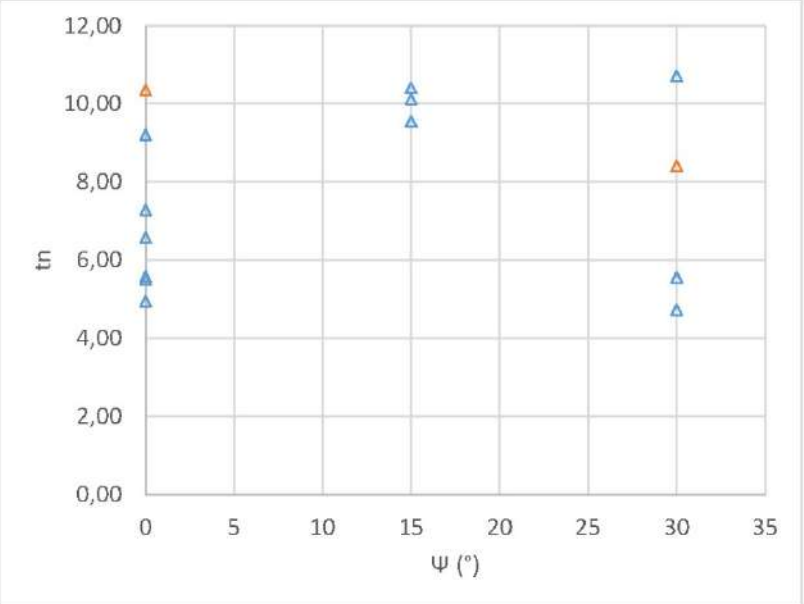

Figure 6. Test results level 6: tn as a function of Ψ.

From the test results mean values and coefficient of variation (COV) are determined, se Table 2 and 3. It is seen that the COVs vary between 0,04 and 0,45 idicating that for some of the parameters very large uncertainties need to be accounted for in determining design values and in reliability calculations. The number of tests for Ψ =15º and 30º is quite low and therefore the values for these two cases should be carefully.

Ψ (°)	0	15	30
Number of tests	5	2	3
J0 (mJ/mm2)	0,24	0,38	0,28
JSS (mJ/mm2)	0,94	0,80	0,56
tn	6,70	10,0	6,99

Table 2. Mean values and number of tests.

Ψ (°)	0	15	30
J0 (mJ/mm2)	0,45	0,07	0,39
JSS (mJ/mm2)	0,10	0,06	0,12
tn	0,22	0,04	0,38

Table 3: Coefficient of variation.

Correlation coefficients for Ψ=0° are estimated to:

- corr J0,JSS: -0,28
- corr J0,tn: 0,00
- corr JSS,tn: 0.60

Bladena
Banestrøget 13, 1
DK-2630 Taastrup

Taastrup, June 28, 2023

and the corresponding test results are shown in the Figure 7-9.

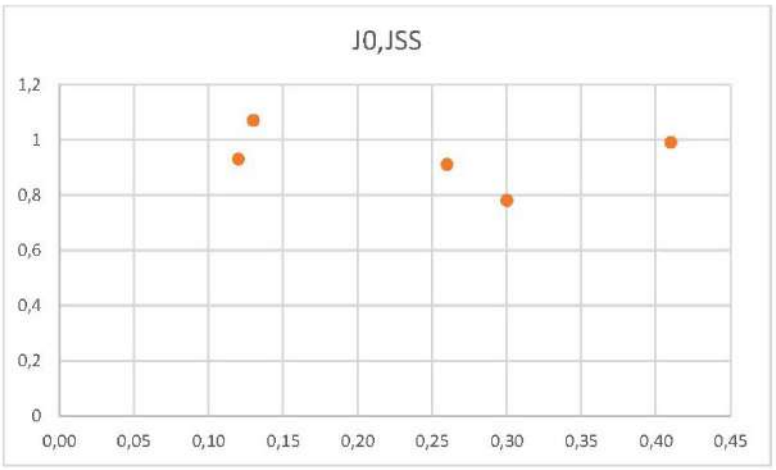

Figure 7. Test results for J0 and JSS for $\Psi=0$.

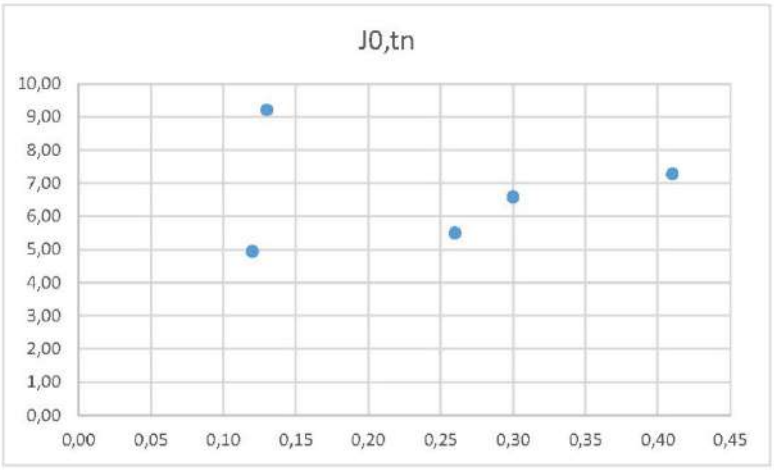

Figure 8. Test results for J0 and tn for $\Psi=0$.

Bladena
Banestrøget 13, 1
DK-2630 Taastrup

Taastrup, June 28, 2023

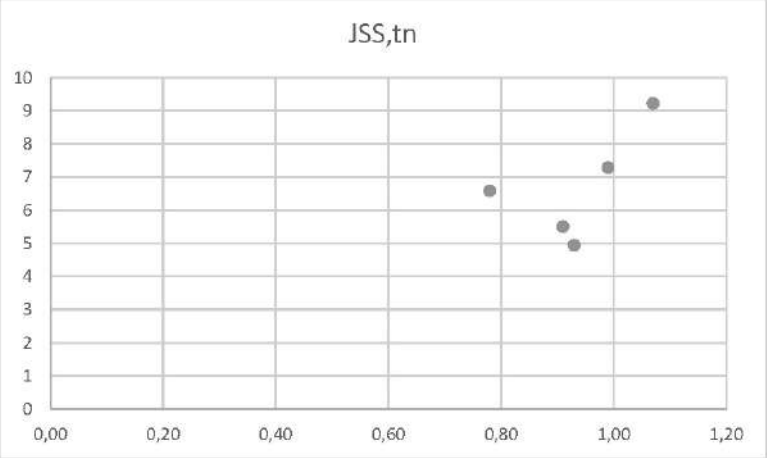

Figure 9. Test results for JSS and tn for Ψ=0.

When more test data from characterization tests are available on $\alpha, \beta, \varepsilon_{th}$, statistical analyses are to be performed.

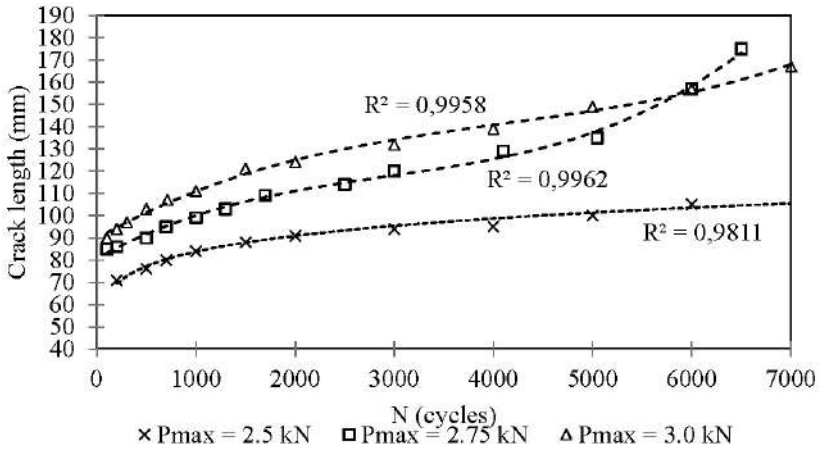

Figure 10. Crack length as function of number of cycles.

Figure 10 shows the crack length as a function of number of cycles. It is seen that the crack growth is almost linear as function of time which is partly due to change in fatigue mode. This is important for planning of O&M planning allowing to increase time intervals between inspections significantly compared to cases where the fatigue growth is exponential wrt time.

Bladena
Banestrøget 13, 1
DK-2630 Taastrup

Test results from subcomponent tests at level 4 and 5 to be included here – and statistical analyses performed...

6. Conclusions

A framework for stochastic modelling of tests for design and assessment of wind turbine blades is presented. The stochastic modelling is based on a crack growth model using a cohesive law approach. The tests can be described by a test pyramid where very few full-scale tests are perfomed, more sub-component tests and may characterization tests. Six levels are used in this paper and an approach to modelling physical, model and statistical uncertainties is presented. Human / gross errors are not included in the modelling. The stochastic modelling is linked to a numerical model to estimate the crack growth using a cohesive law and to a more simple model based on Paris law.

Illustrative tests results form the CORTIR II project are presented. More tests results to be included when the tests are finalized.

The stochastic models obtained by the tests together with numerical models for modelling the crack growth can be used to estimate the reliability of blades for selected failure modes and further be used for cost-optimal planning of operation & maintenance.

Acknowledgments

Financial support is greatly acknowledged to the Energy Development and Demonstration Program (EUDP) under the grant number: 64021-1054 CORTIR II Project.

7 References

DNV-ST-0376 (2021) Rotor blades for wind turbines.

IEC 61400-1 (2019) Wind turbine generator systems – Part 1: Safety requirements. 4th edition.

IEC 61400-5 (2020) Wind turbine generator systems – Part 5: Wind turbine blades.

ISO 2394 (2015) General principles on reliability for structures.

Jensen, F. et al. (2023) CORTIR II - Cost, Risk and Transition Zone Innovative Reinforcement – Final Report, EUDP Project 64021-1054.

Kardomateas, G.A., C. Berggreen & L.A. Carlsson (2013) Energy-Release Rate and Mode Mixity of Face/Core Debonds in Sandwich Beams. AIAAJ Aeronautics, Volume 51, Number 4.

Khoramishad, H. et al. (2010) Predicting fatigue damage in adhesively bonded joints using a cohesive zone model. International Journal of Fatigue, vol. 32, pp. 1146–1158.

Lindley, D.V. (1976) Introduction to Probability and Statistics from a Baysian Viewpoint. Cambridge University Press: Cambridge, UK.

Madsen, H. O., Krenk, S. & Lind, N.C. (1986) Methods of Structural Safety, Dover Publications.

Rasmussen, D.S. (2022) Cohesive web joints in wind turbine blades using cohesive zone modelling to predict crack growth under fatigue loading. Master Thesis, DTU, Department of Mechanical Engineering, Denmark.

Bladena
Banestrøget 13, 1
DK-2630 Taastrup

Taastrup, June 28, 2023

Sørensen, B. (2010) Cohesive laws for assessment of materials failure: Theory, experimental methods and application. Doctoral thesis, Technical University of Denmark, Risoe-R; No. 1736.

Sørensen, J.D.&Toft, H.S. (2014) Safety Factors – IEC 61400-1 ed. 4 – background document. DTU Wind Energy-E Report-0066 (EN).

Bladena
Banestrøget 13, 1
DK-2630 Taastrup